Fabricating Robust Nanoporous Materials and Polymer Electrolyte Membranes from Reactive Block Copolymers by Metathesis Reactions

A THESIS
SUBMITTED TO THE FACULTY OF THE GRADUATE SCHOOL
OF THE UNIVERSITY OF MINNESOTA

Liang Chen

IN PARTICAL FULFILLMENT OF THE REQUIREMENTS
FOR THE DEGREE OF
DOCTOR OF PHILOSOPHY

Marc A. Hillmyer, Advisor

June 2009

Acknowledgements

First, I would like to express my sincere gratitude to my advisor, Prof. Marc Hillmyer, for his guidance, support, and encouragement during my graduate study, for providing me with a great opportunity to study novel block copolymers toward potential applications. Numerous challenges during my research have greatly enhanced my research abilities and motivated me to continually explore new ideas.

I am grateful to the members in Hillmyer group I have worked with, for their generosity and friendliness. The personal and working relationships with them are the best memory of my graduate study at UMN. Specifically, I express my sincere thanks to Javid Rzayev, Rajeswari Kasi, and Nate Lynd for their helpful discussion and suggestions, Pedro Arrechea for teaching me anionic polymerization, Zhiyong Wang in Stein Group and Huiming Mao for their patient training for BET experiments, Kwanho Chang and Chun Liu for their generous help with TEM experiments, Benjamin Hamilton for performing TGA experiments, Marc Rodwogin for acquiring XPS data, Louis Pitet for collecting some synchrotron X-ray data, Yiyong He in Lodge group for some conductivity measurements, and Chun Liu also for training for DLS and SEC experiments. Additionally, Karen Switek, Kathleen Schreck, Mark Amendt, Louis Pitet, and Jennifer Lowe deserve special thanks for patiently proofreading my written dossier, manuscripts, and thesis draft. I also want to thank my friends at UMN for their help and memorable experiences with them.

I must thank all my collaborators: Mark Amendt, Bill Phillip and Prof. Cussler in CEMS at UMN for their significant contributions of diffusion measurements and valuable discussion, and Dan Hallinan and Prof. Elabd at Drexel University for their conductivity measurements.

Lastly but not least, I should not forget to thank my parents and my uncle, for their instruction and dedication, and my wife, Jing Xiao, for her endless support and encouragement.

Abstract

Polymer membranes have been studied for several decades, and conventional utility of these membranes has been realized over a wide range of applications such as water purification, gas separation, and fuel cells. Separation performance of polymer membranes for these applications can be evaluated from different aspects including selectivity, material cost, and thermal and mechanical stabilities.

This research focused on the design of crosslinked polymer membranes from reactive block copolymers, which could possess some attractive features such as controlled functionality and morphology. Novel block copolymers containing a chemically crosslinkable block and a chemically modifiable block were of particular interest. Metathesis reactions were employed to crosslink these copolymers with additional tough polymers such as polycyclooctene (PCOE) and polydicyclopentadiene (polyDCPD), to realize enhanced toughness in the resulting materials.

First, a norbornene-functionalized polystyrene-polylactide (PNS-PLA) block copolymer was synthesized. A self-assembled blend containing this copolymer and DCPD was cured by metathesis reactions, and nanoporous monoliths with a cylindrical morphology were successfully produced after removing the PLA component. These monoliths exhibited pronounced mechanical and thermal stabilities superior to nanoporous polystyrene (PS).

Second, polymerization induced phase separation (PIPS) during the ring-opening metathesis polymerization (ROMP) of DCPD in the presence of the PNS-PLA copolymer rendered continuous PLA nanodomains in a crosslinked PNS/polyDCPD matrix. Upon etching the PLA component, the resultant nanoporous membranes exhibited well-defined percolated nanopores and good thermal and mechanical stabilities. Preliminary diffusion measurements demonstrated potential utility of such membranes in ultrafiltration.

Third, crosslinked polymer electrolyte membranes (PEMs) were fabricated from a PNS-poly(*n*-propyl-*p*-styrenesulfonate) (PSSP) block polymer and COE/DCPD via the PIPS

scheme followed by deprotection of the PSSP block. These PEMs possessed a bicontinuous morphology and mechanical and thermal robustness. Select PEMs exhibited high proton conductivity similar to Nafion at high humidity and reduced methanol crossover. Tunable domain size and mechanical strength of the resulting PEMs are advantageous attributes of this preparation protocol. Additionally, the use of such PEMs for NH_3 separation from gas mixtures was demonstrated.

The appendix chapter represented our efforts to produce amine-functionalized polymer membranes from PNS-poly(dimethylaminoethylmethacrylate) (PNS-PDMAEMA) and COE by metathesis reactions, potentially useful for CO_2 separation from gas mixtures.

Table of Contents

List of Tables

List of Figures

List of Schemes

Chapter 1

Background

This chapter gives an introduction to polymer membranes and the underlying theories for membrane separation. The self-assembly principles of diblock copolymer systems are then briefly described. Current membrane developments using block polymers are reviewed in two areas: nanoporous membranes and polymer electrolyte membranes. Finally, following a concise overview of metathesis polymerization, my thesis research of toughening block polymer membranes by metathesis reactions is outlined.

1.1 Polymer membranes

1.1.1 Introduction

A membrane is defined as an interface between two adjacent phases acting like a selective barrier that regulates mass transfer between two compartments. Among various kinds of membranes, polymer membranes (including natural and synthetic polymers) constitute the most useful category. Polymer membranes have been developed for over 50 years, and conventional utility of these membranes has been realized over a wide range of applications such as water purification,[1] gas separation,[2] solvent dehydration,[3] fuel cells,[4] lithium batteries,[5] biosensors and biomaterials,[6] and medical dialysis.[7] In comparison with traditional industrial separation processes such as adsorption, extraction, and distillation, membrane technology holds inherent advantages (e.g., no chemical additives), and therefore low energy consumption and high performance in membrane separations can be potentially realized.

Performance of polymer membranes can be assessed based on the following aspects: flux and selectivity, cost in production, thermal and chemical stabilities, fouling, and mechanical strength.[8] Generally, these properties are fundamentally related to the chemical and physical nature of polymers, and during the last few decades, tremendous research efforts have been made to clarify the relationships between them. Specific applications of polymer membranes can be categorized based on the membrane microstructures (Table 1.1). Membranes with different ranges of pore sizes can be employed in diverse size-selective filtrations, while the utility of nonporous membranes has been demonstrated in other advanced gas separations. Among all separation processes, pressure is commonly utilized as the cross-membrane gradient to drive the mass transfer.

Table 1.1. Classification of membrane separation processes.[9]

Membrane barrier structure	Cross-membrane gradient		
	Concentration	Pressure	Electric field
Nonporous	Pervaporation (PV)	Gas Separation (GS) Reverse Osmosis (RO)	Electrodialysis (ED)
Microporous size < 2 nm	Dialysis (D)	Nanofiltration (NF)	
Mesoporous size = 2–50 nm	Dialysis (D)	Ultrafiltration (UF)	Electrodialysis
Macroporous size =50–500 nm		Microfiltration (MF)	

From a broad standpoint, a successful membrane separation generally depends on three factors: material selection, membrane formation, and system design (Figure 1.1). Besides the fundamental aspect of material selection, membrane formation plays a critical role in order to meet commercial interest. Early on, free-standing membranes possessing a uniform distribution of the barrier structure were investigated to achieve tailored membrane selectivity. Nevertheless, the major disadvantage of such membranes was low mass flux across the membrane due to the membrane thicknesses of typically > 20 μm. Later, the developments of anisotropic polymer membranes, either with a gradient porous structure or with a thin selective layer (< 1 μm) deposited over a macroporous substrate, were major breakthroughs of membrane technology to realize high flux and low cost in membrane production. Separation system design is a more complicated process toward final applications, and will not be discussed here.

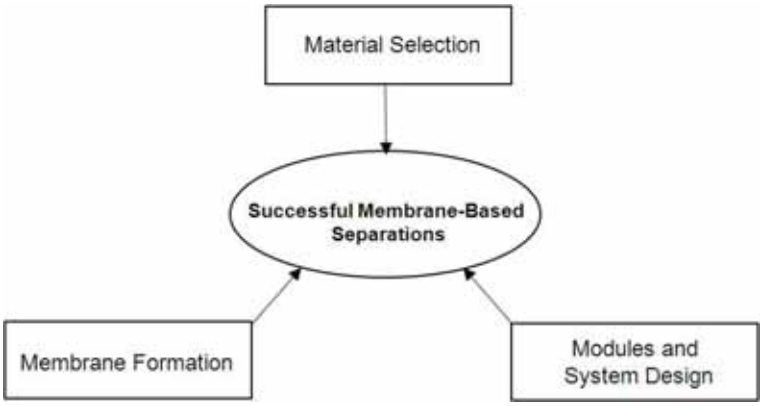

Figure 1.1. Critical factors for membrane-mediated separations.

In the following section, the primary focus will be on material selection, and a brief overview on membrane applications of polymer materials will be given in four areas: CO_2 separation from gas mixtures, water purification, direct methanol fuel cells, and pervaporation.

1.1.2 Applications of polymer membranes

1.1.2.1 CO_2 separation

Gas separations using polymer membranes have been extensively documented.[10] There have been many gas separation systems of practical relevance, for example, air separation,[11] hydrogen recovery,[12] natural gas purification,[13] and olefin-paraffin separations.[14] Among all of these, the capture and isolation of CO_2 from gas mixtures are particularly important, for the purpose of not only protecting the global environment by controlling CO_2 emission but also improving fuel efficiency (e.g. natural gas) by removing the CO_2 impurity. Conventional physical adsorption methods to remove CO_2 require high energy consumption, so there is a motivation to design new polymer membranes that favor CO_2 diffusion over other gases. Numerous polymers have already been explored to clarify the relationship between the polymer structures and CO_2 diffusibility. One category of such polymers is polyimide derivatives, which possess extraordinary thermal and mechanical stabilities.[15] Despite a long history of studying such polymers, innovation in the chemistry and fabrication processes is still needed. For example, Ghanem *et al.* reported some complex polyimide membranes, which exhibited excellent CO_2 selectivity in gas mixtures with CH_4. For these polyimides, high CO_2 flux and selectivity were attributed to a combination of high percentage of micropores (< 1 nm) that enhanced the gas flow, and the presence of interior polar groups that strengthened the polymer-CO_2 interactions and thereby promoted CO_2 diffusion.[16] Similarly, Park and coworkers reported the performance of dense vitreous polymers from polyimide precursors that enabled outstanding CO_2 separation performance, which surpassed the limits of conventional polymers. In particular, the micropores in these materials were

systematically tuned by the degree of thermally driven rearrangement of the original polyimide chains.[17] Nevertheless, for most uncrosslinked glassy polyimide membranes, a tradeoff between gas selectivity and permeability is commonly observed and is typically attributed to the plasticization of the polymer matrix by the absorption of excess CO_2 at high operating pressures. In order to circumvent this problem, chemical crosslinking of the polyimide side chains can be used to retain the membrane selectivity at high operating pressures.[18]

Polyethylene oxide is another attractive material for CO_2 separation from gas mixtures containing CH_4 or H_2. In the process of separating a CO_2/H_2 gas mixture, a high CO_2 permeability through dense PEO polymers was observed.[13] In practice, high crystallinity in linear PEO not only deteriorated the membrane strength but also severely hindered the CO_2 separation efficiency. Amorphous PEO phases existing in a copolymer form (such as with polyamide or polyurethane) have exhibited improved efficiency in CO_2 separation.[13] Recently, a new amorphous and crosslinked PEO membrane synthesized by crosslinking poly(ethylene glycol) acrylates containing branches with methoxy end groups exhibited good separation performance for H_2 purification by removing acidic gases such as CO_2 and H_2S from the gas mixture.[19] At high CO_2 partial pressures, these materials maintained a high CO_2 selectivity along with an increased flux. Likewise, enhanced polymer-CO_2 interactions can be realized by the incorporation of base or polar groups in polymer membranes. For example, poly(allylamine) with base amine groups, in the pure state and in blends, gave rise to high CO_2/H_2 selectivity.[20] Poly(vinylbenzyltrimethylammonium fluoride) displayed high CO_2 selectivity over other gases, and the facilitated CO_2 transport was mainly attributed to the favored interaction between CO_2 and F^-/NH_4^+ ions.[21] Polymer backbones with pendant ionic liquid moieties also showed potential in the separation of CO_2 and SO_2 from CH_4 gas mixtures.[22]

In the above CO_2 separation systems, the structure-separation relationship is well

understood. Polymer functionality that favors the interaction with CO_2 plays a vital role in achieving the facilitated transfer of CO_2. In addition, chemical crosslinking in these polymer membranes, which helps control mechanical strength, is normally required to maintain the high performance of membranes under a variety of experimental conditions. To date, scientific and technological innovation in the development of CO_2 separation membranes has still lagged behind practical requirements due to high cost in membrane fabrication and lack of a combination of good selectivity and high flux.[23]

1.1.2.2 Water purification

Facile water purification is an urgent and challenging task in the coming years for the entire world.[24] Water purification (including disinfection, decontamination, and desalination) is commonly conducted using small molecules, while the use of membrane technologies could potentially reduce the cost of producing clean water in a more sustainable manner. Water purification using polymer membranes involves removal of bacteria and macromolecules and ions by ultrafiltration, reverse osmosis, and nanofiltration.

For ultrafiltration, polymer membranes with pore sizes typically in the range of 5 to 500 nm have been commercialized, including track etched membranes (e.g. porous polycarbonate, Nuclepore[25]), phase inversion membranes (e.g. polysulfone, Udell[26]), and expanded-film membranes (e.g. microporous polypropylene, Celgard [27] and polytetrafluoroethylene, Gore-Tex[28]). Track etched membranes typically have a well-defined pore size and size distribution but a relatively low porosity resulting in a low flux; additionally, large scale production of such membranes is impractical. Based on the balance between membrane cost and performance, phase-inversion porous membranes with a combination of macropores and nanopores have been developed. These membranes are typically manufactured by introducing a poor solvent into a homogeneous polymer solution, where the polymer can be poly(vinylidene fluoride) [29] polyacrylonitrile [30] poly(ether sulfone), [31] chitosan, [32] and polypropylene. [33] Recently, porous poly(vinylidene fluoride-co-hexafluoropropylene)

membranes have also been prepared using a supercritical fluid-phase separation process where CO_2 acts as the nonsolvent.[34] Surface-modified polysulfones[35] have been mostly applied in water purification plants. These materials display desirable performance for aqueous separation including high flux, good selectivity, and mechanical robustness. Despite their broad applications, these membranes possess some deficiencies such as relatively large pore size distributions and poor control on functionality of pore walls, and thus an opportunity for further improvements exists. Tailored functionality of these size-selective UF membranes for selective removal of toxic ions was implemented by incorporating a chelating polymer such as polyethyleneimine in the cellulose acetate membrane.[36]

Desalination by reverse osmosis is also important, since the production of fresh water from sea water at low cost could be a potential solution to the shortage of drinking water.[37] Reverse osmosis by composite membranes is a process to remove hydrated salt ions and larger solutes from water, irrespective of their charge and size. Reverse osmosis membranes for water desalination, such as aromatic polyamides,[38] polyamide/polysulfone composites,[39] and widely utilized cellulose acetate membranes,[40] are fabricated either by a similar phase inversion process but forming a thin dense polymer layer on the membrane surface or by interfacial polymerization over a macroporous substrate.[41] Currently, diverse RO membranes are commercially available from, for example, GE[42] and Dow.[43] Future developments of RO membranes for water desalination is challenging due to the low cost and good efficiency of cellulose membranes. In standard RO processes, salt ions are rejected by the membrane surface while water preferably permeates. Eventually the salts aggregate on the membrane surface and hinder effective and continuous operations. High pressure or electric field gradients are typically required to drive the water to diffuse through the RO membranes. It was posited that implementation of an active transport processes would lead to sustainable and efficient water purification, where the concentrated salt solution was removed from the feed.[1]

Nanofiltration (NF) membranes are similar to RO membranes, but the polymer active layer is microporous (0.5 to 1 nm diameter voids). NF membranes could be efficient in water purification by screening large molecules and even salt ions simultaneously.[44] NF membranes are mainly fabricated by the phase inversion process with subtle control of pore size on the skin surface, and membrane materials are mostly similar to those polymers in the RO membranes. Other synthetic methods have been less developed due to the difficulty in achieving controlled sub-nanometer pores in the skin layer of NF membranes. In 2007, a new type of microporous polymer capable of efficient water desalination was introduced.[45] This material, based on a crosslinked continuous phase templated by self-assembled surfactants, had an effective pore size of 0.75 nm and showed high salt rejection, with water permeability similar to that of some commercial membranes. Besides applications in water purification, NF membranes have demonstrated attractive utility like removal of macromolecular catalysts in organic synthesis.[46]

Overall, no matter what type of polymer-mediated separation is involved, high selectivity and permeability, and high resistance to fouling and chemical degradation are indispensable.

1.1.2.3 Direct methanol fuel cells

Fuel cells are promising alternative energy delivery devices capable of highly efficient chemical energy conversions for a range of practical applications spanning portable electronic to automotive technologies.[47] A key component that defines the fuel cell operation is the proton conducting membrane (PCM). The main function of PCMs is to separate the anodic and cathodic reaction chambers by preventing reactant crossover while allowing proton transfer.[48] Examples of PCMs include acidic inorganic salts and polymer electrolytes, with the polymer electrolyte membranes (PEMs) being more attractive than their inorganic counterparts due to lower cost, high performance, and tunable mechanical strength.

One specific example of fuel cells is the direct methanol fuel cell (DMFC).[49] The DMFC has received increasing attention due to their high power densities, sustainable nature,[50] and

convenient fuel storage.[51] The energy density of methanol is an order of magnitude high than hydrogen, which makes the DMFCs ideal for applications in mobiles phones and laptops. The biggest interest in using DMFCs is for automobile applications, because potentially doubled fuel efficiency can be achieved compared with current combustion engines. For this application, the U.S. Department of Energy has currently established a guideline of 120 °C and 50% relative humidity as operating conditions with conductivity of 0.10 S cm^{-1}, but current PEMs have not achieved this goal.[52] In order to accommodate broad applications, there are many challenges in DMFC operations to overcome, such as cell component stability, catalyst efficiency,[53] methanol crossover, poor methanol oxidation kinetics, and PEM efficiency and stability.[49]

PEMs are typically comprised of hydrophobic polymer backbones, such as polystyrene, PTFE, and poly(arylether ketone), and ion conducting groups (e.g., sulfonic acid), and upon hydration in aqueous methanol solutions continuous hydrated ionic channels regulate the proton transport.[54] As for proton transport, the sulfonic acid groups dissociate in water and thus generate protons as charge carriers into the membrane, while the remaining hydrated SO^{3-} groups provide media for protons and water molecules move. Generally, two mechanisms have been proposed for the proton transport: protons hop from one hydrated sulfonic acid group to another across the membrane, and electro-osmotic drag, where hydrated protons ($H^+(H_2O)_x$) drag one or more water molecules across the membrane.[55]

Useful PEMs should satisfy general criteria including high proton conductivity, good oxidative and thermal stability, high mechanical strength, and low fabrication cost. As for the oxidative stability, experimental results suggested fluorinated materials possess highest thermal and oxidative stability.[56] Nafion, a perfluorinated ionomer membrane introduced by DuPont, has been regarded as the benchmark material for fuel cell applications, because of its high proton conductivity and excellent chemical, oxidative and mechanical stability.[57] The proton conductivity of Nafion is dictated by the internal ion structure. Thus, work has sought

to determine the relationship between the Nafion's structure and its high conductivity. The well-known cluster model indicates the ion clusters less than 5 nm are in a matrix connected by narrow channels (1 nm in diameter) in the fully hydrated state.[58]

In addition to Nafion, polystyrene sulfonic acid (PSSA) was the first explored PEM material, but the low oxidative stability of hydrocarbon membranes hindered any practical interest. Nevertheless, the oxidative stability of PSSA membranes could be greatly improved in corresponding fluorinated forms.[59] In a recent example, Zhou *et al.* introduced the production of PEMs from miscible liquid precursors of end-capped PFPE and protected styrenesulfonate ester by UV crosslinking. Following fluorination reactions using 1 % F_2 in N_2, these partially fluorinated PEMs exhibited improved oxidative stability and better proton conductivity compared with their hydrocarbon precursors and Nafion. These crosslinked PFPE/PSSA membranes having high ion content displayed better fuel cell performance than Nafion 117 under mild operation conditions (e.g. 50 °C and 75 % relative humidity (RH)). In particular, micron-sized features were molded on the surfaces of these PEMs by using imprint lithographic techniques to increase the catalyst-PEM interface and thus promote the power output.[60]

To date, the state-of-the-art Nafion has been restricted to DMFC at low operating temperatures, due to some severe disadvantages, such as dehydration at temperatures higher than 100 °C and permeation of methanol through the membrane materials used, known as methanol crossover. High methanol crossover would cause serious potential loss at the cathode and limit power output efficiency.[61] Because of this concern, instead of using pure methanol as the fuel, aqueous methanol solutions (e.g. 2 M) have been commonly utilized to reduce the methanol crossover, but the potential power output is reduced. In order to circumvent this problem, new PEMs such as sulfonated polyimides, polyphosphazenes, and poly(arylene ether)s have been developed. They demonstrated comparable proton conductivity to Nafion and good thermal stability, but reduced methanol crossover. Notably,

sulfonated polyimides exhibit narrow ionic channels (~ 1 nm) upon hydration similar to Nafion, but swell less in methanol due to the rigid backbone.[62] Furthermore, crosslinking in the above PEMs could lead to improved thermal and mechanical stabilities as well as reduce methanol crossover without sacrificing the proton conductivity.[63] Additionally, research on composite PEMs, where particles of suitable fillers are dispersed in the ionomer matrix like Nafion, have been developed to improve the mechanical properties, promote thermal stability, and overcome methanol leakage while retaining high proton conductivity.[64]

At high temperatures or low humidities, most PEMs tend to dehydrate, which leads to elimination of continuous hydrated channels and reduction of proton conductivity. Generally, water in hydrated sulfonated polymers can be in either free or in bonded form, where free water significantly contributes to proton transport at low temperatures, but also methanol diffusion. Water in PEMs bonded with sulfonic groups could benefit the proton conductivity at high temperatures above 80 °C.[65]

1.1.2.4 Pervaporation

Pervaporation membranes have been widely applied in the processes of dehydration of organic solvents, removal of organic impurities from aqueous solutions, and organic liquid separations. In these processes, a membrane acts as a selective barrier between the liquid phase feed and the vapor phase, which is typically under mild vacuum. The permeate diffuses through the membrane and evaporates into the vapor phase. Separation of compounds depends on the difference in transport rate of different molecules through the membrane.

For liquid-liquid separations, simple theoretical comparisons favor the pervaporation process as pervaporation offers a separation factor[a] above 100, while single plate distillation can only achieve a factor of 2. Qualitatively, pervaporation selectivity can be predicted from the solubility parameters of polymers and solvents, which are typically comprised of three

[a] A measure of the ability of the system to separate two solutes: the distribution ratio in the isolated solution divided by that in the feed.

components: hydrogen bonding, polar interaction, and dispersion interaction. When the combined solubility parameters of two components are quite different, separation of them by pervaporation will be easy to achieve. For instance, water has strong hydrogen bonding, so dehydration of organic solvents is relatively easy to accomplish, while separation of organic species with subtle difference in solubility parameters is quite challenging.[66]

The application of polymer membranes in solvent dehydration has been widely examined.[67] Removal of water from alcohol has been the most explored area. Distillation of ethanol from aqueous ethanol gives an azeotrope containing approximately 4 wt % water, but membrane technology is promising to produce dehydrated alcohols with less than 1 wt % water. For this purpose, polymers such as polyimides,[68] poly(vinyl alcohol),[69] chitosan,[70] and PEMs like Nafion[71] have been investigated and exhibited great potential in alcohol dehydration. Noticeably, proper crosslinking of these membranes is required to avoid plasticization of these membranes and provide proper mechanical strength.

Removal of organic species from water is a long-standing topic for environmental protection, and adsorption technologies play a key role in this area. Membrane separations, as environmentally benign and continuous processes, can potentially compete with conventional adsorption technologies. For example, poly(dimethylsiloxane) (PDMS) has been reported as a good candidate for removing volatile organic residues from aqueous solutions.[72] Recently, Uragami reviewed the progress in refining bio-ethanol using PDMS-containing membranes, where continuous and economic extraction of ethanol from bio-based feedstock could be realized.[73]

In the area of separating organic mixtures, current pervaporation designs have not yet met the requirements for commercial applications. Much work has been performed to identify a polymer possessing different interactions with organic molecules. Tanihara and coworkers reported the separation of aromatics from alkanes/aromatics mixtures using polyimide-containing membranes by pervaporation.[74] A binary polymer blend was prepared

that achieved a good combination of permeation flux and separation factor in separating organic species.[75] In order to differentiate the mobility of organic species in polymer membranes, ionic additives blended into the membrane have shown promise, particular for promoting selective transport of alkenes. Koval *et al.* prepared perfluorosulfonate/Ag^+ (styrene-philic) membranes for the separation of styrene from a styrene/ethylbenzene mixture.[76] In a recent review of membrane pervaporation, the authors suggested that crosslinked glassy polymers and composite membranes containing inorganic species are the most promising candidates for achieving successful separation of organic mixtures.[66]

Other novel separation systems are receiving growing attention. For example, separation of chiral species using polymer membranes may be useful in advanced applications in biological systems. Chiral polymer membranes, prepared by depinanylsilylation of poly(diphenylacetylene) having only one-handed helical conformation, exhibited good efficiency in the separation of (*R*)-butanol from (*S*)-butanol, where the enantio-selectivity of the membranes resulted from the main chain chirality.[77]

1.1.3 Outlook

Membrane technologies have shown tremendous success in the last several decades, and primary structure (polymer functionality) and secondary structure (polymer architecture) of diverse membranes have been tailored to realize selective separations. To improve the efficiency in aforementioned separations, new chemistries and material designs must be explored. For example, in gas separations, high mechanical strength and thermal stability of such membranes are of critical importance to sustain high operating pressures while maintaining high flux and selectivity. In this regard, crosslinked polymers and polymer blends have been proposed to meet these requirements.[78] For DMFCs, seeking new PEMs that outperform Nafion is urgent. Using binary PEM blends or chemical crosslinking, it can be challenging to achieve well-controlled ionic morphologies, low methanol crossover, and

minimal membrane dehydration. Instead, copolymer PEMs have been introduced as a promising approach, and will be discussed in a later section.

Designing new high-performance membranes viable for complex applications such as catalysis or multiple-step separations is attracting increasing attention. Stimuli responsive membranes, which combine liquid and polymer separations, have gained unique applications in the medical arena, where mass transfer could be tuned by additional factors. Multifunctional responsive gel membranes present a new and promising platform for the development of membranes for bio-separation, biosensors, and controlled drug release. Among synthetic polymers, temperature, pH, and solvent stimulus systems will attract more interest in the future.[79]

In the following section, in order to better understand the membrane-mediated separations, fundamental relationships describing the function and basic principles of membrane separations will be briefly discussed.

1.2 Theory of membrane separations

Mass diffusion through polymers membranes is well understood. Based on the architecture of the barrier phase, separation membranes can be mainly divided into two categories: porous membranes and homogeneous dense membranes. The main function of polymer membranes is to control the rate of permeation of different species, based on the membrane chemistry and structures. Nonetheless, there is no uniform theory applicable to all separation processes. Generally, description of the transport processes fall into two models as shown in Figure 1.2: the solution-diffusion model, where a substance transfers through a membrane normally via a concentration gradient, and the pore-flow model where permeates are transfered by pressure-driven convective flow and separation occurs due to size exclusion of permeates.

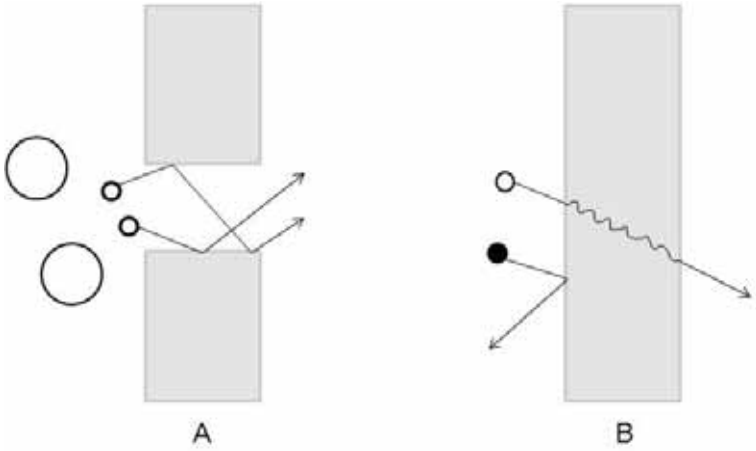

Figure 1.2. Molecular transport through polymer membranes: porous membranes by molecular filtration (A) and dense solution-diffusion membranes by differences in the solubility and mobility of permeates in the membrane (B).

1.2.1 Solution-diffusion membranes[80]

The solution-diffusion model can be applied to a variety of membrane separation processes such as reverse osmosis, pervaporation and gas permeation. Reverse osmosis uses a large pressure difference across the membrane to separate water from salt solutions. In pervaporation, the pressure difference across the membrane is small, and the process is driven by the vapor pressure difference between the feed liquid and the low partial pressure of the permeate vapor. Gas permeation involves transport of gases down a pressure or concentration gradient. Similarly, individual permeating molecules in the membrane move by the same random process of molecular diffusion no matter which process is involved.

There are no permanent porous channels in non-porous membranes. However, due to fluctuation of polymer chains, temporary created voids facilitate the mass transfer. From a molecular viewpoint, the rate-controlling process in diffusion is the creation of gaps in the polymer matrix large enough to accommodate diffusing molecules by thermally-driven fluctuation.[81] Simple permeation through nonporous membranes can be described by Fick's law,[b] although in reality, mass transport through a polymer medium can be complicated as it

[b] Fick's first law relates the diffusive flux to the concentration gradient.

involves many factors such as chemical interaction, hydrogen bonding, and electric fields, which will not be included in below discussion.

In the solution-diffusion model, the flux of a substance cross a membrane, J_i (g cm^{-2} s), can be described by a gradient in its chemical potential, μ_i

$$J_i = -L_i \frac{d\mu_i}{dx} \quad \textbf{1.1}$$

L_i is a coefficient related to the gradient across the membrane and x is a position in the membrane. Simply assuming that only pressure and concentration affect the driving force, the change of chemical potential can be described as

$$d\mu_i = RTd\ln(\gamma_i n_i) + v_i dp \quad \textbf{1.2}$$

where γ_i is the activity coefficient, $\gamma_i n_i$ denotes the solvent activity, p is the pressure, and v_i is the molar volume of component i. Thus, by combining equations 1 and 2, the flux of component i can be represented by the following equation.

$$J_i = -\frac{RTL_i}{n_i}\frac{dn_i}{dx} \quad \textbf{1.3}$$

In the above derivation, one key assumption is that the gradient in chemical potential from one side of the membrane to the other is continuous. This assumption implies that the rate of diffusion through the membrane is much smaller than the rates of absorption and desorption at the membrane interface. Another key assumption indicates that the pressure within a membrane is constant and that the chemical potential gradient across the membrane is only dependent on a concentration gradient.[80] In the following section, detailed analysis of the gas diffusion process is given based on the solution-diffusion mechanism.

1.2.1.1 Gas diffusion

In gas separations, equation 3 can be written in the following form[80]

$$J_i = \frac{P_i^G}{l}(p_{io} - p_{il}) \quad \textbf{1.4}$$

Where P_i^G is the molar gas permeability, nearly a material constant, relatively independent of the composition and pressure of the feed and permeate gases. The parameters p_{io} and p_{il} are the partial pressures of component *i* in the feed gas and permeate side, respectively. The flux strongly depends on the membrane thickness (*l*), so reduction in membrane thickness is the most straightforward and effective approach to increase gas flux. In practice, asymmetric composite membranes having a thin active polymer layer are mostly utilized.

One key issue in gas separations is the intrinsic relationship between the gas selectivity and the chemical structure of the membrane. Based on the solution-diffusion model, gas selectivity is a key factor for measuring membrane performance. The permeability (*P*) is the product of the solubility of gas in the membranes (*S*) and the gas diffusion coefficient (*D*), and thereby the selectivity of a polymer membrane for gas A to gas B can be written as

$$\alpha_{A/B} = \frac{P_A}{P_B} = \frac{S_A D_A}{S_B D_B} \qquad \textbf{1.5}$$

In 1991, Robeson[82] systematically studied the relationship between gas permeability and selectivity through rubbery and glassy polymers in many binary gas mixtures, which indicated that the empirical upper bound relation of gas permeability and selectivity is, in fact, universal. Specifically, the well-known tradeoff relationship between permeability and selectivity has been recognized in all size-selective separations (selective for small gas molecules like H_2): polymers that are more permeable are generally less selective and vice versa (Figure 1.3). The upper bound in terms of permeability and selectivity is represented by the following equation

$$\alpha_{A/B} = \beta_{A/B} / P_A^{\lambda_{A/B}} \qquad \textbf{1.6}$$

where β and λ are constants in a specific gas separation process, and λ is related to the difference in the kinetic diameters of gas molecules.

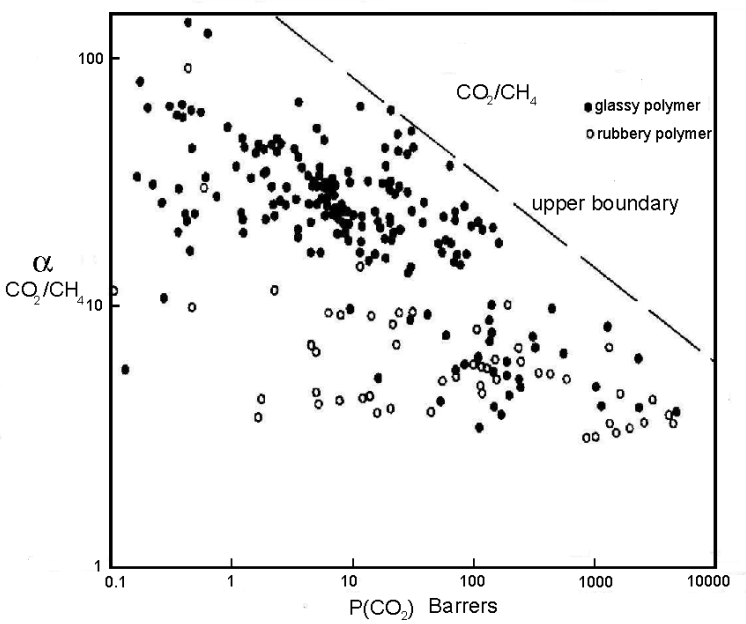

Figure 1.3. Literature data for CO_2/CH_4 separation factor versus CO_2 permeability. Reproduced with permission from Ref 82a. Copyright 1991 Elsevier.

In 1999, Freeman[83] presented detailed analysis of the above relationship based on the activation energy concept for the gas diffusion through polymers, and the two parameters used above were defined by the following equations

$$\beta_{A/B} = \frac{S_A}{S_B} S_A^{\lambda_{A/B}} \exp\left\{-\lambda_{A/B}\left(b - f(1-a)/RT\right)\right\} \quad \textbf{1.7}$$

$$\lambda_{A/B} = (d_B / d_A)^2 - 1 \quad \textbf{1.8}$$

The *d* is the diameter of the permeating molecules. For the size-selective separation (small molecule A is more permeable through the membrane than B), $\lambda_{A/B}$ is normally positive. *a* (<1) and *b* are constants independent of polymers, while *f* is related to the polymer stiffness and free volume in polymers. Based on the above equations, the effect of polymer structures on the tradeoff curve can be envisioned. The most effective pathway for development of higher performance polymer membranes for conventional size-selective gas separation is to systematically increase $\beta_{A/B}$, for example through enhancement of solubility selectivity (S_A/S_B). Simply increasing chain stiffness would cause improved selectivity but reduced flux.

Nonetheless, the above argument would be invalid when the interchain spacing becomes large enough that the polymer segmental motion no longer governs the diffusion of permeates.[84]

1.2.2 Porous membranes

Pore-flow membranes have permanent porous structures in them, where the solution-diffusion mechanism cannot be applied. For gas diffusion through a macroporous membrane, the self-diffusion of gas molecules is predominant. Hence, the diffusion coefficient (D_{CE}) can be expressed by the following equation using the kinetic theory of Chapman and Enskog[85]

$$D_{CE} = \left(\frac{4\sqrt{2}}{3\pi^{3/2}} \right) \frac{\left(k_B T\right)^{3/2}}{P\sigma^2 \tilde{m}^{1/2} \Omega} \qquad \textbf{1.9}$$

where P is the pressure, σ is the collision diameter, Ω is a dimensionless function of temperature, and $\tilde{m}$ is the molar mass of the permeate. For this type of diffusion, the kinetic theory predicts that the diffusion coefficient varies inversely with pressure but is independent of pore size.

Gas diffusion through continuous pores in a small diameter (5–50 nm) falls into the Knudsen regime,[85] where the interaction of the molecules with the pore walls plays the crucial role and the intramolecular collisions can be neglected. The number of gas molecules that pass through the pores is proportional to the pressure of the gas and inversely proportional to its molecular weight. Partial separation of a mixture of gases with different molecular weights can be realized.[86] Gas diffusion through a nanoporous membrane in the Knudsen regime predicts the diffusion coefficient D_{Kn}

$$D_{Kn} = \frac{\varepsilon}{\tau} \frac{d}{3} \left(\frac{2k_B T}{\tilde{m}} \right)^{1/2} \qquad \textbf{1.10}$$

where ε is the porosity, d is the average pore diameter, τ is the membrane tortuosity. l represents the ratio of length of the average pore compared to the membrane thickness, for

example, a cylindrical porous structure has a tortuosity equal to 1.

The selectivity of this membrane ($\alpha_{i/j}$), which is proportional to the ratio of gas permeabilities, is given by

$$\alpha_{i/j} = \sqrt{\frac{m_j}{m_i}} \qquad \textbf{1.11}$$

Additionally, liquid flow through a nanoporous membrane can be described by the Hagen-Pouiseuille relationship,[87] giving an average velocity of pure fluid v

$$v = \frac{\varepsilon}{\tau}\langle v \rangle = \frac{\varepsilon}{\tau}\frac{d^2 \Delta P}{32 \mu \ell} \qquad \textbf{1.12}$$

where ε is the porosity, τ is the membrane tortuosity, $<v>$ is the average velocity of fluid in a single pore, d is the pore size, ΔP is the pressure drop, μ is the liquid viscosity and l is the membrane thickness. Separation of macromolecular solutes or particles in liquid solutions that permeates in ultrafiltration and nanofiltration membranes takes place at the membrane surface according to either a screen filtration mechanism or a capture mechanism inside membranes.[80]

1.3 Self-assembly of diblock copolymer systems

1.3.1 Diblock copolymers in bulk

Covalently connecting two distinct homopolymer chains at one end forms a diblock copolymer. In the copolymer, incompatibility between two different polymers produces interesting phase-separated structures in bulk on the nanoscopic scale (typically 5–50 nm), which are significantly smaller than that in a binary blend of immiscible homopolymers. Furthermore, self-assembly of coil-coil (polymers with flexible backbones) diblock copolymers has been well understood on both theoretical and experimental levels. Early experimental study[88] indicated that the self-assembly of PS-PI diblock copolymers can adopt one of these morphologies: lamellae (L), bicontinuous gyroid (G), percolated lamellae (PL), hexagonally packed cylinders (C), and spheres on a body-centered cubic lattice (S),

depending on the volume fraction of one component and the molecular weight. Matsen and Bates presented the theoretical study of the principles of diblock copolymer self-assembly, and found that the equilibrium phases suggested in the PS-PI study are, in fact, universal.[89] In the phase diagram shown in Figure 1.4, N is the overall degree of polymerization, where $N = N_A + N_B$; f is the volume fraction of block A characterized by $f_A = N_A/N$; χ is the Flory-Huggins interaction parameter between PA and PB.

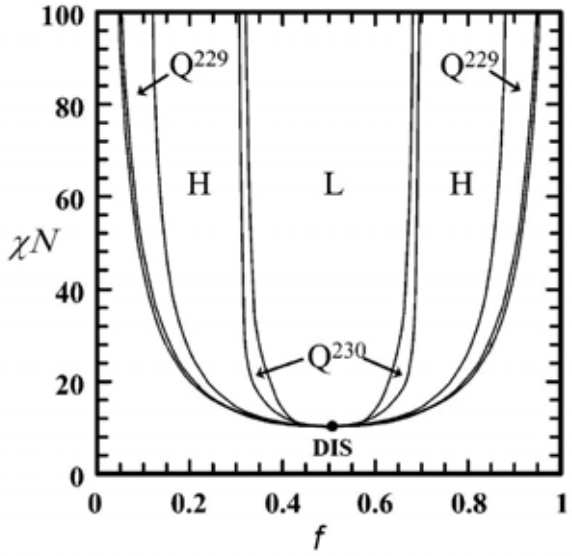

Figure 1.4. Mean-field phase diagram for a diblock copolymer in bulk. f is the volume fraction of one component. Phases are labeled as L (lamellar), H (hexagonal cylinders), Q^{230} (bicontinuous cubic), Q^{229} (bcc spheres), and Dis (disordered). Reproduced with permission from Ref 90. Copyright 2005 American Chemical Society.

According to the established theory,[91] the ensemble of chain configurations that produces the minimum overall Gibbs energy (G) represents the equilibrium state in bulk block copolymers. G is related to the enthalpy (H) and entropy (S) terms of the copolymer system. Parameter χ accounts for the enthalpic interactions between A and B segments, for example, $\chi>0$ implying A and B segments tend to separate. Consequently, both blocks stretch away from an interface at the joints of A and B blocks, to minimize the enthalpically unfavorable contacts. Meanwhile, chain stretching in both blocks results into an increase of the entropic cost. As an overall effect, as $\chi N <10$, no microscopic structures appear as the entropy

dominates to give a disordered state; as χN >10, driven by the enthalpy, four different microscopic phases are theoretically predicted, depending on the volume fraction of each block. For example, a volume fraction f of 0.5, the two blocks stretch about the same distance, resulting in flat interfaces or a lamellar morphology; f = 0.7, the longer block chains reside on the convex side of the block copolymer interface, so a cylindrical morphology resulted.

1.3.2 A-B diblock copolymer with additives

Many researchers have also paid attention to the morphology in blends comprised of a block copolymer (PA-PB) and homopolymers (PA and PB).[92] In the phase diagram presented by Bates and Fredrickson,[93] an isopleth represents a blend composition where the volume fractions of two homopolymer components are equal. Phase behavior at this specific composition demonstrates that upon addition of two homopolymers (PA and PB), the nanoscopic domains of the PA-PB copolymer (e.g. in a lamellar morphology) can be swelled by the chemically identical homopolymers to certain extent. When the enthalpically favored demixing of two homopolymers overcomes the stabilization effect of copolymers at the interfaces, macrophase separated phases (L_A and L_B) occurs. In this particular system, the unique phenomenon is the appearance of a new thermodynamically stable phase, namely a bicontinuous microemulsion, in which each of two distinct phases is interconnected, similar to the gyroid morphology, but lack high order symmetries. A representative phase map of such a tertiary blend is shown below (Figure 1.5b).

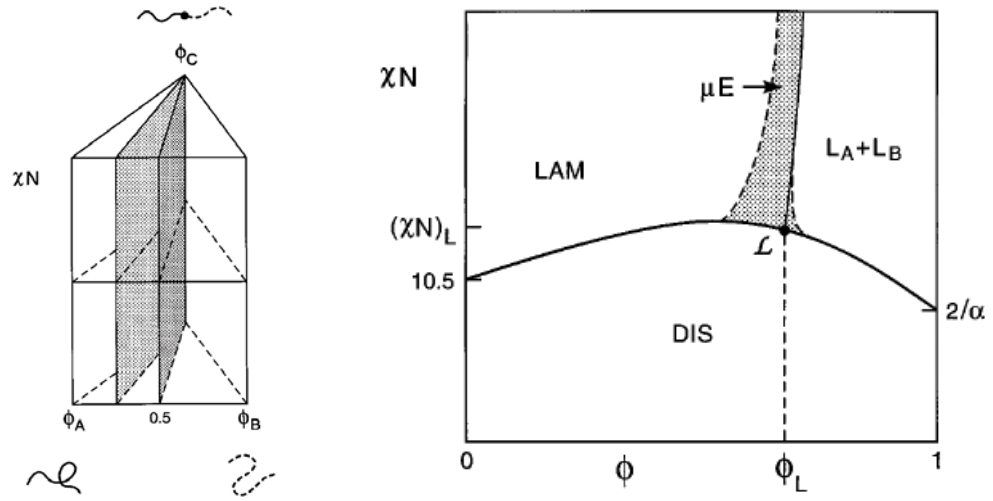

(a) (b)

Figure 1.5. The phase prism for a ternary blend comprised of PA-PB and PA, PB homopolymers (a) and the phase map of the isopleth plan where Φ_A and Φ_B are equal (b). Φ_A, Φ_B and Φ_C are the volume fractions of PA, PB, and the copolymer PA-PB, respectively. The y-axis of the right figure is the segregation strength χN. Phase boundaries from experiments and theoretical calculation are indicated by the solid curve and dotted curves, respectively. μE denotes the bicontinuous microemulsion and L denotes the Lifshitz point in theory. Reproduced with permission from Ref 93. Copyright 1997 Wiley-VCH Verlag GmbH & Co. KGaA.

In addition to copolymers blended with homopolymers, solvent additives in diblock copolymers can bring about interesting morphological transitions as well. Lodge[94] and Register[95] and their coworkers carried out detailed experimental studies on the phase behavior and morphological transitions of block copolymers with either selective or neutral solvents. By introducing an additional solvent component into a polymer blend, the phase diagram will be expanded into 3 dimensions (Figure 1.6). Three sets of phase diagram could be extracted by varying one pair of variables, such as a phase map of ϕ vs T at fixed f. Therefore, for the same copolymer, morphological transitions can be tuned by the selectivity or the composite of the solvent.

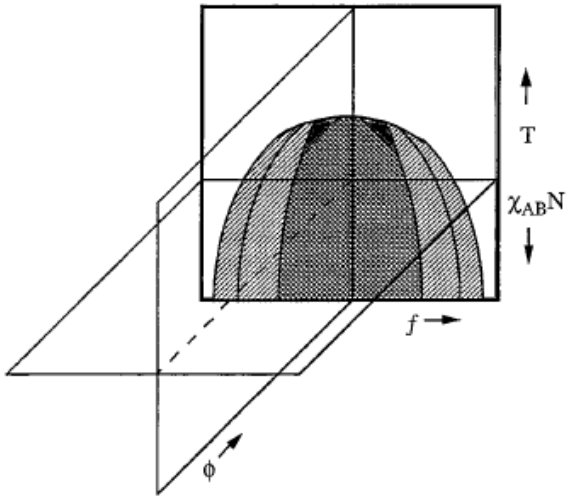

Figure 1.6. Schematic illustration of the phase cube of a block copolymer solution, as a function of temperature, T, copolymer composition, f, and copolymer concentration, ϕ. The shaded plane corresponds to the bulk phase map of diblock copolymers. Reproduced with permission from Ref 94. Copyright 2002 American Chemical Society.

Two circumstances could be expected by adding a solvent to a melt copolymer, where the solvent can be either selective or neutral for the copolymer. The neutral solvent has no preference in partitioning into two blocks, so the effective χ between the two blocks is reduced, which can yield swelled morphologies but decreased temperatures of order-disorder and order-order transitions. Self-assembly of a copolymer with a selective solvent is more intriguing, since the solvent selectively dissolves into one block. For a block copolymer and a selective solvent at a fixed temperature, by varying the solvent composition, one block can be swelled from the minor phase to the major phase so as to access different morphologies; at low temperatures and lower copolymer contents, micelle structures could be detected. For a specific copolymer with fixed solvent composition, by varying the temperature, similar to the order-disorder transition in copolymer melts, the solvent becomes less selective as temperature increases, and leads to curved phase boundaries and various thermally accessible order-order morphological transitions.

1.4 Membrane applications of block copolymers

In the last 20 years, theoretical developments in block copolymer self-assembly have been more complete. These advances are closely linked with the developments of new synthetic tools for copolymer synthesis, allowing for precise arrangement of multiple monomers into desired architectures. Anionic polymerization is one such method, and it provides a controlled synthetic route for various active alkenes.[96] Anionic polymerization combined with end group modification allows for the synthesis and study of diverse copolymer architectures. Furthermore, emerging new synthetic techniques such as atom transfer radical polymerization (ATRP),[97] reversible addition chain fragmentation transfer (RAFT) polymerization,[98] nitroxide-mediated polymerization (NMP),[99] ring opening polymerization (ROP),[100] and ring opening metathesis polymerization (ROMP),[101] offer reliable living techniques for polymer chemists to design new copolymer structures with novel functionality, and meet broad challenges in the utility of block copolymers. Block copolymers have found growing industrial applications, such as macromolecular surfactants,[102] nanostructure templates,[103] and toughened plastics,[104] and there have been several books reviewing the developments in block copolymer science and technology.[105] In the following sections, nanoporous membranes and PEMs produced derived from block copolymers will be discussed in detail.

1.4.1 Nanoporous membranes templated from block copolymers[c]

In the last decades, researchers have paid much attention to block copolymers particularly as attractive template precursors, for creating nanoporous materials with well-defined structures by simply removing one of the blocks.[106] For example, polylactide (PLA) is a particularly attractive sacrificial block due to the straightforward synthesis of various PLA-containing block copolymers and the susceptibility of PLA to hydrolytic degradation

[c] This section is adapted in part with permission from Olson, D. A.; Chen, L.; Hillmyer, M. A. *Chem. Mater.***2008**, *20*, 869–890. Copyright 2008 American Chemical Society.

under relatively mild conditions. Nanoporous polystyrene (PS) monoliths can be prepared from various self-assembled PLA-containing block copolymers.[107,108] Another interesting system is a PS-*b*-poly(methylmethacrylate) (PS-PMMA) block copolymer, as PMMA can be selectively removed by UV etching. These materials have been widely studied by the Russell and Hawker groups in the last decade,[109] and the main utility exists in nanolithographic applications for the microelectronics industry.[110] In addition to the utility of nanoporous polymers for templating other nanostructures,[111] applications of such materials as separation membranes[112] and antireflection coatings[113] have been reported. Herein, an overview will be presented on membrane applications of nanoporous materials from block copolymer precursors.

In 2006, Uehara *et al.*[114] reported the preparation of semicrystalline nanoporous polyethylene (PE) films from polyethylene-*b*-polystyrene (PE-PS) precursors. The resulting films showed significant mechanical strength. Self-assembly of the PE-PS was governed by not only the melt-phase thermodynamics but also the crystallization-induced segregation. The results revealed that the isothermal crystallization temperature was crucial (preferably at 90 °C for 3 d) for the formation of a bicontinuous morphology from an annealed blend cooled from 150 °C. The amorphous PS domains were subsequently etched with fuming nitric acid for 30 min. The resulting bicontinuous nanoporous PE membrane had a surface area of 17 $m^2\ g^{-1}$ by BET analysis and excellent mechanical strength. More importantly, the gas permeation rate of this membrane was 1.4 times that of a commercially available porous polyolefin membrane. This is breakthrough work that demonstrated the production of a highly flexible nanoporous material from copolymers, which could find utility in a variety of membrane applications.

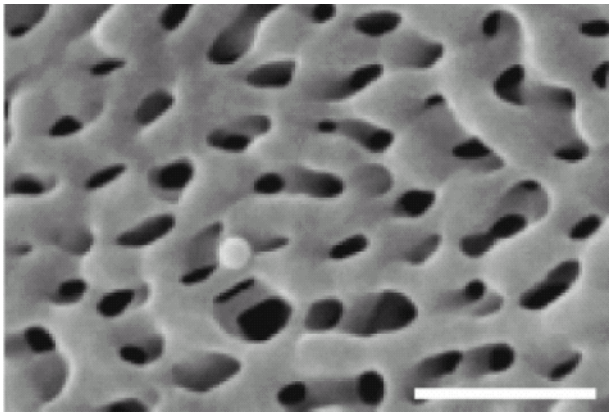

Figure 1.7. SEM of the nanoporous PE membrane produced from PS-PE. The scale bar is 200 nm. Reproduced with permission from Ref 114. Copyright 2006 American Chemical Society.

In a recent paper,[115] Uehara and coworkers prepared several nanoporous PE membranes from the same PE-*b*-PS copolymer with the pore size tuned in the ranging of 5 to 30 nm by varying the etching time of PS. In fact, the porosity in these membranes was strongly dependent on the etching time: either a long or a short etching time caused low porosity. Subsequently, all of these resultant nanoporous membranes were permeable to glucose but retained albumin permeation based on molecular size. The authors claimed that the size selective molecular separation of these robust nanoporous PE membranes could be useful in implanted glucose sensors.

Yang *et al.* prepared a blend of a PS-PMMA block copolymer and a PMMA homopolymer and then deposited it on a silicon wafer that had been treated with a random PS-PMMA copolymer.[112a] Perpendicular orientation of the cylindrical microdomains was observed in a thin film that was about 80 nm thick. This film was removed from the underlying silicon substrate using HF, deposited over a macroporous polysulfone membrane, and the PMMA homopolymer was then removed by acetic acid to generate nanopores about 15 nm in diameter. This supported membrane assembly was then evaluated in the filtration of viruses from an aqueous dispersion. The authors compared the separation efficiency of the block copolymer derived membrane with a commercially available track etch polycarbonate

membrane with similar pore size. Both separation membranes were extremely effective at removing human rhinovirus, but more importantly, the flux through the block copolymer membrane was more than 100 times higher than the polycarbonate membrane. The increase in flux was attributed to a combination of smaller film thickness and larger pore fraction in the block-copolymer derived membrane.

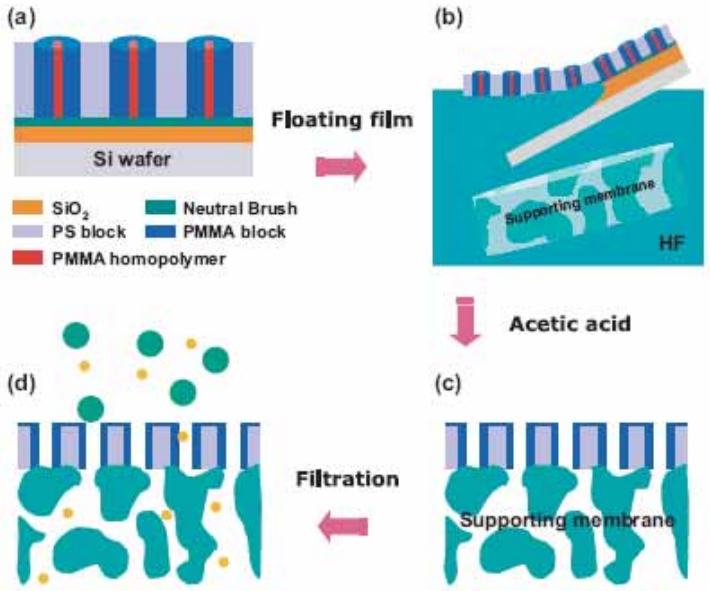

Figure 1.8. Schematic illustration of fabricating asymmetric nanoporous membranes from a PS-PMMA copolymer. Reproduced with permission from Ref 112a. Copyright 2006 Wiley-VCH Verlag GmbH & Co. KGaA.

The above PS-PMMA membrane was only mechanically stable at low operating pressures (0.2 MPa) without forming large porous cracks and suffered from low resistance to organic solvents as well. In a subsequent paper, Yang *et al.* reported thicker nanoporous PS (PS layer was 160 nm) composite membranes following a similar protocol. The PS-PMMA was spin coated from a 4 wt % toluene solution and annealed at 170 °C to form a cylindrical morphology. The vertical orientation of cylindrical nanopores was observed on the top and bottom surfaces while the middle part of the membrane exhibited a mixed orientation of cylindrical nanopores. The cylindrical PMMA microdomains were removed by UV irradiation followed by rinsing with acetic acid, and the nanoporous PS membrane was then

deposited on a supporting porous substrate. Up to 2 bar pressure was applied to this supported membrane, and high water selectivity and flux were maintained. The authors argued that the disordered internal structure of the membrane gave rise to better mechanical stability. Additionally, the UV irradiation promoted adhesion between the polymer layer and the substrate, and increased the solvent-resistance of the membrane, due to slight crosslinking of PS. This membrane could be used under harsh filtration conditions such as in strong acid (or base) solutions.[116]

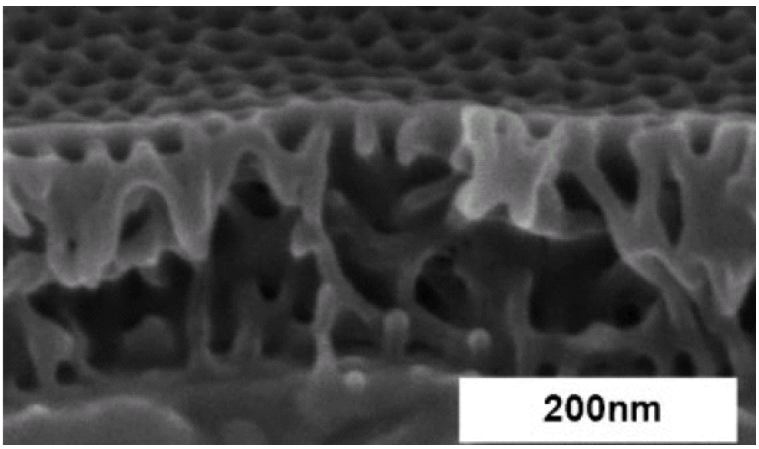

Figure 1.9. Cross-sectional SEM image of the nanoporous film prepared from PS-*b*-PMMA. Reproduced with permission from Ref 116. Copyright 2008 Wiley-VCH Verlag GmbH & Co. KGaA.

In 2006, two other papers describing gas and liquid transport through nanoporous plastics templated from block copolymers appeared. Cooney *et al.*[117] used a liquid diffusion cell to measure the diffusion coefficient for an aqueous NaOH solution through a 2 mm piece of a nanoporous membrane prepared from a PS-PLA block copolymer. Diffusion coefficients for NaOH were determined using either the measured breakthrough time, or the steady-state diffusivity based on the flux of hydroxide ions through the membrane. Poor wetting of the membrane and imperfections in the pore structure in pure aqueous solutions were attributed to the inconsistency between the two diffusion measurements.

Using nanoporous monoliths produced from a self-assembled PS-poly(dimethyl

acrylamide) (PDMA)-PLA triblock terpolymer by etching the PLA component, Phillip *et al.*[112b] performed complementary transport measurements in both gas and liquid cells. Based on the gas diffusion experiments for He, Ar, N_2, and O_2, the permeability and the diffusion coefficient (accounting for the void fraction of the membrane and the tortuosity) were calculated. The experimental diffusion coefficients for the four gases through these membranes were in quantitative agreement with predicted values based on a Knudsen diffusion mechanism. In addition, liquid water flow through the same membranes gave fluxes consistent with pores of about 13 nm in diameter. The results of this study verified the promising potential of copolymer membranes in ultrafiltration applications. In addition, the authors included a comparative analysis of idealized block copolymer based membranes and commercially available membranes for the separation of bovine serum albumin. Block copolymer membranes could simultaneously exhibit dramatically enhanced hydraulic permeabilities and selectivities.

In addition to aforementioned strategies in producing nanoporous membranes selectively etched under UV or base solution conditions, mild and facile fabrication processes are preferred to reduce the fabrication cost and improve the efficiency of membrane production. In 2007, Peinemann *et al.*[118] reported the formation of a nanoporous structure from a solution-cast PS-P4VP copolymer film in DMF (as a good solvent), which was subjected to a H_2O (as a non-solvent) to induce phase inversion before reaching the dry state. At the initial stage after casting the film onto the substrate, the block copolymer solution is homogeneous. Then evaporation of DMF led to the cylindrical domains on the surface layer. After dipping this still highly swollen film into water, the water first exchanged with DMF in the cylindrical domains of swollen P4VP block. Meanwhile, DMF diffused out of the swollen polystyrene domains and induced the PS to precipitate. Underneath the highly ordered layer, water in contact with the remaining copolymer/DMF solution led to the precipitation of the PS with swollen P4VP into a sponge-like structure. Removal of water from the P4VP

domains of this membrane yielded a nanoporous structure.

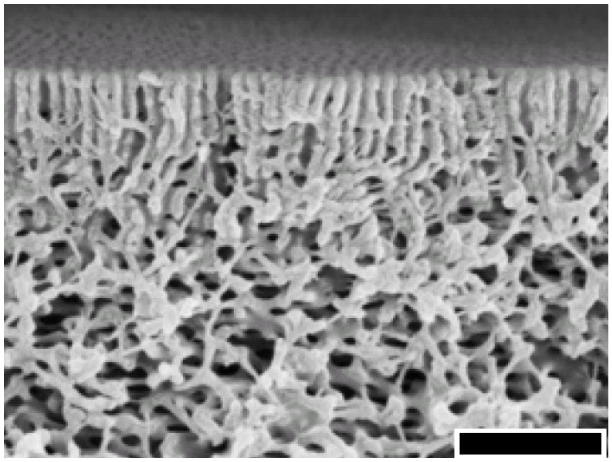

Figure 1.10. SEM image of the cross section of the nanoporous PS-*b*-P4VP film. The scale bar is 500 nm. Reproduced with permission from Ref 118. Copyright 2007 Macmillan Publisher.

A water flux of 20 L m^{-2} h^{-1} through this membrane (~ 80 μm thick) was determined at a 0.5 bar pressure. This example nicely presents a new route combining the phase inversion concept with copolymers, to produce copolymer membranes relying on thermodynamic structure, and achieves well-controlled continuous nanostructures in membranes that have the potential for size-selective separations. This process readily achieved sufficient long-range order without compromising the scale-up synthesis in practical membrane fabrication.

1.4.2 Polymer electrolyte membranes from copolymers

Understanding the relationship between the ionomer architecture on the resultant proton conductivity is critically important for guiding future membrane innovations. During the last several years, PEMs from block copolymers have received growing interest, where the mechanical strength, ionomer morphology, and water uptake could be exquisitely controlled. Sulfonated PS in diverse copolymer formats has been the most explored, due to its amenability to many polymerization schemes compatible in copolymer synthesis.

The first strategy of producing nanostructured copolymer PEMs involves the use of ionic

graft copolymers. Holdcroft and coworkers pioneered the strategy of chemically grafting sulfonated PS on a PS backbone.[119] In 2001, a communication[120] first demonstrated the synthesis of such a graft copolymer (Figure 1.11). Nitroxide-mediated polymerization of sodium styrenesulfonate was conducted followed by an end-capping reaction with one divinylbenzene unit. The formed macromonomer was sequentially copolymerized with styrene to yield a graft polystyrene ionomer (PS-*g*-PSSNa), where the length and density of grafted arms were finely controlled. PS-*g*-PSSNa was hot-pressed and soaked in 0.5 M H_2SO_4 for 2 d. After that, the resultant PEM (PS-*g*-PSSA) was rinsed with DI water and then dried. For comparison, randomly sulfonated polystyrene (PS-*r*-PSSA) with similar sulfonation levels was synthesized. PS-*r*-PSSA with 12 mol % PSSA showed little evidence of microphase separation in the dry state (Figure 1.12) and thus exhibited low proton conductivity. In contrast, the PS-*g*-PSSA membrane with a similar PSSA content presented compelling evidence that proton conductivity was enhanced by formation of continuous nanochannels of PSSA (5–10 nm wide) in a PS matrix by TEM (Figure 1.12). A linear relationship between log σ (σ is the proton conductivity in produced membranes) and sulfonic acid percentage was observed for the graft copolymers. Conductivities of the graft copolymers were an order of magnitude higher than that of PS-*r*-PSSA with similar ion contents. In particular, a PS-*g*-PSSA membrane with 19.1 mol % SSA containing 37 vol % water showed a conductivity of 0.24 S cm^{-1}, which is 3–5 times larger than that of Nafion 117 with similar water content. This work nicely demonstrated that PEMs with a bicontinuous morphology significantly enhanced the proton conductivity.

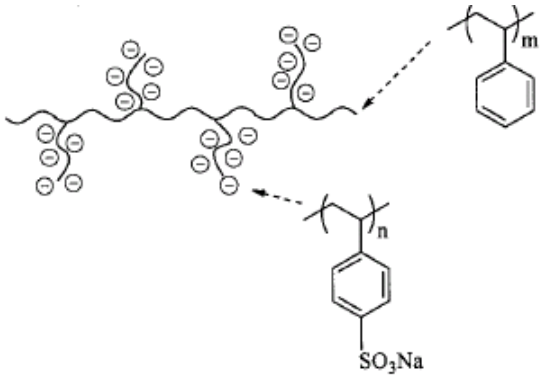

Figure 1.11. Chemical architecture of sulfonated PS grafted on a PS backbone. Reproduced with permission from Ref 121. Copyright 2002 American Chemical Society.

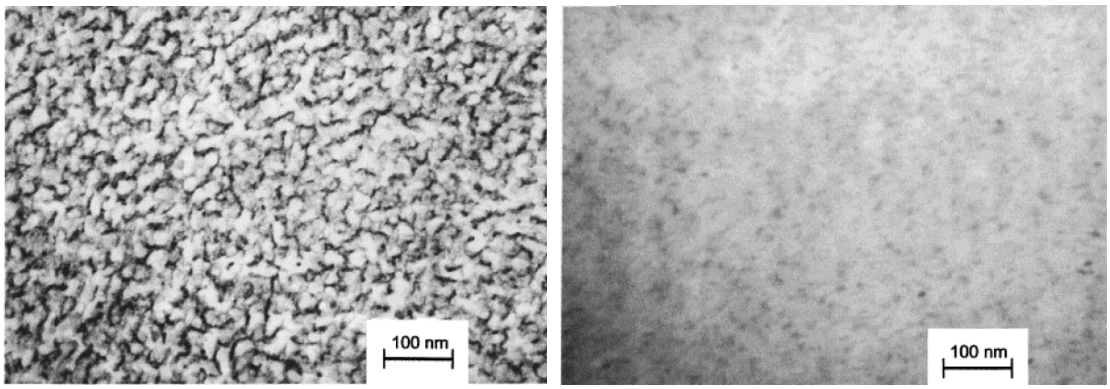

(a) (b)

Figure 1.12. TEM micrographs of a PS-*g*-PSSA graft polymer membrane possessing 19.1 mol % ion contents (a) and of a random copolymer membrane (PS-*r*-PSSA) containing 12.0 mol % ion content (b). The dark domains are PSSA stained by Pb^{2+} ions. Reproduced with permission from Ref 121. Copyright 2002 American Chemical Society.

In a subsequent paper, four different PSSNa macromonomers were utilized to generate four series of grafted copolymers (PS-*g*-PSSA) with tailored sulfonation levels.[d] Generally, using the same PSSNa macromonomer, increased ion content in the resultant PEMs by grafting more PSSNa chains resulted in higher ion conductivity and higher water uptake. At low ion contents, PEMs with shorter PSSA chains had higher proton conductivity than those with longer PSSA chains; at high ion contents, PEMs with longer PSSA chains had higher

[d] Normally known as the ion exchange content (IEC), moles of sulfonic group in 1 gram of polymer, in unit of mmol/g.

proton conductivity than those with shorter PSSA chains. Furthermore, the incremental water uptake with increased ion content was larger in the PEMs having longer grafted PSSA chains, which could be attributed to the following reasons. In the low ion content regime, ionic domains of PEMs having long PSSA side chains were more isolated (less continuous), and thus the proton conductivity was lower. In the high ion content regime, segregation of continuous ionic domains of PEMs with longer PSSA chains was enhanced to give high proton conductivity. Collectively, this work provided a fundamental understanding regarding the design of solid PEMs from graft copolymers.[122]

In 2005, Shi and Holdcroft reported the synthesis and characterization of a poly(vinylidene difluoride-hexafluoropropylene)-*b*-polysulfonatestyrene copolymer. A disruption in the ordered morphology with increasing degrees of sulfonation was indicated by TEM analysis. Membranes having 0.9–1.2 mmol g^{-1} IEC were comprised of interconnected networks of ion channels. For these membranes, the conductivity was similar to Nafion 117, and was significantly higher than PS-*r*-PSSA.[123] In 2007, the Holdcroft group[124] examined two types of copolymers possessing similar ion composition but considerably different architectures (diblock *vs* graft). A diblock copolymer PEM in the previous study was used, and poly(vinylidene difluoride-chlorotrifluoroethylene)-*g*-polystyrenesulfonate was similarly synthesized by an ATRP mechanism. By TEM analysis of the graft copolymer membrane, an interconnected network of small ionic clusters of 2–3 nm in size was revealed, while the diblock PEM possessed a perforated lamellar structure. These lamellar ionic channels were 8 to 15 nm wide parallel to the membrane surface. The diblock membrane swelled excessively at low ion contents (IEC < 1.2 mmol g^{-1}), and high conductivity resulted, but it exhibited highly anisotropic conductivity (through-plane conductivity was much lower). In contrast, the graft PEMs uptook significantly less water at similar IECs and exhibited low conductivity. At a high IEC, high conductivity comparable to that in the diblock copolymer was observed, as the increased water uptake led to continuous ionic phase in the graft copolymer. Isotropic

conductivity in the graft copolymer was obtained due to the 3-dimensional (3D) continuous morphology. The authors concluded that the morphological control (preferably an isotropic morphology) in PEMs from nanostructured copolymers was critically important.

Zhang and coworkers systematically examined a series of poly(vinylidene fluoride) (PVDF)-*g*-PSSA graft copolymers by grafting PS side chains on PVDF copolymers containing some chlorotrifluoroethylene (CTFE) units. Subsequent sulfonation reaction on PS was performed. From two parent PVDF polymers, two series of PVDF-*g*-PSSA graft copolymers with different PSSA graft densities (0.3 to 30 mol %) and arm lengths were synthesized. These graft copolymers with low graft density and long PS arms self-assembled into a microphase-separated morphology with randomly oriented ionic channels embedded in the hydrophobic semicrystalline PVDF matrix. The PEMs derived from a low molecular weight PVDF displayed poor mechanical integrity and high water uptake, while the PEMs from a high molecular weight PVDF gave lower water uptake and high resistance to swelling at high IEC values. For example, the high molecular PVDF-*g*-PSSA graft copolymers with moderately high graft density (1.4–2.4 mol %) showed a cluster-network morphology with small ionic domain size similar to that in Nafion. These materials exhibited high mechanical strength and low water uptake, which yielded notably higher proton conductivity than Nafion at 30–120 °C under high humidities.[125]

Nieh and coworkers grafted PSSA on a fluorinated polyaromatic backbone (Figure 1.13). The resultant PEMs prepared by solution casting showned high proton conductivity coupled with low dimensional swelling upon hydration. These materials exhibited a disordered lamellar morphology,[126] indicated by the TEM micrograph below. Specifically, small-angle neutron scattering (SANS) analysis on the copolymers in D_2O was conducted to resolve the morphological structure. The scattering profile was comprised of two different components: the low q (q is the scattering vector) peak was assigned to the strong interaction among the aggregated hydrophilic and hydrophobic domains, and the high q peak (small domain size)

was attributed to the hydrated PSSA phase, which was nicely fitted by the bicontinuous microemulsion model. Water uptake derived from the proposed model was consistent with the measured value.[127]

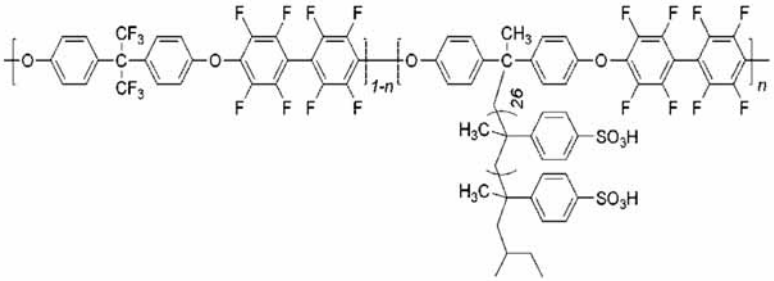

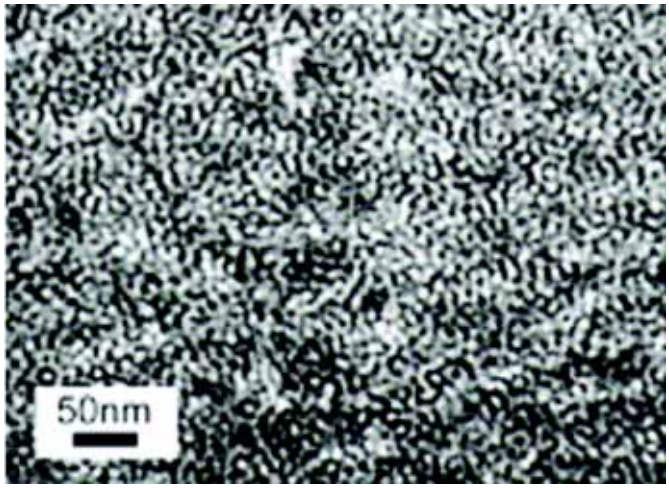

Figure 1.13. Chemical structure of the PEM material and TEM micrograph of the PEM with 32 wt % side chain content. The PSSA domains stained by Pb^{2+} ions. Reproduced with permission from Ref 127. Copyright 2008 American Chemical Society.

In 2002, Kim and coworkers investigated a triblock terpolymer, sulfonated polystyrene-*b*-poly(ethylene-butene)-*b*-polystyrene (*s*-SEBS), with different sulfonation levels. PEMs were prepared from this copolymer using solution casting. The proton conductivity and methanol permeability increased when the sulfonation level of the PS block exceeded 15 mol %. Proton conductivity and methanol permeability equivalent to that of Nafion 117 was observed for *s*-SEBS with 34 mol % sulfonation. Structurally, SAXS analysis did not provide enough morphological information other than the microphase

separation, given that no high order reflections were observed by SAXS.[128]

In addition, Elabd and coworkers studied similar triblock PEMs with a well-defined cylindrical morphology. The styrene in the PS-PIB-PS precursor polymer was post-sulfonated to achieve different sulfonation levels. Ion contents had a clear effect on the resulting morphologies of PEMs. The original morphology of these sulfonated block copolymers at high ion contents was disrupted upon hydration, resulting in a bicontinuous ionic network that substantially increased proton transport. The PEM with an IEC of 2.0 had proton conductivity 3 times higher than that of Nafion, but unfortunately it swelled extensively in water at elevated temperatures causing severe methanol crossover in fuel cell tests. Additionally, solution cast membranes were produced by using different solvents. By SAXS analysis, the casting solvent had a significant effect on the resulting conductivity by affecting the order and orientation of the sulfonated cylindrical domains. In conclusion, this example implied that production of PEMs from self-assembled triblock terpolymers demanded delicate control in the membrane preparation step.[129]

Serpico *et al.* studied sulfonated poly(ethylene-*s*-styrene) (*s*-SE) possessing short alternating units with styrene between 30 and 75 wt % and compared the proton conductivity with a triblock terpolymer, SEBS with 29 wt % PS. Sulfonation of PS was applied to the copolymers afterwards to afford 40 to 50 % conversion. For *s*-SE with the lowest styrene content, minimal proton conductivity was observed, with moderate swelling up to 140 % water uptake. The *s*-SEBS membrane similar in composition had a high conductivity due to extensive swelling to 400 % in water. The *s*-SE membranes with higher styrene content displayed a similar dependence of conductivity on humidity as Nafion. X-ray and neutron scattering studies revealed the presence of a bicontinuous network of hydrophilic and hydrophobic domains (~ 5 nm) in hydrated state, but no phase separation in the dry state. In the fully hydrated state, these materials tend to absorb up to 500 % water and exhibit proton conductivity as high as 0.1 S/cm. At low water contents, the conductivity of *s*-SE is several

orders of magnitude lower than that of Nafion, and the authors suggested that the high basicity of phenylsulfonate anions limited hydrated proton mobility. Normally, the natural microphase separation of the block copolymer affords interconnected sulfonated styrene domains and thereby good proton conductivity. For *s*-SE, water played a dual role of creating a bicontinuous network and conducting protons. The authors concluded that these materials were promising candidates for fuel cell applications at low temperatures.[130]

Park and coworkers reported the preparation of a series of model polymethylbutylene (PMB)-*b*-PS block copolymers with partially sulfonated PS, and complete morphological characterization of these PEMs was performed. The sulfonation content in six model PS-PMB copolymers was tailored, and in each of them a morphological transition was observed driven by the change in the sulfonation level.[131] Additionally, changes in humidity affected the water uptake in each PEM and consequently drove the morphological transition.[132] Those PEMs with > 40 % sulfonation of PS with a gyroid or percolated lamellar morphology exhibited the highest proton conductivities. Notably, some fully hydrated PEMs with ionic domain sizes < 5 nm exhibited increases in conductivity with increasing temperature up to 90 °C. The authors proposed that the suppression of water evaporation from the PEMs was due to the capillary condensation of the water in confined nanochannels thus reducing its chemical potential. Temperature-dependent SANS experiments confirmed significantly enhanced water retention observed in the PEMs made from the low molecular weight copolymers.[133] This example indicated a promising pathway to overcome PEM dehydration at high temperatures.

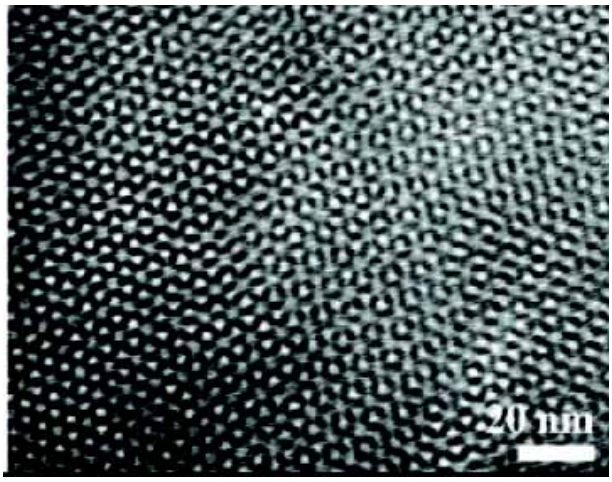

Figure 1.14. Cross-sectional TEM image of a stained PS-PMB (1.8-1.4 kg mol^{-1}) with a gyroid morphology. The PSSA domains stained by RuO_4 appear dark. Reproduced with permission from Ref 133. Copyright 2007 American Chemical Society.

1.4.3 Outlook of copolymer membranes

Self-assembled block copolymers allow precise control of morphology and domain size. They have also shown some potential to introduce multiple functionalities for advanced separations. Besides, block copolymer membranes bring new attributes to some traditional membrane applications, such as battery electrodes and separators,[134] liquid separations,[135] and gas separations.[136] In all of these applications, the morphological control of microphase-separated membranes will play a vital role in achieving selective permeability. Block copolymer membranes containing a pH or temperature-responsive block exhibited regulated selectivity and flux due to the morphological transition or hydrophilic/hydrophobic transition. Those smart membranes could find applications in aqueous separations and possessed better mechanical integrity comparing with the corresponding homopolymers.[137]

Nevertheless, the mechanical stability of most copolymer membranes is still insufficient. Therefore, crosslinking techniques can offer a facile route to circumvent this problem. The subject of improving mechanical and thermal properties of copolymer membranes is of particular interest. It can be realized through chemical incorporation of tough polymers in these membranes by metathesis reactions. Metathesis reaction can be extremely efficient to

produce tough polymers useful as polymer membranes. A brief overview of ring-opening metathesis polymerization (ROMP) is given in the subsequent section.

1.5 Polymers by ROMP

The Nobel Prize in 2005 was awarded to Chauvin, Schrock, and Grubbs in recognition of their contributions to the development of metathesis reactions, which have found applications in various areas from organic synthesis to polymer synthesis.[138] Since the 1980s, extensive research has been carried out exploring new highly reactive metathesis catalysts. Schrock *et al.* reported molybdenum-based catalysis that possessed extremely high reactivity, but were quite sensitive to air or moisture.[139] In 1995 and 1999, the 1st and 2nd generation Grubbs catalysts were introduced.[140] Grubbs catalysts have great tolerance toward diverse functional groups, and consequently use of metathesis reactions have been extended to synthesize bioactive molecules applicable in drug delivery.[141] Additionally, metathesis reactions have been widely applied to polymerize cyclic alkenes to produce unique functional polymers.[142] The general ROMP scheme is depicted as follows

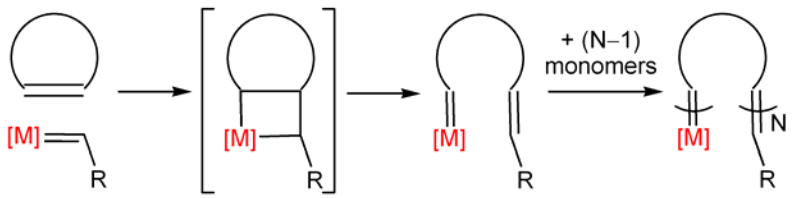

Figure 1.15. ROMP of cyclic alkenes. A cyclic monomer coordinates with the metathesis catalyst to form a metallacyclobutane. If the ring opens in another position, a new catalytic species is generated. Upon more monomer additions, the chain grows. The release of ring strain in the monomer provides the driving force to polymerization.

Tough polymers produced from ROMP, such as polydicyclopentadiene (polyDCPD) and polycyclooctene, are very attractive. PolyDCPD is one important commercial material, which can form elastomers to rigid plastics at different crosslinking densities.[143] Currently, Major polyDCPD products have reached about $50 million in sales for products such as industrial corrosion-resistant parts. One active research area is the direct reaction injection mold (RIM)

of parts with high toughness and corrosion resistance. For example, a spaceship hull is a very strong material, but over time, small microcracks in the structure can form. A new material, with potential application in the construction of spaceship hulls, contained a Grubbs catalyst and small capsules of DCPD. When a crack in the hull formed, the capsules of DCPD were ruptured and contacted with the Grubbs Catalyst, and were polymerized to seal the crack.[144] Additionally, various modified polyDCPD thermosets have been explored to attain better ductility or thermal stability. For example, ROMP of cyclohexenyl norbornene (CHNB) produced more elastic and less crosslinked materials, and upon modification by this rubbery component in polyDCPD, enhanced impact resistance was achieved. Due to less exothermic polymerization with less catalyst load, this PCHNB polymer is also amenable to RIM processes.[145] Recently, Jeong and Kessler reported the preparation of carbon nanotube (MWNT)/polyDCPD nanocomposites by ROMP reactions. Tensile toughness was shown to increase by more than 9 times compared with neat polyDCPD by incorporation of only 0.4 wt % norbornene-functionalized MWNTs. Modest increases in strength and glass transition temperature were also observed with increasing nanotube loadings.[146] In addition, crosslinked monolithic materials of polyDCPD[147] or PCOE[148] have found potential applications as separation media for chromatographic techniques. By means of a polymerization induced phase separation process, pores in packed stationary phases were created by using nonporous polyDCPD particles with small diameters (1–2 μm). In addition, chemically crosslinked PCOE could be applied as shape memory materials.[149]

Although some block copolymers containing a PCOE block have been demonstrated by ROMP using a chain transfer approach,[150] incorporation of crosslinked polyDCPD into copolymer membranes with well-controlled morphology is quite challenging.

1.6 Thesis Outline

The goal of my research is to design crosslinked copolymer membranes from reactive block copolymers with metathesis-reactive monomers (e.g. DCPD or COE) by metathesis

crosslinking reactions. The produced membranes can be elastic to plastic depending on stoichiometry of crosslinking reactions. During this process, morphology of these crosslinked membranes can be controlled.

In Chapter 2, the synthesis and characterization of a norbornene-functionalized polystyrene-polylactide (PNS-PLA) block copolymer is described. A self-assembled blend containing this copolymer and DCPD was cured by metathesis reactions, and nanoporous monoliths with a cylindrical morphology were produced upon etching the PLA component. In Chapter 3, polymerization induced phase separation (PIPS) during ROMP of DCPD in the presence of the PNS-PLA copolymer rendered 3D continuous PLA nanodomains in a crosslinked PNS/polyDCPD matrix. Upon etching PLA, the resultant nanoporous membranes exhibited well-defined bicontinuous nanopores with good thermal and mechanical stabilities. In Chapter 4, crosslinked PEMs were fabricated from PNS-poly(*n*-propyl-*p*-styrenesulfonate) (PSSP) and COE/DCPD via the PIPS scheme. Select PEMs exhibited high proton conductivity similar to Nafion at high humidity but with reduced methanol crossover. In the appendix chapter, crosslinked amine-functionalized membranes were produced from a PNS-poly(dimethylaminoethylmethacrylate) (PNS-PDMAEMA) block polymer and COE.

1.7 References

[1] Shannon, M. A.; Bohn, P. W.; Elimelech, M.; Georgiadis, J. G.; Marinas, B. J.; Mayes, A. M. *Nature* **2008**, *452*, 301–310.

[2] Freeman, B. D.; Pinnau, I. *Polymer membranes for gas and vapor separation: chemistry and materials science*. Washington, DC: American Chemical Society, **1999**.

[3] Chapman, P. D.; Oliveira, T.; Livingston, A. G.; Li, K. *J. Membr. Sci.* **2008**, *318*, 5–37.

[4] Hickner, M. A.; Ghassemi, H.; Kim, Y. S.; Einsla, B. R.; McGrath, J. E. *Chem. Rev.* **2004**, *104*, 4587–4612.

[5] (a) Sadoway, D. R. *J. Power Sources* **2004**, *129*, 1–3. (b) Armand, M.; Tarascon, J. M. *Nature* **2001**, *414*, 359–369.

[6] (a) Koopal, C. G.; de Ruiter, B.; Nolte, R. J. M. *J. Chem. Soc. Chem. Commun.* **1991**, 1691–1692. (b) Wang, P.-C.; DeVoe, D. L.; Lee, C. S. *Electrophoresis* **2001**, *22*, 3857–3867. (c) Adhikari, B.; Majumdar, S.

Prog. Polym. Sci. **2004**, *29*, 699–766. (d) Charcosset, C. *Biotech. Adv.* **2006**, *24*, 482–492.

[7] Pastan, S.; Bailey, J. *New Engl. J. Med.* **1998**, *338*, 1428–1437.

[8] Strathmann, H. *AIChE Journal* **2001**, *47*, 1077–1087.

[9] Ulbricht, M. *Polymer* **2006**, *47*, 2217–2262.

[10] (a) Koros, W. J.; Fleming, G. K. *J. Membr. Sci.* **1993**, *83*, 1–80. (b) Stern, S. A. *J. Membr. Sci.* **1994**, *84*, 1–65. (c) Koros, W. J.; Mahajan, R. *J. Membr. Sci.* **2000**, *175*, 181–196.

[11] Nagai, K.; Masuda, T.; Nakagawa, T.; Freeman, B. D.; Pinnau, I. *Prog. Polym. Sci.* **2001**, *26*, 721–798.

[12] Perry, J. D.; Nagai, K.; Koros, W. J. *MRS Bulletin* **2006**, *31*, 745–749.

[13] Lin, H.; Freeman, B. D. *J. Mol. Struct.* **2005**, *739*, 57–74.

[14] Ho, W. S.; Dalrymple, D. C. *J. Membr. Sci.* **1994**, *91*, 13–25.

[15] (a) Tanaka, K.; Kita, H.; Okano, M.; Okamoto, K. *Polymer* **1992**, *33*, 585–592. (b) Ghosal, K.; Chern, R. T.; Freeman, B. D.; Daly, W. H.; Negulescu, I. I. *Macromolecules* **1996**, *29*, 4360–4369.

[16] Ghanem, B. S.; McKeown, N. B.; Budd, P. M.; Selbie, J. D.; Fritsch, D. *Adv. Mater.* **2008**, *20*, 2766–2771

[17] Park, H. B.; Jung, C. H.; Lee, Y. M.; Hill, A. J.; Pas, S. J.; Mudie, S. T.; Wagner, E. V.; Freeman, B. D.; Cookson, D. J. *Science* **2007**, *318*, 254–258.

[18] Hillock, A. M. W.; Koros, W. J. *Macromolecules* **2007**, *40*, 583–587.

[19] Lin, H.; Wagner, E. V.; Freeman, B. D.; Toy, L. G.; Gupta, R. P. *Science* **2006**, *311*, 639–642.

[20] (a) Kim, T.-J.; Li, B.; Hagg, M.-B. *J. Polym. Sci. B: Polym. Phys.* **2004**, *42*, 4326–4336. (b) Zou, J.; Ho, W. *J. Membr. Sci.* **2006**, *286*, 310–321.

[21] (a) Quinn, R.; Laciak, D. V.; Pez, G. P. *J. Membr. Sci.* **1997**, *131*, 49–60. (b) Quinn, R.; Laciak, D. V.; Pez, G. P. *J. Membr. Sci.* **1997**, *131*, 61–69.

[22] Radosz, M.; Shen, Y. US Patent 0119302A1, **2007**.

[23] Sridhar, S.; Smitha, B.; Aminabhavi, T. M. *Separation & Purification Reviews* **2007**, *36*, 113-174.

[24] *Nature Mater.* **2008**, *7*, 341.

[25] Fleischer, R. L.; Alter, H. W.; Furman, S. C.; Price, P. B.; Walker, R. M. *Science* **1972**, *178,* 255–263.

[26] Michaels, A. S. High Flow Membrane, US Patent 3,615,024, **1971**.

[27] Bierenbaum, H. S.; Isaacson, R. B.; Bruin, M. L.; Plovan, S. G. *Ind. Eng. Chem. Prod. Res. Dev.* **1974**, *1*, 2–9.

[28] Gore, R. W. Porous Products and Process Therefore, US Patent 4,187,390, **1980**.

[29] Hester, J. F.; Mayes, A. M. *J. Membr. Sci.* **2002**, *202*, 119–135

[30] Ulbricht, M.; Oechel, A.; Lehmann, C.; Tomaschewski, G.; Hicke, H.-G. *J. Appl. Polym. Sci.* **1995**, *55*, 1707–1723.

[31] Pieracci, J.; Wood, D. W.; Crivello, J. V.; Belfort, G. *Chem. Mater.* **2000**, *12*, 2123–2133.

[32] Xu. D.; Hein, S.; Wang, K. *Mater. Sci. Tech.* **2008**, 1076–1087.

[33] Matsuyama, H.; Yuasa, M.; Kitamura, Y.; Teramoto, M.; Lloyd, D. R. *J. Membr. Sci.* **2000**, *179*, 91–100.

[34] (a) Reverchon, E.; Cardea, S. *Ind. Eng. Chem. Res.*, **2006**, *45*, 8939–8945. (b) Cardea, S.; Gugliuzza, A.; Sessa, M.; Aceto, M. C.; Drioli, E.; Reverchon, E. *ACS Appl. Mater. Interfaces*, **2009**, *1*, 171–180.

[35] (a) Ulbricht, M.; Belfort, G. *J. Membr. Sci.* **1996**, *111*, 193–215. (b) Nabe, A.; Staude, E.; Belfort, G. *J. Membr. Sci.* **1997**, *133*, 57–72.

[36] Nagendran, A.; Vijayalakshmi, A.; Arockiasamy, D. L.; Shobana, K. H.; Mohan, D. *J. Hazardous Mater.* **2008**, *155*, 477–485.

[37] Vainrot, N.; Eisen, M. S.; Semiat, R. *MRS Bulletin* **2008**, *33*, 16–20.

[38] Strathmann, H.; Kock, K.; Amar, P.; Baker, R. W. *Desalination* **1975**, *16*, 179–203.

[39] Freger, V. *Langmuir* **2003**, *19*, 4791–4797.

[40] Lonsdale,H. K.; Merten, U.; Riley, R. L. *J. Appl. Polym. Sci.* **1965***, 9*, 1341–1362.

[41] (a) Cadotte, J. E.; Petersen, R. J.; Larson, R. E.; Erickson, E. E. *Desalination* **1980**, *32*, 25–31. (b) Jeong, B.-H.; Hoek, E. M. V.; Yan, Y.; Subramani, A.; Huang, X.; Huiwitz, G.; Ghosh, A. K.; Jawor, A. *J. Membr. Sci.* **2007**, *294*, 1–7.

[42] http://www.osmolabstore.com.

[43] http://www.dow.com/liquidseps.

[44] Cadotte, J.; Forester, R.; Kim, M.; Petersen, R.; Stocker, T. *Desalination* **1988***, 70*, 77–88.

[45] Zhou, M.; Nemade, P. R.; Lu, X.; Zeng, X.; Hatakeyama, E.; Noble, R. D.; Gin, D. L. *J. Am. Chem. Soc.* **2007**, *129*, 9574–9575.

[46] (a) Datta, A.; Ebert, K.; Plenio, H. *Organometallics* **2003**, *22*, 4685–4691. (b) Akthakul, A.; Hochbaum, A. I.; Stellacci, F.; Mayes, A. M. *Adv. Mater.* **2005**, *17*, 532–535. (c) de Pater, J. J. M.; Deelman, B.-J.; Elsevier, C. J.; van Koten, G. *Adv. Synth. Catal.* **2006**, *348*, 1447–1458.

[47] (a) Carrette, L.; Friedrich, K. A.; Stimming, U. *ChemPhysChem* **2000**, *1*, 162–193. (b) Neburchilov, V.; Martin, J.; Wang, H.; Zhang, J. *J. Power Sources* **2007**, *169*, 221–238.

[48] Wieser, C. *Fuel Cells* **2004**, *4*, 245–250.

[49] Wasmus, S.; Küver, A. *J. Electroanal. Chem.* **1999**, *461*, 14–31.

[50] Olah, G. A.; Goeppert, A.; Prakash, G. K. S. *Beyond Oil and Gas: The Methanol Economy*; Wiley-VCH, **2006**.

[51] Service, R. F. *Science* **2002**, *296*, 1222–1224.

[52] Garland, N. L.; Kopasz, J. P. *J. Power Sources* **2007**, *172*, 94–99.

[53] McNicol, B. D.; Rand, D. A. J.; Williams, K. R. *J. Power Sources* **2007**, *83*, 15–31.

[54] Hicker, M. A.; Pivovar, B. S. *Fuel Cells* **2005**, *5*, 213–229.

[55] Pivovar, B. S.;Wang, Y.; Cussler, E. L. *J. Membr. Sci.* **1999**, *154*, 155–162.

[56] Souzy, R.; Ameduri, B. *Prog. Polym. Sci.* **2005**, *30*, 644–687.

[57] Mauritz, K.; Moore, R. *Chem. Rev.* **2004**, *104*, 4535–4585.

[58] Hsu, W. Y.; Gierke, T. D. *Macromolecules* **1982**, *15*, 101–105.

[59] Rajendran, R. G. *MRS Bulletin* **2005**, *30*, 587–590.

[60] Zhou, Z.; Dominey, R. N.; Rolland, J. P.; Maynor, B. W.; Pandva, A. A.; DeSimone, J. M. *J. Am. Chem. Soc.* **2006**, *128*, 12963–12972.

[61] Deluca, N. W.; Elabd, Y. A. *J. Polym. Sci. B: Polym. Phys.* **2006**, *44*, 2201–2225.

[62] (a) Rikukawa, M.; Sanui, K. *Prog. Polym. Sci.* **2000**, *25*, 1463–1502. (b) Smitha, B.; Sridhar, S.; Khan, A. A. *J. Membr. Sci.* **2005**, *259*, 10–26.

[63] Park, H. B.; Lee, C. H.; Sohn, J. Y.; Lee, Y. M.; Freeman, B. D.; Kim, H. J. *J. Membr. Sci.* **2006**, *285*, 432–443.

[64] Alberti, G.; Casciola, M. *Annu. Rev. Mater. Res.* **2003**, *33*, 129–154.

[65] Karlsson, L. E.; Wesslen, B.; Jannasch, P. *Electrochimica Acta* **2002**, *47*, 3269–3275.

[66] Shao, P.; Huang, R. Y. M. *J. Membr. Sci.* **2007**, *287*, 162–179.

[67] Semenova, S. I.; Ohya, H.; Soontarapa, K. *Desalination* **1997**, *110*, 251–286.

[68] Xu, Y. X.; Chen, C. X.; Li, J. D. *Chem. Eng. Sci.* **2007**, *62*, 2466–2473.

[69] Chiang, W.-Y.; Lin, Y.-H. *J. Appl. Polym. Sci.* **2002**, *86*, 2854–2859.

[70] Nam, S. Y.; Lee, Y. M. *J. Membr. Sci.* **1999**, *153*, 155–162.

[71] Cabasso, I.; Liu, Z.-Z. *J. Membr. Sci.* **1985**, *24*,101–119.

[72] Bennett, M.; Brisdon, B. J.; England, R.; Feld, R. W. *J. Membr. Sci.* **1997***, 137*, 63–88.

[73] Uragami, T. *Polym. J.* **2008**, *40*, 484–494.

[74] Tanihara, N.; Tanaka, K.; Kita, H.; Okamoto, K. *J. Membr. Sci.* **1994**, *95*, 161–169.

[75] Neel, J.; Aptel, P.; Clement, R. *Desalination* **1985**, *53*, 297–326.

[76] Koval, C.A.; Spontarelli, T.; Nobel, R.D. *Ind. Eng. Chem. Res.* **1989**, *28*, 1020–1024.

[77] Teraguchi, M.; Suzuki, J.; Kaneko, T.; Aoki, T.; Masuda, T. *Macromolecules* **2003**, *36*, 9694–9697.

[78] Baker, R. W. *Ind. Eng. Chem. Res.* **2002**, *41*, 1393–1411.

[79] Tokarev, I.; Minko, S. *Adv. Mater.* **2008**, *20*, 1–7

[80] Baker, R. W. *Membrane technology and applications,* 2nd Ed. John Wiley & Sons Ltd, West Sussex, England, **2004**.

[81] Smit, E.; Mulder, M. H. V.; Smolders, C. A.; Karrenbeld, H.; van Eerden, J.; Feil, D. *J. Membr. Sci.* **1992**, *73*, 247–257.

[82] (a) Robeson, L. *J. Membr. Sci.* **1991**, *62*, 165–185. (b) Robeson, L. M.; Borgoyne, W. F.; Langsam, M.; Savoca, A. C.; Tien, C. F. *Polymer* **1994**, *35*, 4970-4978.

[83] Freeman, B. D. *Macromolecules* **1999**, *32*, 375–380.

[84] Pinnau, I.; Toy, L. G. *J. Membr. Sci.* **1996**, *116*, 199–209.

[85] Cussler, E. L. In *Diffusion, mass transfer in fluid systems;* Cambridge University Press: New York,

1997; pp 580.

[86] Huizenga, D. G.; Smith, D. M. *AICHE J.* **1986***, 32*, 1–6.

[87] Bird, R. B.; Stewart, W. E.; Lightfoot, E. N. *Transport phenomena*; Wiley: New York, **2002**; pp 895.

[88] Khandpur, A. K.; Forster, S.; Bates, F. S.; Hamley, I. W.; Ryan, A. J.; Bras, W.; Almdal, K.; Mortensen, K. *Macromolecules* **1996**, *28*, 8796–8806.

[89] Matsen, M. W.; Bates, F. S. *Macromolecules* **1996**, *29*, 1091–1098.

[90] Cochran, E. W.; Garcia-Cervera, C. J.; Fredrickson, G. H. *Macromolecules* **2006**, *39*, 2449–2451.

[91] Bates, F. S.; Fredrickson, G. H. *Physics Today* **1999**, 32–38.

[92] (a) Bates, F. S.; Maurer, W. W.; Lipic, P. M.; Hillmyer, M. A.; Almdal, K.; Mortensen, K.; Fredrickson, G. H.; Lodge, T. P. *Phys. Rev. Lett.* **1997**, *79*, 849–852. (b) Jeon, H. S.; Lee, J. H.; Balsara, N. P. *Phys. Rev. Lett.* **1997**, *79*, 3274–3277. (c) Thompson, R. B.; Matsen, M. W. *Phys. Rev. Lett.* **2000**, *85*, 670–673.

[93] Bates, F. S.; Fredrickson, G. H. *J. Polym. Sci. B: Polym. Phys.* **1997**, *35*, 2775–2786.

[94] Lodge, T. P.; Pudil, B.; Hanley, K. J. *Macromolecules* **2002**, *35*, 4707–4717.

[95] Lai, C.; Russel, W. B.; Register, R. A. *Macromolecules* **2002**, *35*, 841–849.

[96] Hadjichristidis, N.; Pitsikalis, M.; Pispas, S.; Iatrou, H. *Chem. Rev.* **2001**, *101*, 3747–3792.

[97] Braunecker, W. A.; Matyjaszewski, K. *Prog. Polym. Sci.* **2007**, *32*, 93–146

[98] Moad, G.; Rizzardo, E.; Thang, S. H. *Polymer* **2008**, *49*, 1079–1131.

[99] Hawker, C. J.; Bosman, A .W.; Harth, E. *Chem. Rev.* **2001**, *101*, 3661–3688.

[100] Dechy-Cabaret, O.; Martin-Vaca, B.; Bourissou, D. *Chem. Rev.* **2004**, *104*, 6147–6176.

[101] Bielawski, C. W.; Grubbs, R. H. *Prog. Polym. Sci.* **2007**, *32*, 1–29.

[102] Discher, B.M.; Won, Y.-Y.; Ege, D.S.; Lee, J. C.-M.; Discher, D.E.; Hammer, D.A. *Science* **1999**, *284*, 1143–1146.

[103] Warren, S. C.; Messina, L. C.; Slaughter, L. S.; Kamperman, M.; Zhou, Q.; Gruner, S. M.; DiSalvo, F. J.; Wiesner, U. *Science* **2008**, *320*, 1748–1752.

[104] Ruzette, A.-V.; Leibler, L. *Nature Mater.* **2005**, *4*, 19–31.

[105] (a) Hamley, I. W. *The Physics of Block Copolymers*; Oxford University Press: Oxford, **1998**. (b) Hadjichristidis, N.; Pispas, S.; Floudas, G. A. *Block Copolymers: Synthetic Strategies, Physical Properties, and Applications*; Wiley-Interscience: New York, **2003**. (c) *Developments in block copolymer science and technology*, Hamley, I. W. Ed.; John Wiley & Sons Ltd, West Sussex, England; **2004**. (d) *Block copolymer in nanoscience*, Lazzari, M.; Liu, G.; Lecommandoux, S. Eds.; WILEY-VCH Verlag GmbH & Co. KGaA, Weinheim; **2006**.

[106] (a) Lodge, T. P. *Macromol. Chem. Phys.* **2003**, *204*, 265–273. (b) Hamley, I. W. *Angew. Chem. Int. Ed.* **2003**, *42*, 1692–1712. (b) Park, C.; Yoon, J.; Thomas, E. L. Polymer **2003**, *44*, 6725–6760. (d) Hillmyer, M. A. *Adv. Polym. Sci.* **2005**, *190*, 137–181. (e) Olson, D. A.; Chen, L.; Hillmyer, M. A. *Chem. Mater.* **2008**, *20*, 869–890.

[107] (a) Zalusky, A. S.; Olayo-Valles, R.; Taylor, C. J.; Hillmyer, M. A. *J. Am. Chem. Soc.* **2001**, *123*, 1519–1520. (b) Zalusky, A. S.; Olayo-Valles, R.; Wolf, J. H.; Hillmyer, M. A. *J. Am. Chem. Soc.* **2002**, *124*, 12761–12773.

[108] (a) Rzayev, J.; Hillmyer, M. A. *J. Am. Chem. Soc.* **2005**, *127*, 13373–13379. (b) Mao, H.; Arrechea, P. L.; Bailey, T. S.; Johnson, B. J. S.; Hillmyer, M. A. *Faraday Discuss.* **2005**, *128*, 149–162. (c) Bailey, T. S.; Rzayev, J.; Hillmyer, M. A. *Macromolecules* **2006**, *39*, 8772–8781.

[109] (a) Kim, S. H.; Misner, M. J.; Xu, T.; Kimura, M.; Russell, T. P. *Adv. Mater.* **2004**, *16*, 226–231. (b) Ryu, D. Y.; Shin, K.; Drockenmuller, E.; Hawker, C. J.; Russell, T. P. *Science* **2005**, *308*, 236–239. (c) Bang, J.; Kim, S. H.; Drockenmuller, E.; Misner, M. J.; Russell, T. P.; Hawker, C. J. *J. Am. Chem. Soc.* **2006**, *128*, 7622–7629. (d) Tang, C.; Lennon, E. M.; Fredrickson, G. H.; Kramer, E. J.; Hawker, C. J. *Science* **2008**, *322*, 429–432.

[110] Hawker, C. J.; Russell, T. P. *MRS Bull.* **2005**, *30*, 952–966.

[111] Thurn-Albrecht, T.; Schotter, J.; Kastle, G. A.; Emley, N.; Shibauchi, T.; Krusin-Elbaum, L.; Guarini, K.; Black, C. T.; Tuominen, M. T.; Russell, T. P. *Science* **2000**, *290*, 2126–2129.

[112] (a) Yang, S. Y.; Ryu, I.; Kim, H. Y.; Kim, J. K.; Jang, S. K.; Russell, T. P. *Adv. Mater.* **2006**, *18*, 709–712. (b) Phillip, W. A.; Rzayev, J.; Hillmyer, M. A.; Cussler, E. L. *J. Membr. Sci.* **2006**, *286*, 144–152.

[113] (a) Walheim, S.; Schaffer, E.; Mlynek, J.; Steiner, U. *Science* **1999**, *283*, 520–522. (b) Joo, W.; Park, M. S.; Kim, J. K. *Langmuir* **2006**, *22*, 7960–7963.

[114] Uehara, H.; Yoshida, T.; Kakiage, M.; Yamanobe, T.; Komoto, T.; Nomura,K.; Nakajima, K.; Matsuda, M. *Macromolecules* **2006**, *39*, 3971–3974.

[115] Uehara, H.; Kakiage, M.; Sekiya, M.; Sakuma, D.; Yamonobe, T.; Takano, N.; Barraud, A.; Meurville, E.; Ryser, P. *ACS Nano* **2009**, *3*, 924–932.

[116] Yang, S. Y.; Park, J.; Yoon, J.; Ree, M.; Jang, S. K.; Kim, J. K. *Adv. Funct. Mater.* **2008**, *18*, 1371–1377.

[117] Cooney, D. T.; Hillmyer, M. A.; Cussler, E. L.; Moggridge, G. D. *Crystallogr. Rev.* **2006**, *12*, 13–24.

[118] Peinemann, K.-V.; Abetz, V.; Simon, P. F. W. *Nature Mater.* **2007**, *6*, 992–996.

[119] Yang, Y.; Holdcroft, S. *Fuel Cells* **2005**, *2*, 171–186.

[120] Ding, J.; Chuy, C.; Holdcroft, S. *Chem. Mater.* **2001**, *13*, 2231–2233.

[121] Ding, J.; Chuy, C.; Holdcroft, S. *Macromolecules* **2002**, *35*, 1348–1355.

[122] Ding, J.; Chuy, C.; Holdcroft, S. *Adv. Func. Mater.* **2002**, *12*, 389–394.

[123] Shi, Z.; Holdcroft, S. *Macromolecules* **2005**, *38*, 4193–4201.

[124] Tsang, E. M. W.; Zhang, Z.; Shi, Z.; Soboleva, T.; Holdcroft, S. *J. Am. Chem. Soc.* **2007**, *129*, 15106–15107.

[125] Zhang, Z.; Chalkova, E.; Fedkin, M.; Wang, C.; Lvov, S. N.; Komarneni, S.; Chung, T. C. M. *Macromolecules* **2008**, *41*, 9130-9139.

[126] Norsten, T. B.; Guiver, M. D.; Murphy, J.; Astill, T.; Navessin, T.; Holdcroft, S.; Frankamp, B. L.;

Rotello, V. M.; Ding, J. *Adv. Funct. Mater.* **2006**, *16*, 1814–1822.

[127] Nieh, M.-P.; Guiver, M. D.; Kim, D. S.; Ding, J.; Norsten, T. *Macromolecules* **2008**, *41*, 6176–6182.

[128] Kim, J.; Kim, B.; Jung, B. *J. Membr. Sci.* **2002**, *207*, 129–137.

[129] Elabd, Y. A.; Napadensky, E.; Walker, C. W.; Winey, K. I. *Macromolecules* **2006**, *39*, 399–407.

[130] Serpico, J. M.; Ehrenberg, S. G.; Fontanella, J. J.; Jiao, X.; Perahia, D.; McGrady, K. A.; Sanders, E. H.; Kellogg, G. E.; Wnek, G. E. *Macromolecules* **2002**, *35*, 5916–5921.

[131] Park, M. J.; Balsara, N. P. *Macromolecules* **2008**, *41*, 3678–3687.

[132] Park, M. J.; Nedoma, A. J.; Geissler, P. L.; Balsara, N. P.; Jackson, A.; Cookson, D. *Macromolecules* **2008**, *41*, 2271–2277.

[133] Park, M. J.; Downing, K. H.; Jackson, A.; Gomez, E. D.; Minor, A. M.; Cookson, D.; Weber, A. Z.; Balsara, N. P. *Nano Lett.* **2007**, *7*, 3547–3552.

[134] (a) Bullock, S. E.; Kofinas, P. K. *J. Power Sources* **2004**, *132*, 256–260. (b) Bullock, S. E.; Kofinas, P. *Macromolecules* **2004**, *37*, 1783–1786. (c) Xue, C.; Meador, M. A. B.; Zhu, L.; Ge, J. J.; Cheng, S. Z. D.; Putthanarat, S.; Eby, R. K.; Khalfan, A.; Bennett, G. D.; Greenbaum, S. G. *Polymer* **2006**, *47*, 6149–6155. (d) Olivetti, E. A.; Kim, J. H.; Sadoway, D. R.; Asatekin, A.; Mayes, A. M. *Chem. Mater.*, **2006**, *18*, 2828–2833

[135] (a) Miyata, T.; Obata, S.; Uragami, T. *Macromolecules* **1999**, *32*, 8465–8475. (b) Dutta, B. K.; Sikdar, S. K. *Environ. Sci. Technol.*, **1999**, *33*, 1709–1716. (c) Arnold, M. E.; Nagai, K.; Spontak, R. J.; Freeman, B. D.; DeSimone, J. M. *et al. Macromolecules* **2002**, *35*, 3697–3707. (d) Ray, S.; Ray, S. K. *J. Membr. Sci.* **2006**, *270*, 73–87. (e) Zhao, Q.; Qian, J.; An, Q.; Zhu, Z.; Zhang, P.; Bai, Y. *J. Membr. Sci.* **2008**, *311*, 284–293. (f) Koh, J. H.; Kim, Y. W.; Park, J. T.; Min, B. R.; Kim, J. H. *Polym. Adv. Technol.* **2008**, *19*, 1643–1648.

[136] (a) Kim, J. H.; Ha, S. Y.; Lee, Y. M. *J. Membr. Sci.* **2001**, *190*, 179–193. (b) Zhao, H.-Y.; Cao, Y-M.; Ding, X.-L.; Zhou, M.-Q.; Yuan, Q. *J. Membr. Sci.* **2008**, *310*, 365–373. (c) Car, A.; Stropnik, C.; Yave, W.; Peinemann, K.-V. *Adv. Funct. Mater.* **2008**, *18*, 2815–2823

[137] (a) Ying, L.; Wang, P.; Kang, E. T.; Neoh, K. G. *Macromolecules* **2002**, *35*, 673–679. (b) Nyknen, A.; Nuopponen, M.; Ruokolainen, J. *et al. Macromolecules* **2007**, *40*, 5827–5834. (c) Wang, W.; Chen, L. *J. Appl. Polym. Sci.* **2007**, *104*, 1482–1486. (d) Xue, J.; Chen, L.; Wang, H. L.; Zhang, Z. B., Zhu, X. L. Kang, E. T.; Neoh, K. G. *Langmuir* **2008**, *24*, 14151–14158.

[138] Nobelprize.org. http://nobelprize.org/chemistry/laureates/2005/index.html.

[139] (a) Murdzek, J. S.; Schrock, R. R. *Organometallics* **1987**, *6*, 1373–1374. (b) Schrock, R. R.; Murdzek, J. S.; Bazan, G. C.; Robbins, J.; DiMare, M.; O'Regan, M. *J. Am. Chem. Soc.* **1990**, *112*, 3875–3886.

[140] (a) Schwab, P.; France, M. B.; Ziller, J. W.; Grubbs, R. H. *Angew. Chem., Int. Ed. Engl.* **1995**, *34*, 2039–2041. (b) Scholl, M.; Ding, S.; Lee, C. W. Grubbs, R. H. *Org. Lett.* **1999**, *1*, 953–956.

[141] *Handbook of Metathesis*; Grubbs, R. H., Ed.: Wiley-VCH: Weinheim, **2003**; Vol. 1.

[142] *Handbook of Metathesis*; Grubbs, R. H., Ed.: Wiley-VCH: Weinheim, **2003**; Vol. 3.

[143] (a) Davidson, T. A.; Wagener, K. B.; Priddy, D. B. *Macromolecules* **1996,** *29,* 786–788. (b) Rule, J. D.; Moore, J. S. *Macromolecules* **2002**, *35*, 7878–7882.

[144] White, S. R.; Sottos, N. R.; Geubelle, P. H.; Moore, J. S.; Kessler, M. R.; Sriram, S. R.; Brown, E. N.; Viswanathan, S. *Nature* **2001**, *409*, 794–797

[145] Kelsey, D. R.; Chuan, H. H.; Ellison, R. H. *J. Polym. Sci. A: Polym. Chem.* **1997**, *35*, 3049–3063.

[146] Jeong, W.; Kessler, M. R. *Chem. Mater.* **2008**, *20*, 7060–7068.

[147] (a) Sinner, F.; Buchmeiser, M. R. *Macromolecules* **2000,** *33,* 5777–5786. (b) Martina, A. D.; Hilborn, J. G. *J. Mater. Res.* **2001**, *16*, 2045–2052.

[148] Bandari, R.; Prager-Duschke, A.; Kuhnel, C.; Decker, U.; Schlemmer, B.; Buchmeiser, M. R. *Macromolecules* **2006**, *39*, 5222–5229.

[149] Liu, C.; Chun, S. B.; Mather, P. T. *Macromolecules* **2002**, *35*, 9868–9874.

[150] (a) Bielawski, C. W.; Morita, T.; Grubbs, R. H. *Macromolecules* **2000**, *33*, 678–680. (b) Mahanthappa, M. K.; Bates, F. S.; Hillmyer, M. A. *Macromolecules* **2005**, *38*, 7890–7894.

Chapter 2

Fabrication of Robust 1-D Nanoporous Monoliths Using Norbornene-Functionalized Block Polymers[a]

This chapter explores a new method of incorporating polydicyclopentadiene (polyDCPD) into the matrix of ordered nanoporous monoliths with enhanced mechanical and thermal stabilities. Polylactide (PLA)-containing diblock copolymers and DCPD may form ordered nanostructures and undergo further metathesis reactions. After etching the PLA component, crosslinked nanoporous plastics can be obtained. To realize such a scheme, norbornene-functionalized polystyrene-*b*-PLA block polymers were synthesized and fully characterized. The resultant crosslinked nanoporous monoliths with a hexagonally packed cylindrical morphology exhibit enhanced thermal and mechanical properties.

[a] Reproduced in part with permission from Chen, L.; Hillmyer, M. A. *Macromolecules* **2009**, *42*, 4237–4243. Copyright 2009 American Chemical Society.

2.1 Introduction

Nanoporous polymers can be fabricated from diblock copolymers by selectively removing one sacrificial block via ozonolysis,[1] chemical etching,[2] or dissolution.[3] These materials have found interesting applications in templating other nanostructures,[4] size-selective membranes[5] and anti-reflection coatings.[6] Nanoporous polystyrene (PS) has been widely studied, due to the facile syntheses of PS-containing block copolymers and high stiffness in PS. However, limited thermal stability, intrinsic brittleness, and poor solvent resistance of nanoporous PS has been limiting, particularly in separation membrane applications.[5]

Several approaches have been adopted to combat the thermal instability of such nanoporous materials. Wolf *et al.* prepared nanoporous polycyclohexylethylene (PCHE) monoliths from an ordered PCHE-*b*-polylactide (PLA) copolymer, which exhibited enhanced thermal stability of nanopores to about 140 °C;[7] nanoporous PS collapses at the glass transition temperature (T_g) of PS (e.g., 100 °C).[8] Additionally, crosslinking reactions have been utilized to improve the thermal stability of nanoporous polymers. One method developed by Hawker and coworkers involved the thermolysis of benzocyclobutane (BCB) units in BCB-modified PS-containing block copolymers, having polymethylmethacrylate (PMMA) or PLA as a degradable block. Enhanced thermal stability of thin nanoporous PS films to temperatures exceeding 150 °C resulted.[9] Crosslinking double bonds through a free radical mechanism in ordered polydimethylsiloxane (PDMS)-*b*-polyisoprene (PI)[10] or PDMS-*b*-polybutadiene (PBD)[11] block copolymers having PDMS as a degradable block has been reported to impart good solvent-resistance and thermal stability in the resulting monoliths. Zhou *et al*. reported the crosslinking of PI by S_2Cl_2 in a bicontinuous microemulsion of PS/PS-*b*-PI/PI, and after solvent extraction of PS, the resultant nanoporous monoliths were thermally stable to 160 °C without pore collapse. Tensile tests on these monoliths indicated an elongation at break of 2 % with a tensile strength of 50 MPa; the

brittleness of these nanoporous monoliths was attributed to extensive crosslinking of the PI phase.[12]

Improved thermal stability of nanoporous polymer monoliths was demonstrated in above examples, but mechanical toughness, another critical property of such materials, has not been achieved by crosslinking. To solve this problem, incorporating tough polymers into the matrix of nanoporous monoliths can be helpful. In 2006, Uehara *et al.* reported the fabrication of nanoporous semicrystalline polyethylene (PE) membranes from a PE-PS block copolymer.[13] These materials were particularly tough and had 3-dimensional (3D) continuous nanopores with a well-defined pore size distribution. This work was a breakthrough in the development of robust nanoporous membranes for separation applications. Recently, Jones and Lodge described the preparation of a bicontinuous microemulsion of polypropylene (PEP), PE-*b*-PEP, and PE, and the subsequent production of 3D continuous nanoporous PE through selectively washing away the PEP homopolymer. The resultant nanoporous PE monoliths exhibited outstanding strength and solvent resistance.[14] Likewise, Bluemle and coworkers attempted to use tough multi-block polymers as the matrix of nanoporous monoliths. A continuous network morphology was identified in PCHE-*b*-PE-*b*-PCHE-*b*-PDMS[15] and nanopores were later generated upon removal of the PDMS phase. Preliminary tensile tests indicated superior mechanical strength of these nanoporous monoliths.[16] Tough polymers have shown great promise in producing robust nanoporous membranes and will continue to be pursued. Nevertheless, control of the self-assembly of these precursor copolymers can be complicated, due to the crystallinity and poor solubility of the tough PE component.

The crosslinking strategies described previously failed to accomplish the goal of toughening nanoporous monoliths. In the previous examples, crosslinkable groups like double bonds existed on the polymer backbone. The resultant mechanical strength of crosslinked polymers was largely dependent on the crosslinking efficiency of the polymer

backbones. Since reactive polymer chains in bulk are less mobile than low molecular weight reactants, high catalyst loading was typically required to attain high crosslinking density. For example, as high as 30 wt % of dicumyl peroxide was needed to efficiently crosslink PI-PDMS.[10] Therefore, new crosslinking strategies need to be developed.

Incorporation of tough thermosets by crosslinking reactions into the matrix phase of nanoporous monoliths can be a promising approach. Templating nanostructures in thermosets using block polymers has been widely examined in epoxy resins[17] and polyimides,[18] but no effort has been made to produce nanoporous thermosets by etching one block of the copolymers. Herein, templating nanostructures into polydicyclopentadiene (polyDCPD) could be an interesting approach. PolyDCPD can be synthesized by ring-opening metathesis polymerization (ROMP) under desirable synthetic conditions (e.g., mild reaction condition and low catalyst loading), and polyDCPD possesses appealing thermal and mechanical stabilities.[19] Schematically, a curable mixture comprised of a PLA-bearing copolymer and DCPD with a cylindrical morphology could be prepared and subsequently cured with the microstructure retained. After crosslinking reactions, improvements in thermal and mechanical properties can be realized. Finally, the PLA phase in the crosslinked materials can be removed to leave well-defined nanopores (Figure 2.1).

In this chapter, we (i) examine the criteria of copolymer structure and reactivity in order to successfully template nanostructures in polyDCPD through metathesis reactions, (ii) address the synthesis and characterization of a new norbornene-functionalized monomer and derived block copolymers, (iii) prepare crosslinked monoliths with ordered cylindrical nanopores using blends containing a PLA-*b*-poly(4-norbornenylethylstyrene-*s*-styrene) (P(N-S)) block copolymer with DCPD and a metathesis catalyst. Through our efforts, the utility of metathesis reactions can be extended to facile preparation of tough nanoporous monoliths, and applications of nanoporous monoliths can be potentially broadened.

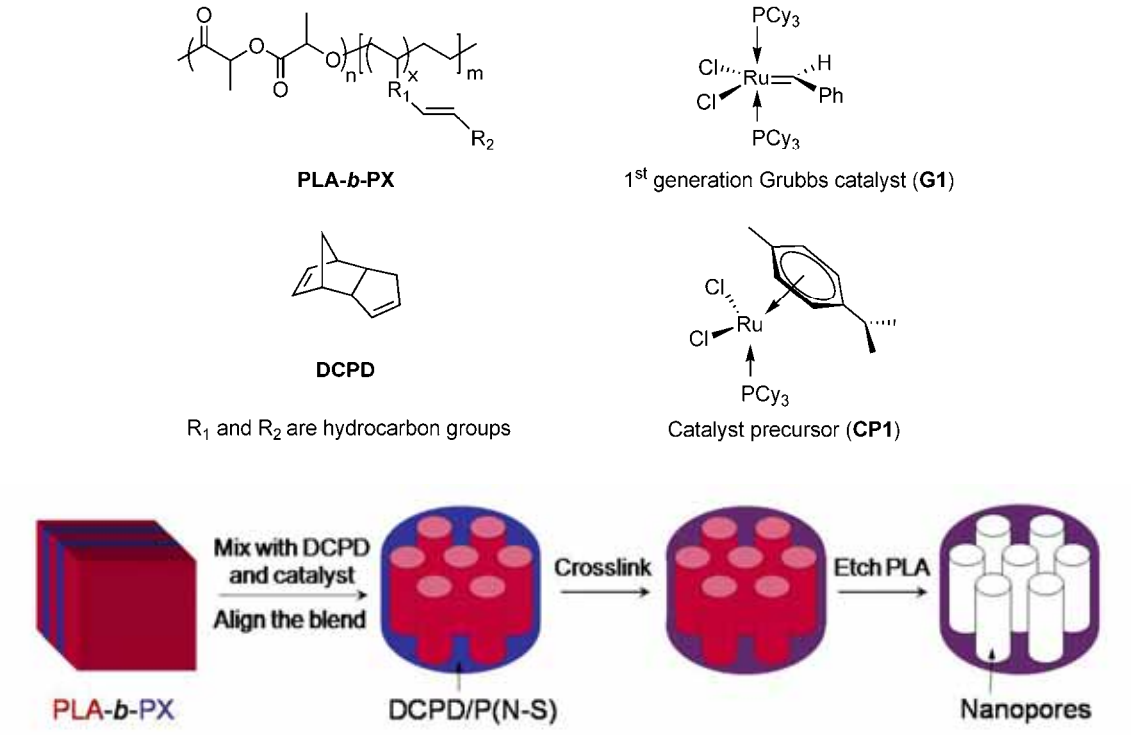

Figure 2.1. Chemical structure of a PLA-*b*-PX copolymer, DCPD, and metathesis catalysts and schematically illustration of fabricating crosslinked nanoporous monoliths by metathesis reactions.

2.2 Experimental section

2.2.1 Materials

Unless specified, all chemicals were used without further purification. 1,3-Butadiene was first stirred with *n*-butyl lithium for 1 h to remove protic impurities, followed by three freeze-pump-thaw cycles. Then butadiene was distilled under static vacuum to another air-free flask containing dibutyl magnesium followed by three freeze-thaw-pump cycles, and stirred at 0 °C for 1 h. Finally, butadiene was distilled into a tared burret and stored in a dry ice/isopropanol bath. Ethylene oxide was purified by vacuum distillations from dibutyl magnesium twice following the same procedure. Styrene was passed through a short alumina column to remove the inhibitor and distilled over CaH_2 under reduced pressure. THF (HPLC grade) was degassed under N_2 purge and purified by passage through a home-built solvent

purification system equipped with activated alumina, to remove traces of protic impurities.[20] Degassed toluene (HPLC grade) was purified by passage through a home-built solvent purification system equipped with activated alumina and a supported copper catalyst. CH_2Cl_2 (HPLC) was purified through using an MBraun solvent purification system equipped with alumina and molecular sieves. The radical inhibitor in 4-chloromethylstyrene was removed by passage through a short alumina column. D,L-lactide was recrystallized from ethyl acetate and dried under reduced pressure at RT, and stored in a nitrogen glovebox. Azoisobutyronitrile (AIBN) was recrystallized from methanol, dried under reduced pressure, and stored under nitrogen.

2.2.2 Materials characterization

2.2.2.1 General methods

Nuclear Magnetic Resonance (NMR) spectra were recorded on a Varian VI-300 spectrometer, and samples were prepared in deuterated chloroform (Cambridge) of approximately 1 wt % for NMR experiments. Size exclusion chromatography (SEC) experiments were performed on a Hewlett-Packard 1100 series liquid chromatograph equipped with Jordi polydivinylbenzene columns with pore sizes of 10000, 1000, and 500 Å as well as a Hewlett-Packard 1047A refractive index detector. THF (HPLC) was used as the mobile phase at 40 °C with a flow rate of 1 mL/min. The SEC instrument was calibrated with PS standards (Polymer Laboratories). Differential scanning calorimetry (DSC) analysis was conducted on a TA Q1000 instrument at a scan rate of 20 °C/min, and T_g was recorded on the 2nd heating run. Mass Spectrometry (MS) analysis was performed on an Finnigan MAT 95 instrument with the sample introduced by Hewlett-Packard Series II Model 5890 Gas Chromatograph. Fourier Transform Infrared (FT-IR) spectra were acquired on a Nicolet Magna-IR Spectrometer 550, and liquid samples were sandwiched between two NaCl plates, while solid polymer samples were ground with KBr and subsequently pressed into transparent pellets by using a screw-press. Tensile tests on monolithic bars (10×2×1 mm)

were carried out on a Rheometric Scientific MINIMAT instrument under ambient conditions, operated at crosshead speed of 2 mm/min with a load cell of 1000 N; a pulling force was applied along the length direction that is parallel with the cylinders axes of the monoliths. Elemental analysis was performed by Atlantic Microlab. Scanning Electron Microscope (SEM) micrographs were acquired on a Hitachi S-900 FE-SEM instrument using a 3.0 kV accelerating voltage. Prior to SEM analysis, the polymer sample was cryo-fractured in liquid nitrogen and mounted on a brass shim using carbon glue (colloidal graphite suspension in isopropanol from Ted Pella, Inc.). A 1.0 nm thick Pt layer was coated on the fractured sample surface via direct Pt sputtering before SEM analysis.

2.2.2.2 Small angle X-ray scattering (SAXS)

All SAXS experiments were conducted on a 230 cm custom built beam line at the University of Minnesota. CuKα X-rays (λ = 1.542 Å) were generated through a Rigaku RU-200BVH rotating anode fitted with a 0.2×2 mm^2 microfocus cathode and Franks mirror optics. Polymer samples were placed in a rubber O-ring and sandwiched between two Kapton films (DuPont). Under helium purge, all samples were equilibrated for 5 min at each temperature before experiment. Two-dimensional (2-D) diffraction patterns were recorded using a Siemens area detector and corrected for detector response before analysis. 2-D images were azimuthally integrated to a 1-D plot of intensity versus q where $q=4\pi/\lambda \sin(\theta/2)$ and θ and λ are the scattering angle and X-ray wavelength, respectively. The domain spacing (D) of polymer samples was calculated based on the principal peak at q^*

$$D = 2\pi / q^* \qquad \textbf{2.1}$$

Morphologies of copolymer samples are indicated by high order reflections. For example, in a cylindrical morphology, peaks relative to the principal peak at $\sqrt{3}, \sqrt{4}, \sqrt{7}, \sqrt{9}$, *et al.* are expected. The periodic distance (l) in the lattice is related to D differently in diverse morphologies,[21] for example in a cylindrical morphology,

$$l = 2D/\sqrt{3} \quad \textbf{2.2}$$

The cylinder domain size (*d*) can be further calculated given a volume fraction of the cylindrical phase (*f*) by

$$\frac{\pi(d/2)^2}{l \times D} = f \quad \textbf{2.3}$$

Additionally, for a polymer sample in a cylindrical morphology where the cylindrical domains are aligned along one direction, SAXS analysis can be used to assess the degree of the alignment of cylinders. In the 2D scattering pattern, at the q^* position, two scattering spots are observed when the incident beam is perpendicular to the cylinders axes. The degree of alignment of the cylindrical phase can be quantified based on the following equations using the two spots pattern.[22] At the principal peak q^*, intensity of a narrow region of Δq equal to the half-peak-width versus the azimuthal angle (β) was plotted, and from a second-order orientation factor (F_2) is extrapolated (1 for a perfectly aligned sample; 0 for an isotropic sample).

$$F_2 = 1 - 3\int_0^{\pi} \cos^2\phi P(\phi) \sin\phi d\phi \quad \textbf{2.4}$$

$$P(\phi) = \frac{I(q^*,\phi)q^{*2}}{\int_0^{\pi} I(q^*,\phi)q^{*2} \sin\phi d\phi} \quad \textbf{2.5}$$

2.2.2.3 N_2 adsorption measurement

N_2 adsorption experiments were performed on a Micromeritics ASAP 2000 instrument, and nanoporous samples were degassed at 50 °C under vacuum overnight to remove absorbed volatiles. Detailed operating procedures have been described elsewhere.[23] During experiment, the amount of gas adsorbed in nanoporous materials (in unit of $cm^3\ g^{-1}$) was measured. The accumulated adsorbed gas as a function of equilibrium relative pressure (p/p^o, p^o is the saturation pressure) at a constant temperature (77 K) was plotted as an isotherm. Nanoporous polymers typically exhibited a type Ⅳ isotherm, where the a hysteresis

between adsorption and desorption curves are typically present.[24] Calculation of the surface area was done following the Brunauer-Emmett-Teller (BET) method,[25] and the average pore diameter and pore size distribution from the adsorption isotherm were calculated using the Barrett-Joyner-Halenda (BJH) method.[26]

2.2.3 Materials synthesis

2.2.3.1 Synthesis of hydroxyl-terminated 1,2-polybutadiene (1,2-PBD-OH)[27]

A 1L glass reactor was equipped with a glass-coated magnetic stir bar and fitted with four Teflon plugs and one Y-connector. The Y-connector was equipped with three ports: one capped with a Teflon-coated septum and two with Teflon-capped valves interfaced to a vacuum/argon manifold and a pressure gauge. The sealed reactor was evacuated to 20 mtorr and flame-dried. After cooling, the Teflon plugs were replaced (under argon purge) with an air-free flask containing dry THF (0.5 L) and pre-tared burets of purified butadiene (35.5 g, 0.65 mol) and purified ethylene oxide (25.0 g, 0.57 mol), which were emerged in a dry ice/isopropanol bath. The reactor was evacuated and backfilled with argon six times and flame-dried. After that, the pressure was set to 3 psi and the reactor was isolated from the manifold. The pressure was monitored to ensure the absence of leaks. Next, THF (0.50 L) was added to the reactor, followed by the addition of *sec*-butyl lithium (3.7 mL, 1.35 M in cyclohexane, this concentration was not titrated) through the Teflon-coated septum using an air-tight syringe. The flask was immersed in a dry ice/isopropanol bath (−78 °C) for 20 min. Butadiene was slowly added to the reaction flask. The reaction solution was stirred for 6 h at −78 °C. The reactants were warmed up to 0 °C at the end of the reaction. Then, ethylene oxide was added at a steady rate. The reaction was allowed to stir for 20 h at RT. Pressure inside the reactor was monitored throughout this process. The reaction was quenched with degassed acidic methanol (1 M, 5 mL). The resulting polymer was precipitated in 4 L methanol. The viscous polymer was recovered by carefully decanting methanol and was

subsequently dried under vacuum at 25 °C overnight, in 4.5 g yield.[b] According to ^{1}H NMR end group analysis, the number average molecular weight (M_n) was 7.2 kg/mol and the molar fraction of 1,4-addition of butadiene was 10 %. 1,2-PBD-OH was dried further at 50 °C under reduced pressure for 2 d, to ensure no residue methanol remained in the polymer. ^{1}H NMR spectrum of 1,2-PBD-OH δ ppm (multiplicity, identity): 5.4 (m, CH2-C**H**=C**H**-CH2- and CH2=C**H**-CH), 4.9 (m, C**H2**=CH-CH-), 2.0 (b, C**H2**-CH=CH-C**H2**- and CH2=CH-C**H**-), 1.2 (m, CH2=CH-C(R)H-C**H**2-), 0.9 (m, -C**H3** resonance from the initiator), 3.65 (m, -C**H2**-OH).

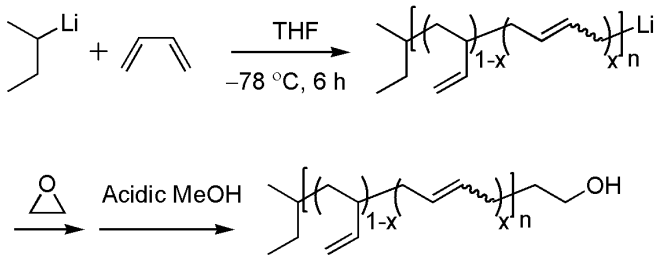

Scheme 2.1. Synthesis of 1,2-PBD-OH by living anionic polymerization. The x indicates the molar fraction of 1,4-addition of butadiene.

2.2.3.2 Synthesis of PBD-*b*-PLA[c]

In a nitrogen atmosphere glovebox, a Teflon coated stir bar, 1,4-PBD-OH (0.95 g, 0.12 mmol), and toluene (11.3 mL) were mixed in a high-pressure vessel. A 1 M solution of $AlEt_3$ in toluene (60 μL, 0.06 mmol) was slowly added to the flask using a syringe, and the mixture was allowed to stir at RT overnight. After formation of the macroinitiator in Scheme 2.2, D,L-lactide (1.70 g, 11.8 mmol) was added to the flask in the glovebox. The flask was sealed and removed from the glovebox, and immersed into an oil bath at 90 °C. After 4 h, the reaction was quenched with aqueous HCl (2 M, 1 mL), and the block copolymer was

[b] Most PBDOH was not precipitated out after 1 d. By NMR analysis, the conversion of butadiene was nearly complete based on the content of initiators. In order to fully recover the product, most THF should be removed after reaction before precipitation in methanol.

[c] PBD-OH was thoroughly dried before growing a second block. Taking the synthesis of 1,4-PBD-*b*-PLA as an example.

precipitated in cold methanol and subsequently dried under vacuum at RT for 1 d. About 2.24 g of block copolymer was recovered. ^{1}H NMR spectrum of 1,4-PBD-PLA δ ppm (multiplicity, identity): 5.2 (m, -C(O)-C(**H**)(CH3)-O-) for the PLA block; 5.4 (m, -CH2-C**H**=C**H**-CH2- and CH2=C**H**-CH-), 4.9 (m, C**H**2=CH-CH-). The M_n of the PLA block was calculated by NMR end group analysis.

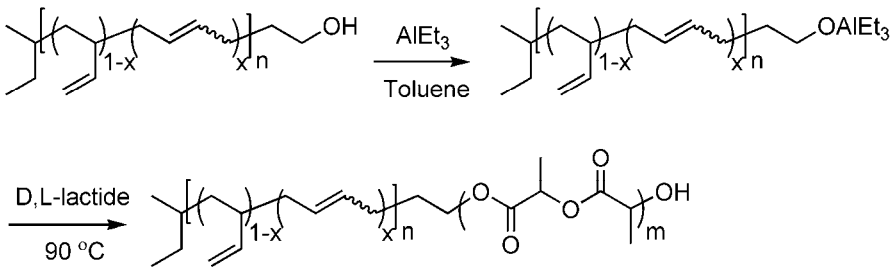

Scheme 2.2. Synthetic scheme for the production of PBD-*b*-PLA block copolymers.

2.2.3.3 Synthesis of a metathesis catalyst precursor (CP)

A metathesis precursor, $RuCl_2$(Cymene)PCy_3, was synthesized using a reported protocol.[28] Hydrated ruthenium trichloride (0.50 g) in ethanol (25 mL) was heated under reflux with α-phellandrene (3.2 mL) for 4 h. The purple precipitate was filtered, washed with cold methanol, and dried under vacuum (0.39 g) ^{1}H NMR spectrum of $[RuCl_2(Cymene)]_2$ δ ppm (multiplicity, identity): 5.39 (d, d, Ph-**H**), 2.16 (s C**H3)**, 2.92 (m, C**H**(CH3)3), 1.28 (d, CH(C**H3**)2). $[RuCl_2(Cymene)]_2$ (0.30 g) suspended in *n*-hexanes (20 mL) with tricyclohexanylphosphine (PCy_3) (0.45 g) was heated to reflux for 4 h. After decanting the supernatant liquid, the dark orange product was dried under vacuum (0.35 g). ^{1}H NMR spectrum of **CP** δ ppm (multiplicity, identity): 5.58 (s Ph-**H**), 2.11 (s, C**H3**, s), 2.83 (m, C**H**(CH3)3), 1.28 (d, CH(C**H3**)2), 1–2 (m, P**Cy3**). In the product, unreacted $[RuCl_2(Cymene)]_2$ of about 10 % was the only impurity. For preliminary crosslinking tests, no further purification of **CP** was attempted.

2.2.3.4 Synthesis of a chain transfer reagent

S-1-dodecyl-S'-(α,α'-dimethyl-α''-acetic acid) trithiocarbonate (**CTA**) was prepared according to a reported procedure.[29] 1-Dodecanethiol (26.9 g, 133.3 mmol), aliquot 336 (tricaprylylmethylammonium chloride, 2.16 g, 5.33 mmol), and acetone (64 g) were mixed in a three-neck reactor under nitrogen purge and cooled down below 10 °C. To the solution, a 50 wt % NaOH solution (11.2 g, 140 mmol) was added over 15 min, and white foam formed in the reactor. After the solution was stirred for 10 min, carbon disulfide (10.2 g, 0.133 mol) in acetone (13.45 g, 0.69 mol) was added over 15 min, and the solution turned orange. After 10 min, chloroform (23.75 g, 0.20 mol) was added, followed by the addition of a 50 wt % NaOH solution (53 g) over 30 min. After reaction at RT for 16 h, water (200 mL) and concentrated aqueous HCl (33 mL) were added. Nitrogen was purged through the solution with vigorous stirring to evaporate the acetone. The solid was collected by vacuum filtration and then stirred in isopropanol (300 mL). A light yellow solid was removed by filtration. After concentration of the isopropanol solution, the resulting viscous product (dark red) was recrystallized from hexanes (4 times) to yield approximately 15 g of produce as a yellow solid. ^{1}H NMR spectrum of **CTA** δ ppm (multiplicity, identity): 0.99 (t, -CH2-C**H3**), 1.37–1.47 (m, C**H2**), 1.75 (s, -C(C**H3**)2-), 3.42 (t, S-C**H2**), 13.05 (s, COO**H**).

2.2.3.5 Synthesis of a macro chain transfer agent (PLA-TC)[30]

In the glovebox, triethylaluminum (1.0 M in heptane, 0.175 mL, 1.75×10^{-4} moles), benzyl alcohol (0.036 mL, 3.5×10^{-4} moles), and dry toluene (35 mL) were mixed in an air-free pressure flask and stirred at RT overnight. D,L-Lactide (5.0 g) was added to the reaction mixture, and the flask was sealed and placed in an oil bath at 90 °C. After 3 h, the reaction was quenched with aqueous HCl (1 M, 2 mL), and the product was precipitated in cold methanol. After decanting methanol, the polymer was dissolved in CH_2Cl_2, precipitated in pentane, and dried at 50 °C under reduced pressure overnight. 2.8 g of hydroxyl-terminated polylactide (PLA-OH) was recovered. ^{1}H NMR spectrum of PLAOH δ ppm (multiplicity, identity): 7.3 (m, Ph-**H**), 5.2 (m, -C(O)-C(**H**)(CH3)-O-), 4.3 (m, C(**H**)(CH3)-OH). ^{1}H NMR

end group analysis indicated the M_n of 10.3 kg mol^{-1}. Oxalyl chloride (0.15 g, 1.6 $\times 10^{-3}$ mol) and **CTA** (0.2 g, 5.5×10^{-4} mol) were mixed in dry CH_2Cl_2 (5 mL) under nitrogen atmosphere and stirred at RT until gas evolution stopped (2 h). After removing any volatile components under reduced pressure, the residue was dissolved in dry CH_2Cl_2 (10 mL). To the solution PLA-OH (10.3 kg mol^{-1}, 2.80 g) dissolved in dry CH_2Cl_2 (20 mL) was added under N_2 atmosphere. The mixture was stirred at RT for 24 h, and the polymer was recovered through precipitation in methanol. The polymer was then dissolved in CH_2Cl_2 (20 mL), precipitated in pentane, and dried at 50 °C under vacuum overnight. A slightly yellow polymer (PLA-TC) (2.50 g) was collected. ^{1}H NMR spectrum of PLA-TC (multiplicity, identity) δ ppm: 3.26 (q, C(**H**)(CH3)-O-CTA), other signals were identical to those of PLA-OH. ^{1}H NMR analysis of PLA-TC confirmed the complete coupling of the hydroxyl end groups of PLAOH with CTA.

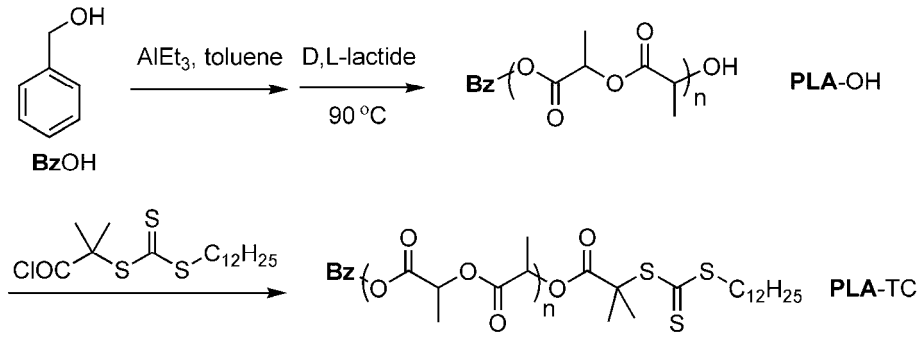

Scheme 2.3. Synthetic protocol for the PLA-attached chain transfer agent (PLA-TC).

2.2.3.6 Synthesis of 4-bromomethyl styrene

4-bromomethyl styrene was synthesized using a reported procedure.[31] A mixture of 4-vinylbenzyl chloride (10.23 g, 67.3 mmol), N-methyl-2-pyrrolidinone (NMP) (220 mL), ethyl bromide (210 mL), and sodium bromide (5.6 g, 54.4 mmol) were refluxed at 65 °C using a Friedrich condenser for 2 d. The mixture was then cooled to RT, poured into a mixture of ice and water, and extracted with diethyl ether three times. The organic fractions were washed with DI water and brine (three times each). The organic phase was dried over $MgSO_4$. After removing $MgSO_4$, ethyl bromide and diethyl ether were evaporated. The crude

product was purified by vacuum distillation (85 °C, 150 mtorr), to afford a light yellow oil (13.2 g, in 95 % yield and 98 % conversion). ^{1}H NMR spectrum δ ppm (multiplicity, identity): 7.4 (m, 4H, Ph-**H**), 6.73 (m, -C**H**=CH2), 5.31 and 5.79 (d, -CH=C**H2**), 4.51 (s, -C**H2**-Br). ^{13}C NMR spectrum (75 MHz) δ ppm: 137.9, 137.4, 136.3, 129.4, 126.7, 114.8, 33.5.

2.2.3.7 Synthesis of 5-bromomethyl norbornene (NBr)

NBr was prepared following a literature procedure.[32] DCPD (80 g) was placed in a round-bottomed flask with a magnetic stir bar and a Vinreux column fitted with a distillation head, and the receiving flask was immersed in a dry ice/isopropanol bath. By slowly heating the flask with stirring at 160 °C, fractioned cyclopentadiene (CPD) was collected under normal atmosphere pressure (boiling point of CPD ~ 46 °C). CPD (30 mL, 224 mmol), allyl bromide (46 mL, 537 mmol), and hydroquinone (150 mg) were mixed in an autoclave under 20 psi N_2, and reacted at 165 °C for 20 h. After cooling down to RT, excess allyl bromide was evaporated. The product was extracted from the remaining black oil by fractional distillation (55 °C, 500 mtorr), to afford 51 g of product as clear liquid. ^{1}H NMR spectrum (main peaks were assigned to the majority *endo* isomer) δ ppm (multiplicity, identity): 6.08–6.24 (m, -C**H**=C**H**-), 3.22 (d d, -C**H2**-Br) 3.05 (t, -C**H2**-Br) 3.00 (s, CH-C**H**-CH=), 2.89 (s, CH2-C**H**-CH=), 2.54 (m, C**H**-CH2-Br), 1.96 (m, -CH-C**H2**(exo)-CH-), 1.50 (m, -CH-C**H2**-CH-), 1.31 (d, -CH-C**H2**-CH-), 0.60 (m, 1H, -CH-C**H2**(endo)-CH-). ^{13}C NMR spectrum of the *endo* isomer δ ppm: 138.3, 131.7, 49.8, 45.6, 43.2, 42.2, 38.4, 32.9.

2.2.3.8 Synthesis of 5-cyclohexenyl norbornene[33]

An autoclave charged with hydroquinone (50 mg) was evacuated to 200 mtorr, refilled with argon (repeated three times), and finally sealed under vacuum. A solution of 4-vinylcyclohexene (39 mL), CPD (20 mL) in an air-free flask was degassed for 10 min and added into the autoclave. After heating the mixture at 230 °C for 5 h, the resultant viscous mixture was subjected to fractional distillation (150 mtorr, 40 °C) to afford 20 g of clear

liquid. ^{1}H NMR spectrum δ ppm (multiplicity, identity): 6.12 and 5.93 (m, CH-C**H**=C**H**-CH), 5.65 (t, CH2-C**H**=C**H**-CH2), 2.87, 2.95, and 2.78 (b, C**H**-CH=CH-C**H** in two isomers), 0.5–2.2 (m, C**H**2-CH=CH-C**H**2 and other saturated C**H** or C**H2**). ^{13}C NMR spectrum (75 MHz) of two main *endo* isomers: 137.2(×2), 132.3, 132.2 (norbornene), 126.6, 126.8, 126.9, 127.2 (cyclohexene), 49.2, 49.4 (bridging methylene), 45.4, 44.9, 44.0, 43.9, 42.3 (×2), 38.5, 38.1, 31.4, 31.2(×2), 30.9, 28.2, 27.7, 25.6, 25.0.

2.2.3.9 Synthesis of bisnorbornene[34]

Following the above procedure, a solution of bicyclo[2.2.1]hepta-2,5-diene (23 g), CPD (16 g), and hydroquinone (0.20 g) were heated to 190 °C for 16 h, to afford a light yellow viscous solution. The resulting viscous mixture was subjected to fractional distillation (1 torr, 46–52 °C) to yield clear viscous liquid (5 g).[d] ^{1}H NMR spectrum of the three isomers δ ppm (multiplicity, identity): 6.21, 6.04, and 5.31 (t, t, t, CH-C**H**=C**H**-CH), the ratio of the three isomers was 2.4:2.3:1 based on the NMR integrations. Other signals between 1 and 3 ppm were not assigned.

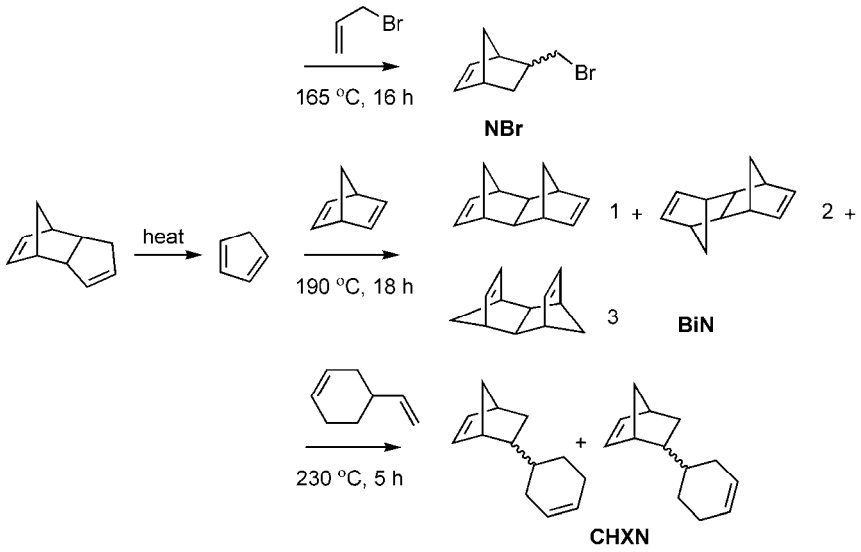

Scheme 2.4. Syntheses of some norbornene derivatives.

[d] Residue mixture was solid-like after cooling down to RT, mainly containing multi-adducts of CPD.

2.2.3.10 Synthesis of a norbornene-functionalized styrene[35]

5-bromomethyl norbornene (4.42 g, 23.5 mmol) was added dropwise to magnesium powder (0.65 g, 27 mmol) in anhydrous THF (25 mL) and reacted at 40 °C for 16 h. The Grignard reagent in THF was isolated from excess magnesium, and added dropwise to a solution of 4-chloromethylstyrene (3.04 g, 20 mmol) in anhydrous THF (15 mL) with Li_2CuCl_4 solution (3 mL, 0.1 M in THF) at −78 °C under argon. The reaction solution was kept at −78 °C for 6 h and then warmed up to RT. The solution was quenched with saturated aqueous NH_4Cl and extracted with diethyl ether twice. The combined ether phase was washed with saturated Na_2CO_3 aqueous solution and brine, and dried over $MgSO_4$. After removing $MgSO_4$, concentration of the organic phase under reduced pressure yielded a pale yellow oil. Purification of this crude product by column chromatography (silica, hexanes) afforded a colorless oil (about 3 g). ^{1}H NMR spectrum of the major *endo* isomer δ ppm (multiplicity, number of Hs, identity): 7.35(d, 2H, Ph-**H**), 7.15 (d, 2H, Ph-**H**); 6.72 (t, 1H, -C**H**=CH2); 6.06–6.19 (m, 2H, -C**H**=C**H**-), 5.73 (1H, d, -CH=C**H2**),5.21 (d, 1 H, -CH=C**H2**), 2.81 (d, 2H, -C**H**-CH=CH-C**H**-), 2.61 (t, 2H, Ph-C**H2**-), 1.99–2.08 (m, 1H, -C**H**-CH2-CH2-Ar), 1.89 (m, 1H, -CH-C**H2**(*exo*)-CH-), 1.36–1.50 (m, 3H, -CH-C**H2**-CH- and -C**H2**-CH2-Ar), 1.24 (d, 1H, -CH-C**H2**-CH-), 0.57 (m, 1H, -CH-C**H2**(*endo*)-CH-). ^{13}C NMR spectrum of the *endo*-N (75 MHz) ppm: 142.9, 137.2, 136.8, 135.1, 132.4, 128.6, 126.2, 112.9, 49.7, 45.4, 42.7, 38.4, 36.7, 35.0, 32.5. MS: 224.2 (M+), 66 (C5H6+), 117.1 (C2H3-Ph-CH+), 158.1 (C2H3-Ph-CH2CH2CH=CH2+). FT-IR (cm^{-1}): (stretching) C=C, 1630, 1610; Ph-H, 1570, 1510, 1450; -C-H, 2870, 2970; =C-H, 3060, 3080; (vibrating of =C-H) the vinyl group, 990, 904; *p*-substituted benzene, 830; norbornene, 717. Elemental analysis: C 90.70 % and H 9.16 % (found); C 91.01 % and H 8.99 % (calculated). This monomer was further stirred with CaH_2, passed through dry alumina, and stored over molecular sieves.

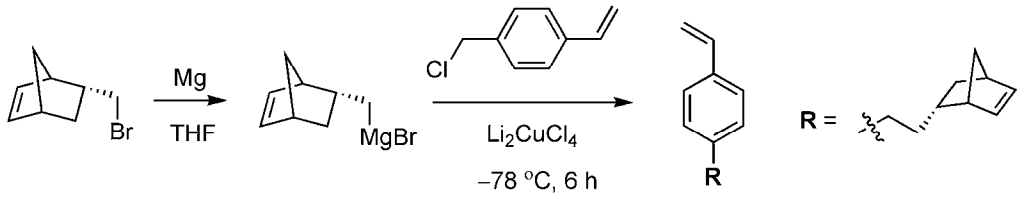

Scheme 2.5. Synthesis of *p*-norbornenylethylstyrene (N) via the Grignard reaction.

2.2.3.11 Polymerization reactions of N

Anionic polymerization (PN_1 in Table 2.5): In the glovebox, *s*-butyl lithium (1.35 M in cyclohexane, 20 μL) was added into dry toluene (3 mL) and N (0.224 g) in a pressure vessel. The mixture was reacted at 50 °C for 4.5 h. Then, the mixture was quenched with degassed acidic methanol under argon, and the resultant polymer was recovered through precipitation in methanol. Anionic polymerization (PN_2): In a similar procedure but using THF instead, the reaction was performed in a dry ice/isopropanol bath at −78 °C for 0.5 h. Conversion of N was nearly quantitative in both polymerizations. Free radical polymerization (PN_3): AIBN (4 mg) and monomer N (2.0 g) was mixed in toluene (3 mL), degassed, and reacted at 60 °C for 14 h. Approximately 0.20 g of polymer (10% conversion) was recovered through precipitation in methanol. Metathesis polymerization (PStN): Monomer N (0.1 g) was dissolved in CH_2Cl_2 (4 ml) under N_2 atmosphere, and the 2nd generation Grubbs catalyst (1 mg) dissolved in minimum CH_2Cl_2 was added into the solution at RT. The reaction was quenched with acidic methanol after for 1 h.[e] ^{1}H NMR spectrum of PN_2 δ ppm (multiplicity, identity): 6.2–7.3 (b, PH-**H**), 5.9–6.2 (b, CH-C**H**=C**H**-CH), 2.7–2.9 (b, -C**H**-CH=CH-C**H**-), 2.4–2.6 (b, Ph-C**H2**-), 1.0–2.3 (b, other C**H** or C**H**2), 0.5–0.6 (b,-CH-C**H2**(*endo*)-CH-). ^{1}H NMR spectrum of PStN δ ppm (multiplicity, identity): 6.9–7.4 (b, Ph-**H**), 6.7 (b, Ph-C**H**=CH2), 5.5–6.5 (b, Ph-C**H**=C**H**-CH-, *trans* and *cis*), 5.2, 5.7 (d, d, Ph-CH=C**H2**), 5.0 and 5.3 (b, CH-C**H**=C**H**-CH, , *trans* and *cis*), 1–3 (b, other C**H** and C**H2**).

[e] Polymerization for longer than 2 h yielded insoluble product.

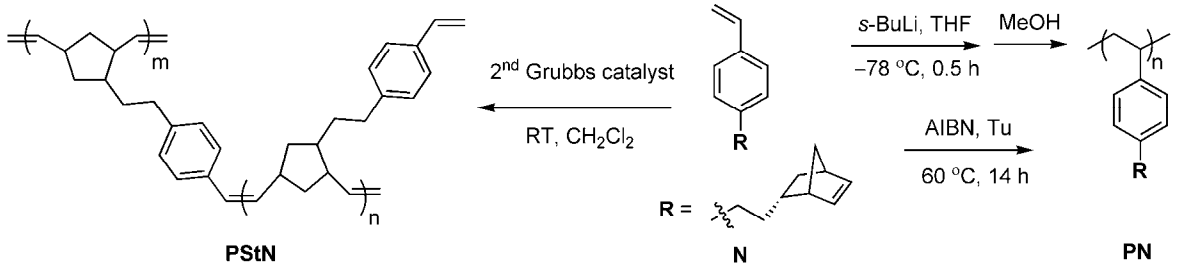

Scheme 2.6. Different polymerization schemes of N.

2.2.3.12 Kinetics study in copolymerization of styrene and N

Condition 1: CTA (3.5 mg), and styrene and N (totally 0.5 mL at different ratios) were placed in a 10 mL reactor, and sealed under argon atmosphere after three freeze-pump-thaw cycles. Condition 2: CTA (3.5 mg), dry toluene (0.5 mL), and styrene and N (totally 0.5 mL at different ratios) were placed in a 10 mL reactor, and sealed under vacuum after three freeze-pump-thaw cycles. Under these conditions, styrene vaporization during polymerization that resulted in increasing f_N (molar ratio of N) was negligible. Polymerization reactions were conducted at 120 °C for 1 to 2 h, where the reaction time was increased with decreasing N concentrations in the feed. Final monomer conversion was between 3 to 6 wt % based on recovered polymers through precipitation in methanol and molecular weight by NMR spectroscopy. Molar ratios in the feed were calculated using ρ(styrene) and ρ(N) = 0.9 g mL^{-1} at 25 °C, while molar ratios in polymers were calculated from the NMR spectra by comparing the signal of C**H**=C**H** with the signal of Ph-**H**.

2.2.3.13 Synthesis of PLA-*b*-P(N-S) and PLA-*b*-PN

PLATC (0.2 g, 0.019 mmol, M_n= 10.6 kg/mol, PDI = 1.09), monomer N and styrene (total volume of 1.0 mL) at different ratios, were mixed in an air-free flask, followed by three freeze-pump-thaw cycles, and sealed under vacuum, and finally polymerized at 120 ± 1 °C for around 4 h. Some polymerization reactions were carried out in toluene as follows: PLATC (0.2 g, 0.019 mmol), N and Styrene (1.0 mL), and AIBN (0.35 mg, 0.002 mmol) were dissolved in toluene (1.0 mL) in an air-free flask followed by three freeze-pump-thaw

cycles, and reacted at 70 °C for 20 h. The resultant copolymers were recovered through precipitation in methanol, followed by dissolution in CH_2Cl_2 and re-precipitation in pentane, and finally dried under vacuum. The overall monomer conversion was between 20 and 30 wt % determined through NMR analysis. ^{1}H NMR spectrum of PLA-*b*-P(N-*s*-S) (multiplicity, identity) δ ppm: 6.2–7.2 (b, Ph-**H**), 5.9–6.2 (b, -C**H**=C**H**-), 5.1–5.3 (b, -C(O)-C**H**(CH3)-O-), 2.8 (b, -C**H**-CH=CH-C**H**-), 2.55 (b, Ph-C**H2**-), 2.0 (b, -C**H**-CH2-CH2-Ar), 1.86 (b, -CH-C**H2**(*exo*)-CH-), 1.39 (b, -CH-C**H2**-CH- and -C**H2**-CH2-Ar), 1.25 (d, -CH-C**H2**-CH-), 0.55 (b, -CH-C**H2**(*endo*)-CH-).

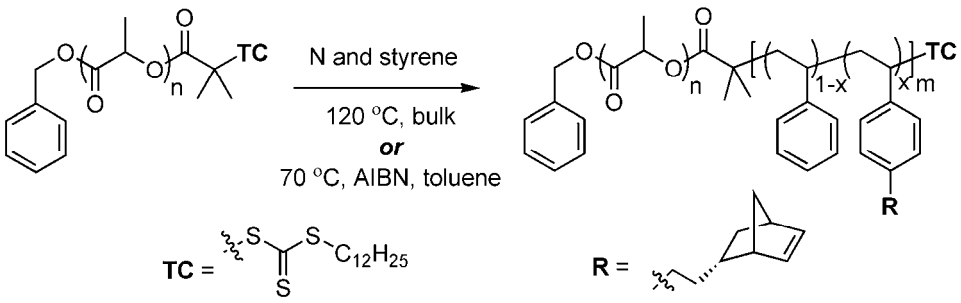

Scheme 2.7. Synthetic scheme for PLA-*b*-P(N-S) copolymers. The x denotes the mole fraction of N in the PNS block.

2.2.4 Monolith fabrication

2.2.4.1 Preparation of the copolymer blends

PLA-*b*-PX (0.2 g) and DCPD (0.1 to 0.2 g) were dissolved in CH_2Cl_2 (1.5 mL), and then most of the CH_2Cl_2 and some DCPD were removed under reduced pressure over 10 to 30 min. The composition of the resultant blend was estimated by mass and precisely determined by NMR spectroscopy.

2.2.4.2 Crosslinking of the copolymer blends

A metathesis catalyst (using the catalyst **CP** of 3 wt %, or using catalyst **G1** of 0.5 wt% with PPh_3 of 1.5 wt %, relative to the overall mass of copolymer/DCPD), PLA-*b*-PX (0.2 g) and DCPD (0.1 ~ 0.2 g) were dissolved in CH_2Cl_2 (0.2 mL) at RT and stirred for 20 s until a

homogenous solution formed. Then, most of the CH_2Cl_2 and some DCPD were removed by placing the mixture under vacuum for about 20 min or longer to achieve a desired PLA composition. The exact composition was calculated by NMR spectroscopy immediately after the blend preparation. Polymer samples were then aligned using a home-made channel die.[8] The resultant orange waxy blend was pressed into thin films at RT between two Teflon sheets, and then carefully peeled off Teflon after soaking in liquid N_2. The pressed films were placed vertically in the channel die and then pressed at 50 °C to form long rectangular bars (the cylindrical PLA domains oriented along the flow direction). The aligned samples were placed in a sealed pressure vessel under positive argon pressure and cured at 70 °C for 12 h and annealed at 110 °C for 3 h using **G1** (at 93 °C for 16 h for blends containing **CP**). The crosslinked monoliths were dried under vacuum overnight prior to further analysis.

2.2.4.3 PLA Degradation in the crosslinked monoliths

The PLA component in these crosslinked samples was degraded in a NaOH solution (a mixture 4:6 (v/v) of methanol and water) for 7 d at 70 °C. The resultant nanoporous monoliths were rinsed with methanol and DI water, and subsequently dried under reduced pressure at 60 °C for 2 d.

2.3 Results and discussion

2.3.1 Crosslinking reaction of PBD-*b*-PLA and DCPD

Self-assembly of block copolymers in a selective solvent has captured much attention.[36,37] For instance, PS-*b*-PI (15-13 kg mol^{-1}) in a PS-selective solvent diethyl phthalate can adopt various morphologies, such as spheres, cylinders, and lamellae depending on fraction of the solvent.[36a] Using a selective solvent that can crosslink with the solvent-philic block, improvements in thermal and mechanical properties of the composites are expected, and the blend morphology is tailored by the solvent.

To template nanostructures in polyDCPD, a tough plastic material, by metathesis reactions, a PLA-PX copolymer (PX is a hydrocarbon polymer containing double bonds reactive to metathesis catalysts, see Figure 2.1) might be useful if DCPD could be efficiently crosslinked with the PX block. To this end, PBD was chosen as a suitable polymer for initial investigation.

The PBD-OH homopolymer was synthesized by living anionic polymerization of butadiene followed by end capping reaction with ethylene oxide (Scheme 2.1). The resultant polymer possessed well-defined hydroxyl end groups susceptible to subsequent polymerization. Under the living anionic polymerization conditions, 1,4-PBD-OH and 1,2-PBD-OH polymers containing about 91 and 10 % 1,4-PBD repeating unit, respectively, based on NMR analysis, were produced. Using PBD-OH as a macro initiator and $AlEt_3$ as a catalyst, the PBD-*b*-PLA copolymers were produced by ring-opening polymerization of D,L-lactide (Scheme 2.2). All produced polymers are summarized in Table 2.1.

The resulting copolymers exhibited low polydispersity indices (PDIs) and well-defined polymer structures. Lamellar morphology in these two PBD-PLA copolymers was indicated by SAXS analysis, in agreement with the 50 % PLA composition.

Table 2.1. Summary of polymers used in the crosslinking studies.

[a]	Mn (SEC)[b] kg mol^{-1}	Mn (NMR)[c] kg mol^{-1}	PDI[d]	T_g (°C)	f_{PLA}[e] (%)	Morphology[f]	Domain spacing (nm)
1,4-PB-OH	16.2	7.9	1.03	–98			
1,2-PB-OH	16.3	7.3	1.06	–20			
1,4-BL_1	28.7	19.2	1.11	–98/46	50.6	L	29.9
1,2-BL_2	20.1	16.9	1.24	–20/45	48.6	L	29.3

a. This sample was provided by a former group member, synthesized via anionic polymerization of butadiene in cyclohexane at 45 °C; BL indicates PBD-*b*-PLA. *b*. based on PS standards. *c*. Molecular weight was obtained by NMR end group analysis: the integration value of the double bond signals divided by the end group signal gave the number of butadiene repeating unit. *d*. PDI: polydispersity index; *e*. Volume fraction of PLA was calculated based on polymer densities at RT: ρ(PBD) = 0.90,[38] ρ(PLA) = 1.254 g cm^{-3}.[39] *f*. Morphologies of copolymers were indicated from SAXS experiments at RT after annealing the polymer samples at 100 °C.

The miscibility of DCPD with PBD and PLA was first evaluated. DCPD was completely miscible with PBD at 60 °C, while it slightly swelled PLA at a high temperature of 90 °C, suggesting that DCPD would be strongly selective for the PBD block in a PBD-PLA/DCPD blend. The selectivity of DCPD was theoretically evaluated as well by calculating the Flory-Huggins parameters (χ) from solubility parameters (δ). The solubility parameter of polybutadiene δ_{PBD} is 8.35 $(cal/cm^3)^{0.5}$ and δ_{DCPD} of 8.03$(cal/cm^3)^{0.5}$, and calculation of δ_{PLA} is shown in Table 2.2 using a group contribution method.[40] Using the reference volume of DCPD (v) calculated by M/ρ = 134 $cm^3\ mol^{-1}$, the pairwise χs were calculated using equation 2.6: $\chi_{(D/PLA)}$=0.73, $\chi_{(D/PBD)}$=0.02, and $\chi_{(PBD/PLA)}$=0.46. These χ values also indicate that DCPD is a poor solvent for PLA but a good solvent for PBD.

Table 2.2. Calculation of the solubility parameter for PLA.

		(CO)-O	CH	CH3	Sum
Cohesion energy $\mathbf{F}_{Hoy}$	$(cal\ cm^3)^{0.5}\ mol^{-1}$	2(326.6)	2(86.0)	2(148.3)	1121.8
Molar volume $\mathbf{V}_r$	$cm^3\ mol^{-1}$	2(24.6)	2(9.85)	2(22.8)	114.5

$$\delta_{PLA} = \frac{\sum F_{Hoy}}{\sum V_r} = 1121.8/114.5 = 9.8(cal/cm^3)^{0.5}$$

$$\chi_{12} = \frac{v}{RT}(\delta_1 - \delta_2)^2 \qquad \textbf{2.6}$$

With the knowledge of the selective miscibility of DCPD in PBD-*b*-PLA, a blend of these two components was then prepared, and the morphology of the resultant blend was characterized by SAXS experiments. For example, SAXS analysis of a blend containing 1,4-BL_1 and DCPD at a mass ratio of 2:1 is shown in Figure 2.2. Although the morphology of the blend was not clear at RT, after annealing the blend at high temperatures a well-defined cylindrical morphology was observed. During the SAXS experiments, the waxy blend was kept in a sealed sample holder, and the evaporation of DCPD was negligible. The morphological transition from lamellae (the morphology of PBD-PLA not shown in Figure 2.2) to cylinders confirmed the selectivity of DCPD for the PBD phase, because for a neutral solvent, equal swelling of both blocks would be expected and the lamellar morphology would

be retained.[41] The resultant cylindrical morphology of the blend was stable over a range of temperatures, which would be proper for later crosslinking reactions.

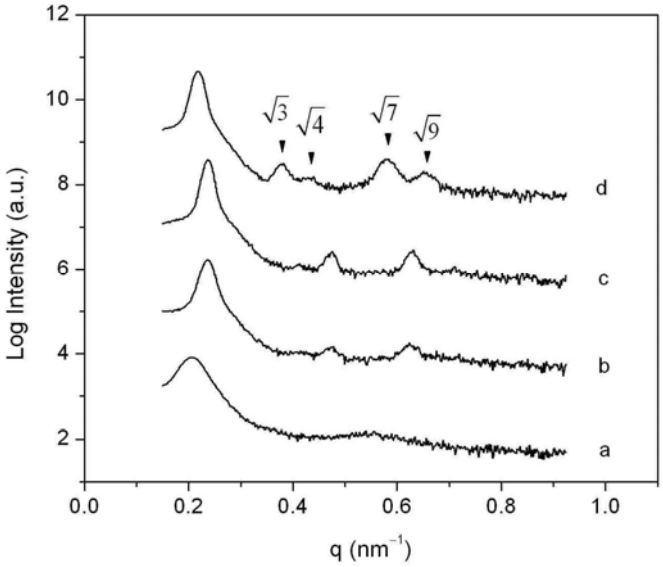

Figure 2.2. SAXS profiles of a 1,4-PBD-PLA/DCPD blend (mass ratio = 2:1) with a cylindrical morphology. Traces a, b, c, and d indicate SAXS signals at 25 °C (5 min), 100 °C (20 min), 100 °C (50min), and 25 °C (60 min).

DCPD was polymerized through the norbornene double bond with metathesis catalysts and further underwent crosslinking reaction on the double bond of the cyclopentene ring upon heating by a combination of metathesis and radical crosslinking reactions.[42] Blends comprised of DCPD and a copolymer were prepared using methylene chloride as a cosolvent, which was removed under reduced pressure after blending at RT (see Section 2.2.4.2). A latent metathesis catalyst (**CP**, see Figure 2.1) was mixed into the blend. This precursor catalyst generates reactive species when heated to temperatures above 80 °C, so it allows facile preparation of a precursor blend in a desired composition without crosslinking.[43] Then, the crosslinking reaction would be promoted by simply heating the blend. First, the reactivity of the PBD phase by metathesis reactions was evaluated through the reaction of the PBD homopolymer and the precursor catalyst at 80 °C for 24 h. After reaction, more than 50 % gel

fraction in the crosslinked PBD/polyDCPD was observed by soaking the crosslinked sample in THF overnight, indicating the modest reactivity of PBD with this catalyst.

Two copolymers (1,4-PB-PLA and 1,2-PB-PLA) were utilized to prepare reactive blends with DCPD as shown in Table 2.3. The mass ratio of PBD-PLA to DCPD in the blend was kept at 2:1, and the catalyst precursor **CP** was 3–4 wt % in the blend relative to the overall mass of PBD-PLA and DCPD. The morphology of prepared blends was identified by SAXS at RT.

Table 2.3. Initial metathesis crosslinking studies using PBD-*b*-PLA.

	Transparency	f_{PLA} %	Morphology[b]
1,4-BL_1/D	Clear	25	C
1,4-BL_1/D*[a]	Opaque		N
1,2-BL_2/D	Clear	25	C
1,2-BL_2/D*[a]	Opaque		N

a. Cured blend. *b*. C and N denote a cylindrical morphology and not determined morphology, respectively.

Both PBD-*b*-PLA/DCPD samples were soft after crosslinking, and the gel fraction in these samples (the mass of insoluble component after soaking the sample in THF overnight) was less than 70 %, indicating insufficient crosslinking in these two samples. This result was not surprising, since the PBD block was modestly reactive to the metathesis catalyst. Despite that, the appearance of the cured samples was opaque after reaction, and SAXS analysis of these samples indicated the disappearance of the pre-assembled cylindrical morphology. Moreover, time-dependent SAXS experiments were performed to monitor the crosslinking process, (Figure 2.3). Blends were crosslinked in a sealed ampoule and a partial sample was taken for SAXS analysis after some time.

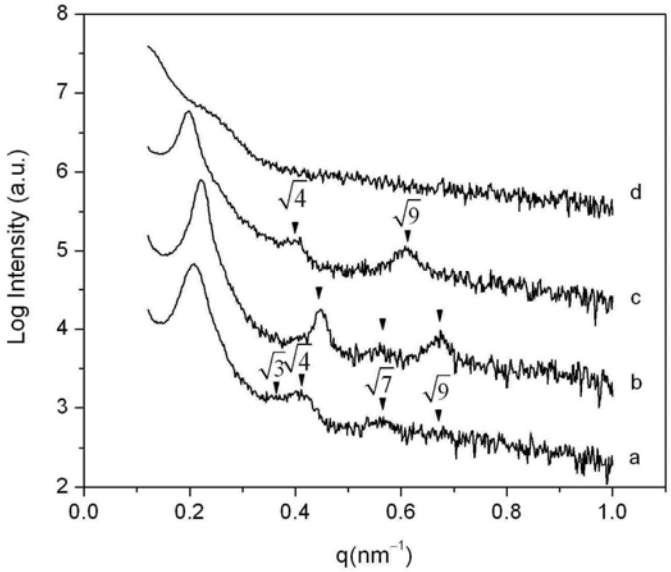

Figure 2.3. Time-dependent SAXS analysis of a 1,4-PBD-PLA/D blend by metathesis reactions, containing 3 wt % precursor catalyst at 100 °C. Signals a, b, c, and d were collected at 5 min, 30 min, 1 h, and 24 h at RT, respectively.

During the experiments, morphology changes caused by the evaporation of DCPD were assumed to be trivial. The phase transition from cylinders to lamellae (Figure 2.3) during the reaction might suggest the exclusion of polyDCPD from the PBD-PLA phase, as the PBD block was slightly reacted with polyDCPD. Meanwhile, some PBD chains could be cleaved off the PLA block from the 1,4-butadiene units by metathesis reactions. Thus, a PLA-predominant phase could form leading to the disappearance of the lamellar morphology of the original PBD-PLA copolymers. Due to the strong segregation between polyDCPD and PLA, the PLA-containing phase was finally phase-separated from polyDCPD on a macroscopic scale.

Block copolymers have been used to template nanostructures in epoxy resins without macrophase separation, including these made with unreactive poly(ethyl ethylene)-*b*-poly(ethylene oxide) (PEE-PEO) copolymers.[17a] The self-assembled nanostructure of a blend containing PEE-PEO and epoxy resin precursors was stable during curing reactions, likely due to a high viscosity in the blend which kinetically inhibited macrophase separation

of the copolymers from the epoxy resins. In contrast, in the DCPD system studied here, the DCPD component with low viscosity at a crosslinking temperature of 100 °C could segregate with PBD-PLA copolymers more easily. Most importantly, the χ of epoxy resin/PEE-PEO is relatively low, which is advantageous for stabilizing the assembled microscopic structure; χ(DCPD/PLA) was quite large as previously calculated, so during the polymerization of DCPD, the PLA-containing phase was driven to separate from the polyDCPD matrix. In order to overcome this problem, a highly metathesis-reactive block in PX-PLA would be helpful to implement the crosslinking scheme by metathesis reactions.

2.3.2 A norbornene-functionalized monomer

2.3.2.1 Background

In order to increase the reactivity of the PX block to metathesis reactions, functional monomers having cyclic alkene groups (e.g., norbornene) are preferred. Such monomers could be polymerized readily into a PLA-containing block copolymer. Norbornene-functionalized initiators have been widely explored with examples including a norbornene-containing ATRP initiator,[44] a norbornene-functionalized RAFT initiator,[45] and a norbornene-containing diphenylethylene anionic polymerization initiator.[46] They also have been examined for the synthesis of norbornene-functionalized macro-monomers and comb-like block polymers by ROMP. For example, a dual-polymerizable norbornene derivative, namely norbornenylmethyl acrylate, has been applied in an electro-grafting reaction on an electrode, followed by a graft polymerization of norbornene by ROMP.[47] This monomer could be useful to produce a norbornene-functionalized block copolymer. Nevertheless, the ester linkage between the norbornene and acrylate groups could be susceptible to hydrolysis.

Functionalized styrene derivatives have attracted great attention due to the fact that various controlled polymerization approaches, such as anionic and free radical polymerizations, can be utilized to selectively polymerize the vinyl group of styrene,[48] giving rise to complex

PS-based copolymers.[49,50] A styrene derivative containing norbornene functionality would be chemically robust, and the resulting polymers will be chemically resistant in base or acid conditions, making them applicable under diverse crosslinking conditions.

2.3.2.2 Monomer synthesis and characterization

4-Norbornenylethyl styrene (N) would be a good candidate for synthesizing a norbornene-functionalized block copolymer. Norbornenylethyl magnesium bromide (NMgBr) has been used in excess to react with a bromomethyl styrene derivative at −30 °C.[32] In order to accommodate a large-scale monomer synthesis, this coupling reaction has to be conducted in a more atom-economical way. Several studies indicated Li_2CuCl_4 was an efficient catalyst for Grignard coupling reactions with alkyl magnesium halides.[51] Different synthetic conditions were examined and are summarized below in Table 2.4. Without using Li_2CuCl_4, poor coupling efficiency resulted (Entries 1 and 5), although 4-bromomethyl styrene was more effective in coupling with NMgBr than 4-chloromethyl styrene. Using 4-chloromethyl styrene (commercially available) at lower temperatures, the formation of byproducts, mainly the homo-coupling compounds of the reactants, were effectively suppressed. As a result, the condition used in entry 4 of Table 2.4 was chosen.

Column chromatography of the crude N removed most of the major byproducts. The purification process must be careful operated as one byproduct, 1,2-norbornenylethyl-ethane, eluted before the monomer. The ^{13}C and ^{1}H NMR spectra of purified N (Figures 2.4 and 2.5) indicate a product of high purity and all resonances are consistent with the structure. Infrared spectroscopy, gas chromatography-mass spectrometry, and elemental analysis are corroborative (see Section 2.2.3.10).

Table 2.4. Synthetic conditions for N.[a]

Entry[b]	Mole ratio of NBr:XMeSt	Temperature (°C)	Time (h)	Conversion[c] (%)
1	1.2:1	0	2	<5
2	1.2:1	–20	3	54
3	1.2:1	–78	3	62
4	1.2:1	–78	6	89
5	1.2:1[3]	0	2	60
6	1.2:1	–78	6	92

a. All reactions carried out at the indicated temperature and then warmed up to RT overnight. *b*. Entries 1 to 4 were using 4-chloromethyl styrene, while entries 5–6 were using 4-bromomethyl styrene. In entries 1 and 5 Li_2CuCl_4 was not used in the coupling reaction. *c*. Conversion of XMeSt was obtained through NMR analysis of the isolated crude product.

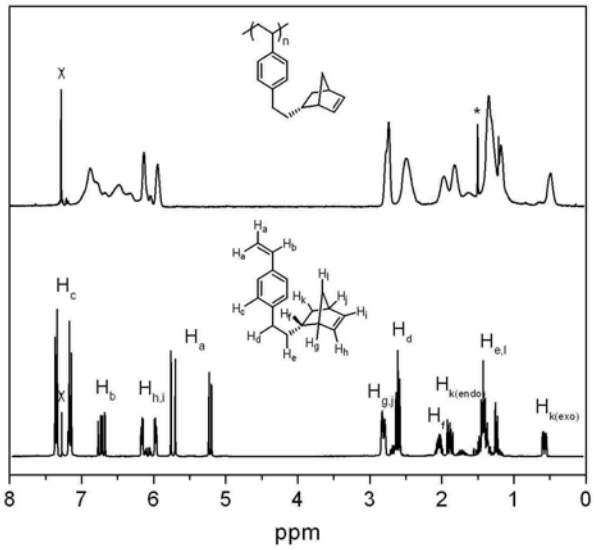

Figure 2.4. ^{1}H NMR spectra of monomer N (the bottom graph, mainly the *endo* isomer) and corresponding polymer PN. The peak labeled with asterisk indicates residue water in $CDCl_3$ and peaks labeled with cross correspond to $CDCl_3$.

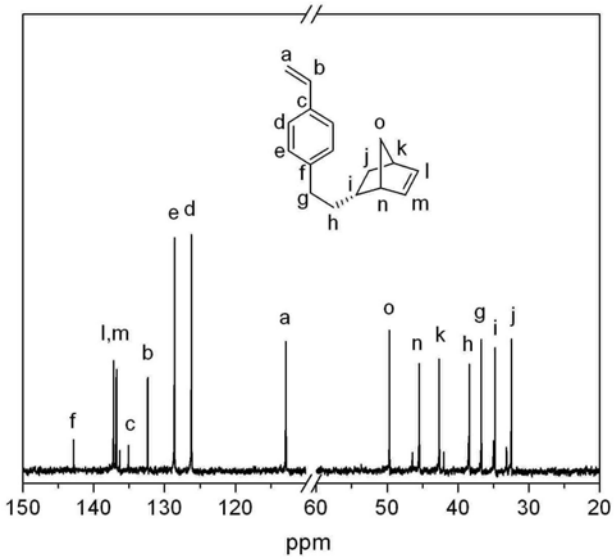

Figure 2.5. ^{13}C NMR spectrum of monomer N, with all major peaks assigned to the major *endo* isomer of N. Side peaks associated with main peaks between 30 and 50 ppm likely correspond to the *exo* isomer of N.

2.3.2.3 Polymerization of N

The new norbornene-containing styrene (N) was subjected to orthogonal polymerization techniques including anionic polymerization, which has been widely employed as a robust technique to synthesize numerous functionalized styrene monomers.[48a] Two anionic polymerization conditions were examined. For the anionic polymerization in cyclohexane, the resultant PN polymer exhibited a shoulder peak in SEC analysis with molecular weight double that of the main peak and a relatively broad PDI. This may be attributed to a coupling reaction of the norbornene groups. Polymerization of N in THF at a low temperature (–75 °C) successfully eliminated this problem. The ^{1}H NMR spectrum of the resultant polymer confirmed complete retention of norbornene groups throughout the polymerization. Using anionic polymerization, followed by sequential addition of another monomer or end-capping reaction with ethylene oxide,[52] various norbornene-functionalized block copolymers could be produced.

Free radical polymerization of N in toluene using AIBN was quite slow and gave a lower yield compared with the polymerization of styrene, presumably due to the large steric hindrance of monomer N compared with polymerization of styrene. In metathesis polymerization, the low reactivity of the vinyl group caused the formation of branched polymers (see Section 2.2.3.11) and a longer polymerization time yielded insoluble polymers.

Table 2.5. Polymerization reactions of N.

Entry	Scheme	Monomer to initiator molar ratio	M_n (SEC) (kg mol^{-1})	PDI	Yield[b] (%)	T_g (°C)
PN_1	anionic	37	6.7[a]	1.21	100	
PN_2	anionic	40	6.7	1.04	100	81
PN_3	free radical	360	5.4	1.56	10	
PStN	metathesis	340	6.2	2.03	100	

a. SEC of PN_1 indicated bimodal peaks with molecular weight of 6.6 and 13.4 kg mol^{-1} respectively. *b*. Based on the mass of recovered polymers.

2.3.2.4 Controlled free radical copolymerization of N and styrene

In norbornene-functionalized polymers, the number of norbornene groups needs to be tuned in order to control subsequent crosslinking reactions. For this reason, a copolymer of N and styrene is more appealing. The copolymerization of N and styrene following a RAFT scheme was explored using a trithiocarbonate (see Section 2.2.3.12) as the chain transfer agent. Copolymerizations at various feed compositions were carried out to low conversions, and the resultant copolymers were analyzed by ^{1}H NMR spectroscopy to determine the relative amounts of incorporated N and styrene. Specifically, copolymerization reactions were carried out under two different conditions: (1) bulk reaction under positive argon pressure and (2) solution reaction in toluene under reduced pressure. The overall monomer conversions were determined to be lower than 6 wt %, based on the mass of recovered polymers and molecular weight determination through NMR analysis. The mole fraction of N incorporated in the copolymer (F_N) as a function of mole fraction of N in the feed (f_N) is shown in Figure 2.6. These data were fitted using the copolymerization equation (Equation 1),

where r_N and r_S are the reactivity ratios for N and styrene (S), respectively, and determine r_N = 0.72 and r_S = 0.97 (bulk), and r_N = 0.56 and r_S = 0.94 (solution). That r_N is somewhat greater than r_S is consistent with the bulky norbornene substituent in N. The related radical copolymerization of the bulky *p*-n-decylstyrene styrene and styrene showed both reactivity ratios close to 1.[53]

$$F_N = \frac{f_N(r_N f_N + 1 - f_N)}{f_N(r_N f_N + 1 - f_N) + (1 - f_N)(r_S(1 - f_N) + f_N)} \quad \textbf{2.7}$$

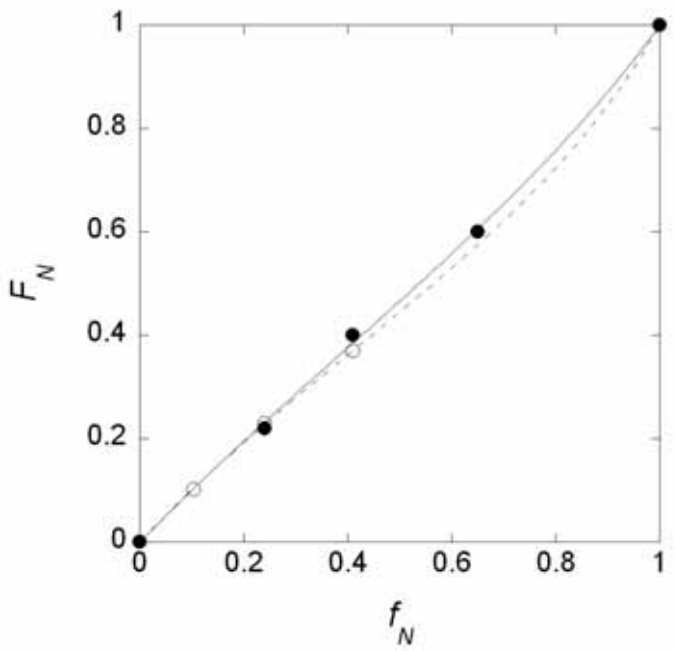

Figure 2.6. The mole fraction of N in the copolymer (F_N) as a function of the mole fraction of N in the feed (f_N) for the RAFT copolymerization of N and S. The filled circles are for the bulk copolymerization (condition 1) and the open circles are for solution polymerization (condition 2). The solid (condition 1) and dashed (condition 2) lines are non-linear fits of the data according to Equation 2.8.

2.3.3 PLA-*b*-P(N-S) block polymers

2.3.3.1 Copolymer synthesis

With knowledge of the copolymerization kinetics of N and styrene, block copolymers were prepared employing a PLA-attached RAFT chain transfer agent (PLA-TC).[30] The synthetic

scheme for PLA-*b*-P(N-*s*-S) copolymers is shown in Scheme 2.7, and characterization of these block copolymers is summarized in Table 2.6.

Table 2.6. Summary of PLA-*b*-P(N-S) synthesized by RAFT polymerization.

Entry	Polymer[a]	M_n (SEC) (kg mol^{-1})	PDI	M_n(NMR)[b] (kg mol^{-1})	f_{PLA}[c] (%)	T_g(PNS) (°C)	N molar ratio Feed	N molar ratio Polymer	Morphology at 140 °C
0	PLATC	13.7	1.09	10.6					
1	NSL(0.11)	23.1	1.27	23.6	39.4	90	0.10	0.11	C+L
2	NSL(0.23)	23.6	1.26	23.0	40.5	86	0.24	0.23	C+L
3	NSL(0.44)	23.2	1.37	23.0	40.5	82	0.41	0.44	C
4	NSL(0.67)	22.4	1.34	22.4	41.7	79	0.65	0.67	C
5	NSL(0.46)	19.9	1.17	19.2	49.3	78	0.41	0.46	L
6	NSL(0.34)	30.4	1.30	30.2	30.9	93	0.32	0.34	C
7	NSL(0.48)	15.0	1.10	13.4	76.0	[d]	0.42	0.48	[d]
8	NSL(1)	21.4	1.19	21.4	43.8	76	1.00	1.000	C
9	NSL(0.31)	21.3	1.20	21.2	44.3	83	0.32	0.31	L
10	NSL(0)	21.4	1.17	21.3	44.0	90	0	0	L

a. Entries 1–7 were synthesized from PLATC, styrene, and N at 120 °C for 4 h via the thermal initiation, while entries 8–10 were prepared in toluene for 20 h at 70 °C initiated by 2,2'-azodiisobutyronitrile. For NSL(x), NSL represents the PLA-*b*-P(N-S) copolymer and x denotes the molar ratio of N in the P(N-S) block. *b*. In NMR analysis, molecular weight of the TC was included in all M_n values, and in entry 0, M_n (PLAOH) = 10.3 kg mol^{-1} *c*. To calculate the PLA volume fraction, the TC group was included as part of the PNS block, and f_{PLA} was based on densities of polymers at 140 °C: ρ(PS) = 0.97 g cm^{-3},[38] ρ(PLA) = 1.154 g cm^{-3},[39] and assuming ρ(PN) = ρ(PS). *d*. Not determined.

SEC traces of the copolymers listed in Table 2.6 showed that these products exhibited narrow molecular weight distributions (Figure 2.7 and Figure 2.8). However, a shoulder with twice the molecular weight of the main peak was apparent with increasing concentrations of N in the feed but became less prevalent at a low reaction temperature, as in NSL(0.31). Additionally, no shoulder was observed in NSL(0) (i.e., no incorporation of N), so the high molecular weight peak in the SEC data was attributed to a minor radical coupling reaction of pendant norbornene groups. Literature indicates that, in a RAFT polymerization using a norbornene-containing initiator, coupling reaction from norbornene groups increased with reaction time.[45] NMR spectra showed an incremental increase of norbornene functionality in

the copolymers. DSC analysis of these copolymers showed two T_gs: one corresponding to the PLA block at 52 °C, and the other one to the P(N-S) block that varied with the N content in the P(N-S) block (see Figure 2.10), consistent with microphase segregation of the PLA and P(N-S) blocks. A statistical distribution of pendant norbornene groups on PS backbone is expected, although composition drift in the batch copolymerizations would lead to P(N-S) blocks with somewhat non-uniform composition distribution along the backbone. Overall, well-defined norbornene-functionalized PLA-based copolymers with tailored N composition were successfully produced.

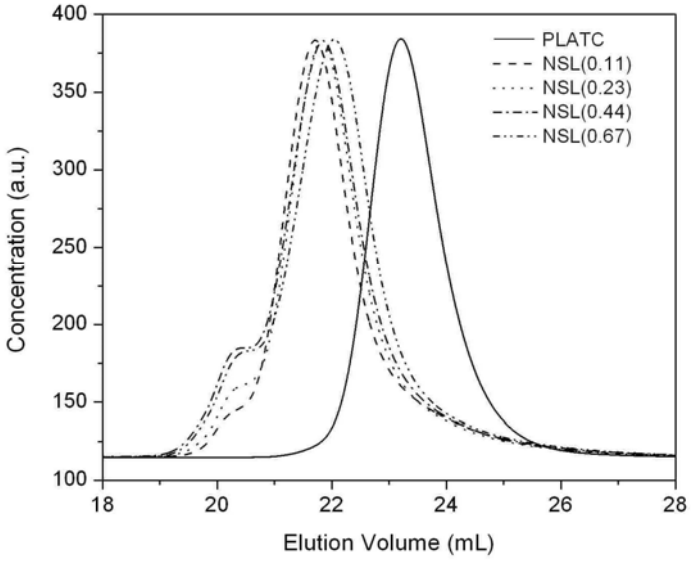

Figure 2.7. SEC curves of PLA-*b*-P(N-S) copolymers produced from bulk RAFT polymerization.

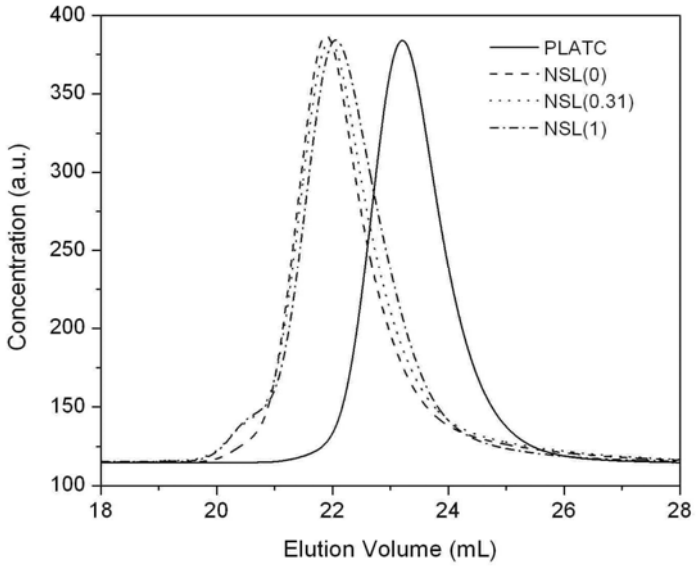

Figure 2.8. SEC curves of PLA-*b*-P(N-S) copolymers produced from RAFT polymerization in toluene.

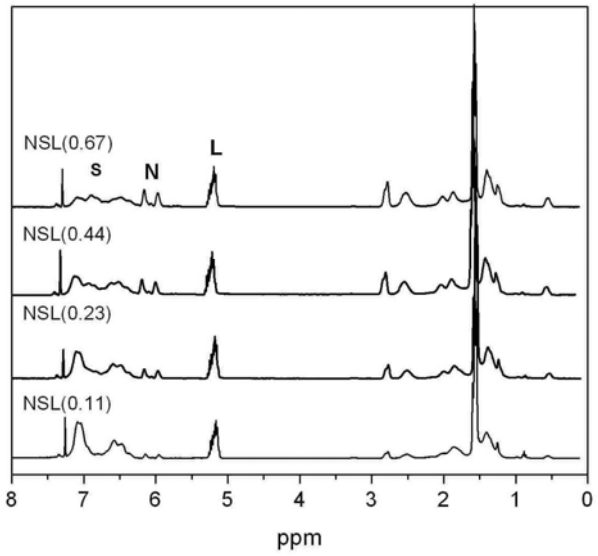

Figure 2.9. NMR spectra of PLA-*b*-P(N-S) copolymers. S, N, and L denote signals relevant to the benzene group, the norbornene group, and -CH group in polylactide, respectively.

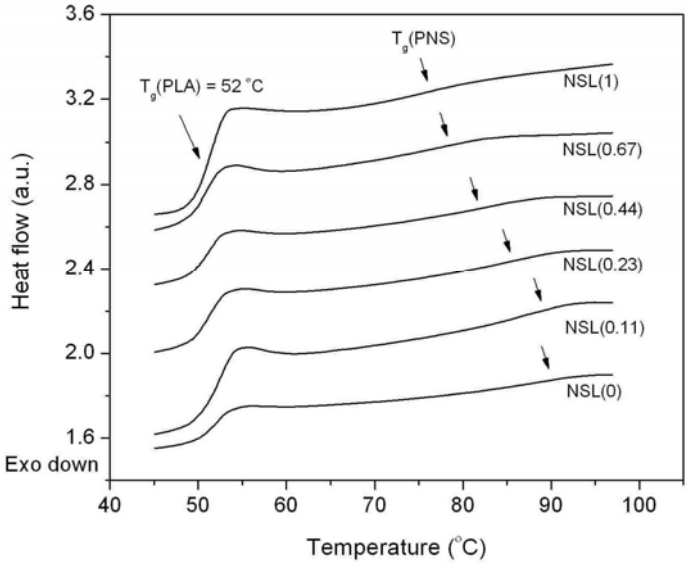

Figure 2.10. DSC traces of PLA-*b*-P(N-S) copolymers (the 2nd heating run), indicating the T_g of PNS block was tuned over 15 °C at different N compositions.

2.3.3.2 SAXS analysis of the PLA-*b*-P(N-S) copolymers

The morphologies of the above PLA-*b*-P(N-S) copolymers were characterized using small angle X-ray scattering (SAXS) (summarized in Table 2.6). The principal scattering peak observed corroborates microphase separation between the P(N-S) and PLA blocks, and higher order reflections imply the long-range order. For instance, NSL(1) exhibited a cylindrical morphology (Figure 2.11). The Flory-Huggins interaction parameter χ in these block copolymers with different norbornene compositions were extracted, based on the temperature dependence of the lamellar or cylindrical domain spacing in the strong-segregation regime ($\chi N > 100$) (equations 2.8 and 2.9).[54] Although equations 2 and 3 were derived for the strong-segregation regime, they have been used in the previous work to provide reasonable estimation of χ for ordered lamellar and cylindrical block copolymers at moderate segregation strengths ($25 < \chi N < 85$).[55]

$$D_{lam} = 1.10 a N^{2/3} \chi_{eff}^{1/6} \quad \textbf{2.8}$$

$$D_{cyl} = 1.12 f^{1/6} (1 + f^{1/2})^{2/3} a N^{2/3} \chi_{eff}^{1/6} \quad \textbf{2.9}$$

$$a = \left(\frac{f_{PLA}}{a_{PLA}^2} + \frac{f_{PNS}}{a_{PNS}^2} \right)^{-0.5} \quad \textbf{2.10}$$

For simplicity, the actual degree of polymerization was used for the number of statistical repeating units N in equations 2.8 and 2.9 even though there would be some quantitative difference between these two values. The average statistical segment length, a, for the block copolymer was calculated using statistical segment lengths for PLA (a_{PLA}) and PS (a_{PS}) of 1.02 nm and 0.71 nm respectively,[8] based on the segment volume of 185 Å^3, assuming $a_{\mathrm{P(N\text{-}S)}}$ was identical to that of PS. f_{PLA} is the volume fraction of PLA and $f_{\mathrm{P(N\text{-}S)}}$ is the volume fraction of P(N-S) block. Based on SAXS measurements, the interaction parameter between the P(N-S) and PLA blocks, χ_{eff}, was obtained by evaluating the principal domain spacing dependence on temperature (Figure 2.12), using PLA-P(N-S) in entries 3, 4, and 6 of Table 1 with cylindrical morphologies, and that in Entry 8 with a lamellar morphology. In the previous work, SAXS analysis of PS-*b*-PLA copolymers indicated $\chi_{PS/PLA}$ = 96.6/T–0.091; herein, $\chi_{PS/PLA}$ = 99.1/T–0.111 was calculated for NSL(0) using equation 2.[8] For NSL(1) having a cylindrical morphology, $\chi_{PN/PLA}$ = 199.1/T–0.174 was obtained using equation 3. Incorporation of hydrophobic pendant norbornene groups led to approximately two-fold increase in segregation strength compared to PS-PLA. Furthermore, the segregation strength between PLA and P(N-S) blocks can be tailored by the level of N incorporation. The group contributions to solubility parameter (Hoy values),[40] δ_{PLA} = 9.8 (cal/cm^3)$^{0.5}$ and δ(PN) = 7.92 (cal/cm^3)$^{0.5}$ (calculation shown in Table 2.7), give a calculated $\chi_{PN/PLA}$ of 181/T using a reference volume of 185 Å^3, in reasonable agreement with the SAXS results.

Table 2.7. Estimation of solubility parameter of PNS.

Group	V_r	F_{Hoy}
5 -CH_2-	16.45×5	133×5
4 –CH=	9.85×4	28×4
-C_6H_4-	61.4	658
-CH=CH-	26	111×2

$$\delta_{PNS} = \frac{\sum F_{Hoy}}{\sum V_r} = 7.92(cal/cm^3)^{0.5}$$

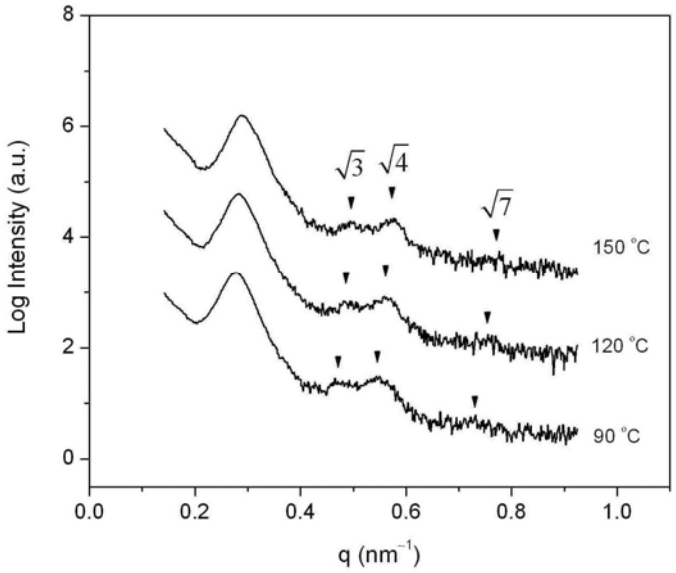

Figure 2.11. SAXS profiles of copolymer NSL(1) at different temperatures. Higher order peaks relative to the principal peak located at $\sqrt{3}$, $\sqrt{4}$, and $\sqrt{7}$ are indicative of a cylindrical morphology.

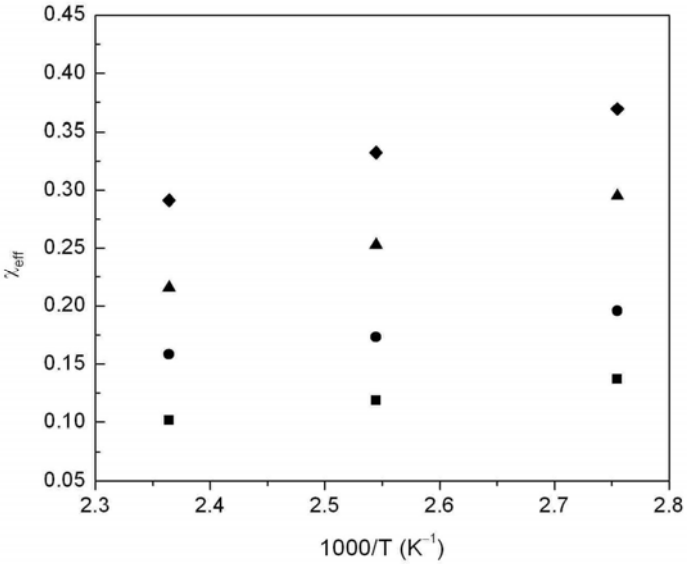

Figure 2.12. Effective Flory-Huggins parameters χ_{eff} of PLA-*b*-P(N-S) copolymers at different temperatures, calculated from fitting the domain spacing (D) determined from SAXS profiles to the copolymer composition. Filled square, circle, triangle, and diamond symbols denote NSL(0), NSL(0.44), NSL(0.67), and NSL(1), respectively.

2.3.4 Preparation of nanoporous monoliths

2.3.4.1 Self-assembly of PLA-*b*-P(N-S)/DCPD blends

For the purposes of crosslinking P(N-S) with DCPD by metathesis reactions, the self-assembly of DCPD and PLA-*b*-P(N-S) mixtures must be addressed. A waxy solid comprised of NSL(0.11) (Entry 1 in Table 2.6) and DCPD at a mass ratio of 2:1 was prepared (see Section 2.2.4.1). DSC analysis of this waxy solid (Figure 2.13) indicates clear shifts of T_g to lower temperatures in both PLA and PNS domains compared to NSL(0.11). Simply treating the changes of T_g using the Fox equation (Equation 2.11),[56] two variables were solved independently: T_g of DCPD and partition of DCPD in two phases. The *w* is the weight fraction of component 1 in the blend.

$$\frac{1}{T_g} = \frac{w}{T_{g1}} + \frac{1-w}{T_{g2}} \qquad \textbf{2.11}$$

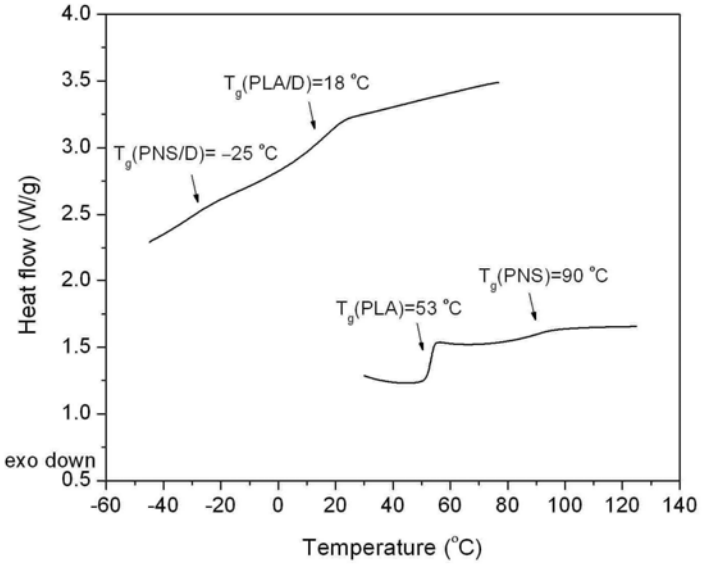

Figure 2.13. DSC traces for NSL (0.11) and a NSL (0.11)/DCPD blend (2:1), respectively.

Based on the calculation using the Fox equation, DCPD was distributed in the PLA and P(N-S) domains at a ratio of 1 to 4, in agreement with the anticipated distribution based on the structural similarity between P(N-S) and DCPD. In the similar way for PLA

aforementioned,[40] the solubility parameter can also be estimated for the PNS block. Thus, $\chi_{PNS/D}$=0.0027 was calculated; experimentally, PNS was miscible with DCPD.

NSL(0.46), in a lamellar morphology (Entry 5 in Table 2.6), was chosen to study the morphology of assembled PLA-*b*-P(N-S)/DCPD mixtures and for subsequent crosslinking reactions. PLA-*b*-P(N-S)/DCPD blends with different PLA volume factions were prepared. The blend composition was determined by ^{1}H NMR spectroscopy. For SAXS analysis, assuming DCPD evaporation was negligible during experiments, a wide region of the cylindrical morphology is evident over a range of temperatures in Figure 2.14; introduction of DCPD in the P(N-S) phase drives the phase transition from lamellae to hexagonally packed cylinders which is the targeted phase for the subsequent crosslinking studies. SAXS profiles of a NSL(0.46)/DCPD blend (f_{PLA}= 30 % by volume) that adopts a cylindrical morphology are shown in Figure 2.15.

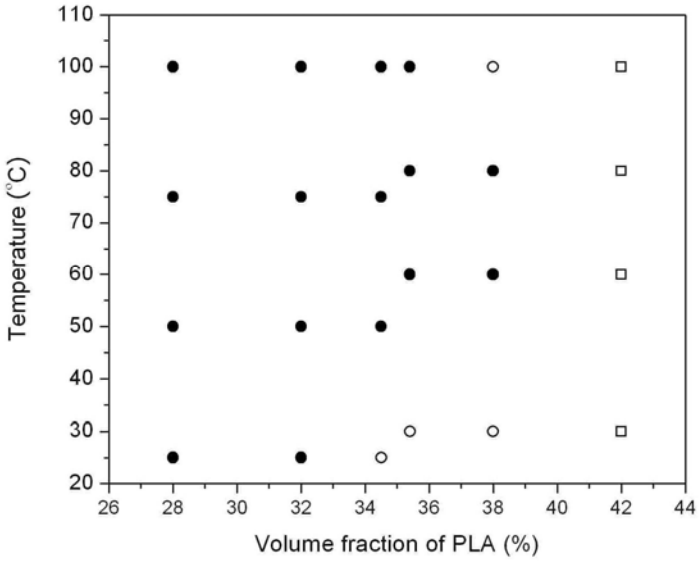

Figure 2.14. Partial morphology map for NSL(0.46)/DCPD blends at different temperatures from SAXS experiments. Filled circle denotes a cylindrical morphology, and open circle and square represent lamellar and unidentified morphologies, respectively. Volume fraction of PLA is calculated assuming densities of PLA and the matrix phase are 1.254[39] and 1.0 g cm^{-3} at RT.

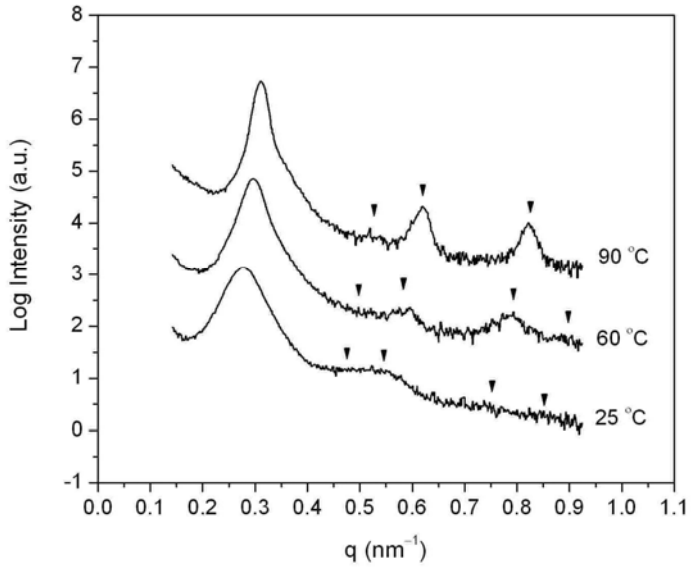

Figure 2.15. Temperature-dependent SAXS profiles of a NSL(0.46)/DCPD blend in a cylindrical morphology (without metathesis catalyst), with the volume fraction of PLA equal to 30 %. Higher order peaks relative to the principal peak located at $\sqrt{3}$, $\sqrt{4}$, $\sqrt{7}$, and $\sqrt{9}$ indicate a cylindrical morphology.

2.3.4.2 Crosslinked monoliths using the precursor catalyst

The crosslinking of PLA-*b*-P(N-S) and DCPD is examined in this section. The catalyst **CP** (Figure 2.1) was chosen for the facile blend preparation. A reactive blend containing NSL(0.34) (0.2 g) and DCPD (0.04 g), and **CP** (9 mg) was prepared. The volume fraction of PLA in the blend was 25.1 %, with residue CH_2Cl_2 of less than 4 wt % in the blend, as found by NMR characterization. Then, the alignment of cylindrical PLA nanodomains was achieved by pressing the blend through a home-made channel die (see Section 2.2.4.2). The prepared samples were then crosslinked in a small sealed tube at 93 °C for 24 h under N_2.

In order to explore the match of reactivity between the reactive monomers and PLA-*b*-PNS by metathesis reactions, three monomers (shown below) besides DCPD were studied in the same blend composition. Resultant monoliths were quite stiff and remained transparent after crosslinking. To evaluate the crosslinking efficiency of these monomers, the sol fractions

were measured by soaking the monoliths in THF overnight and weighing the mass after drying the insoluble component.

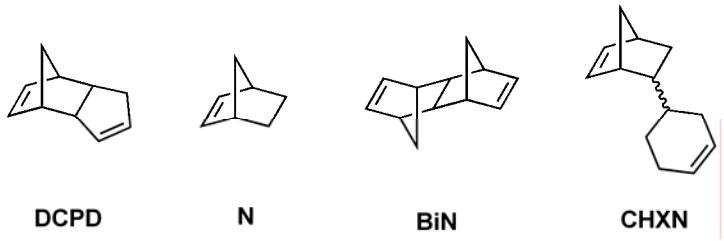

For the crosslinked monoliths produced with DCPD, more than 15 wt % sol fraction resulted, while the sol fraction in the monoliths produced with norbornene was less than 3 wt %. Norbornene was the mostly efficient to crosslink the PNS block, whereas polyDCPD possessed high toughness compared with the other three resultant polymers.

Characterization of the nanoporous monoliths prepared from NSL(0.34) and norbornene is summarized as follows. IR characterization (Figure 2.16) shows the disappearance of the C=O stretching signal at 1750 cm^{-1} after etching PLA, agreeable with nearly complete removal of the PLA component. SAXS characterization (Figure 2.17) confirms the retention of the cylindrical morphology after crosslinking and after PLA degradation. The nanoporous structure is directly visualized by SEM (Figure 2.18), and the pore size of 10 nm agreed with the PLA block size.

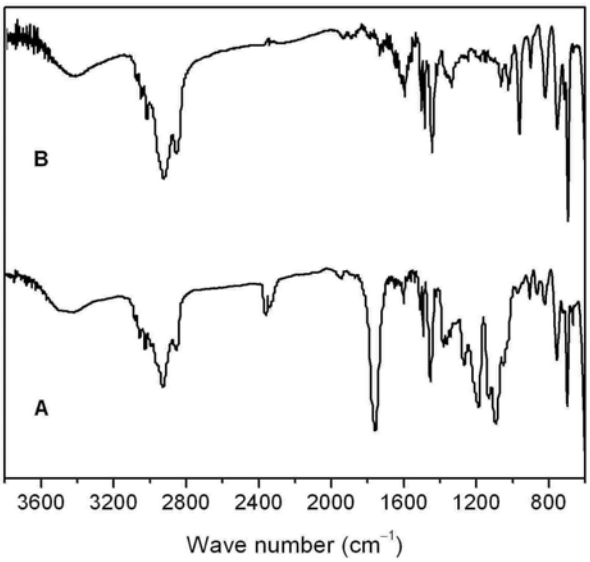

Figure 2.16. Infrared spectra of the crosslinked (A) monoliths prepared from NSL(0.34) and norbornene and the nanoporous (B) monoliths following PLA degradation.

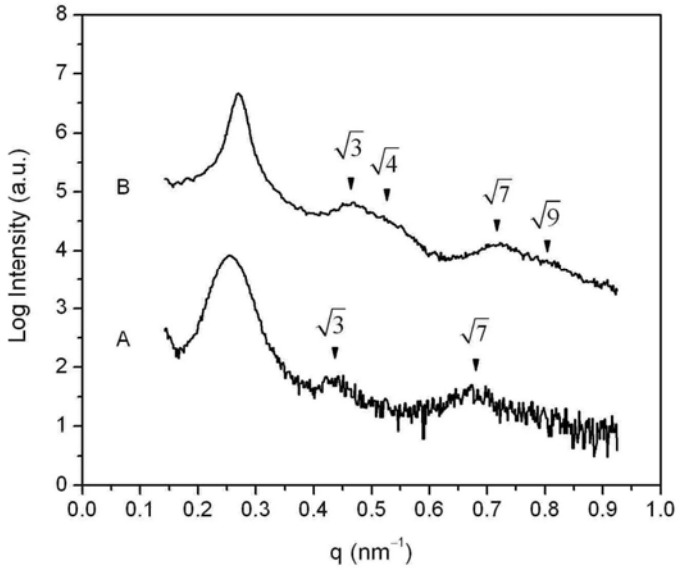

Figure 2.17. SAXS profiles of the crosslinked (A) monoliths prepared from NSL(0.34) and norbornene and the nanoporous (B) monoliths following PLA degradation. Higher order peaks relative to the principal peak located at $\sqrt{3}$, $\sqrt{4}$, $\sqrt{7}$, and $\sqrt{9}$ indicate a cylindrical morphology.

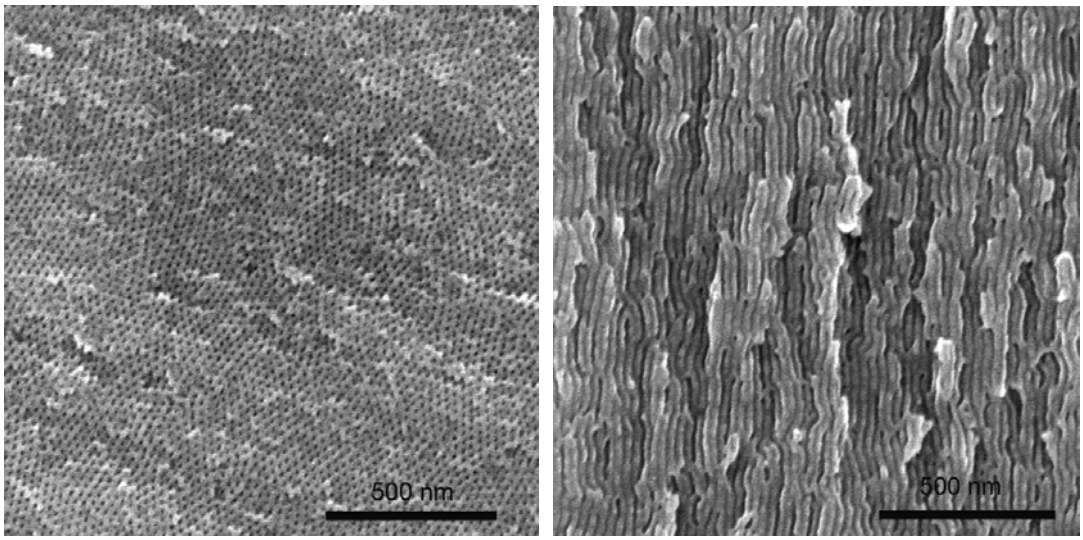

a b

Figure 2.18. SEM images of the nanoporous monoliths prepared from NSL(0.34) and norbornene. a. perpendicular to the cylinders axes; b. parallel to the cylinders axes. The fractured surfaces were coated with 1.5 nm Pt to prevent charging.

Additionally, DSC experiments on the resulting monoliths indicated pore collapses around 100 °C, similar to PS monoliths, and the resulting monoliths were as brittle as uncrosslinked nanoporous PS. Additionally, thermal and mechanical stabilities of crosslinked monoliths containing polyDCPD were also similar to nanoporous PS. One possible explanation is that this precursor catalyst is not efficient enough to achieve high crosslinking density. Besides, high loading of CP (ca. 3 wt %) in these examples is generally unfavorable for monolith fabrication. In sum, metathesis crosslinking reactions of PLA-PNS block polymers and DCPD were successfully demonstrated, but more efficient crosslinking reactions need to be achieved to impart improved thermal and mechanical stabilities in the resulting monoliths.

2.3.4.3 Crosslinked monoliths using the 1st generation Grubbs catalyst

Grubbs catalysts display high reactivity in ROMP. Because of this, incorporation of a Grubbs catalyst (**G1** in Figure 2.1) to the blend resulted in gelation within minutes at RT before removal of the cosolvent for sample preparation. This problem was overcome by addition of PPh_3 to attenuate the catalyst reactivity.[57]

To produce nanoporous monoliths, a NSL(0.46)/DCPD blend with a PLA volume fraction around 30 % was desired. In a prepared NSL(0.46)/DCPD blend containing 0.25 wt % of the 1st generation Grubbs catalyst and 0.75 wt % PPh_3, the ^1H NMR spectrum indicated negligible crosslinking reaction in the resultant waxy orange solid before curing. The DCPD content before crosslinking was 60 wt % relative to the copolymer. A cylindrical morphology was expected given the calculated weight fraction of PLA of 33.5 wt % in this composite (corresponding PLA volume fraction of PLA of 29 % at RT, see Figure 2.14). The waxy solid was aligned through the channel die as previously described (Section 2.2.4.2). After crosslinking, slight mass loss of the blend was apparent due to DCPD evaporation. SAXS analysis indicated that the initial cylindrical morphology was maintained during and after crosslinking. After degradation of PLA, IR spectra (Figure 2.19) showed disappearance of the peak at 1750 cm^{-1} corresponding to C=O stretching, which indicated nearly complete removal of the PLA phase in the crosslinked monoliths. The monoliths lost about 35 wt % of their mass following PLA degradation, slightly higher than the mass fraction of PLA in the composite.

2D SAXS data of the crosslinked samples (Figure 2.20) showed two broad reflection arcs consistent with cylinder orientation in the flow direction. The degree of alignment in nanoporous monoliths (Figure 2.21) was characterized by the second order orientation factor F_2 of 0.83. After PLA removal, the scattering intensity in the monoliths exhibited a 27-fold increase, consistent with the anticipated increase in electron density contrast for a nanoporous sample. The slight shift of the primary peak (q*) to a higher value after PLA removal indicated slight decrease of the domain spacing, which was likely attributed to the slight shrinkage of the crosslinked matrix following PLA hydrolysis. The domain spacing from SAXS of 21.1 nm gave a PLA domain size (pore size) of about 13.8 nm based on the pore volume fraction of 29 %.

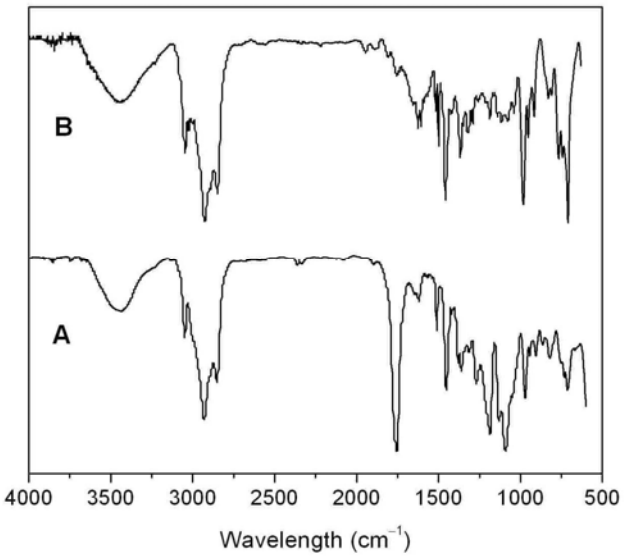

Figure 2.19. IR spectra of crosslinked monoliths prepared from NSL(0.46) and DCPD before (A) and after (B) PLA removal. Moisture in the KBr salt possibly caused the absorption signal around 3500 cm^{-1}.

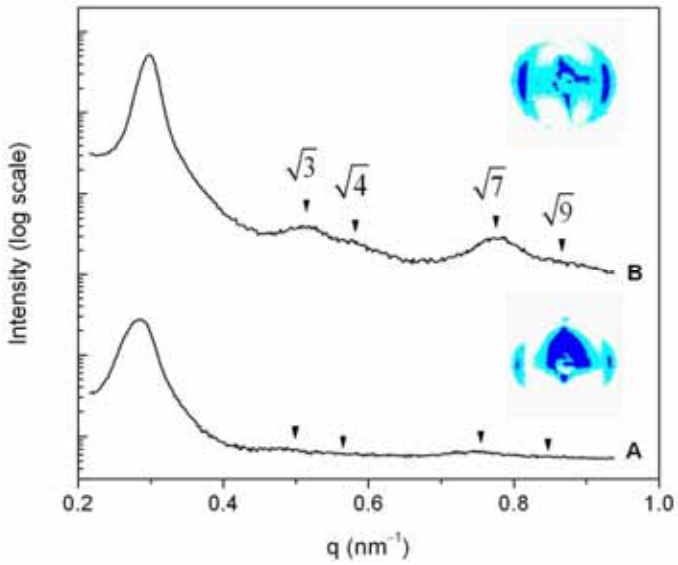

Figure 2.20. SAXS profiles of the crosslinked monoliths prepared from NSL(0.46) and DCPD before (bottom) and after PLA removal (top). The incident X-ray was perpendicular to the cylinders axes. Higher order scattering peaks relative to the principal peak located at $\sqrt{3}$, $\sqrt{4}$, $\sqrt{7}$, and $\sqrt{9}$ indicate a cylindrical morphology.

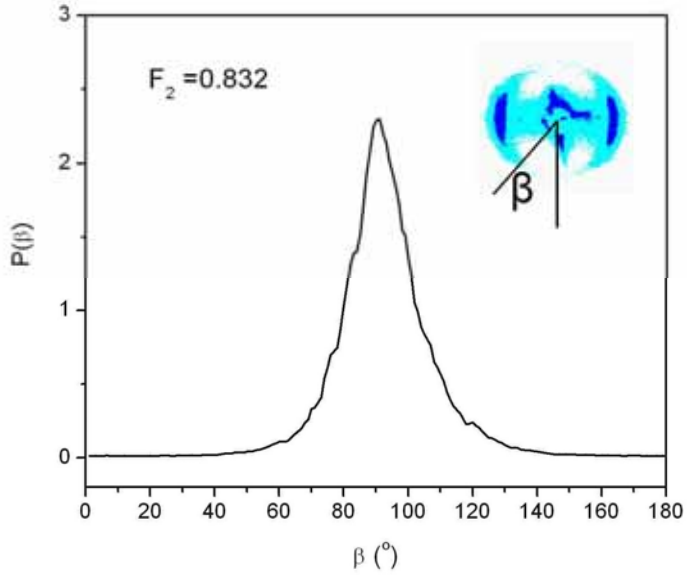

Figure 2.21. Normalized orientation distribution function ($P(\beta)$) for the nanoporous monoliths prepared from NSL(0.46) and DCPD. The azimuthal angle (β) was measured from the direction parallel to the cylinders axes as shown in the inset.

Typical SEM images for fractured surfaces of monoliths in two directions are shown in Figure 2.22: parallel to and normal to the cylinders axes, confirming a structure with an array of hexagonally packed cylindrical pores. Pore diameter determined from SEM image is 11 ± 2 nm (accounting for 1 nm Pt coating). The averaged domain spacing was about 21 ± 2 nm, consistent with the SAXS analysis. In N_2 adsorption experiments, the Brunauer-Emmett-Teller (BET) analysis[24] showed a type IV isotherm and gave a specific surface area of 132 m^2 g^{-1} (Figure 2.23). Analysis of the desorption data gave an average pore diameter of 9.0 nm and a peak width at half height of 3.0 nm. Barrett-Joyner-Halenda (BJH) analysis[24] gave an average pore diameter of 12.5 nm, in agreement with SEM data. The pore diameter calculated from the SAXS (13.8 nm) was somewhat higher than that determined by both SEM and N_2 adsorption analysis. It was suspected this was due to inaccuracies in the estimated density of poly(DCPD)/PS matrix.

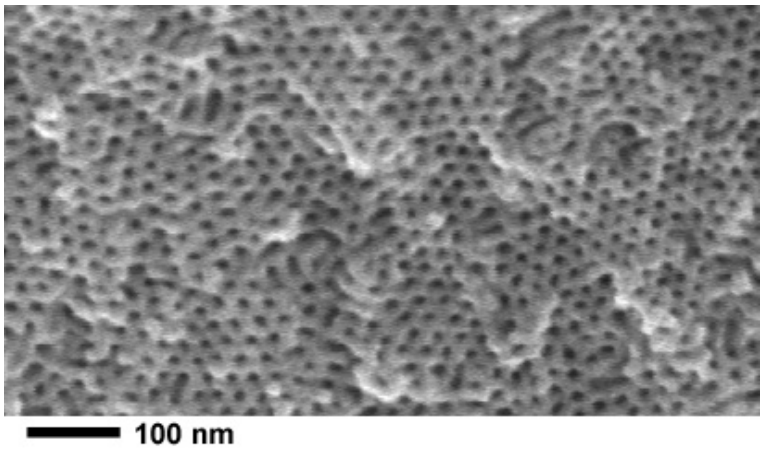

(a)

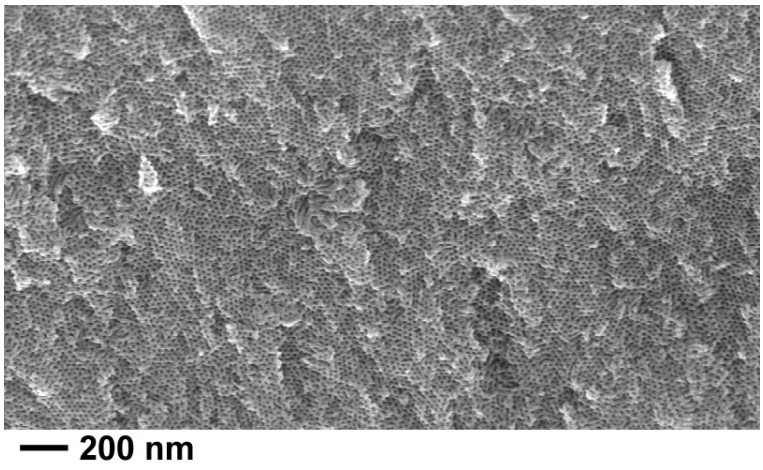

(b)

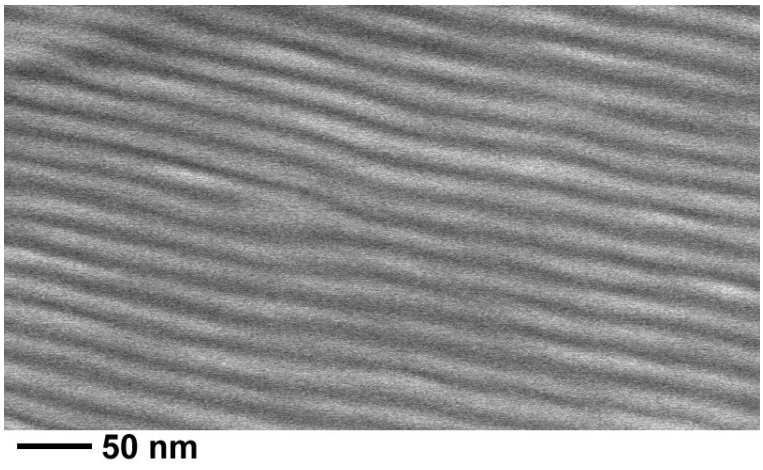

(c)

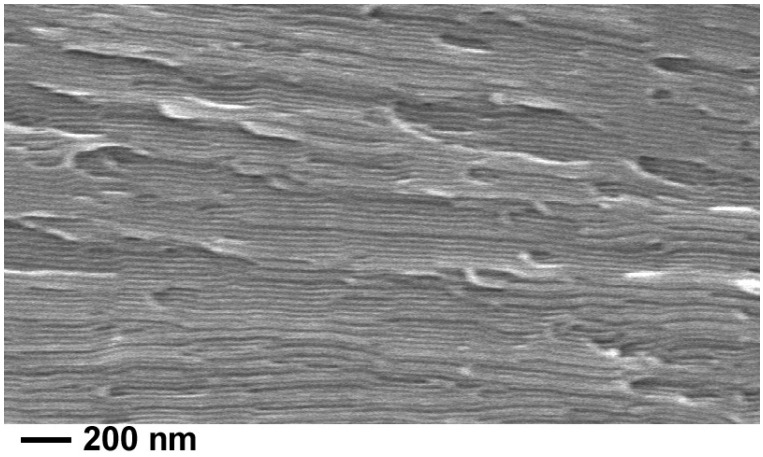

(d)

Figure 2.22. SEM images of the crosslinked nanoporous monoliths prepared from NSL(0.46) and DCPD fractured in two directions: (a) and (b) perpendicular to the cylinders axes; (c) and (d) parallel to the cylinders axes. Samples were cryo-fractured and coated with 1 nm thick Pt via direct sputtering to prevent charging.

In previously reported nanoporous PS monoliths, an exothermic peak in the initial heating trace of the DSC analysis corresponded to the collapse of nanopores above the T_g of PS (100 °C).[8] In the polyDCPD composite monoliths described here, no detectable thermal transition appeared in the DSC thermogram up to 130 °C (Figure 2.24). Furthermore, the nanoporous structure was preserved after heating to 130 °C according to SEM. However, substantial pore collapse was evident after annealing the nanoporous monoliths at 150 °C for 1 h, presumably due to the softening of the polyDCPD-containing matrix (the T_g of polyDCPD is between 140 and 160 °C[33]). The solvent resistance of these monoliths was examined by immersion in THF and subsequently soaking in methanol to allow for plasticization of the polyDCPD-containing matrix before a final drying step, and SEM analysis confirms preservation of the nanoporous structure (Figure 2.25).

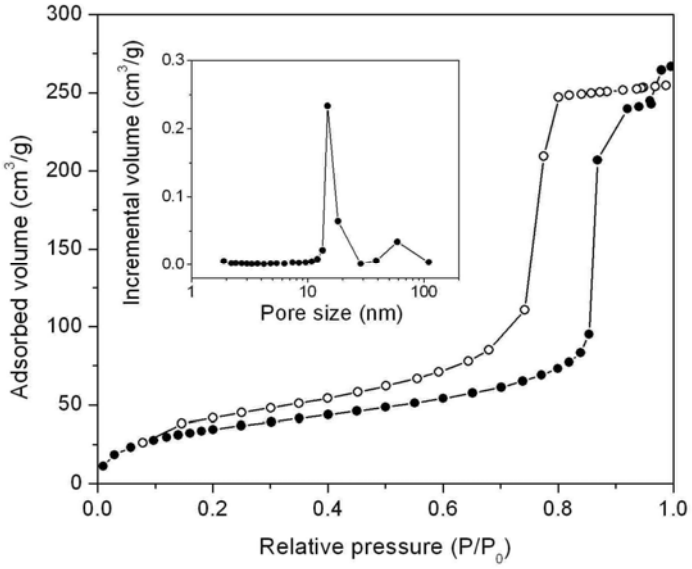

Figure 2.23. Nitrogen adsorption (solid) and desorption (open) isothermal curves of the nanoporous monoliths prepared from NSL(0.46) and DCPD. Inset: pore size distribution calculated from the desorption process.

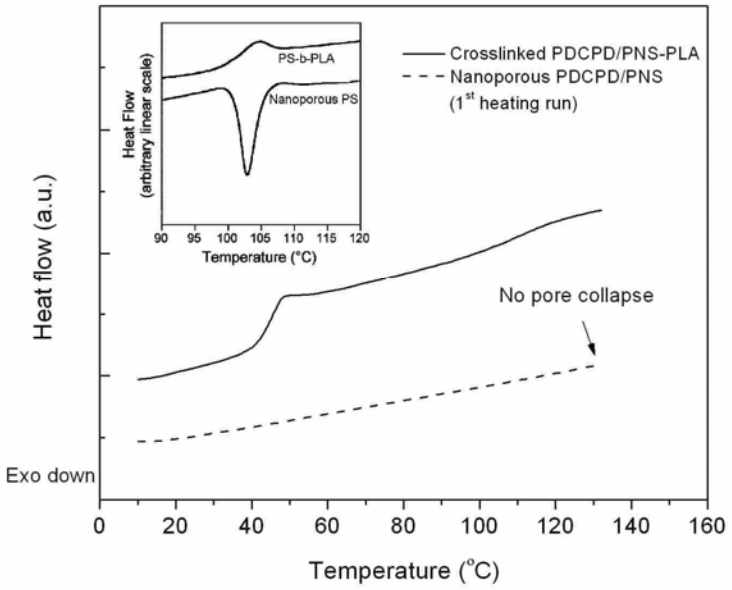

Figure 2.24. DSC traces of crosslinked monoliths prepared from NSL(0.46) and DCPD before and after PLA removal (heating rate: 20 °C/min). Inset: DSC analysis of nanoporous PS where the exothermic peak (the 1st heating run) indicates pore collapse.

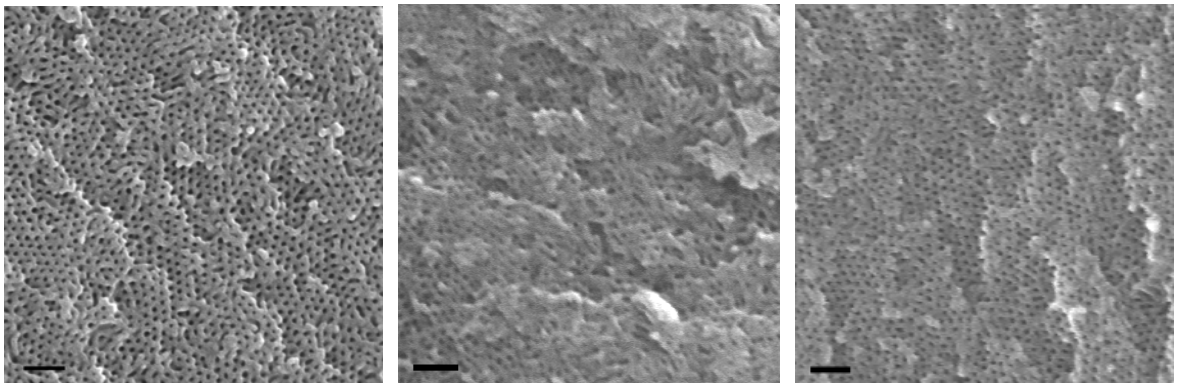

(a) (b) (c)

Figure 2.25. SEM images of fractured nanoporous monoliths prepared from NSL(0.46) and DCPD after annealing for 1 h at 130 °C (a), after annealing at 150 °C (b), and after soaking in THF (monoliths were slowly dried after soaking in methanol to plasticize the monoliths) (c). Samples were coated with 1 nm Pt to prevent charging. (The scale bars are 100 nm)

The mechanical properties of the composite nanoporous monoliths were evaluated by tensile testing with extension parallel to the channel direction (Figure 2.26). The average tensile strength of the resulting crosslinked samples (ca. 90 MPa) was higher than pure crosslinked polyDCPD plastics (55 MPa), which is likely attributed to higher crosslinking density by incorporation of the reactive P(N-S) blocks. For the nanoporous samples, the average elongation at break was about 10 % and the average tensile strength was about 50 MPa, significantly improved in comparison to uncrosslinked nanoporous PS, which was too brittle to be appropriately loaded in the same test. Without DCPD, self-assembled PLA-*b*-PNS could be crosslinked by the metathesis scheme, but the resultant monoliths were as brittle as PS-PLA, likely due to the limited crosslinking density.

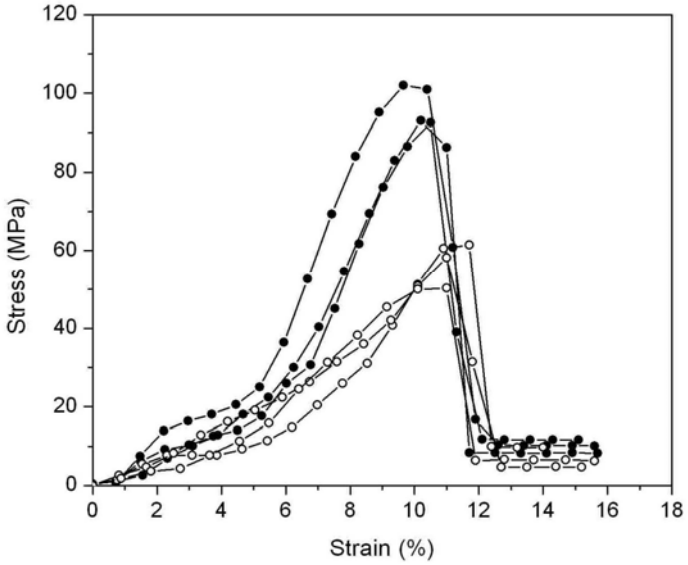

Figure 2.26. Tensile curves of crosslinked monoliths prepared from NSL(0.46) and DCPD before (solid) and after (open) PLA degradation.

2.3.5 Stabilities for nanoporous polymers

Incorporation of a robust polymer into the nanoporous monoliths by crosslinking reactions would not only enhance the mechanical toughness but also result in increased thermal stability. For nanoporous polymers, the thermal stability of nanopores is a critical aspect. Previous work has indicated that the thermal stability of nanopores was closely related to the modulus of the matrix.[10]

Nanoporous monoliths are known to be unstable as the temperature approaches the T_g of the matrix because the polymer softening leads to pore collapse. This phenomenon can be rationalized by using the concept of Laplace pressure caused by the curved surface of nanopores. Assuming an air channel (radius R) sealed in a polymer matrix, P_1 is the air pressure inside the air channel; P_2 is the required pressure inside the matrix to sustain the air channel

$$P_2=P_1+ 2\gamma/R \qquad \textbf{2.12}$$

where the γ is the polymer surface tension (surface energy per unit area) and $2\gamma/R$ is defined

as Laplace pressure. When the matrix is soft or the channel radius is small, the modulus in the polymer matrix may not be capable of supporting the air channel, so the air channel can be excluded from the matrix to minimize the surface energy. The stability limit of nanopores has been defined below[58]

$$\frac{2ER}{3\gamma} > 1 \qquad \textbf{2.13}$$

where E and R denote the Young's modulus of the polymer matrix and the radius of the void, respectively. Overall, increasing the modulus of the matrix will help stabilize nanopores. Crosslinking reactions are efficient to stabilize nanopores because chemically tying polymer chains inhibits the flow of polymers and increase the module of the matrix phase. As an example, crosslinking a self-assembled rubbery copolymer like PI-PLA should give a modulus necessary to stabilize the structure after removing the PLA component. For nanopores of 13 nm in diameter, based on Equation 2.13, the modulus must be greater than 7.4 MPa to prevent pore collapse. Consequently, the maximum molecular weight between crosslinkers allowed at RT was 900 g mol^{-1}.[10]

2.3.6 Bicontinuous morphology in crosslinked monoliths

Nanoporous monoliths with aligned cylindrical pores were thermally robust, mechanically strong and exhibited exceptional solvent resistance. Applications of such nanoporous monoliths include the use as catalyst supports. For filtration applications, a 3D continuous morphology is preferred, as 1D nanoporous monoliths are limited by the long-range alignment of nanochannels. Theoretically, a gyroid morphology could be achieved in the pre-assembled blend based on a related example. In the previous phase map (Figure 2.14) for blends of NSL(0.46) and DCPD, the gyroid phase was not observed. The gyroid phase might exist in a narrow range of compositions or at high temperatures. Therefore, preparing new blends using a lower molecular copolymer like NSL(0.48) (reduce χN) might make achieving the gyroid phase possible. Blends containing 40 to 55 wt % NSL(0.48) in DCPD were

prepared following the standard procedure, and characterized by SAXS. As shown in Figure 2.27, lower order-disorder transition temperatures (below 100 °C) are achieved as anticipated, and a narrow gyroid phase window is observed. SAXS profiles of a NSL(0.48)/DCPD blend with f_{PLA}=36.3 % are shown in Figure 2.28.

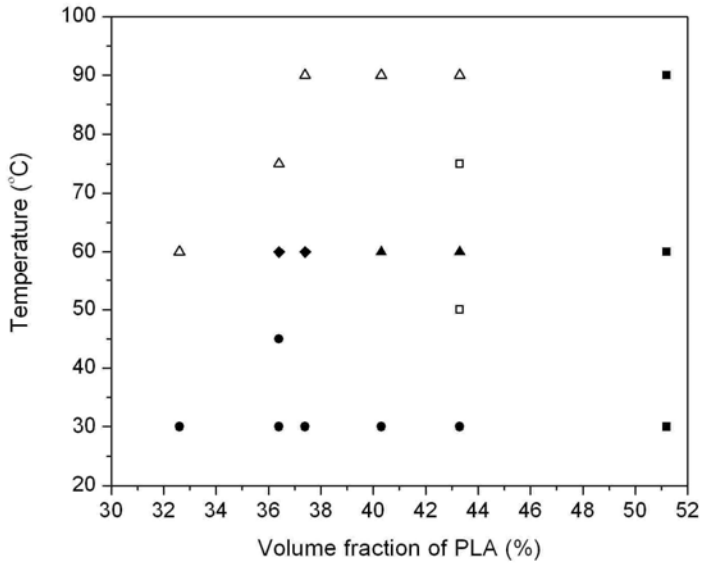

Figure 2.27. Phase map of NSL (0.48)/DCPD blends characterized by SAXS experiments. Open triangle, open square, filled triangle, filled square, and filled diamond denote a disordered phase, an unidentified phase, a lamellar/cylindrical mixture phase, a cylindrical phase, and a gyroid phase, respectively.

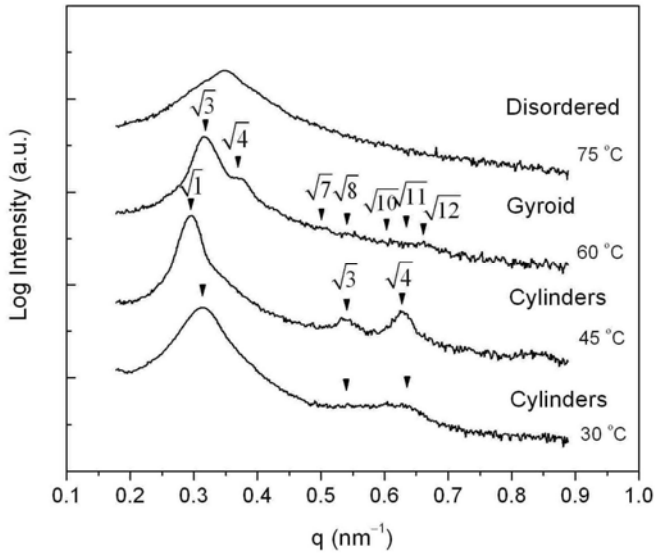

Figure 2.28. SAXS profiles of a NSL(0.48)/DCPD blend with f_{PLA}=36.3 %. The scattering curves are indexed with the predicted peak positions in a cylinder or gyroid morphology.

In further experiments, a blend with a gyroid morphology was prepared in the presence **G1** and PPh_3 (0.5 wt % and 1.5 wt % in the blend respectively). After crosslinking the blend at 60 °C for 0.5 h before the blend was sufficiently crosslinked, the morphology of the blend shifted from gyroid to cylinders. Due to the narrow gyroid phase window, slight evaporation of DCPD or the density change during polymerization could significantly affect the blend morphology; in previous examples, the broad cylindrical phase was less affected. In the future, to avoid the potential heat-induced change of morphology, a new metathesis catalyst that gave high reactivity at RT triggered by UV irradiation[59] may be beneficial for the crosslinking process.

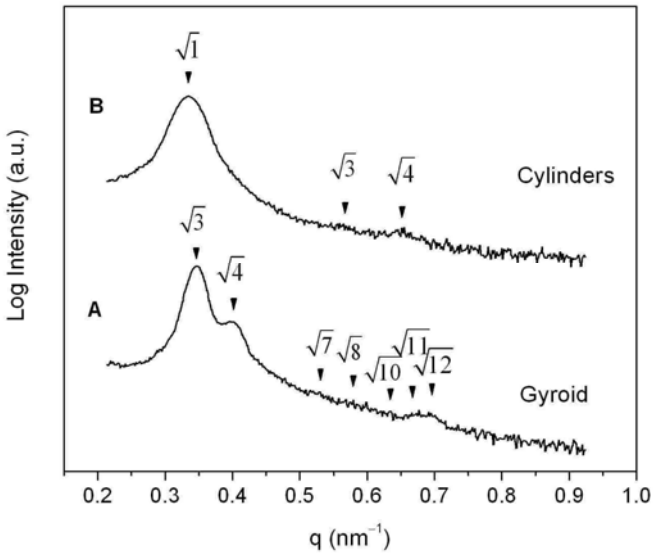

Figure 2.29. SAXS profiles of a prepared NSL(0.48)/DCPD blend with a gyroid morphology before crosslinking (A) and a blend after reacting at 60 °C for 0.5 h (B). The scattering peaks are in agreement with the predicted peaks for a cylinder or gyroid morphology.

2.4 Conclusions and outlook

A new norbornene-functionalized styrene monomer was prepared, and the synthesis of PLA-*b*-P(N-S) block copolymers containing tailored norbornene functionality was demonstrated. DSC and SAXS analysis of these materials confirmed that these block polymers adopted morphologies consistent with their compositions. Crosslinked nanoporous monoliths were produced via metathesis reactions from a pre-assembled reactive blend containing DCPD templated by block copolymers. These monoliths have excellent thermal and mechanical stability and solvent resistance. This approach shows the utility of metathesis chemistry to generate robust nanoporous materials, which are potentially favorable for catalyst supports and other applications. This new method for preparing nanoporous polymers will significantly broaden their applicability.

2.5 References

[1] Lee, J. S.; Hirao, A.; Nakahama, S. *Macromolecules* **1988**, *21*, 274–276.

[2] (a) Zalusky, A. S.; Olayo-Valles, R.; Taylor, C. J.; Hillmyer, M. A. *J. Am. Chem. Soc.* **2001**, *123*, 1519–1520. (b) Mao, H.; Hillmyer, M. A. *Macromolecules* **2005**, *38*, 4038–4039.

[3] Jeong, U.; Kim, H.-C.; Rodriguez, R. L.; Tsai, I. Y.; Stafford, C. M.; Kim, J. K.; Hawker, C. J.; Russell, T. P. *Adv. Mater*. **2002**, *14*, 274–276.

[4] (a) Thurn-Albrecht, T.; Schotter, J.; Kastle, G. A.; Emley, N.; Shibauchi, T.; Krusin-Elbaum, L.; Guarini, K.; Black, C. T.; Tuominen, M. T.; Russell, T. P. *Science* **2000**, *290*, 2126–2129. (b) Johnson, B. J. S.; Wolf, J. H.; Zalusky, A. S.; Hillmyer, M. A. *Chem. Mater*. **2004**, *16*, 2909–2917. (c) Tseng, W.-H.; Chen, C.-K.; Chiang, Y.-W.; Ho, R.-M.; Akasaka, S.; Hasegawa, H. *J. Am. Chem. Soc.* **2009**, *131*, 1356–1357. (d) Zschech, D.; Kim, D. H.; Milenin, A. P.; Scholz, R.; Hillebrand, R.; Hawker, C. J.; Russell, T. P.; Steinhart, M.; Gosele, U. *Nano Lett.* **2007**, *7*, 1516–1520. (e) Crossland, E. J. W.; Ludwigs, S.; Hillmyer, M. A.; Steiner, U. *Soft Matter* **2007**, *3*, 94–98.

[5] (a) Yang, S. Y.; Ryu, I.; Kim, H. Y.; Kim, J. K.; Jang, S. K.; Russell, T. P. *Adv. Mater.* **2006**, *18*, 709–712. (b) Phillip, W. A.; Rzayev, J.; Hillmyer, M. A.; Cussler, E. L. *J. Membrane Sci.* **2006**, *286*, 144–152. (c) Yang, S. Y.; Park, J.; Yoon, J.; Ree, M.; Jang, S. K.; Kim, J. K. *Adv. Funct. Mater.* **2008**, *18*, 1371–1377.

[6] (a) Walheim, S.; Schaffer, E.; Mlynek, J.; Steiner, U. *Science* **1999**, *283*, 520–522. (b) Joo, W.; Park, M. S.; Kim, J. K. *Langmuir* **2006**, *22*, 7960–7963.

[7] Wolf, J. H.; Hillmyer, M. A. *Langmuir* **2003**, *19*, 6553–6560.

[8] Zalusky, A. S.; Olayo-Valles, R.; Wolf, J. H.; Hillmyer, M. A. *J. Am. Chem. Soc.* **2002**, *124*, 12761–12773.

[9] (a) Drockenmuller, E.; Li, L. Y. T.; Ryu, D. Y.; Harth, E.; Russell, T. P.; Kim, H-C.; Hawker, C. J. *J. Polym. Sci. A: Polym. Chem.* **2005**, *43*, 1028–1037. (b) Leiston-Belanger, J. M.; Russell, T. P. Drockenmuller, E.; Hawker, C. J. *Macromolecules* **2005**, *38*, 7676–7683.

[10] Cavicchi, K. A.; Zalusky, A. S.; Hillmyer, M. A.; Lodge, T. P. *Macromol. Rapid Commun.* **2004**, *25*, 704–709.

[11] Guo, F.; Andreasen, J. W.; Vigild, M. E.; Ndoni, S. *Macromolecules* **2007**, *40*, 3669–3675.

[12] Zhou, N.; Bates, F. S.; Lodge, T. P. *Nano. Lett.* **2006**, *6*, 2354–2357.

[13] Uehara, H.; Yoshida, T.; Kakiage, M.; Yamanobe, T.; Komoto, T.; Nomura, K.; Nakajima, K.; Matsuda, M. *Macromolecules* **2006**, *39*, 3971–3974.

[14] Jones, B. H.; Lodge, T. P. *J. Am. Chem. Soc.* **2009**, *131*, 1676–1677.

[15] Bluemle, M. J.; Fleury, G.; Lodge, T. P.; Hillmyer, M. A.; Bates, F. S. *Soft Matter* **2009**, *5*, 1587–1590.

[16] Bluemle, M. J. *et al.* unpublished results.

[17] (a) Hillmyer, M. A.; Lipic, P. M.; Hajduk, D. A.; Almdal, K.; Bates, F. S. *J. Am. Chem. Soc*. **1997**, *119*, 2749–2750. (b) Grubbs, R. B.; Dean, J. M.; Broz, M. E.; Bates, F. S. *Macromolecules* **2000**, *33*, 9522–9534.

[18] Carter, K. R.; DiPietro, R. A.; Sanchez, M. I.; Russell, T. P.; Lakshmanan, P. McGrath, J. E. *Chem. Mater.* **1997**, *9*, 105–118.

[19] Trimmer, M. S. In *Handbook of Metathesis*; Grubbs, R. H., Ed.: Wiley-VCH: Weinheim, **2003**; Vol. 3, 407– 418.

[20] Pangborn, A. B.; Giardello, A.; Grubbs, R. H.; Rosen, R. K.; Timmers, F. J. *Organometallics* **1996**, *15*, 1518–1520.

[21] Roe, R. J. *Methods of X-ray and Neutron Scattering in Polymer Science, Topics in Polymer Science*; Oxford University Press: New York, **2000**.

[22] deGennes, P. G.; Prost, J. *The Physics of Liquid Crystals*; Oxford University Press: New York, **1993**.

[23] Mao, H. Ph.D. thesis "Nanoporous Polymers with Functionalized 1D and 3D Channels from Ordered Block Copolymer Templates", University of Minnesota, **2006**, Chapter 2.

[24] Gregg, S. J.; Sing, K. S. W. *Adsorption, Surface Area and Porosity*; Academic Press: London, **1982**.

[25] Brunauer, S.; Emmett, P. H.; Teller, E. *J. Am. Chem. Soc.* **1938**, *60*, 309–319.

[26] Barrett, E. P.; Joyner, L. G.; Halenda, P. P. *J. Am. Chem. Soc.* **1951**, *73*, 373–380.

[27] Wang, Y.; Hillmyer, M. A. *Macromolecules* **2000**, *33*, 7395–7403.

[28] Bennett, M. A.; Smith, A. K. *J. Chem. Soc., Dalton Trans.***1974**, 233–241.

[29] Lai, J. T.; Filla, D.; Shea, R. *Macromolecules* **2002**, *35*, 6754–6756.

[30] Rzayev, J.; Hillmyer, M. A. *Macromolecules* **2005**, *38*, 3–5.

[31] Willy, W. E.; McKean, D. R.; Garcia, B. A. *Bull. Chem. Soc. Jpn.* **1976**, *49*, 1989–1995.

[32] Dolman, S. J.; Hultzsch, K. C.; Pezet, F.; Teng, X.; Hoveyda, A. H.; Schrock, R. R. J. *Am. Chem. Soc.* **2004**, *126*, 10945–10953.

[33] Kelsey, D. R.; Chuan, H. H.; Ellison, R. H. *J. Polym. Science A: Polym. Chem.* **1997**, *35*, 3049–3063.

[34] Stille, J. K.; Frey, D. A. *J. Am. Chem. Soc.* **1959**, *81*, 4273-4275.

[35] Stubbs, L. P.; Weck, M. *Chem. Eur. J.* **2003**, *9*, 992–999.

[36] (a) Lai, C.; Russel, W. B.; Register, R. A. *Macromolecules* **2002**, *35*, 841–849. (b) Ding, J.; Carver, T. J.; Windle, A. H. *Comp. Theo. Polym. Sci.* **2001**, *11*, 483–490.

[37] Lodge, T. P.; Pudil, B.; Hanley, K. J. *Macromolecules* **2002**, *35*, 4707–4717.

[38] Fetters, L. J.; Lohse, D. J.; Richter, D.; Witten, T. A.; Zirkel, A. *Macromolecules* **1994**, *27*, 4639–4647.

[39] Witzke, D. R.; Narayan, R.; Kolstad, J. J. *Macromolecules* **1997**, *30*, 7075–7085.

[40] Du, Y.; Xue, Y.; Frisch, H. L. in *Physical Properties of Polymers Handbook*; Mark, J. E. *Ed*; AIP Press, **1996**, Chapter 16, Page 232.

[41] Lodge, T. P.; Hanley, K. J.; Pudil, B.; Alahapperuma, V. *Macromolecules* **2003**, *36,* 816–822.

[42] Davidson, T. A.; Wagener, K. B.; Priddy, D. B. *Macromolecules* **1996**, *29*, 786–788.

[43] Hafner, A.; Mühlebach, A.; van der Schaaf, P. A. *Angew. Chem. Int. Ed. Engl.* **1997**, *36*, 2121–2124.

[44] Runge M. B.; Dutta, S.; Bowden, N. B. *Macromolecules* **2006**, *39*, 498–508.

[45] Patton, D. L.; Advincula, R. C. *Macromolecules* **2006**, *39*, 8674–8683.

[46] Cheng, C.; Yang, N.-L. *Macromol. Rapid Commun.* **2005**, *26*, 1395–1399.

[47] Detrembleur, C.; Jérôme, C.; Claes. M.; Louette, P.; Jérôme, R. *Angew. Chem. Int. Ed.* **2001**, *113*, 1308–1311.

[48] (a) Hirao, A.; Loykulnant, S.; Ishizone, T. *Prog. Polym. Sci.* **2002**, *27*, 1399–1471. (b) Hawker, C. J.; Bosman, A. W.; Harth, E. *Chem. Rev.* **2001**, *101*, 3661–3688. Matyjaszewski, K. *Current Org. Chem.* **2002**, *6*, 67–82. (c) Le, T. P.; Moad, G.; Rizzardo, E.; Thang, S. H. PCT Int. Appl. WO 9801478 A1 980115.

[49] (a) Robello, D. R.; Levy, D. H.; Reynolds, J. H.; Southby, D. T.; Twist, S. L. *Macromolecules* **2006**, *39*, 5686–5695. (b) Yamada, S.; Mrozek, T.; Rager, T.; Owens, J.; Rangel, J.; Willson, C. G. M*acromolecules* **2004**, *37*, 377–384. (c) Wang, S.; Li, X.; Xun, S.; Wan, X.; Wang, Z. Y. *Macromolecules* **2006**, *39*, 7502–7507. (d) Mitsukami, Y.; Donovan, M. S.; Lowe, A. B.; McCormick, C. L. *Macromolecules* **2001**, *34*, 2248–2256. (e) Gortz, V.; Ritter, H. *Macromolecules* **2002**, *35*, 4258–4265. (f) Hashimoto, K.; Ohsawa, R.; Imai, N.; Okada, M. *J. Polym. Sci. A: Polym. Chem.* **1999**, *37*, 303–312.

[50] (a) Zhang, H.; Ruckenstein, E. *Macromolecules* **1999**, *32*, 5495–5500. (b) O'Reilly, R. K.; Joralemon, M. J.; Hawker, C. J.; Wooley, K. L. *Chem. Eur. J.* **2006**, *12*, 6776–6786. (c) Trakhtenberg, S.; Warner, J. C.; Nagarajan, R.; Bruno, F. F.; Samuelson, L. A.; Kumar, J. *Chem. Mater.* **2006**, *18*, 2873–2878.

[51] Mirviss, S. B. *J. Org. Chem.* **1989**, *54*, 1948–1951.

[52] Hillmyer, M. A.; Bates, F. S. *Macromolecules* **1996**, *29*, 6994–7002.

[53] Buckley, D. A.; Augostini, P. P. *J. Appl. Polym. Sci.* **1979**, *23*, 311–314.

[54] (a) Leibler, L. *Macromolecules* **1980**, *13*, 1602–1617. (b) Matsen, M. W., Bates, F. S. *J. Chem. Phys.* **1997**, *106*, 2436–2448.

[55] Ren, Y.; Lodge, T. P.; Hillmyer, M .A. *Macromolecules* **2002**, *35*, 3889–3894.

[56] Couchman, P. R. *Macromolecules* **1978**, *11*, 1156–1161.

[57] Sanford, M. S.; Love, J. A.; Grubbs, R. H. *J. Am. Chem. Soc.* **2001**, *123*, 6543–6554.

[58] Muralidharan, V.; Hui, C.-Y. *Macromol. Rapid Commun*. **2004**, *25*, 1487–1490.

[59] Keitz, B. K.; Grubbs, R. H. *J. Am. Chem. Soc.* **2009***, 131*, 2038–2039.

Chapter 3

Robust Nanoporous Membranes Templated by a Doubly Reactive Block Copolymer[a]

This chapter illustrates the polymerization induced phase separation during the ring-opening metathesis polymerization (ROMP) of dicyclopentadiene (DCPD) in the presence of the poly(norbornenylethylstyrene-styrene)-*b*-polylactide (PNS-*b*-PLA) copolymer. Upon etching the PLA component, the resulting nanoporous materials with percolated nanopores exhibit striking thermal and mechanical stabilities. Preliminary water diffusion measurements (e.g., flux and molecular weight cutoff) demonstrate potential utility of such membranes for ultrafiltration. Lastly, preliminary mechanistic investigation of the structure formation is performed.

3.1 Bicontinuous morphologies in block copolymer systems

Nanoporous membranes are useful for separation applications like water ultrafiltration and virus filtration. A continuous porous structure is crucial for such applications, in order to realize fast mass transport. For most commercial membranes, a continuous porous structure is produced via a phase inversion process by adding a poor solvent into a polymer solution, where the polymer precipitates out in a gradient porous phase.[1] Nevertheless, this process commonly resulted in wide pore size distributions, which may cause severe deficiencies in size-selective separations. As discussed in Chapter 1, incorporation of block copolymers in the phase inversion process has demonstrated the ability of reducing the pore size.[2] Alternatively, selectively etching one block in self-assembled block polymers gives rise to well-defined nanoporous membranes with fine control of pore size and pore volume.[3] Hexagonally packed cylindrical nanopores can be ideal for filtration separations, but uninterrupted connectivity of nanochannels across a macroscopically film requires the alignment of defect-free domains and is experimentally challenging. Bicontinuous nanopores[b] in the range of 10–100 nm can be facilely produced using the copolymer strategy. Specifically, production of 3D nanopores from block copolymer precursors can be categorized into the following three schemes.

First, self-assembly of diblock or triblock polymers in bulk yields ordered 3D continuous morphologies, such as the gyroid morphology in diblock copolymers, a double core-shell gyroid morphology in triblock terpolymers.[4] Nanoporous materials in the gyroid morphology have been produced through selectively removing a sacrificial block, for example, nanoporous polystyrene (PS) from PS-polylactide (PLA)[5] and nanoporous poly(4-fluorostyrene) (PFS) from PFS-PLA.[6] Similarly, a nanoporous ceramic film was fabricated from a polyisoprene (PI)-*b*-poly(pentamethyldisilylstyrene)-*b*-PI triblock terpolymer by selectively etching the PI phase.[7] The resultant film possessed continuous

[b] Both the porous and matrix domains are interconnected in 3 dimensions.

nanopores and could be useful for membrane applications. The gyroid morphology has also been demonstrated both theoretically[8] and experimentally[9] in copolymers/homopolymer blends. The gyroid morphology could be obtained by adding a small amount of homopolymer (PA) into the minority domain (PA) of a diblock copolymer (PA-PB) at certain compositions. In this approach, nanoporous membranes have been similarly fabricated by selectively etching away one block, for example, nanoporous poly(4-vinylpyridine) (P4VP) membranes produced from a P4VP-*b*-PI/PI blend.[10]

Second, a bicontinuous phase has been widely observed in a ternary microemulsion blend of water, oil, and a surfactant (e.g., sodium dodecyl sulfate (SDS), poly(ethylene oxide)-poly(propylene oxide)-poly(ethylene oxide) (PEO-PPO-PEO)) at appropriate compositions.[11] Mimicking the oil/water microemulsions, polymer blends containing a diblock polymer and two homopolymers have exhibited the same bicontinuous structure with a natural length scale in the range of 10–100 nm, for example, PEO /poly(ethylene-propylene) (PEP)/PEO-PEP,[12] polybutadiene (PBD)/polyisobutene (PIB)/ PB-PIB,[13] and poly(ethyl ethylene)(PEE)/polydimethylsiloxane (PDMS)/PEE-PDMS.[14] Similar to the gyroid phase, the bicontinuous microemulsion phase, where two polymer domains were interwoven, is thermodynamically stable but possesses no higher order symmetries. Notably, the bicontinuous microemulsion phase is easier to achieve than the gyroid phase due to a relatively broad phase window. Nanoporous membranes have been demonstrated by selectively washing away one homopolymer from the microemulsions, for example, nanoporous crosslinked PI from a PS/PS-PI/PI microemulsion,[15] nanoporous PE from a PE/PE-PEP/PEP microemulsion.[16]

Third, some unconventional 3D continuous morphologies in bulk copolymers are attractive for producing 3D nanoporous membranes, such as a perforated lamellae phase in a PEP-PEE copolymer,[17] an orthorhombic network phase in a PS-PI copolymer,[18] and a disordered network phase in a PE-PS copolymer induced by PE crystallization.[19] Apart from those,

researchers have also found that a random graft copolymer preferably adopted a bicontinuous morphology at certain compositions, presumably due to the low interfacial energy for such a morphology.[20] A random graft copolymer is also effective to stabilize a bicontinuous phase in a tertiary blend (Figure 3.1), for example, a blend prepared by grafting reactions of backbone-functionalized PE and end-functionalized polyamides.[21] To our knowledge, nanoporous membranes have not been fabricated from such systems.

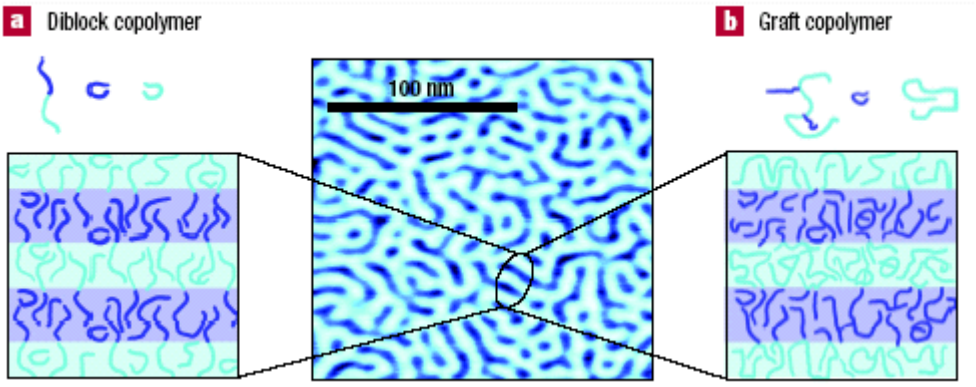

Figure 3.1. A bicontinuous morphology stabilized by (a) diblock or (b) graft copolymers. Reproduced from Ref 22.

Overall, no matter which method is adopted to produce nanoporous membranes from copolymer precursors, mechanical integrity of the resulting membranes is prerequisite for potential separation applications. The main objective of my research is to incorporate a tough polymer like polydicyclopentadiene (polyDCPD) into copolymer membranes by metathesis reactions and then to produce robust nanoporous membranes. In Chapter 2, by using a norbornene-functionalized PS-PLA copolymer (PNS-*b*-PLA), fabrication of tough 1D nanoporous PNS/polyDCPD monoliths by metathesis reactions was illustrated. Those monoliths exhibited excellent thermal and mechanical stabilities. However, using the same scheme, it was difficult to produce nanoporous polyDCPD/PNS membranes with a gyroid morphology.

Macroporous variants of polyDCPD prepared by ROMP of DCPD in the presence of a

porogen via a polymerization induced phase separation (PIPS) process have been demonstrated utility in applications such as chromatographic supports.[23] The PIPS process provides an efficient pathway to realize a bicontinuous phase,[24] and then to produce macroporous thermosets.[25] Motivated by these examples, in this chapter, the PIPS process during the ROMP of DCPD is explored by including a PNS-*b*-PLA block copolymer, and subsequently the production of nanoporous PNS/polyDCPD membranes with a percolating pore structure and significant mechanical strength is demonstrated (Figure 3.3). The utility of such membranes in ultrafiltration is preliminarily explored. Lastly, mechanism of the membrane formation is briefly discussed.

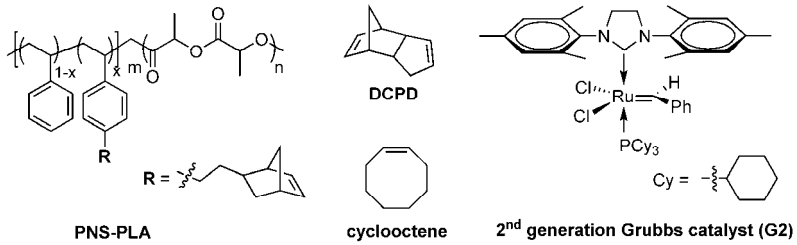

Figure 3.2. Chemical structure of components in the crosslinkable blends.

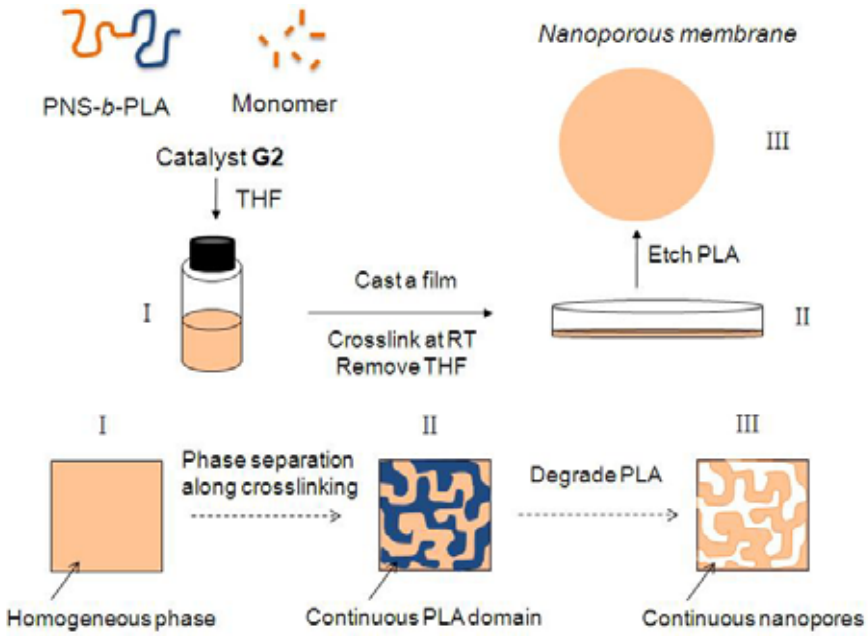

Figure 3.3. Schematic illustration of fabricating nanoporous PNS/polyDCPD membranes.

3.2 Experimental section

3.2.1 Materials

Unless specified, all chemicals were used without further purification. Ethylene oxide was purified by vacuum distillation over dibutyl magnesium twice following the procedure in Chapter 2. Styrene and cyclooctene were passed through short alumina columns to remove the inhibitors, and then distilled over CaH_2 under reduced pressure. Purification of THF, toluene, and CH_2Cl_2 was described in Chapter 2. D,L-lactide was recrystallized from ethyl acetate and dried under reduced pressure at RT, and stored in a nitrogen atmosphere glovebox. Azoisobutyronitrile (AIBN) was recrystallized from methanol and dried under reduced pressure. Monomer 4-norbornenylethyl styrene (N) was synthesized and purified following the procedures in Chapter 2. N was stirred over CaH_2 at RT to remove protic impurities. After removing CaH_2 by filtration, the monomer was dried at RT for 1 d under reduced pressure of 20 mtorr and refrigerated before use.

3.2.2 Characterization

Two different size exclusion chromatography (SEC) systems were used in this study. Some SEC data were acquired on a Hewlett-Packard 1100 series liquid chromatograph equipped with Jordi polydivinylbenzene columns with pore sizes of 10000, 1000, and 500 Å as well as a Hewlett-Packard 1047A refractive index detector. THF was used as the mobile phase at 40 °C with a flow rate of 1 mL/min. Other SEC data were recorded using the same chromatograph equipped with three Varian PLgel mixed C columns and a PLgel 5 μm guard column using $CHCl_3$ as the elute phase at 35 °C and a flow rate of 1 mL/min. These two systems were calibrated with polystyrene standards (Polymer Laboratories). Scanning electron microscopy (SEM) experiments were performed on a Hitachi S-900 FE-SEM using 3.0 kV accelerating voltage. Before SEM analysis, the freeze-fractured polymer membrane was mounted on a brass shim and coated with a 1–3 nm thick Pt layer through direct Pt sputtering. Transmission electron microscopy (TEM) analyses were conducted on a JOEL

1210 transmission electron microscope using 120 kV accelerating voltage. Polymers were cyro-microtomed at −120 °C and stained with OsO_4 vapor (4 % OsO_4 aqueous solution from Ted Pella Inc.) for 15 min. FT-IR spectra were acquired on a Nicolet Magna-Infrared Spectrometer 550. Thick samples were ground with KBr and pressed into transparent pellets. Thermogravimetric analysis (TGA) was performed on a Perkin-Elmer TGA 7 instrument under air. N_2 adsorption experiments were carried out on a Micromeritics ASAP 2000 instrument. Polymer samples were degassed under high vacuum at 60 °C overnight before analysis. Tensile tests were conducted using a Rheometric Scientific MINIMAT instrument at crosshead rate of 2 mm/min with a 1000 N load cell under ambient conditions. Membranes before and after degradation were cut into the dogbone shape (1.0 cm in length). Some SAXS experiments were conducted at the Argonne National Labs using the Advanced Photon Source. Other SAXS measurements were performed on a 2.3 m or 4.4 m custom built beam line at the University of Minnesota. Dynamic light scattering (DLS) measurements were carried out at 25 °C using a home-built photometer.[26] The polymer solution was passed through a 0.45 μm microfilter (Millipore) into a clean optical glass tube. The intensity autocorrelation function, $g_2(t)$, was recorded at 90° scattering angle.

3.2.3 Materials synthesis

3.2.3.1 PLA-*b*-PNS copolymers by reversible addition-fragmentation chain transfer (RAFT) polymerization[c]

Hydroxyl group terminated polylactide (PLA-OH) was prepared via aluminum-catalyzed ring-opening polymerization of D,L-lactide, and PLA-attached trithiocarbonate (PLA-TC) as a RAFT chain transfer agent was synthesized following a reported procedure.[27] PLA-TC (0.45 g, 0.0132 mmol), 4-norbornenylethyl styrene (N) (1.1 mL), styrene (1.1 mL), and AIBN (0.21 mg) were dissolved in dry toluene (1.3 mL) in an air-free flask, and after three freeze-pump-thaw cycles, the mixture was reacted at 70 ± 1 °C for 20 h. Copolymers were

[c] Taking the synthesis of NSL(48) in Table 3.1 as an example.

recovered through precipitation in methanol followed by dissolution in CH_2Cl_2, precipitation in pentane, and drying under vacuum at 50 °C overnight. Calculated comonomer conversion by mass was 12 wt %. By NMR spectroscopy, the number average molecular weight (M_n) of the PNS block was calculated based on the pre-determined PLA block, instead of end group analysis. ^{1}H NMR spectrum of PLA-*b*-PNS (multiplicity, identity) δ ppm: 6.2–7.2 (b, Ph-**H**), 5.9–6.2 (b, -C**H**=C**H**-), 5.1–5.3 (b, -C(O)-C**H**(CH3)-O-), 2.8 (b, -C**H**-CH=CH-C**H**-), 2.55 (b, Ph-C**H2**-), 1.6 (b, -C(O)-C(H)(C**H3**)-O-), 1.1–1.5 and 1.7–2.2 (b, b, other C**H** and C**H2**), 0.55 (b, -CH-C**H2**(*endo*)-CH-).

3.2.3.2 Synthesis of PNS-OH by living anionic polymerization[d]

A 1L glass reactor was equipped with a glass-coated magnetic stir bar and fitted with four Teflon plugs and one Y-connector. The Y-connector was equipped with three ports: one capped with a Teflon-coated septum and two with Teflon-capped valves connected to a vacuum/argon manifold and a pressure gauge. The sealed reactor was evacuated to 20 mtorr and baked at 120 °C overnight. After cooling down the reactor, the Teflon plugs were replaced (under slow argon purge) with an air-free flask containing dry THF (0.15 L), pre-tared burets of purified styrene (8.8 g) and purified ethylene oxide (EO) (3.0 g). The buret containing EO was emerged in a dry ice/isopropanol bath. Monomer N (2.05 g) was first introduced into the reactor through the septum using an air-tight syringe, and the reactor was evacuated and backfilled with argon six times, after which the pressure was set to 3 psi, which was isolated from the manifold. The pressure was monitored to ensure the absence of leaks. THF was added to the reactor, and the flask was immersed in a dry ice/isopropanol bath (−78 °C). After 20 min, the styrene was added to the reaction flask, and the initiator *sec*-butyl lithium (0.37 mL, 1.35 M in cyclohexane[e]) was quickly added through the Teflon-coated septum using an air-tight syringe. The reaction solution turned orange upon

[d] Taking the synthesis of PNS-OH in Table 3.1 as an example.

[e] The initiator concentration was used without titration.

addition of the initiator. The reaction solution was stirred for 0.5 h at −78 °C. After that, EO was added at a steady rate. The color of the solution faded slowly (over 5 min). After maintaining the reactor at −78 °C for 2 h, the reactor was warmed up to 0 °C overnight with stirring. The pressure inside the reactor was monitored throughout this process. Finally, the reaction was quenched with degassed acidic methanol (1 M, 2 mL). The polymer was precipitated in 1 L methanol. About 8 g of white polymer was recovered through vacuum filtration and was subsequently dried under vacuum at 60 °C overnight. The resultant polymer was sufficiently dried before growing a second PLA block. By NMR end group analysis, the M_n and the number of N unit were precisely determined (details see Table 3.1). ^{1}H NMR spectrum of PNS-OH δ ppm (multiplicity, identity): 6.2–7.3 (b, Ph-**H**), 5.9–6.2 (b, CH-C**H**=C**H**-CH), 2.7–2.9 (b, -C**H**-CH=CH-C**H**-), 2.4–2.6 (b, Ph-C**H2**-), 0.9–2.3 (b, other C**H** or C**H**2), 0.55 (b,-CH-C**H2**(*endo*)-CH-), 0.9 (m, -C**H3** resonance from the initiator), 3.65 (m, -C**H2**-OH).

3.2.3.3 Synthesis of a PNS-*b*-PLA copolymer using PNS-OH[f]

A typical reaction procedure was described as follows: In the glovebox, PNS-OH (1.0 g, 0.0385 mmol) and toluene (25 mL) were mixed in a high-pressure vessel. A 1 M solution of $AlEt_3$ in toluene (20 μL, 0.02 mmol) was added to the flask, and the mixture was allowed to stir at RT overnight. D,L-lactide (3.0 g) was added to the flask. The flask was sealed and removed from the glovebox and immersed into an oil bath at 105 °C. After 3 h, the reaction was quenched with aqueous HCl (2 M, 1 mL), and the resultant block copolymer was precipitated in cold methanol followed by filtration and subsequently dried under vacuum at 50 °C overnight. About 3.5 g of product was collected (83 % conversion of lactide). The M_n of the PLA block calculated based on the PNS block was consistent with the M_n calculated by end group analysis (details see Table 3.1). ^{1}H NMR spectrum of PNS-*b*-PLA δ ppm (multiplicity, identity) δ ppm: 6.2–7.2 (b, Ph-**H**), 5.9-6.2 (b, -C**H**=C**H**-), 5.1–5.3 (b,

[f] For example, NSL_4 in Table 3.1

-C(O)-C**H**(CH3)-O-), 2.8 (b, -C**H**-CH=CH-C**H**-), 2.55 (b, Ph-C**H2**-), 1.6 (b, -C(O)-C(H)(C**H3**)-O-), 1.1–1.5 and 1.7–2.2 (b, b, other C**H** or C**H2**), 0.55 (b, -CH-C**H2**(endo)-CH-), 4.3 (m, -C**H**(CH3)OH).

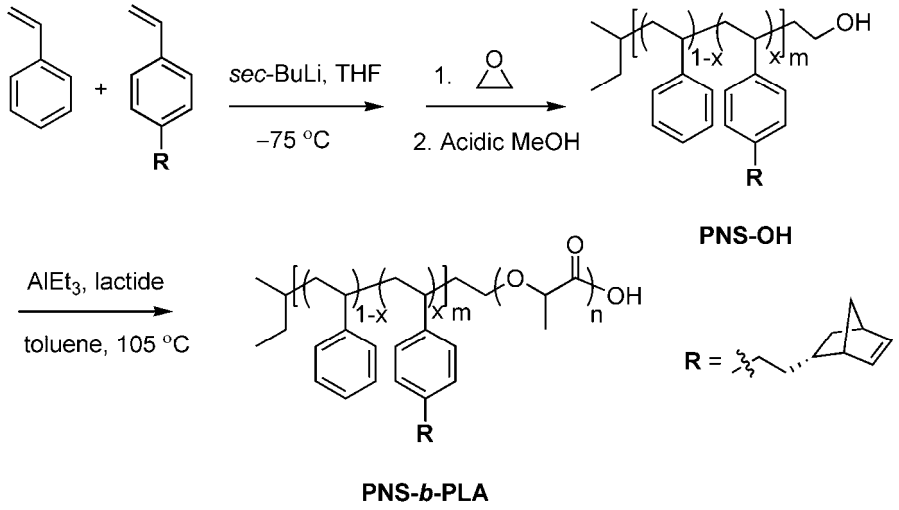

Scheme 3.1. Synthetic protocol for a PNS-b-PLA copolymer by combined anionic and ring-opening polymerizations.

3.2.3.4 Synthesis of 5-hydroxyl-1-cyclooctene[28]

To bulk 1,5-cylcooctadiene (14.5 g), a chloroform solution (300 mL) of *m*-chloroperbenzoic acid (24 g, 76 % pure) was added dropwise over 1 h with stirring at RT. After reaction overnight, a white solid (*m*-chlorobenzoic acid) was removed by filtration, and the resulting solution was concentrated to afford crude epoxy-cyclooctene as a colorless oil. Pure product (9.0 g) was obtained by column chromatography (silica gel, hexanes). A $LiAlH_4$ solution in THF (1 M, 40 mL) was added dropwise into a mixture of dry THF (80 mL) and epoxy-cyclooctene (9.0 g) in a three-necked flask at 0 °C under argon atmosphere. The reaction was stirred at RT overnight. The solution placed in an ice bath was slowly quenched with water. Insoluble salts were removed by filtration and then washed with diethyl ether. Concentration of the combined organic fractions yielded a clear crude product. Further purification by vacuum distillation yielded about 7.0 g of product as a viscous oil. ^{1}H NMR

of spectrum δ ppm (multiplicity, identity): 5.6 (m, CH2-C**H**=C**H**-CH2), 3.75 (m, C**H**-OH), 1.4–2.4 (m, other C**H** and C**H2**). ^{13}C NMR spectrum (75 MHz) δ ppm: 130.0, 129.4, 72.5, 37.4, 36.1, 25.4, 24.7, 22.6.

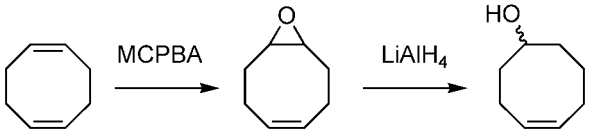

Scheme 3.2. Synthesis of 5-hydroxy-1-cyclooctene.

3.2.3.5 Synthesis of 5-hydroxymethyl norbornene[29]

An autoclave charged with hydroquinone (50 mg) was evacuated to ~200 mtorr and backfilled with argon three times and sealed under vacuum. A solution of allyl alcohol (39 mL) and DCPD (20 mL) in an air-free flask was degassed for 10 min by bubbling N_2 through the mixture and added through the side valve into the autoclave. The Diels-Alder reaction was conducted at 165 °C for 16 h. After cooling the reaction, the resultant viscous mixture was subjected to fractional distillation (150 mtorr, at 40 °C) and afforded 20 g of product as a clear oil. The ratio of endo/exo isomers was approximately 4:1 based on NMR analysis. ^{1}H NMR spectrum (mainly the *endo* isomer) (multiplicity, identity) δ ppm: 6.14 and 5.95 (m, m, CH-C**H**=C**H**-CH), 3.20 and 3.38 (t, t, CH-C**H2**-OH), 2.92 and 2.80 (s, s, C**H**-CH=CH-C**H**), 2.28 (m, C**H**-CH2-OH), 1.81 (m, -CH-C**H2**(exo)-CH-), 1.45 and 1.26 (m, -CH-C**H2**-CH-), 0.50 (m, -CH-C**H2**(endo)-CH-). ^{13}C NMR spectrum (75 MHz) of the *endo* isomer: 137.3, 132.0, 66.3, 49.3, 43.3, 42.0, 41.4, 28.5; the *exo* isomer: 136.6, 136.3, 67.3, 44.7, 43.0, 41.6, 41.3, 29.3.

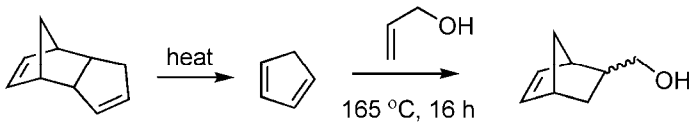

Scheme 3.3. Synthesis of 5-hydroxymethyl norbornene by the Diels-Alder reaction.

3.2.3.6 Synthesis of norbornene-terminated PLA (PLA-N)[g]

In the glovebox, triethylaluminum (1.0 M in heptane, 0.175 mL, 1.75×10^{-4} moles), 5-hydroxymethyl norbornene (0.043 g, 3.5×10^{-4} moles), and dry toluene (35 mL) were mixed in a air-free pressure flask and stirred at RT for 16 h. D,L-Lactide (5.0 g) was added to the reaction mixture, and the flask was sealed and placed in an oil bath at 90 °C. After 3.5 h, the reaction was quenched with aqueous HCl (1 M, 5 mL), and the polymer was precipitated in cold methanol. After decanting the methanol, the polymer was dissolved in CH_2Cl_2, precipitated in pentane, and dried at 50 °C under reduced pressure overnight. 3 g of PLA-OH was yielded (~ 60 % conversion of lactide). SEC analysis gave M_n= 15.0 kg mol^{-1} and PDI = 1.10. ^{1}H NMR end-group analysis gave M_n of 10.3 kg mol^{-1}. ^{1}H NMR spectrum of PLAN δ ppm (multiplicity, identity): 5.9–6.2 (m, b, CH-C**H**=C**H**-CH), 5.2 (m, -C(O)-C**H**(CH3)-O-), 4.36 (t, C(**H**)(CH3)-OH), 3.7–4.3 (m, CH-C**H2**-O-), 2.8 and 2.65 (b, b, -C**H**-CH2-C**H**-), 1.6 (b, -C(O)-CH(C**H3**)-O-), other minor peaks were not specified.

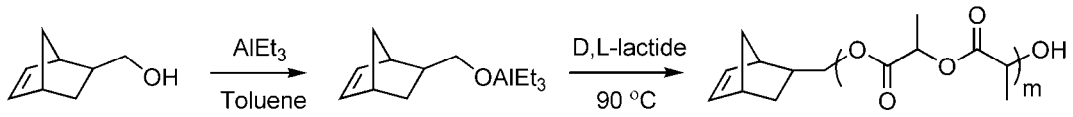

Scheme 3.4. Synthesis of norbornene-attached PLA.

3.2.3.7 Synthesis of PCOE-*g*-PLA[h]

A PCOE-*g*-OH polymer was synthesized by a ring opening metathesis polymerization scheme with a chain transfer initiator, *cis*-1,4-diacetoxy-2-butene (**CT**).[30] To a flask, dry COE (5.0 g) and COE-OH (0.5 g) were added dropwise into a solution of **CT** (44 mg) and the 2nd generation Grubbs catalyst (**G2**) (8.2 mg) in CH_2Cl_2 (25 mL) under argon atmosphere. The resultant solution was stirred at RT for 24 h. After polymerization, the polymer was recovered through precipitation in acidic methanol (2 mL concentrated HCl in 300 mL methanol). Finally, the polymer was collected by vacuum filtration, washed with methanol

[g] For example, the synthesis of the PLA-N(10) in Table 3.4.
[h] PCOE-g-PLA_1 of Table 3.4

until pH = 7, and dried at 60 °C overnight. The M_n and the average number of hydroxyl groups per chain were determined through NMR end group analysis. ^{1}H NMR spectrum (multiplicity, identity) δ ppm: 5.36 (b, CH2-C**H**=C**H**-CH2), 4.51 and 4.62 (d, d, C**H2**-O-C(O)-CH3), 3.6 (b, C**H**-OH), 2.0 (b, C**H2**-CH=CH-C**H2**), 1.3 (b, other C**H2**). For PCOE-*g*-PLA synthesis, in the glovebox, triethylaluminum (1.0 M in heptane, 0.30 mL, 3.0×10^{-4} moles), PCOE-*g*-OH (1.0 g, 21.4 kg mol^{-1}; about 13 hydroxy groups per chain), and dry toluene (20 mL) were mixed in a air-free pressure flask and stirred at RT for 16 h. D,L-lactide (2.0 g) was added to the reaction mixture. The flask was sealed, removed from the glovebox, and placed in an oil bath at 90 °C. After 4 h, the reaction was quenched with aqueous HCl (1 M, 2 mL), and the product was precipitated in cold methanol. After decanting the methanol, the polymer was dissolved in CH_2Cl_2, precipitated in pentane, and dried at 50 °C under reduced pressure overnight. The yield of PCOE-*g*-PLA was 2.0 g (55 % conversion of lactide). ^{1}H NMR spectrum (multiplicity, identity) δ ppm: 5.36 (b, -CH2-C**H**=C**H**-CH2), 5.2 (m, -C(O)-C(**H**)(CH3)-O-), 4.51 and 4.62 (d, d, C**H2**-O-C(O)-CH3), 4.36 (t, C**H**(CH3)-OH), 3.6 (b, C**H**-O-C(O)-), 2.0 (b, C**H2**-CH=CH-C**H2**), 1.6 (b, -C(O)-CH(C**H3**)-O-), 1.3 (b, other C**H2**).

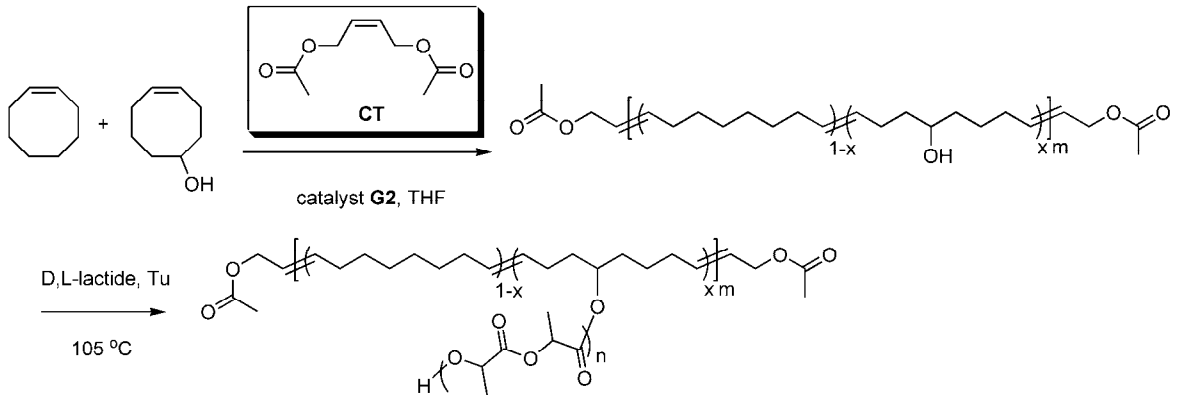

Scheme 3.5. Synthesis of a PCOE-*g*-PLA graft copolymer.

3.2.4 Membrane preparation

PNS-*b*-PLA (0.20 g), DCPD (0.10 g), and a good solvent such as THF (variable, e.g., 1.0 mL) were pre-mixed in a glass vial with stirring and added to a solution of **G2** (variable, e.g., 1.2 mg) in THF (0.2 mL). Solution-cast film on a glass substrate gelled within 1 min, and was allowed to cure at RT for 6 h and at 100 °C for 1 h in air. During the process, much of the THF evaporated from the film, and the 100 °C treatment led to nearly complete removal of the THF (as determined by mass loss). The resultant optically transparent film was easily peeled from the glass substrate. After that, the PLA component in the film was degraded in 0.5 M NaOH solution of a 40/60 (v/v) mixture of methanol and water at 70 °C for 3 d. Finally, the resulted membrane was rinsed with methanol and DI water, and dried under vacuum at 50 °C for 24 h.

3.3 Results and discussion

3.3.1 Copolymer synthesis

PNS-*b*-PLA block copolymers were prepared using two different schemes. RAFT polymerization of N and styrene using a PLA-attached chain transfer reagent (PLA-TC) was demonstrated in Chapter 2. Herein, the PLA-TC samples with three different molecular weights (11, 34, and 43 kg mol^{-1}) were prepared to yield three corresponding PLA-*b*-PNS copolymers, respectively, as summarized in Table 3.1. The overall conversion of styrene and N in these three polymerizations was below 20 %, which resulted into minimized coupling reactions on the norbornene groups. By SEC analysis, low polydispersity indices (PDIs) of the resultant copolymers (< 1.3) indicated good control in the RAFT polymerizations.

Another scheme was combining living anionic polymerization of N and styrene and ring opening polymerization (ROP) of D,L-lactide, similar to the previously reported synthesis of PS-*b*-PLA.[31] Anionic polymerization of monomer N was discussed in Chapter 2, where a key issue was the purification of monomer N. If using less purified monomer N, a broad PDI in the resultant polymer was observed. Additionally, coupling reactions of PNS chains occurred in the anionic polymerization of N and styrene in cyclohexane at 45 °C. To prevent

these problems, anionic polymerization of N and styrene was performed in THF at −78 °C. Herein, instead of quenching the PNS anions with methanol, end-capping reaction of PNS anions with one ethylene oxide (EO) unit at −78 °C was conducted to introduce the hydroxyl end groups. Experimentally, the coupling step was relatively slow, as the orange color of PNS anions in THF faded within 5 min. As a result, a minor coupling peak resulted after end capping with EO (Figure 3.4) by SEC analysis, although the resulting PNS-OH has a relatively narrow PDI of 1.1. The M_n revealed by ^{1}H NMR end group analysis was 25.6 kg mol^{-1}, a bit higher than the theoretical value of 20 kg mol^{-1}. This discrepancy was possibly attributed to either the error of the initiator concentration or residual impurities in N. Next, the PNS-OH polymer was utilized to grow a PLA block. SEC analysis of the resulting polymer (Figure 3.4) indicated the presence of some homopolymer in the PNS-*b*-PLA copolymer. The residual homopolymer was mostly isolated by wash the resultant copolymer with cyclohexane at 40 °C. By NMR spectroscopy, the isolated polymer was PNS homopolymer without the hydroxyl end group, suggesting that the end capping reaction of PNS anions with EO at −78 °C was incomplete. The termination reaction of the PNS anionic chains likely occurred in the end-capping step. Possibly, the allyl H on the norbornene group was more susceptible to the nucleophilic attack by the alkoxy anions (PNS-O$^-$) than PNS$^-$. In the future, synthesis of PNSOH could be improved by performing anionic polymerization at lower temperatures to suppress this undesired termination reaction or using a protected anionic initiator that could be subsequently converted into a hydroxy end group.[32]

Overall, anionic polymerization provides an efficient pathway to produce PNS-PLA copolymers to high monomer conversions, with decent control of functionality and molecular weight.

Table 3.1. Summary of the PNS-PLA copolymers.

Entry[a]	M_n(SEC)[b] kg mol^{-1}	PDI	M_n(NMR) kg mol^{-1}	f_{PLA}[d] %	N # per chain
PLATC(11)	15	1.09	10.6	100	0
PLATC(34)	40	1.27	33.5	100	0
PLATC(43)	66	1.11	43.0	100	0
NSOH(26)	19.2	1.15	25.6	0	19
NSL(19)	19.9	1.17	19.2	49.3	24
NSL(48)	50.6	1.25	48.3	65.5	27
NSL(63)	83	1.13	63.3	63.9	46
NSL(91)	93.9	1.10[c]	90.6	68.0	32

a. NSOH and NSL denote PNS-OH homopolymer and PNS-*b*-PLA copolymer, respectively. Number in the brackets denotes the M_n by NMR analysis. NSL (19), (48) and (63) were synthesized from PLATC(11), (34), and (43) via a RAFT polymerization scheme, respectively; NSL (91) was produced from NSOH(26). *b*. Based on PS standards. *c*. The homopolymer peak was not included. *d*. Volume fraction of PLA was calculated based on densities of polymers at RT: ρ(PS) = 1.05 g cm^{-3},[33]. ρ(PLA) = 1.25 g cm^{-3},[34] and assuming ρ(PN) = ρ(PS).

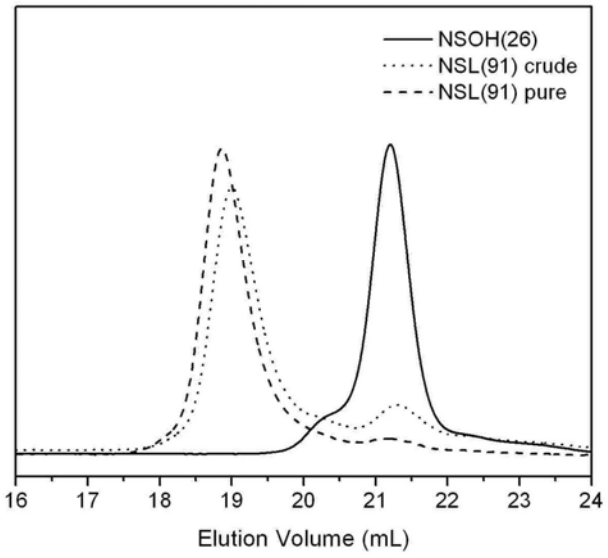

Figure 3.4. SEC traces of NSOH(26), crude NSL(91), and purified NSL(91).

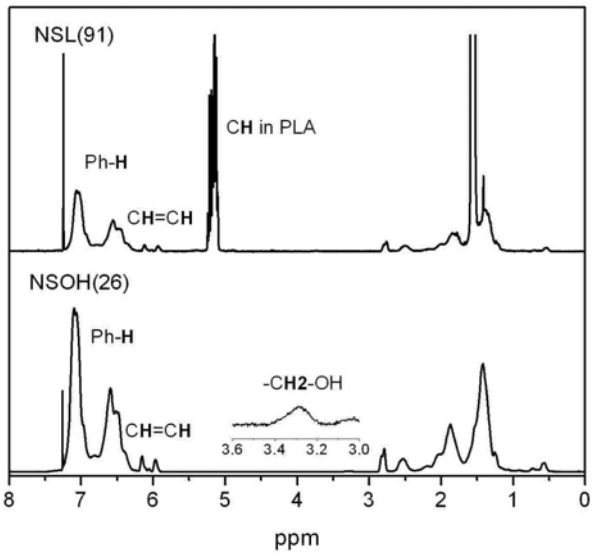

Figure 3.5. NMR spectra of NSOH (26) and NSL (91). Representative group signals are labeled accordingly.

3.3.2 Preparation and characterization of crosslinked nanoporous membranes

The ROMP of DCPD in the presence of PS-*b*-PLA in THF yielded polymers with little mechanical integrity and the macrophase separation was evident based on the opaque appearance. This observation led us to use a PNS-*b*-PLA block copolymer that contained two reactive constituents: a metathesis reactive block and a chemically etchable block. Incorporation of the reactive block into the thermosetting matrix during the reaction should help arrest phase separation. Furthermore, the incompatibility of the PLA block and polyDCPD would likely result in nanoscopic organization of these two components.

A reactive blend amenable to PIPS typically possesses no microstructure initially, such as the example of producing macroporous polyDCPD,[23] while the structure develops during crosslinking. Since the blends of PNS-*b*-PLA and DCPD have exhibited various nanostructures at RT (shown in Chapter 2), two methods could be used to prepare blends in a disordered state. The disordered state was demonstrated in a PNS-*b*-PLA/DCPD blend at high temperatures in the last section of Chapter 2. In practice, due to the volatility of DCPD

at high temperatures, the first approach could cause loss of DCPD during crosslinking, which is disadvantageous for membrane preparation. Moreover, the lifetime of metathesis catalysts at high temperatures is limited,[35] which might cause low crosslinking efficiency. Alternatively, introducing a good solvent for both components (PNS-*b*-PLA and DCPD) can result in a homogeneous polymer solution with no micellular structure. This approach could be conducted at RT and thus was more convenient for membrane preparation. The metathesis catalyst **G2** (structure shown in Figure 3.2) was chosen due to its great tolerance of impurities and moderate reactivity.

A clear solution containing NSL(19) in Table 3.1 (0.10 g), DCPD (0.08 g), CH_2Cl_2 (0.30 mL) was prepared in a vial by direct dissolution. To this solution, **G2** (0.9 mg) dissolved in CH_2Cl_2 (0.10 mL) was added, and the resultant mixture was sealed and cured at RT overnight. After removing CH_2Cl_2, a transparent plastic material (~ 0.18 g) resulted, and the calculated PLA weight fraction was 30 %. The resulting sample was insoluble in organic solvents and had minimum sol fraction. Subsequently, this sample was subjected to base hydrolysis to degrade the PLA component. The mass loss of approximately 27 wt % agreed with the original PLA composition. Additionally, IR spectrum of the membrane after PLA hydrolysis confirmed the successful removal of the PLA component.

In the fabrication of 1-D nanoporous monoliths discussed in Chapter 2, poor alignment of the cylindrical domains caused incomplete PLA degradation. Herein, it was strongly suggested that the PLA phase percolated throughout the macroscopic film. Further SAXS and SEM experiments were performed to confirm the nanostructure. From SAXS characterization, a single broad peak was observed (Figure 3.6), implying a disordered state where PLA and PNS/polyDCPD domains were nanoscopically segregated. The overall domain spacing was about 21 nm, which was comparable with the domain spacing of the parent copolymer NSL(19) of 20 nm. The SEM images (Figure 3.7) of the fractured surface of the degraded film corroborated the nanoporous structure, where the isotropically percolated nanopores

were approximately 10 nm.

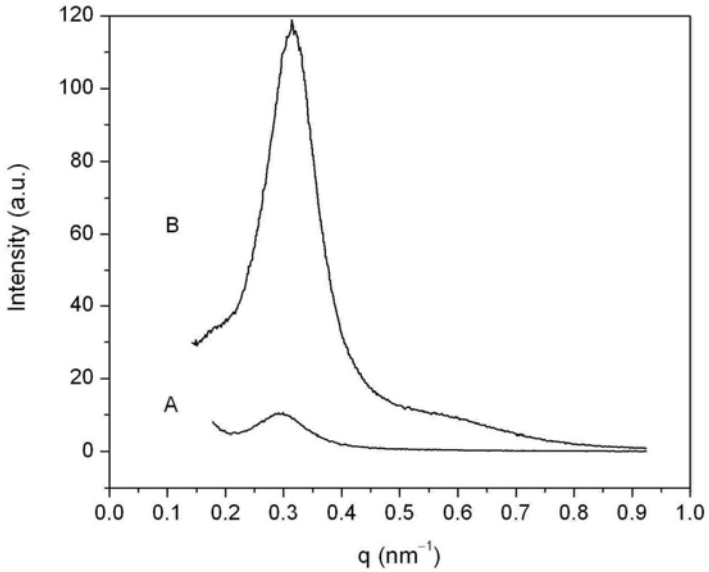

Figure 3.6. 1D SAXS profiles of the crosslinked membrane (A) fabricated from NSL(19) and DCPD by metathesis reactions and the nanoporous (B) membrane after PLA degradation.

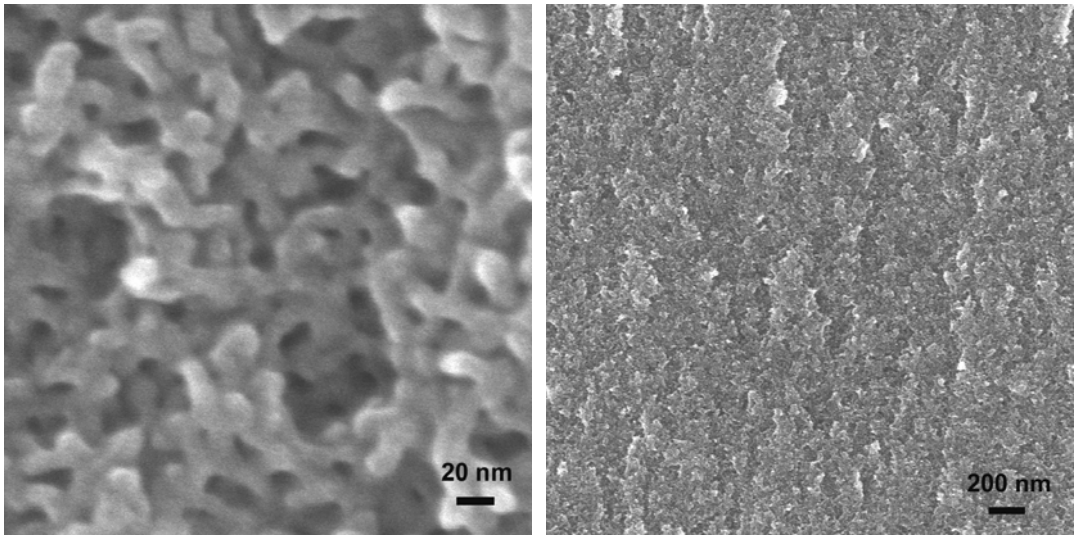

Figure 3.7. SEM micrographs of the fractured surface of the nanoporous membrane fabricated from NSL(19) and DCPD, coated with 1 nm thick Pt to prevent charging.

Combined, these data confirmed the formation of a robust thermoset with nanopores templated by the PNS-*b*-PLA block copolymer. The inclusion of the reactive

norbornene-containing block resulted in control of the PIPS process leading to nanoscopic organization of the PLA segments in the polyDCPD/PNS composite. This initial experiment has shown a facile way to prepare a robust membrane with percolated nanopores. However, further characterization of the pore continuity in the film by nitrogen adsorption encountered some difficulties, such as slow degassing of the sample and long equilibrium time, presumably due to the small pore size and low porosity in the nanoporous film.

Therefore, A PNS-PLA copolymer containing a large PLA block was selected to increase the PLA fraction in the crosslinked film. A film was casted on a substrate, and THF was utilized to dissolve all crosslinkable components, which would allow for slow solvent evaporation during crosslinking. Following the same preparation, NSL(48) in Table 3.1 (0.20 g), DCPD (0.10 g), THF (1.0 mL) were pre-mixed in a glass vial with stirring and added to a solution of **G2** (1.2 mg) in THF (0.20 mL). A cast membrane from this solution formed gel within 30 s and then cured at RT for 6 h. After annealing the membrane at 100 °C and removing the residual solvent, a transparent and flexible membrane was obtained. The SAXS data of the membrane (Figure 3.10) exhibited a single scattering peak at 0.19 nm^{-1} consistent with a microphase separated but disorganized structure on a 33 nm length scale. Furthermore, TEM analysis of the resulting membrane supported the phase separation between the PLA and polyDCPD/PNS domains. In the TEM image (Figure 3.8), dark regions are associated with polyDCPD/PNS domains with double bonds in polyDCPD stained by OsO_4, and white regions are unstained PLA domains. Based on this micrograph, the width of PLA channels are approximately 20 nm.

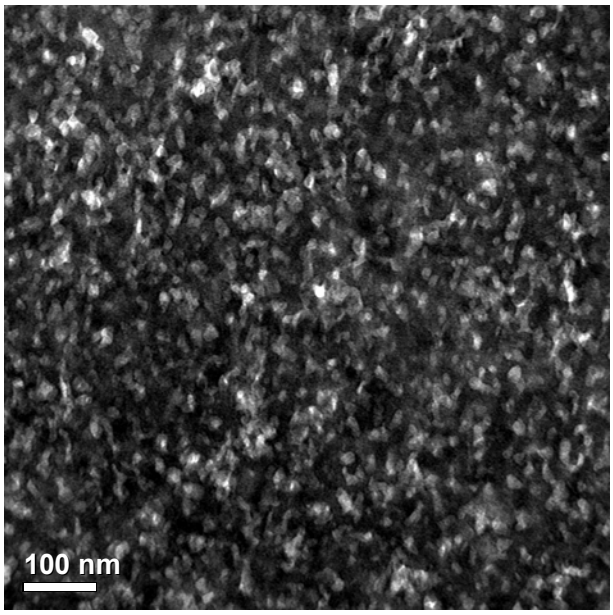

Figure 3.8. TEM micrograph of the crosslinked membrane fabricated from NSL(48) and DCPD before PLA degradation. Bright regions correspond to the PLA domains that were not stained by OsO_4.

Next, the PLA component was hydrolyzed by soaking the resulting membrane in a 0.5 M solution of NaOH in methanol and water. Complete PLA removal was corroborated by mass loss and IR spectroscopy. In the IR spectra (Figure 3.9), the peak at 1750 cm^{-1} is indicative of carbonyl groups from PLA and is nearly absent after treatment with aqueous base. The peaks at 970 cm^{-1} correspond to *trans* double bonds in polyDCPD, and after curing the film residual double bonds were not affected. A pore volume fraction in membranes is 40 % based on the mass loss after PLA degradation that consists with the initial PLA composition in the crosslinked membrane. After PLA degradation, the membrane (0.1 mm thick) was flexible and could be rolled up without breaking.

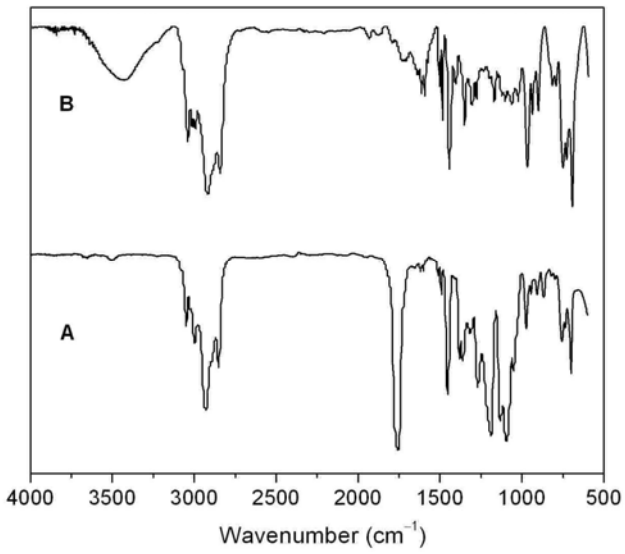

Figure 3.9. IR spectra of the crosslinked membrane fabricated from NSL(48) and DCPD before (A) and after (B) PLA removal.

The resulting nanoporous film was analyzed by SAXS using the synchrotron source (Figure 3.10). The peak position is unchanged after PLA degradation, but enhancement in the scattered intensity is about 28 times due to porosity. A simple calculation is given below because scattered intensity is proportional to the square of the electron density difference between two phases. The total electron density for PS is 0.560 mol e^- cm^{-3}, for PLA 0.665 mol e^- cm^{-3}, for polyDCPD 0.545 mol e^- cm^{-3}, and for vacuum approximately 0 mol e^- cm^{-3}. Therefore, the expected enhancement in scattering intensity is $(0.550-0)^2/(0.55-0.665)^2 = 23$, which agrees with the experimental value. Furthermore, the pore size can be estimated from the domain spacing given the pore volume fraction of 40 %. Since these is no established correlation between the pore size and the domain spacing (D) in a disordered bicontinuous morphology, the pore size was just estimated by taking the average value of hypothetic pore sizes in a lamellar or cylindrical morphology. With a pore volume fraction of 40 %, for a hexagonally packed cylindrical morphology, a calculated PLA cylinder diameter (d_1) is about 25.3 nm ($\sqrt{3}\pi d^2/8D^2 = 0.40$); a calculated PLA lamellar thickness (d_2) is 13.5 nm (D×0.40).

Hence, for a bicontinuous morphology, the pore size (the PLA domain size) is presumably 19.4 nm ((d_1+d_2)/2), in a good agreement with the result from TEM analysis.

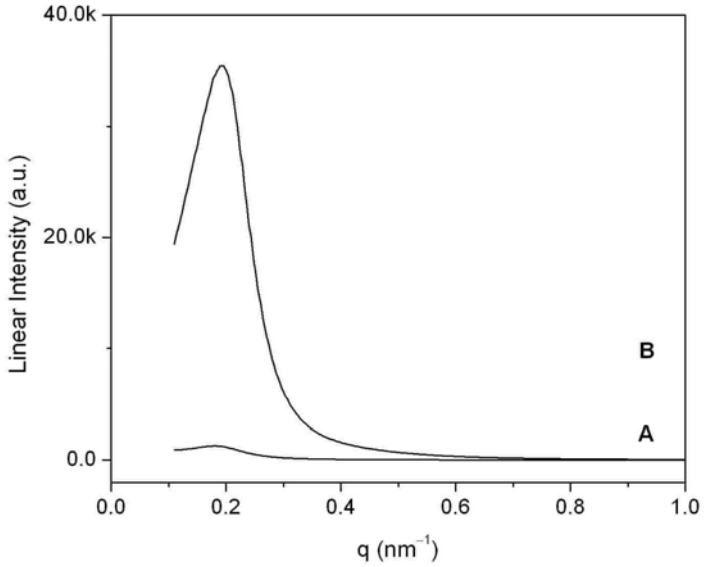

Figure 3.10. Synchrotron SAXS profiles of the crosslinked membranes fabricated from NSL(48) and DCPD before (A) and after (B) etching the PLA component.

SEM images (Figure 3.11) of the fractured surface of the nanoporous membrane revealed a bicontinuous structure containing percolating pores; the average diameter of the pores estimated from the SEM image was near 20 nm, comparable to the SAXS data and the TEM image. The bicontinuous structure is uniform throughout the macroscopic film. In addition, the pore diameter is larger than that shown in Figure 3.7, consistent with the fact than the pore size is simply templated by the PLA block.

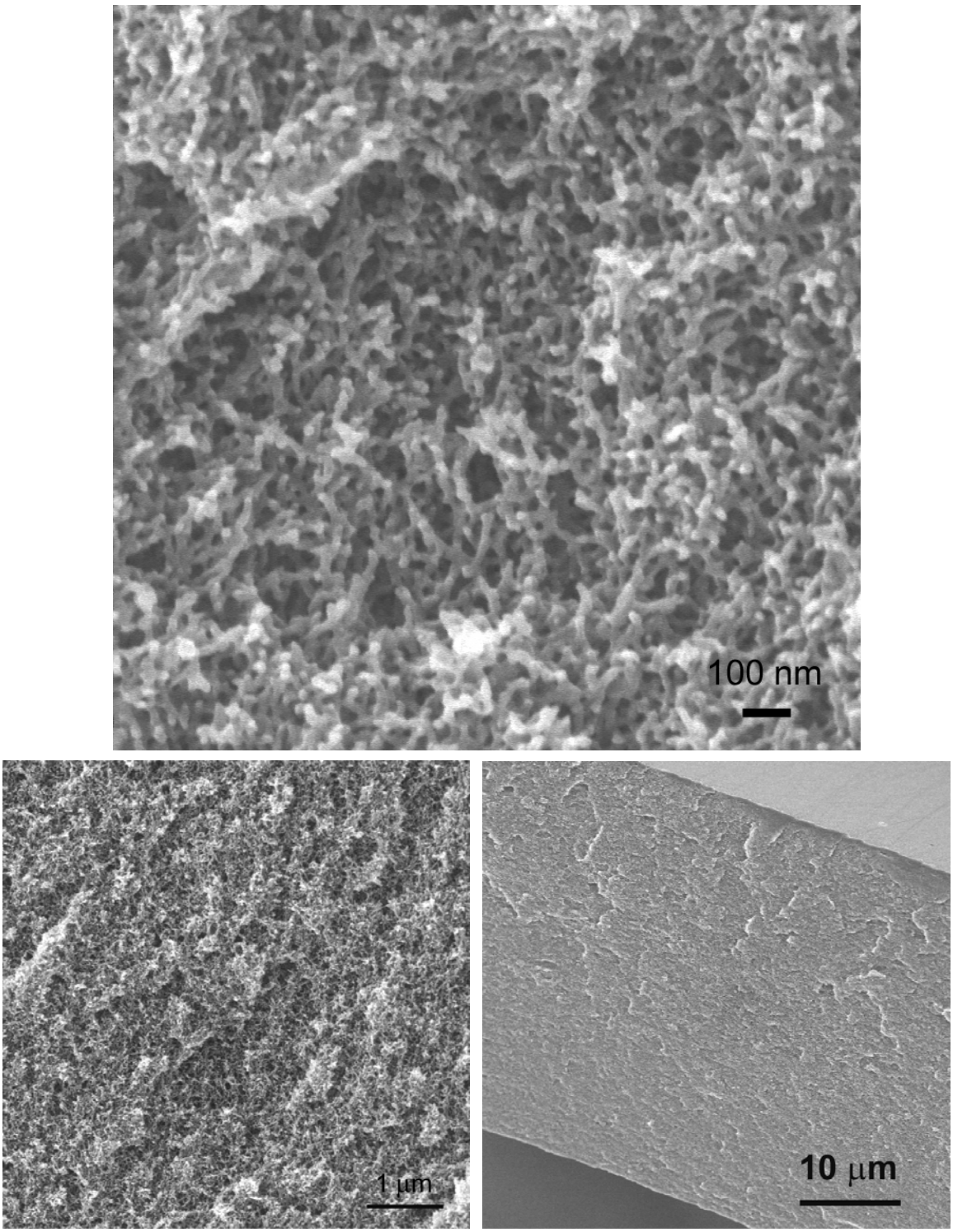

Figure 3.11. SEM images of the cryo-fractured surface of the nanoporous membrane fabricated from NSL(48) and DCPD. The fractured surface was coated with 2 nm thick Pt to prevent charging.

Next, nitrogen adsorption experiments confirmed the porosity of the films.[36] BET analysis showed a type IV isotherm and gave a specific surface area of 160 m^2 g^{-1} and BJH analysis gave a peak pore diameter of 20 nm, an average pore diameter of 17 nm, and a peak width at half height of 7 nm (Figure 3.12).

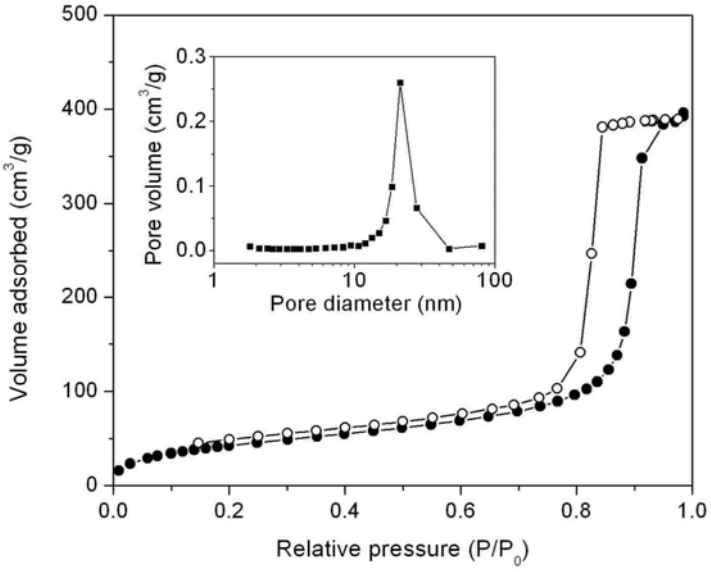

Figure 3.12. Nitrogen adsorption (filled circles) vs desorption (open circles) isotherms of the nanoporous membranes fabricated from NSL(48) and DCPD. Inset: pore size distribution from the adsorption data.

The nanoporous membrane retained their structure after annealing at 140 °C for 1 h or after swelling in THF followed by slow drying as revealed by both SAXS and SEM (Figure 3.13). In addition, the DSC trace (Figure 3.14) of the nanoporous membranes did not exhibit a glass transition temperature (T_g) for PLA but a strong exothermic peak at 150 °C was indicative of the pore collapse. Based on these results, the thermal stability of nanopores in such membranes was strikingly improved from the nanoporous PS (pore collapse at 100 °C).[31] TGA experiments (Figure 3.15) were performed to examine the thermal stability of the membrane. The PLA component in the crosslinked films started to degrade at 150 °C in air, while the nanoporous film retained > 95 % of their mass upon heating to 450 °C in air and was mostly decomposed by 500 °C.

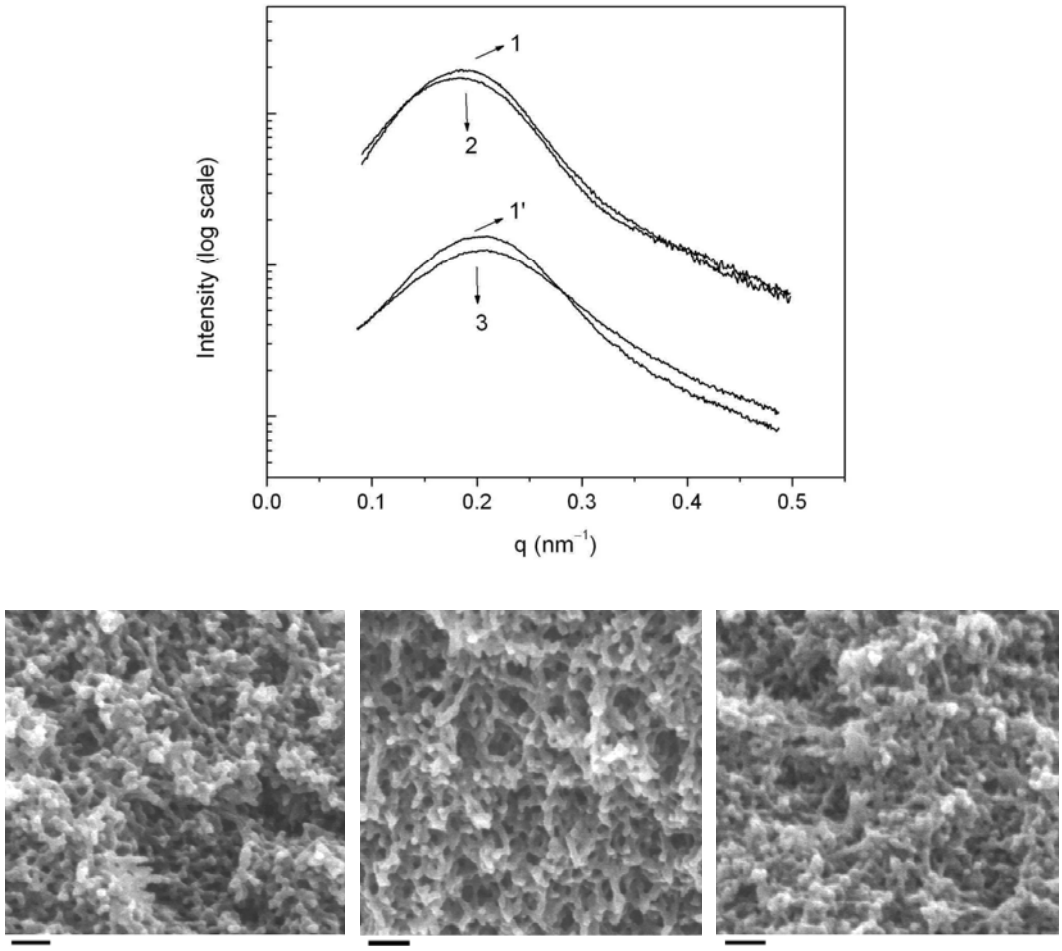

Figure 3.13. SAXS profiles of the crosslinked membrane fabricated from NSL(48) and DCPD after PLA etching at RT: 1(1'). no annealing; 2. after annealing at 140 °C for 1 h; 3. dried from THF (after soaking in THF, slow solvent-exchange with methanol was performed before drying). SEM images corresponding to the freeze-fractured samples 1, 2, and 3 (the scale bars above are 100 nm).

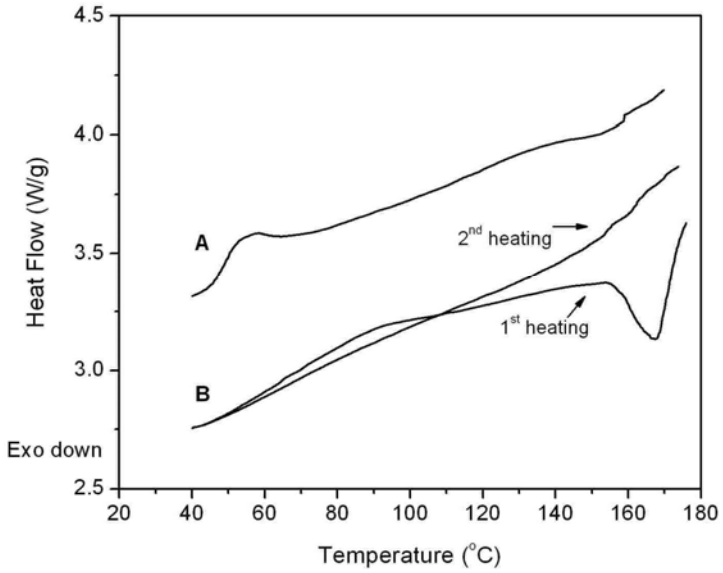

Figure 3.14. DSC of the crosslinked membranes fabricated from NSL(48) and DCPD before (A) and after (B) removing the PLA component (heating rate = 10 °C /min).

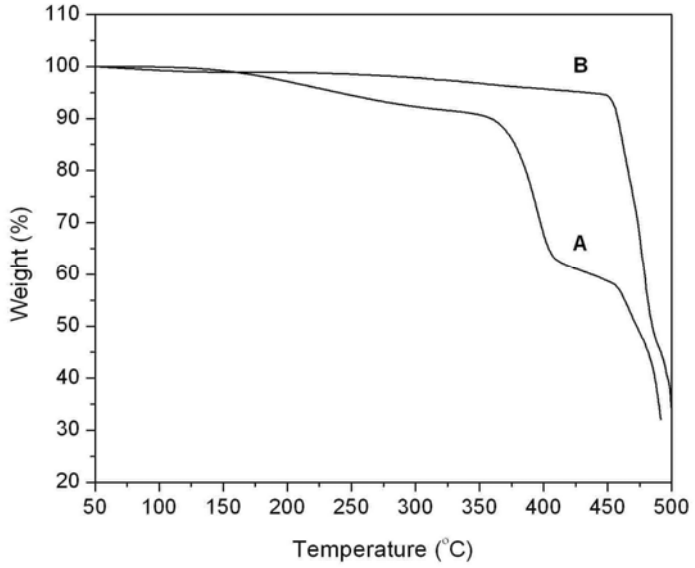

Figure 3.15. Thermogravimetric analysis of the crosslinked membranes fabricated from NSL(48) and DCPD before (A) and after (B) PLA removal (in air, heating rate = 20 °C /min).

Tensile tests on the crosslinked thin films before and after removal of the PLA were performed (Figure 3.16). The average tensile strength for the crosslinked film is

approximately 45 MPa with the average elongation at break around 15 %. The average ultimate elongation of the nanoporous membrane (ca. 10 %) was similar to the PLA-containing precursor, and the average tensile strength was 32 MPa, comparable to the films before removal of the PLA (45 MPa) and pure polyDCPD plastics (55 MPa).[29] The remarkable mechanical strength of these nanoporous membranes is contrasted with other block copolymer templated membranes such as nanoporous PS membranes that are typically too brittle to be practically evaluated.

For applications as separation membranes, these nanoporous thin films should ideally exhibit robust mechanical properties and a percolating pore structure. To demonstrate the porosity and the pore continuity in a macroscopic measurement, the nanoporous films was filled with an ionic liquid (IL), 1-ethyl-3-methylimidazolium bis(trifluoromethylsulfonyl)imide ([Emim][TFSI]).[37] For the sample preparation, a piece of nanoporous film was floating on the surface of the IL in a glass vial; while pulling vacuum on the IL at 60 °C, small air bubbles were slowly released from the nanoporous film, and eventually the film sank into the IL. Below are two SEM images of two fractured surfaces (Figure 3.17): the left image is the original nanoporous membrane and the right image is the sample filled with the IL. Based on the SEM image, the IL percolates throughout the film.

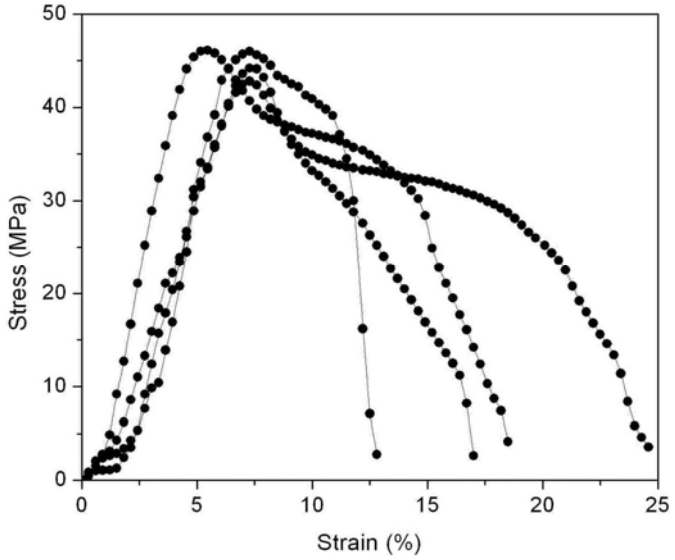

(a)

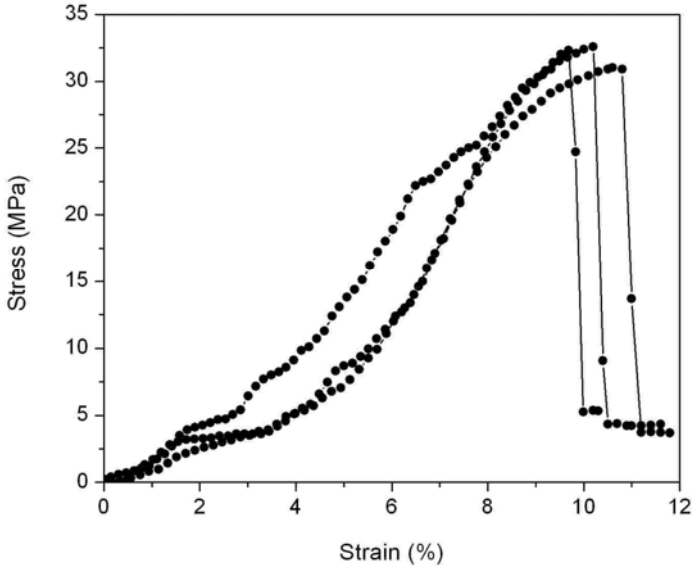

(b)

Figure 3.16. Tensile tests on the crosslinked membranes fabricated from NSL(48) and DCPD before (a) and after (b) removing PLA.

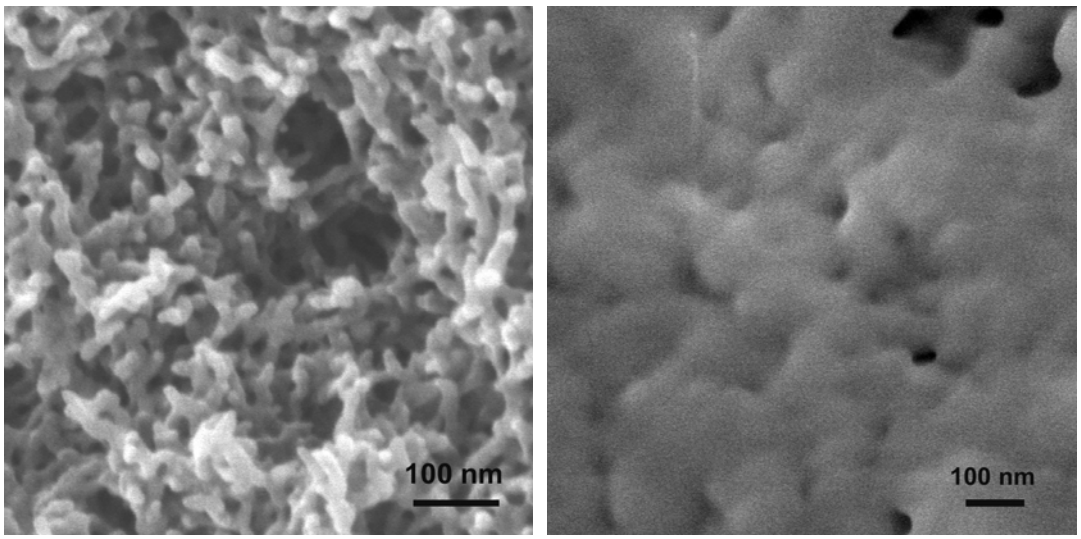

Figure 3.17. SEM images of the fractured surface of the nanoporous film fabricated from NSL(48) and DCPD and the membrane filled with [Emim][TFSI].

Conductivity of pure IL at 25 °C is 9.0×10^{-3} S cm^{-1} as measured by AC impedance.[38] This IL-filled membrane (size: 3.6×3.0×0.51 mm) had an impedance of 335 ohms at high frequency, and an ionic conductivity was 1.49×10^{-3} S cm^{-1} (1.058×cell constant/resistance). Accounting for the pore volume fraction of 0.40, the tortuosity was 2.48, which is a typical value for a disordered structure. These data confirm that the bicontinuous structure percolates through the entire film.

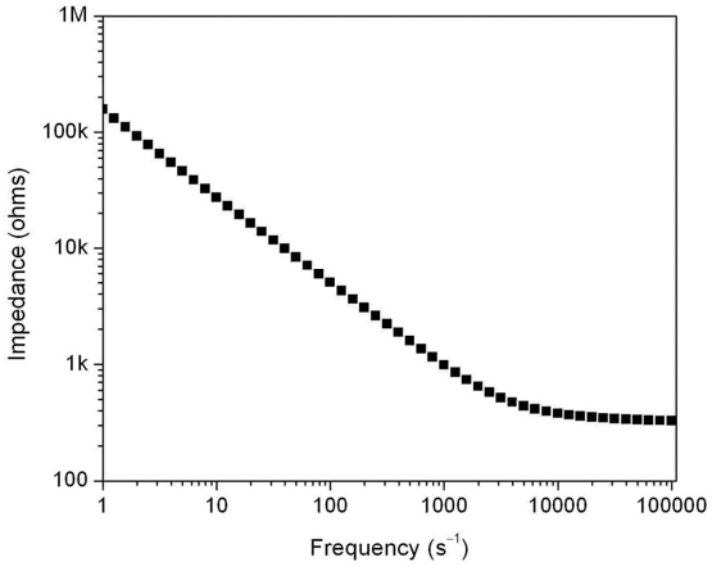

Figure 3.18. Conductivity measurement of the nanoporous membrane filled with the ionic liquid [Emim][TFSI] at 25 °C.

In sum, above characterizations of the nanoporous PNS/polyDCPD membrane have provided compelling evidence for well-controlled bicontinuous nanopores and excellent thermal and mechanical stabilities. More significantly, preparation of such a membrane has been realized from *in situ* metathesis polymerization of DCPD and PNS-*b*-PLA followed by PLA degradation. This process can be quite tolerant of compositional deviations of the copolymer and can be advantageous over other approaches using self-assembled copolymers. Besides the above membrane, another two nanoporous membranes have been prepared from NSL(63) or NSL(91), respectively, as summarized in Table 3.2. These two membranes will be used in later experiments.

Table 3.2. Summary of the nanoporous PNS/polyDCPD membranes.[a]

Membrane	Precursor copolymer	Porosity (%)	BET surface area ($m^2\ g^{-1}$)	Averaged pore size[b] (nm)
A	NSL(48)	40	162	20
B	NSL(63)	40	150	23
C	NSL(91)	40	[c]	[c]

a. For membrane preparation, the mass ratio of PNS-*b*-PLA to DCPD was approximating 2:1, and the G2 catalyst content was 0.4 wt %. *b*. The average pore diameter by N_2 adsorption experiment was calculated from the adsorption isotherm using the Barrett-Joyner-Halenda (BJH) method.[39] *c*. Not performed.

3.3.3 The membrane skin layer

As just demonstrated, these PNS/polyDCPD films exhibit a 3D nanoporous structure throughout the film. However, the surface layer was mostly nonporous and likely coated with polyDCPD homopolymer (Figure 3.19a). The formation of such a skin layer was attributed to the solvent evaporation during the crosslinking process. As the solvent evaporated, some DCPD was brought to the surface, and was then polymerized into a dense polyDCPD layer. Additionally, polyDCPD was preferred to form at the interfaces because a polar polymer like

PLA possesses higher surface energy than typical hydrocarbon polymers.[i] In order to characterize the continuity in these nanoporous membranes and demonstrate their potential utility, the skin layer must be removed. Physical abrasion and chemical etching (e.g., oxidants) methods failed to uniformly remove the surface layers. Nevertheless, reactive ion etching, a common tool in copolymer lithography,[40] successfully removed the surface layer. For example, a preliminary etching test was performed on membrane B of Table 3.2. After 30 s of etching,[j] the surface was nearly as porous as the interior (Figure 3.19b). After 2 min treatment of O_2 plasma, the nonporous surface was completely removed to display a nanoporous structure instead. Noticeably, pillar-like domains were fabricated on the membrane surface after 2 min etching and were caused by some etching-resistant regions or oxidation residues from polyDCPD. In fact, a short etching time (e.g., 1 min) is typically sufficient to remove the skin layer.

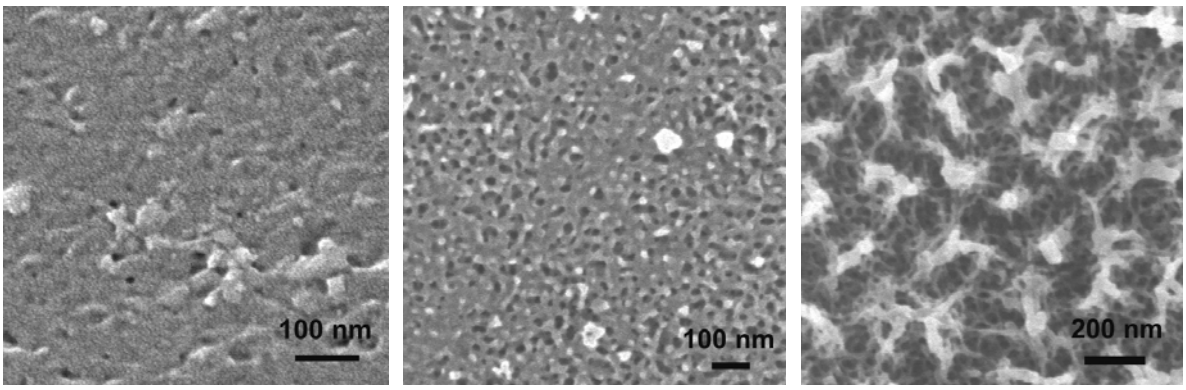

(a) (b) (c)

Figure 3.19. SEM images of the surface of the nanoporous membrane: the original surface (a), after O_2 plasma etching for 30 s (b), and after O_2 plasma etching for 120 s (c), coated with 2 nm of Pt.

In addition to the O_2 plasma etching, effect of the solvent in the crosslinking process was investigated as a means of controlling the skin layer. For the membrane preparation, the

[i] This can be roughly indicated from solubility parameters for these polymers, see Chapter 2.

[j] The etching rate of PS was approximated 1 nm per second based on the description in the Nanofabrication Center at UMN.

initially solution was homogeneous without any supermolecular aggregates, while the bicontinuous nanostructure was developed by a PIPS process. Many solvents such as toluene and THF, which can readily dissolve both PNS-PLA and DCPD, were used in the crosslinking study. Consequently, the use of different solvents had no influence on the membrane morphology but did affect the thickness of the dense skin polyDCPD layer. Using CH_2Cl_2 or THF, the surface layer was nearly nonporous; using toluene, the surface layer was more porous (not shown below). One possible reason for such results was the solvent evaporation rate. For a less volatile solvent, less DCPD was brought to the surface before gelation of the solution.

An alternative idea of controlling the surface structure was adding a volatile solvent that preferably dissolves PLA in the crosslinking process. When this solvent evaporated to the membrane surface, more PLA-containing copolymers would locate at the surface, and thus after crosslinking, the PLA phase at the surface could be etched away to leave nanopores. Acetone is a good candidate solvent, since it can readily dissolve the PLA phase but is incompatible with polyDCPD.[23] Experimentally, when a small amount of acetone (10 % relative to THF) was used in the crosslinking, the surface layer was notably more porous after PLA degradation, shown in Figure 3.20b.

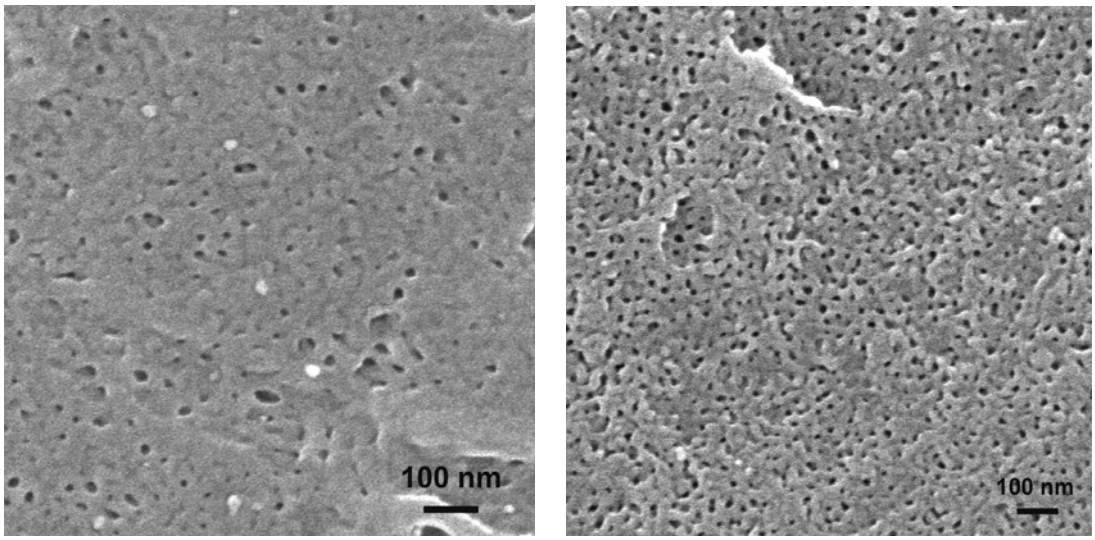

(a) (b)

Figure 3.20. SEM micrographs of the membrane surface to air, coated with 2 nm of Pt. (a) no acetone in the initial THF solution; (b) with acetone. The surface to the substrate was affected in a similar manner.

3.3.4 Diffusion measurements on the nanoporous membranes[k]

Gas diffusion measurements have been performed on membrane B in Table 3.2 as previously described.[41] As expected, effective diffusion coefficients are higher for gases with lower molecular weights. The close agreement between the experimental and Knudsen coefficients showed that the transport through the pores occurs by a Knudsen mechanism. Knudsen diffusion is the result of collisions between the gas molecules and pore wall as opposed to intermolecular collisions between the gas molecules. This is the expected result because the pore diameter (23 nm) is smaller than estimates of the gases' mean free path. Finally, Table 3.3 summarizes the gas selectivity relative to helium as calculated through experiments and Knudsen theory.[42]

[k] The gas and water diffusion experiments were performed by Bill Phillip and Mark Amendt, respectively.

Table 3.3. Experimental and predicted diffusion coefficients and selectivities.

Solute	D^a	$D_{Kn}{}^b$	α_{exp}	α_{Kn}
He	0.089	0.085	1.00	1.00
N_2	0.031	0.032	2.82	2.66
Ar	0.027	0.027	3.27	3.15

Effective, Knudsen and kinetic theory diffusion coefficients have units of $cm^2\ sec^{-1}$. *a*. Experimental data. *b*. Prediction from the Knusen theory using a tortuosity of 2.3.

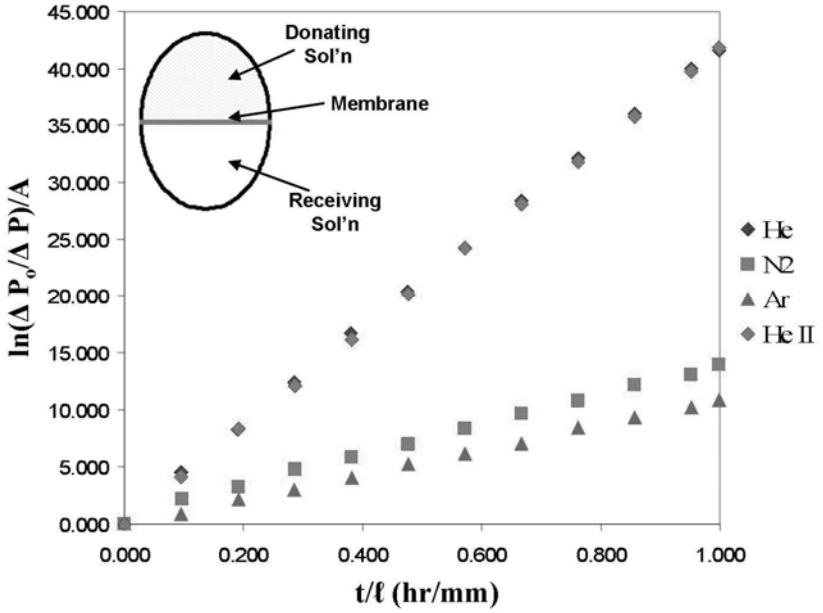

Figure 3.21. Diffusion data for different gases through the nanoporous membrane B. The two helium runs show the typical reproducibility between samples. Reproduced from Ref 41. Copyright 2007 American Chemical Society.

Additionally, water diffusion through these membranes was reported in a recent paper, disclosing the relationship between the bicontinuous nanoporous structure and diffusion properties.[43] Herein, the ultrafiltration experiment is highlighted. The MWCO curves of two membranes[1] were measured according to "Standard Test Method for Molecular Weight Cutoff Evaluation of Flat Sheet Ultrafiltration Membranes,"[44] using a dextran solution with molecular weights ranging from 1×10^3 to 1×10^6 g mol^{-1}. The resulting MWCO curves for the membranes are shown below with a commercial ultrafiltration membrane. These

[1] Compositionally similar to membranes A and C in Table 3.2.

crosslinked membranes templated from PNS-PLA block copolymers had sharper MWCO curves, and by tailoring the molecular weight of the PLA block the pore size and selectivity can be tuned. However, the fluxes of the membranes were an order of magnitude less than that of the commercial membrane: the sample membranes had a flux of 74.9 L hr^{-1} MPa^{-1} m^{-2} while the commercial membrane had a flux of 1070 L hr^{-1} MPa^{-1} m^{-2}.

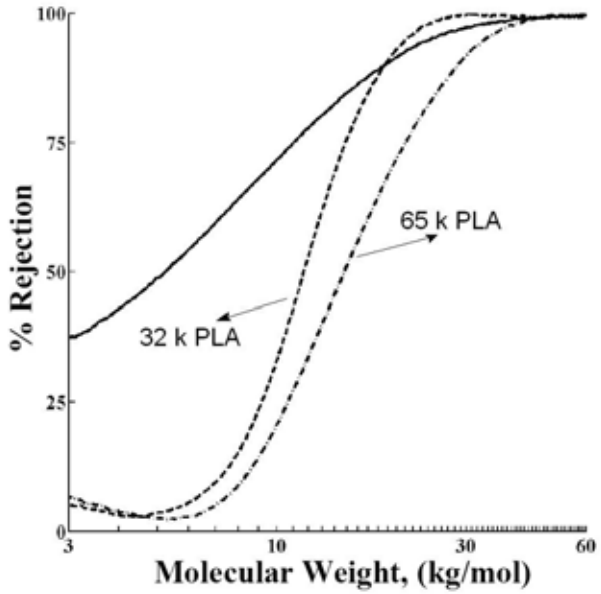

Figure 3.22. PNS/polyDCPD membranes showing sharper MWCO curves than the membrane made by phase inversion. Reproduced with permission from Ref 43. Copyright 2009 American Chemical Society.

The lower flux of the sample membranes presumably arose from the relative thickness of the active barrier, as the flux across a membrane depends inversely on the thickness of the membrane. The barrier layer for the sample membrane is the thickness of the entire membrane, ca. 120 μm, while the commercial membrane is an asymmetric membrane with a thin barrier layer of less than 1 μm. In the future, new fabrication methods should be explored in order to overcome the membrane thickness, such as by coating an active layer on a macroporous substrate.

3.3.5 Other crosslinked films

3.3.5.1 Crosslinked films with additives

For the membrane preparation, an additional component such as a PLA homopolymer can be added to potentially tune the pore size. Initially, the limit of PLA homopolymer that was added to a reactive blend was examined. A blend comprised of NSL(19), DCPD, PLA (10.3 kg mol^{-1}), **G2**, and THF at a mass ratio of 18:41:41:0.4:400 was prepared. After crosslinking, the resulting membrane was opaque white and turned white upon etching the PLA component. IR characterization indicated complete PLA removal in the resultant membrane. Tensile tests on the crosslinked membranes suggested that mechanical integrity was substantially reduced after PLA removal: a tensile strength of 75 MPa with an elongation at break of 15 % before PLA removal; a tensile strength of 20 MPa with an elongation at break of 5 % after PLA removal. The opaque appearance implied that macrophase separation occurred in this membrane, which was confirmed by SAXS characterization where no scattering peak was observed. Furthermore, the SEM micrographs (Figure 3.23) of the fractured membrane after PLA degradation show large irregular pores of < 0.5 μm. The large pores were templated from the PLA homopolymer. In the PIPS process, the PNS-*b*-PLA copolymer stabilized the interfaces between the PLA and polyDCPD domains to some extent, and thus shrank the PLA domain size as opposed to the circumstance without using the copolymer.[m] However, the copolymer composition (e.g., 18 % in the crosslinked film) fell below the limit where uniform nanodomains could be effectively stabilized. In separate studies, incorporation of less PLA homopolymer (~30 wt % to the copolymer) could give rise to bicontinuous PLA nanodomains, where the domain spacing could increase about 50 %.[n]

---

[m] In Section 3.3.6.2, pores of > 2 μm in polyDCPD were templated by PLA (10 kg mol^{-1}) through a PIPS process.

[n] This work was described in Mark Amendt's written dossier.

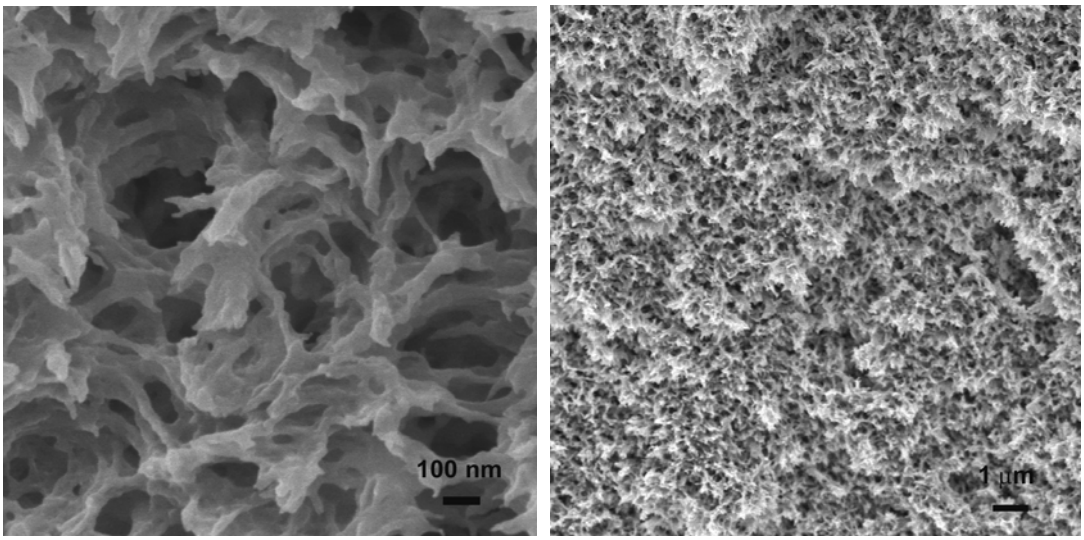

Figure 3.23. SEM images of the fractured surface of the porous polyDCPD/PNS membrane, coated with 3 nm Pt.

Additionally, expanding the pore size using a high boiling point solvent such as acetylacetone was investigated. Acetylacetone is a good solvent for the PLA block but incompatible with polyDCPD. Due to the low volatility of acetylacetone, it would mostly remain in the PLA domains after crosslinking. Through incorporation of this compound in the crosslinkable solution (acetylacetone:THF=2:3 by volume), the domain spacing of the prepared membrane increased about 20 % by SAXS measurements. Nonetheless, the expansion of the domain spacing was not simply correlated with the acetylacetone composition.

Collectively, the above examples demonstrated that the preparation of nanoporous membranes from a PNS-PLA copolymer could be generally applicable in blend systems, where additives (e.g. homopolymers or small molecules compatible with the PLA phase) can be incorporated to facilely tune the pore size.

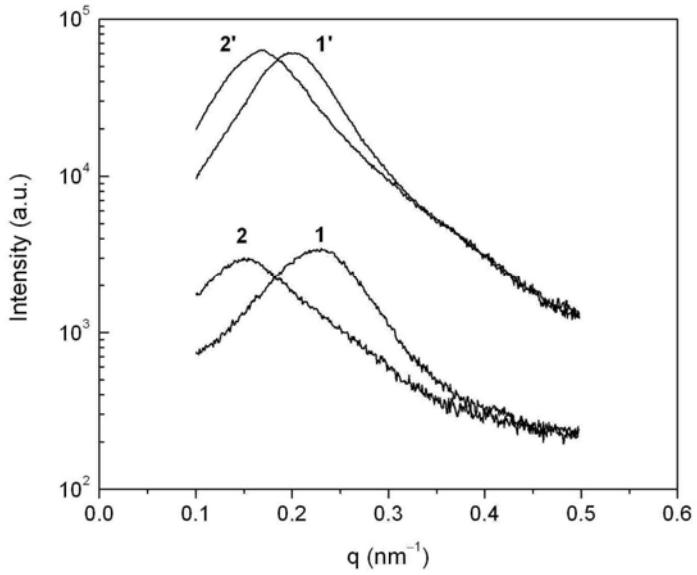

Figure 3.24. SAXS profiles of the crosslinked membranes before (1,2) and after (2,2') removing PLA. Membrane 2 was prepared in the presence of acetylacetone.

3.3.5.2 Crosslinked films containing PCOE

In previous examples, polyDCPD was mostly utilized as a robust component to toughen the nanoporous membranes. In practice, other tough polymers produced by ROMP like PCOE could also be crosslinked with PNS-*b*-PLA, to achieve high strength and high ductility in the resultant membrane. A blend was prepared from NSL(48) and COE in the same composition as membrane A in Table 3.2. The resultant crosslinked film exhibited great elasticity similar to the parent PCOE. Tensile tests (Figure 3.25) on the membrane indicated a tensile strength exceeding 20 MPa and an elongation at break of about 200 %, which was largely attributed to the semicrystalline PCOE component. SAXS experiments (Figure 3.26) indicated a similar scattering peak as in previous crosslinked polyDCPD/PNS-PLA membranes. Furthermore, TEM characterization was performed to examine the morphology and indicated a disordered network morphology (Figure 3.27), similar to the image in Figure 3.8.

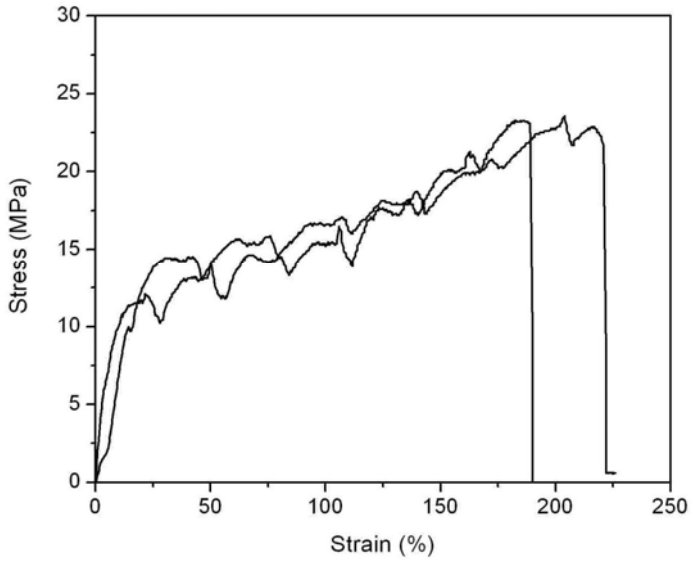

Figure 3.25. Tensile tests on the crosslinked film containing PCOE.

Next, this membrane was subjected to base hydrolysis to degrade PLA. Using the standard procedure (see Section 3.2.4), less than 20 wt % PLA was successfully removed based on the sample mass. By SAXS analysis, the scattering intensity of the degraded film decreased, against the formation of nanopores in the film. Possibly, the degradation temperature of 70 °C was too high to collapse formed nanopores. Thus, PLA degradation was performed under a mild degradation condition, using a 0.5 M base solution containing 0.5 wt % SDS at 50 °C.[45] The PLA component in the crosslinked film was completely removed after 30 d, based on the mass loss and IR spectra. Nevertheless, SAXS analysis of the degraded film exhibited no scattering peak (Figure 3.26), and SEM analysis did not reveal any nanoporous structure (not shown below). Clearly, pore collapse still occurred during the PLA degradation. PCOE homopolymer has a melting temperature around 50 °C and a T_g below 0 °C. Although PCOE chains were tethered between PNS chains, the resultant matrix could become soft at 50 °C and therefore collapse nanopores. Based on this example, for the crosslinking membrane from PNS-PLA, the choice of a reactive monomer should satisfy certain criteria like high T_g and desirable stiffness, in order to successfully template nanopores from the PLA

phase.

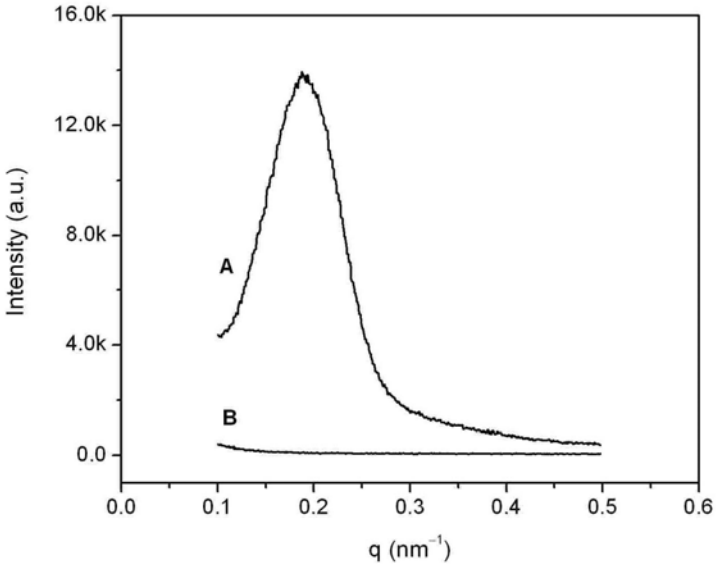

Figure 3.26. SAXS profiles of the crosslinked film produced from NSL(48) and PCOE by metathesis reactions before (A) and after (B) PLA removal.

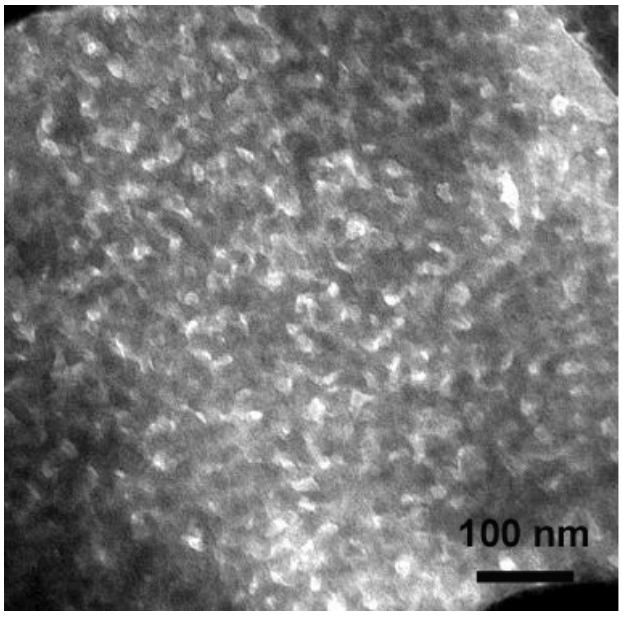

Figure 3.27. TEM image of the crosslinked membrane produced from NSL(48) and PCOE. The sample was cryo-microtomed at −120 °C and the double bonds in PCOE were stained by OsO_4.

3.3.6 Mechanism studies of the structure formation

3.3.6.1 Direct investigations

The fabrication of nanoporous membranes via a PIPS scheme combined with PNS-*b*-PLA block copolymers has been successfully demonstrated in previous sections. Following this, understanding how the bicontinuous nanostructure formed through the PIPS process is critically important. Next, additional experiments were performed to study the crosslinking process.

First, in the crosslinking process, the catalyst concentration did not affect the membrane morphology but influenced the resulting mechanical strength. In previous examples, about 0.4 wt % metathesis with respect to PNS-PLA/DCPD was used and yielded robust crosslinked membranes. When using a low catalyst loading (e.g., 0.1 wt %), the mechanical strength was reduced in the resultant membrane. Theoretically, all norbornene groups would be fully crosslinked even using a low catalyst loading. In fact, all membranes were prepared in air and the metathesis catalyst would degrade at a slow rate thereby causing insufficient crosslinking using a low catalyst loading.[35]

Second, the effect of solvent content in the PIPS process was briefly examined. Two membranes were produced using the same composition as membrane C in Table 3.2. In a 10 % THF solution, gelation occurred at 5 min and a well-defined bicontinuous structure was observed by SEM after etching PLA (Figure 3.28a). In a 5 wt % THF solution, no gelation was observed within 1 h during crosslinking. However, after THF evaporation, a crosslinked film was produced, in which the PLA phase was then completely removed. SEM image of the resultant film (Figure 3.28b) exhibited nanopores and large voids of > 200 nm. Moreover, the membrane produced from the dilute THF solution was mechanically weak, agreeable with the presence of large voids. The formation of such an irregular porous structure was likely attributed to the following reasons. For the crosslinking reaction in a dilute solution, some crosslinked PNS-PLA/polyDCPD domains could not be connected (no gelation), although these domains finally overlapped after THF evaporation. In the resultant membrane, regions

between these domains might be not sufficiently crosslinked and thereby leave large voids. From these experiments, a proper concentration of the initial THF solution (for example containing 10–20 % PNS-PLA and DCPD) is preferred to yield robust crosslinked films with uniform nanopores.

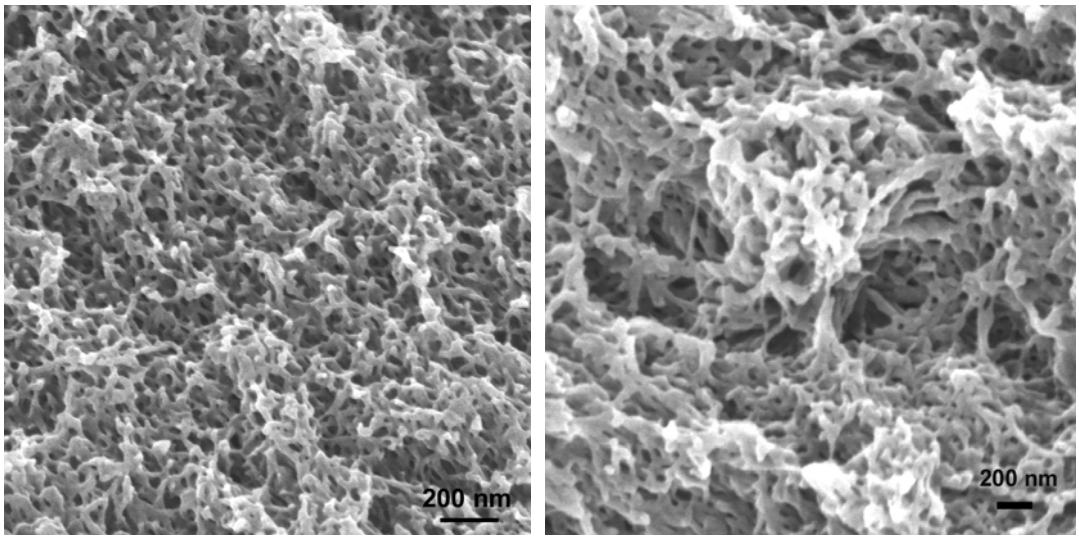

(a) (b)

Figure 3.28. SEM images of nanoporous membranes produced from NSL(91) and DCPD at a mass ratio of 2:1, coated with 2 nm Pt. The initial THF concentrations were 15 % (a) and 5 % (b), respectively.

Third, the reaction time affected both the mechanical properties and the morphology in resulting membranes. Certain reaction time (ca. 1 h) was required to render all components fully crosslinked, while the development of the bicontinuous structure along crosslinking occurred within 1 h. Time-dependent experiments on the crosslinking process might be helpful to elucidate the formation of the bicontinuous morphology.

SAXS experiments using the synchrotron source were first performed on crosslinkable solutions in THF and cured films. For either a dilute (10 %) or concentrated (30%) solution containing NSL(19) and DCPD (mass ratio of 2:1) in THF without catalysts, no scattering peak was observed (Figure 3.29a). This result might imply no microscopic structure existent in the initial THF solutions. The crosslinked film with a bicontinuous morphology was stable

in THF, so the swollen film should be microphase-separated. Experimentally, SAXS analysis of the swollen film exhibited no scattering peak (Figure 3.29b), but a scattering peak appeared along with THF evaporation. These unexpected results suggested that THF substantially reduced the scattering contrast. Therefore, the SAXS analysis of the initial crosslinkable solutions could not confirm a homogeneous state without micellular structures, despite the absence of scattering peak.

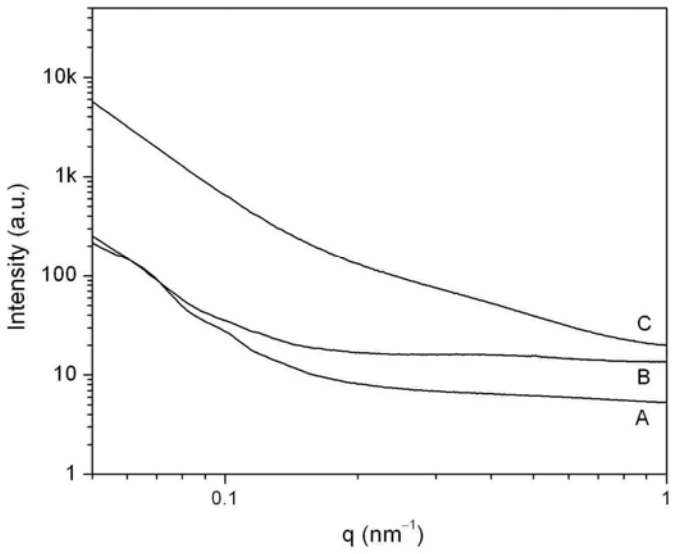

(a)

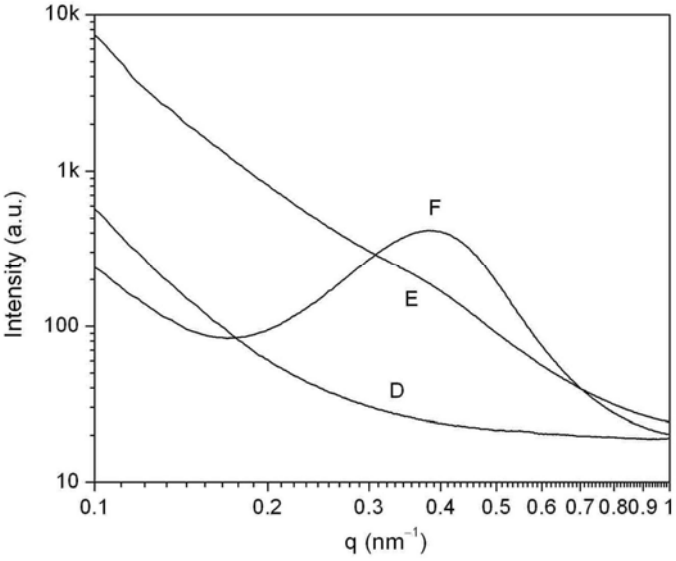

(b)

Figure 3.29. Synchrotron X-ray scattering profiles of the crosslinkable solutions in THF (a), and the crosslinked samples (b). In figure a, the A, B, and C curves represent blank, dilute, and concentrated NSL(19)/DCPD solutions in THF, respectively. In figure b, the D, E, and F curves represent swelled, partially dry, and dried crosslinked samples, respectively.

Next, time-dependent synchrotron SAXS analysis of the crosslinking process was conducted. A THF solution containing NSL(19) and DCPD at a mass ratio of 2:1 (20 wt % in THF) was prepared prior to analysis. After adding a deactivated metathesis catalyst (to attenuate the crosslinking reaction, details described in Chapter 2), the solution was immediately sealed in a quartz capillary tube for SAXS measurements (Figure 3.30). Given the gelation of this reactive blend occurred at about 16 min, the crosslinking process could be monitored by SAXS with an acquisition time of about 2 s. At 8 min, the appearance of a broad scattering peak at 0.25 nm^{-1} indicated a domain spacing (D) of 25 nm; at 12 min, this peak lightly shifted to a higher q value (corresponding to D = 23 nm) and reached a maximum. At 18 min, the scattering peak vanished. Based on the observation, the initial scattering peak could be indicative of the initial crosslinking reaction of PNS chains, where the scattering peak was possibly attributed to heterogeneous THF distribution in the blend. After gelation, the structural development was likely complete, and THF homogeneously distributed in the crosslinked sample thus eliminating the SAXS contrast. By this experiment, the driving force for the change of THF distribution was still not clear. Hypothetically, the initial metathesis reaction of PNS chains was exothermic, so the produced heat possibly drove some THF outside the reacted PNS/THF domains to induce the scattering contrast.

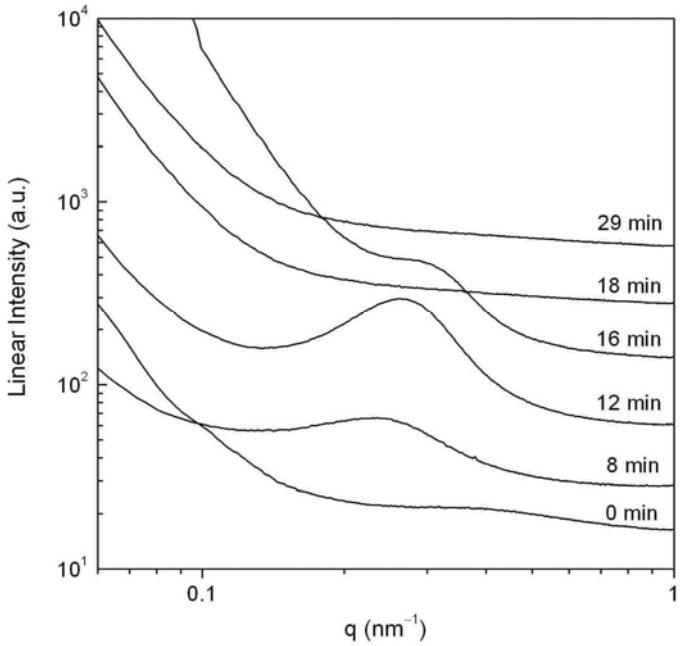

Figure 3.30. Time-dependent SAXS profiles for the PIPS process of a crosslinkable mixture of PNS-*b*-PLA and DCPD in THF. Signals were intentionally shifted vertically.

This PIPS process was different from other conventional PIPS processes in reactive polymer blends, where the scattering contrast from two domains was always present and the scattering peak shifted to a lower q along the PIPS process over several hours.[46] In our examples, the presence of THF and fast metathesis reactions made the crosslinking process difficult to resolve.

To further understand the structure in the initial THF solution, dynamic light scattering experiments was performed on a THF solution containing 15 wt % NSL (19) and 10 % DCPD. A weak scattering signal (Figure 3.31) was detected, consistent with a solution without supermolecular aggregates. The signal fitting resolved a hydrodynamic radius (R_h) of 8.1 nm, close to the size of the free chain size of NSL(19).[o] DLS analysis of a fully crosslinked gel indicated a size in the micrometer length scale, which in fact was not clearly

[o] The domain of NSL (19) was about 18 nm by SAXS, approximately equal to twice of the radius of gyration (R_g) of NSL(19). The R_g of PNS-PLA was 9 nm, comparable to the R_h of PNS-PLA in a good solvent.

understood. Thus, DLS experiments may not be helpful to indicate the crosslinking process, since the structural definition is lacking and relatively long acquisition time is typically needed.

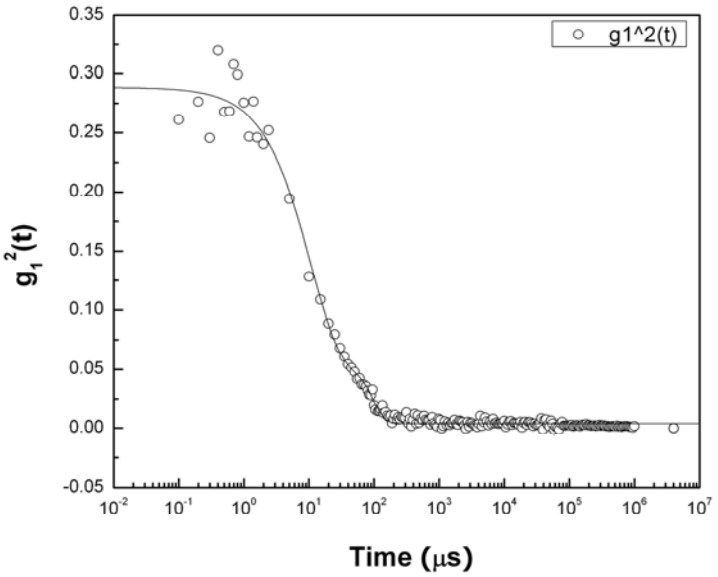

Figure 3.31. Correlation function plotted against the relaxation time in the DLS analysis of a NSL(19)/DCPD mixture in THF (20 wt %). The signal fitting gives the R_h of 8.1 nm.

Additionally, NMR spectroscopy was employed to address the reactivity of all components during crosslinking (Figure 3.32). The same blend as in the SAXS study was prepared in $CDCl_3$ in an NMR tube, and 0.2 mL CH_2Cl_2 was added as a reference. During the NMR experiment, the acquisition signal time (8 s) was much shorter than the gelation time of 20 min. At t=0 min, signals corresponding to each component are clearly observed; before gelation, the signals of the PNS component decreased somewhat, while other signals remained. After gelation (1 h), the signals of the PNS component were reduced, since the group relaxation in the crosslinked PNS phase was largely hindered. At 24 h, all DCPD molecules were fully crosslinked and gave rise to no NMR signals, but the PLA component still gave weak NMR signals. This result strongly suggested that the PLA phase was not incorporated in the crosslinked PNS/polyDCPD phase, but the relaxation of the PLA phase

was somewhat hindered presumably due to the confinement of the PLA phase in a crosslinked matrix. Finally, after performing PLA degradation in the NMR tube,[p] the resulting gel was washed with methanol and swelled in $CH_2Cl_2/CDCl_3$. The NMR signal of the degraded sample indicated the absence of PLA signals, consistent with the complete removal of the PLA component.

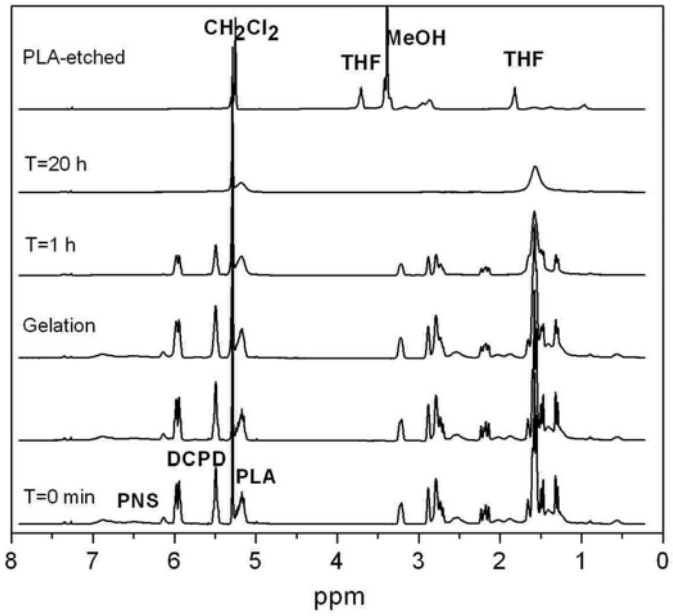

Figure 3.32. NMR spectra of a PNS-PLA/DCPD blend during metathesis reactions.

Collectively, although direct visualization of the structure formation in the PIPS process is still lacking, all above characterizations may shed light on the mechanism for structure formation. Based on a similar PIPS process,[47] the PIPS process during metathesis reactions of PNS-*b*-PLA and DCPD is generically depicted in Figure 3.33. Initially, free polymer chains and DCPD evenly distribute in the THF, and then the metathesis reaction of PNS-*b*-PLA and DCPD generate small crosslinked regions, where the PLA chains are segregated from the reacted PNS/polyDCPD domains. In the below scheme, fewer polymers chains were intentionally drawn in the first two stages to clarify the structure. At a proper

[p] PLA was degraded in a 1M tetrabutyl ammonium fluoride (TBAF) solution in THF at RT for 1 d.

concentration, the crosslinked regions tend to overlap with each other. PLA chains are located around crosslinked PNS/polyDCPD domains and favor a phase with low interfacial energy, for example, a bicontinuous morphology. After gelation, the morphology evolution is mostly complete, while more free DCPD molecules are polymerized in the PNS/polyDCPD domains to achieve high crosslinking density.

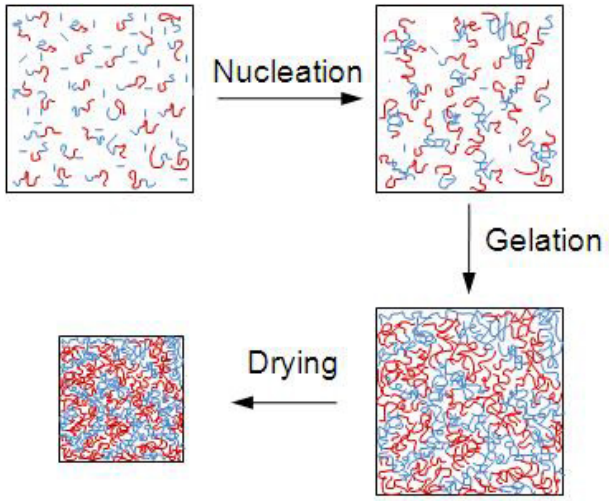

Figure 3.33. Structure formation in the PIPS process of the metathesis crosslinking reactions of PNS-PLA and reactive monomers.

3.3.6.2 Effect of the polymer structure on the morphology

According to the proposed mechanism, without adding DCPD, metathesis reactions of PNS-PLA copolymers in THF would give rise to the same nanostructure and PLA would be completely degraded afterwards, although this resulting material might be brittle; preliminary experimental results were consistent with this hypothesis. Since the role of polyDCPD is just as a tough polymer filled in the PNS domains, the bicontinuous morphology should arise from the highly crosslinked PNS-*b*-PLA.

Some experiments were performed to understand the morphology of *in situ* formed graft polymers. A model graft copolymer PCOE-*g*-PLA_1 was synthesized by a combination of ROMP and ROP schemes (see Section 3.2.3.7). The resultant copolymer possessed a

well-defined chain length of 3 kg mol^{-1} and on average 12 PLA chains grafted on each PCOE backbone. In addition, similar grafted copolymers were produced by *in situ* copolymerizations of COE and norbornene-attached PLA (PLA-N) in THF, summarized in Table 3.4. Two PLA-N macromonomers were utilized in this study, to produce different grafted PLA arms.

Table 3.4. Summary of the graft copolymers

Entry	Polymer	SEC M_n(kg mol^{-1})/PDI	NMR M_n(kg mol^{-1})	SAXS peak	TEM[c]
1	PCOE-*g*-OH	44.8/1.69	21.4		
2	PCOE-*g*-PLA_1	63.2/2.03	44.9	yes	yes
3	PLAN_1	5.5/1.11	2.9		
4	PLAN_2	15/1.1	10.3		
5	PCOE-*g*-PLA_2[a]			no	
6	PCOE-*g*-PLA_3[b]			yes	yes

a. PCOE-*g*-PLA_3 was synthesized by a ROMP process: in THF (20 mL), PLAN_1 (0.9 g) and COE (0.6 g), CT (5 mg), and G2 (1.2 mg, 10 mol % relative to the CT) reacted at RT overnight, and the resulting copolymer was recovered through precipitation in methanol, and on average 4–5 PLAN_1 units were grafted on the PCOE backbone. *b*. PCOE-*g*-PLA_2 was produced with PLAN_2 using the same procedure, on average < 1 PLA were grafted on the PCOE backbone. *c*.TEM images are shown in Figure 3.35.

For the graft copolymer PCOE-*g*-PLA_1, a relatively narrow scattering peak was observed, indicating a disordered but phase separated structure. Using PLAN_2, the resulting graft copolymer was mostly comprised of homopolymers with some PCOE-PLA diblock copolymers, due to the low reaction efficiency of PLAN_2 and COE. As a result, SAXS analysis of PCOE-*g*-PLA_2 did not exhibit a scattering peak, suggesting no microphase-segregated structure. For the resultant PCOE-*g*-PLA_3, a small amount of unreacted PLAN_1 homopolymer was still present in the graft copolymer based on SEC analysis due to the incomplete grafting reaction, but a broad scattering peak was evident for microphase separation.

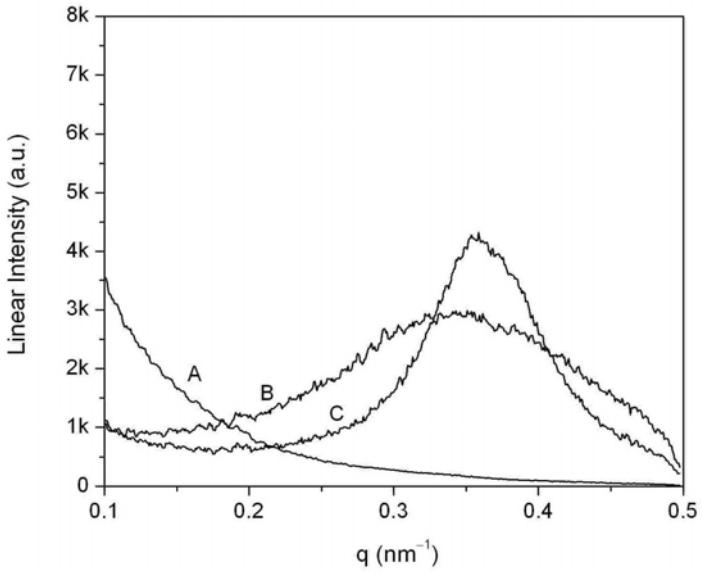

Figure 3.34. SAXS profiles of PCOE-*g*-PLA copolymers in Table 3.4. The A, B, and C curves denote PCOE-*g*-PLA_2, PCOE-*g*-PLA_3, and PCOE-*g*-PLA_1, respectively.

TEM experiments were carried out on two microphase-separated samples (shown in Figure 3.35). PCOE-*g*-PLA_1 exhibited a disordered network structure, similar to the bicontinuous morphology of the PNS-PLA/polyDCPD membranes (Figure 3.8). The TEM image of PCOE-*g*-PLA_3 exhibited less uniform PLA domains in the PCOE matrix, consistent with the broader scattering peak by SAXS. Thus, well-defined graft copolymers can help adopt a bicontinuous structure. In previous examples, PNS-*b*-PLA having more norbornene groups could render a highly graft structure due to multiple reactive sites on each copolymer backbone. When some reactive monomers like DCPD and COE included in the crosslinking process, the bicontinuous morphology would be retained with polyDCPD tethered between PNS domains.

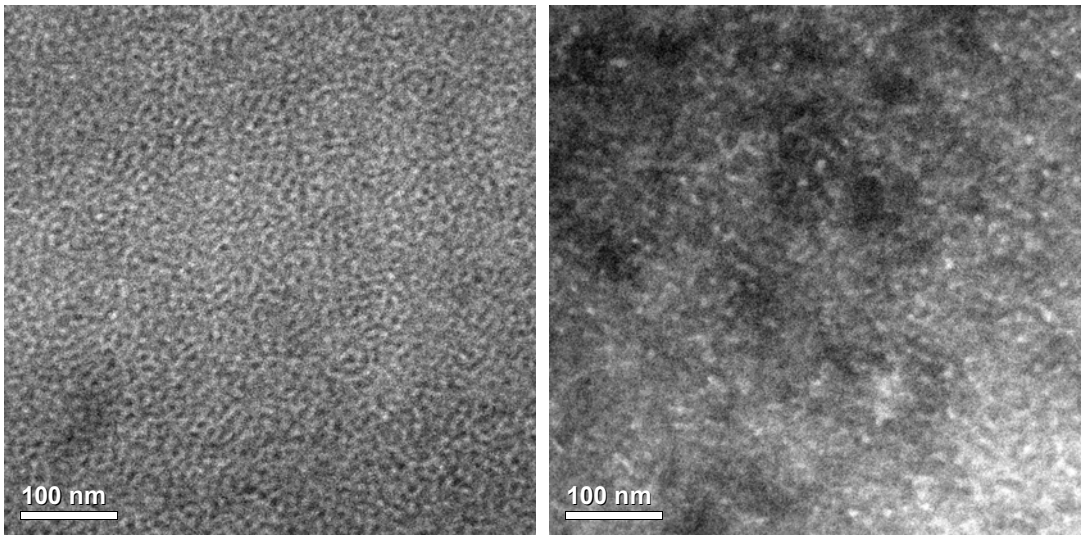

(a) (b)

Figure 3.35. TEM images of PCOE-*g*-PLA_1 (a) and PCOE-*g*-PLA_3 (b). The polymer samples were cryo-microtomed into about 80 nm thick pieces and stained with OsO_4, and bright domains correspond to unstained PLA domains.

Furthermore, the mechanism of the structure formation could be interpreted from a different aspect by focusing on the role of DCPD. Metathesis polymerization of DCPD in a THF solution with PLA (10 kg mol^{-1}) formed an opaque film. Subsequently, the PLA component was completely removed by base hydrolysis. SEM analysis of the resultant film indicated the presence of a bicontinuous macroporous structure (> 2 μm) (Figure 3.37a). As previously demonstrated, 3D nanoporous membranes were produced from crosslinking PNS-PLA with DCPD in THF followed by PLA degradation. Thus, a critical factor in the PIPS process is the number of norbornene groups in the PLA-containing polymer and deserves further exploration. Several model polymers, including PS-PLA, PLAN (10), and PNS-PLA copolymers with different norbornene groups, were studied in the crosslinking process of DCPD and summarized in Table 3.5.

By the ROMP of DCPD in THF with PS-*b*-PLA, the resultant membrane was macrophase-separated containing isolated polyDCPD and PS-PLA domains, while a scattering peak was observed corresponding to scattering from PS-PLA (not shown below). Since the resulting film was extremely brittle, PLA degradation in the film was not attempted.

Using a norbornene-attached PLA (Entry 2 of Table 3.5), the SAXS result indicated no pronounced phase separation similar to the example containing PLA homopolymer. Surprisingly, the PLA composition was completely removed by base hydrolysis, and the SEM image (Figure 3.37b) showed an irregular structure with pore sizes of < 200 nm. From this example, introduction of a reactive group on PLA helped limit the phase separation to prevent coarsening of the PLA domains and thereby yielded smaller pore sizes. For the crosslinked film produced with PNS-*b*-PLA copolymers having 3 norbornene groups per chain (Entry 4 of Table 3.5), after PLA degradation, a well-defined nanoporous structure was still observed. This example clearly indicated that 3 norbornene groups in the PNS chain could be enough to direct a well-defined bicontinuous structure. Lastly, in this example of Entry 5 in Table 3.5, the length of PNS block was relatively short and in the blend the mass ratio of PNS to DCPD was low, although the PNS block has 10 norbornene groups. The final nanoporous structure is quite irregular indicated from the SEM image (Figure 3.37d). This experiment elucidated that the PNS/monomer ratio was another critical factor for preparing the crosslinked membranes with well-defined bicontinuous nanopores. Based on the mechanism shown in Figure 3.33, if more DCPD molecules in the solution were not confined in the swollen PNS chains, the resultant polyDCPD would be formed outside the PNS/polyDCPD domains, which would disrupt the regularity of the bicontinuous structure.

Table 3.5. Summary of crosslinked polyDCPD films with different polymers[a]

Entry	Polymer	Appearance	SEM after PLA deg (pore size)[b]	SAXS peak	Brittle
1	PLAOH (10)	white	> 2 μm	No	Yes
2	PLAN (10)	opaque	< 200 nm	No	Yes
3	PS(11, 0)-PLA(11)[c]	opaque		Yes[d]	Yes
4	PNS(15, 3)-PLA(30)[e]	clear	~20 nm	Yes	No
5	PN(2, 10)-PLA (20)[e]	clear	~15 nm	Yes	No

a. PLA volume fraction and **G2** content in each film was fixed roughly at 40 wt % and 0.3 wt %, respectively, and initially the overall polymer/monomer fraction in THF was about 20 wt %. *b*. PLA was completely degraded. *c*. Obtained from Huiming Mao. *d*. This scattering peak originated from the PS-PLA copolymer *e*. PA(X,Y)-PB(Z) where X, Z indicate the NMR M_n values of each block and Y denotes the

number of norbornene groups per chain. *e*. Synthesized by a combination of anionic polymerization of N and styrene and ROP of D,L-lactide, following the description in Sections 3.2.3.2 and 3.2.3.3.

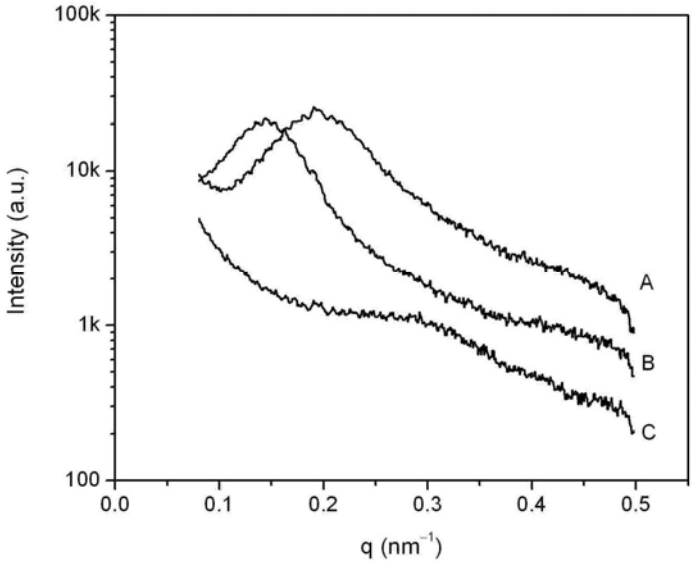

Figure 3.36. SAXS profiles of crosslinked polyDCPD with the PLAN and PNS-PLA copolymers. The A, B, and C curves represent the membranes made with PN-PLA(2-24, 10), PNS-PLA(15-30, 3), and PLAN(10), respectively.

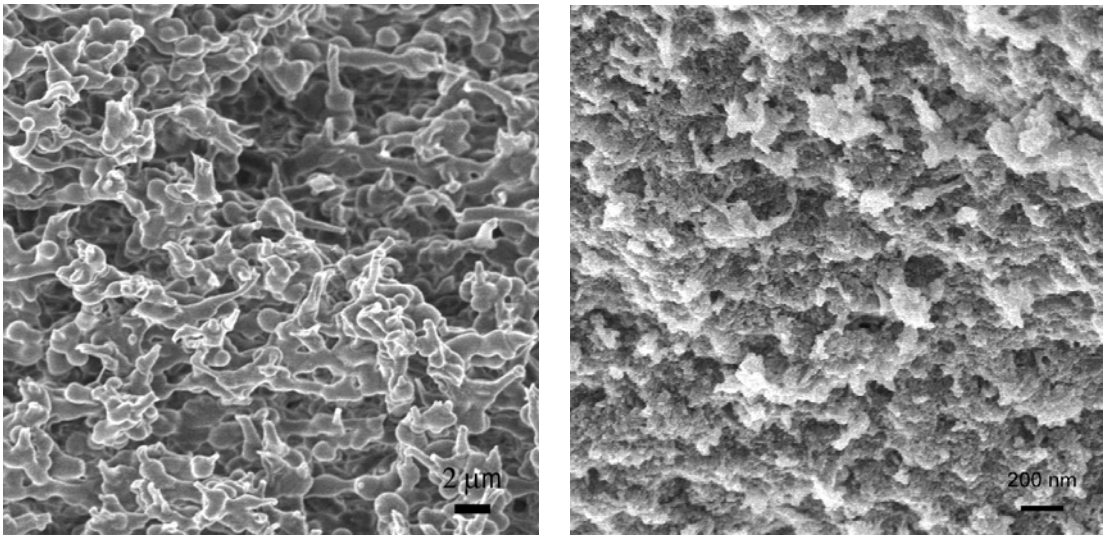

(a) (b)

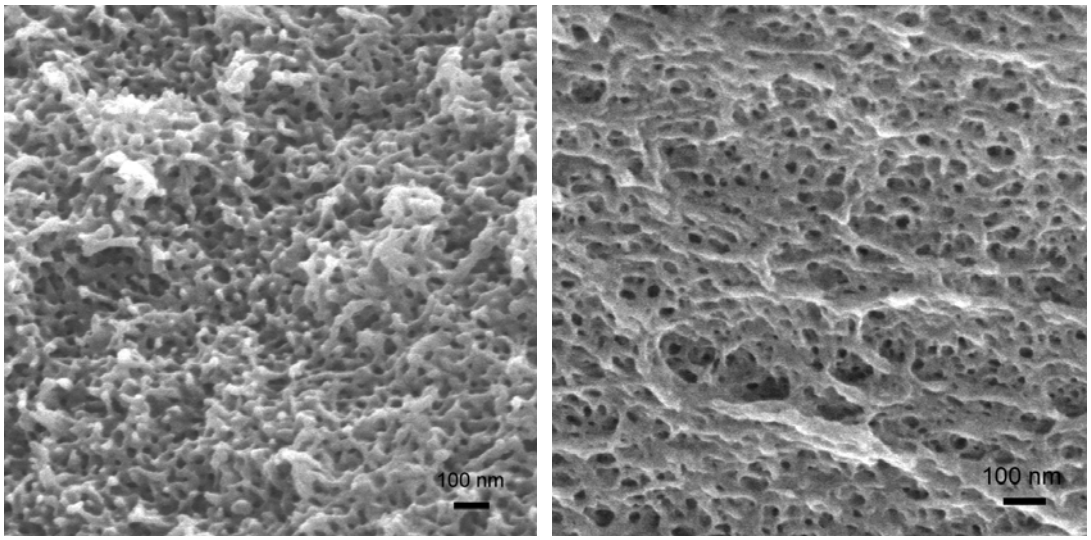

(c) (d)

Figure 3.37. SEM images of the porous membranes. Samples were coated with 2 nm Pt to prevent charging. Images a, b, c, and d correspond to entries 1, 2, 4, and 5 in Table 3.5, respectively.

2.4 Conclusions and outlook

By the combination of a thermosetting monomer (DCPD), a metathesis catalyst, and a doubly reactive block copolymer (PNS-PLA), robust nanoporous PNS/polyDCPD membranes can be generated by a PIPS process. In this preparation, the best bicontinuous nanopores can be achieved from a mixture containing PNS(M kg mol^{-1})-PLA(2M–3M kg mol^{-1}) (x g), DCPD (2x g), and THF (12x–15x g). The resultant membranes contain a percolating porous structure and excellent thermal stability and mechanical toughness. These membranes may have utility as high surface area catalysts supports, size selective membranes, and nanomaterial templates.[48] Preliminary tests have demonstrated potential use as filtration membranes, although technological challenges still exist in fabricating thin membranes.

To broaden the utility of such PIPS scheme, one interesting example is using triblock terpolymers having a short functional block in the middle to produce functional nanoporous membranes. For example, the triblock terpolymers below have been synthesized and nanoporous membranes produced from them have been studied.[49]

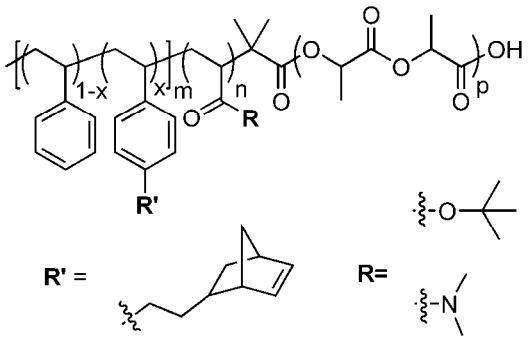

Beyond the metathesis crosslinking scheme, this novel preparation may shed light on new strategies for facile preparation of crosslinked membranes with 3D nanostructures. For instance, block copolymers with a radical-reactive block may be utilized to template 3D continuous nanostructures in crosslinked membranes by free-radical crosslinking.

3.5 References

[1] Strathmann, H.; Kock, K. *Desalination* **1977**, *21*, 241–255.

[2] (a) Peinemann, K.-V.; Abetz, V.; Simon, P. F. W. *Nature Mater.* **2007**, *6*, 992–996. (b) Xue, J.; Chen, L.; Wang, H. L.; Zhang, Z. B., Zhu, X. L. Kang, E. T.; Neoh, K. G. *Langmuir*, **2008**, *24*, 14151–14158.

[3] Olson, D. A.; Chen, L.; Hillmyer, M. A. *Chem. Mater.***2008**, *20*, 869–890.

[4] Bates, F. S.; Fredrickson, G. H. *Physics Today* **1999**, 32–38. Ruzette, A.-V.; Leibler, L. *Nature Materials* **2005**, *4*, 10-31. Bates, F. S. *MRS Bulletin* **2005**, *30*, 525–532**.**

[5] Mao, H.; Hillmyer, M. A. *Soft Matter* **2006**, *2*, 57–59.

[6] Crossland, E. J. W.; Kamperman, M.; Nedelcu, M.; Ducati, C.; Wiesner, U.; Smilgies, D.-M.; Toombes, G. E. S.; Hillmyer, M. A.; Ludwigs, S.; Steiner, U.; Snaith, H. J. *Nano Lett.* **2009**, in press.

[7] Chan, V. Z.-H.; Hoffman, J.; Lee, V. Y.; Iatrou, H.; Avgeropoulos, A.; Hadjichristidis, N.; Miller, R. D.; Thomas, E. L. *Science* **1999**, *286*, 1716–1719.

[8] Matsen, M. W. *Macromolecules* **1995**, *28*, 5765–5773.

[9] (a) Sun, P.; Yin, Y.; Li, B.; Chen, T.; Jin, Q.; Ding, D.; Shi, A.-C. *Phys. Rev. E* **2005**, *72*, 061408. (b) Lammertink, R. G. H.; Hempenius, M. A.; Thomas, E.; Vancso, G. J. *J. Polym. Sci. B: Polym. Phys.* **1999**, *37*, 1009–1021.

[10] (a) Okumura, A.; Nishikawa, Y.; Hashimoto, T. *Polymer* **2006**, *47*, 7805–7812. (b) Hashimoto, T.; Nishikawa, Y.; Tsutsumi, K. *Macromolecules* **2007**, *40*, 1066–1072.

[11] (a) Scriven, L. E. *Nature* **1976**, *263*, 123–125. (b) Kaler, E. W.; Davis, H. T.; Scriven, L. E. *J. Chem. Phys.* **1983**, *79*, 5685-5692. (c) Langevin, D. *Acc. Chem. Res.* **1988**, *21*, 255–260.

[12] Zhou, N.; Lodge, T. P.; Bates, F. S. *J. Phys. Chem. B* **2006**, *110*, 3979–3989.

[13] Ruegg, M. L.; Reynolds, B. J.; Lin, M. Y.; Lohse, D. J.; Balsara, N. P. *Macromolecules* **2006,** *39,* 1125–1134.

[14] Hillmyer, M. A.; Maurer, W. W.; Lodge, T. P.; Bates, F. S.; Almdal, K. *J. Phys. Chem. B* **1999**, *103*, 4814–4824.

[15] Zhou, N.; Bates, F. S.; Lodge, T. P. *Nano. Lett.* **2006**, *6*, 2354–2357.

[16] Jones, B. H.; Lodge, T. P. *J. Am. Chem. Soc.* **2009**, *131*, 1676–1677.

[17] Almdal, K.; Koppi, K. A.; Bates, F. S.; Mortensen. K. *Macromolecules* **1992**, *25*, 1743–1751.

[18] Takenaka, M.; Wakada, T.; Akasaka, S.; Nishitsuji, S.; Saijo, K.; Shimizu, H.; Kim, M. I.; Hasegawa, H. *Macromolecules* **2007**, *40*, 4399–4402.

[19] Uehara, H.; Yoshida, T.; Kakiage, M.; Yamanobe, T.; Komoto, T.; Nomura, K.; Nakajima, K.; Matsuda, M. *Macromolecules* **2006**, *39*, 3971–3974.

[20] Qi, S., Chakraborty, A. K.; Balsara, N. P. *J. Chem. Phys.* **2001**, *115*, 3387–3400.

[21] Pernot, H.; Baumert, M.; Court, F.; Leibler, L. *Nature Mater.* **2002***, 1*, 54–58.

[22] Ryan, A. J. *Nature Mater.* **2002**, *1*, 8–10.

[23] (a) Martina, A. D.; Hilborn, J. G.; Mühlebach, A. *Macromolecules* **2000**, *33*, 2916–2921. (b) Lee, J. K.; Gould, G. L. *J. Sol-Gel Sci. Technol.* **2007**, *44*, 29–40.

[24] Inoue, T. *Prog. Polym. Sci.* **1995**, *20*, 119–153.

[25] Kiefer, J.; Hedrick, J. L.; Hilborn, J. G. *Adv. Polym. Sci.* **1999**, *147*, 161–247.

[26] Pan, C.; Maurer, W.; Liu, Z.; Lodge, T. P.; Stepanek, P.; von Meerwall, E. D.; Watanabe, H. *Macromolecules* **1995**, *28*, 1643–1653.

[27] Rzayev, J.; Hillmyer, M. A. *Macromolecules* **2005**, *38*, 3–5.

[28] Hillmyer, M. A.; Laredo, W. R.; Grubbs, R. H. *Macromolecules* **1995**, *28*, 6311–6316.

[29] Kelsey, D. R.; Chuan, H. H.; Ellison, R. H. *J. Polym. Sci. A: Polym. Chem.* **1997**, *35*, 3049–3063.

[30] Bielawski, C. W.; Scherman, O. S.; Grubbs, R. H. *Polymer* **2001**, *11*, 4939 – 4945.

[31] Zalusky, A. S.; Olayo-Valles, R.; Wolf, J. H.; Hillmyer, M. A. *J. Am. Chem. Soc.* **2002**, *124*, 12761–12773.

[32] Meuler, A. J.; Mahanthappa, M. K.; Hillmyer, M. A.; Bates, F. S. *Macromolecules* **2007**, *40*, 760–762.

[33] Fetters, L. J.; Lohse, D. J.; Richter, D.; Witten, T. A.; Zirkel, A. *Macromolecules* **1994**, *27*, 4639–4647.

[34] Witzke, D. R.; Narayan, R.; Kolstad, J. J. *Macromolecules* **1997**, *30*, 7075–7085.

[35] Dinger, M. B.; Mol, J. C. *Organometallics* **2003**, *22,* 1089–1095.

[36] Gregg, S. J.; Sing, K. S. W. *Adsorption, Surface Area and Porosity*; Academic Press: London, **1982**.

[37] He, Y.; Lodge, T. P. *Chem. Comm.* **2007**, 2732–2734.

[38] He, Y.; Boswell, P. G.; Bühlmann, P.; Lodge, T. P. *J. Phys. Chem. B* **2007**, *111*, 4645–4652.

[39] Barrett, E. P.; Joyner, L. G.; Halenda, P. P. *J. Am. Chem. Soc.* **1951**, *73*, 373–380.

[40] Guo, S.; Rzayev, J.; Bailey, T. S.; Zalusky, A. S.; Olayo-Valles, R.; Hillmyer, M. A. *Chem. Mater.* **2006**, *18*, 1719–1721.

[41] Chen, L.; Phillip, W. A.; Cussler, E. L.; Hillmyer, M. A. *J. Am. Chem. Soc.* **2007**, *129*, 13786–13787.

[42] Cussler, E. L. In *Diffusion, mass transfer in fluid systems;* Cambridge University Press: New York, **1997**; page 580.

[43] Phillip, W. A.; Amendt, M. A.; O'Neil, B.; Chen, L.; Hillmyer, M. A.; Cussler, E. L. *ACS Appl. Materials & Interfaces* **2009**, *1*, 472–480.

[44] ASTM International Standard Test Method for Molecular Weight Cutoff Evaluation of Flat Sheet Ultrafiltration Membranes; **2001**; ASTME 1343–1390.

[45] Bailey, T. S.; Rzayev, J.; Hillmyer, M. A. *Macromolecules* **2006**, *39*, 8772–8781.

[46] Ishii, Y.; Ryan, A. J. *Macromolecules* **2000**, *33,* 158–166.

[47] (a) Ide, N.; Fukuda, T. *Macromolecules* **1999**, *32,* 95–99. (b) Kanamori, K.; Hasegawa, J.; Nakanishi, K.; Hanada, T. *Macromolecules* **2008**, *41*, 7186–7193.

[48] Tseng, W.-H.; Chen, C.-K.; Chiang, Y.-W.; Ho, R.-M.; Akasaka, S.; Hasegawa, H. *J. Am. Chem. Soc.* **2009**, *131*, 1356–1357.

[49] Roerdink, M. *et al.* unpublished results.

Chapter 4

Crosslinked Polymer Electrolyte Membranes from Reactive Block Copolymers[a]

In this chapter, poly(norbornenylethylstyrene-styrene)-poly(*n*-propyl-*p*-styrenesulfonate) (PNS-PSSP) was prepared by sequential atom transfer radical polymerizations. Crosslinked polymer electrolyte membranes (PEMs) were fabricated by metathesis crosslinking reactions of this copolymer and dicyclopentadiene (DCPD) and/or cyclooctene (COE) followed by deprotection of the PSSP component. The resultant PEMs with a bicontinuous morphology hold attractive mechanical and thermal stabilities, and the domain size of the ionic phase is controlled by the PSSP block. Select PEMs exhibit high proton conductivity similar to Nafion at high humidity. Additionally, the use of these PEMs in separating NH_3 from gas mixtures is briefly examined.

[a] Reproduced in part from Chen, L.; Hallinan, D. T.; Elabd, Y. A.; Hillmyer, M. A. manuscript submitted.

4.1 Introduction

Polymer electrolyte membranes (PEMs) have been widely studies as a key component in direct methanol fuel cell operations.[1] Nafion has been the benchmark material for fuel cell applications, due to its high proton conductivity and excellent chemical, oxidative and mechanical stabilities.[2] Besides its high cost, the use of Nafion in direct methanol fuel cells (DMFCs) has been limited to high humidities and low temperatures, because high methanol crossover limits the power output efficiency[3] and Nafion dehydration at high temperatures results into the elimination of continuous hydrated channels and thus reduced proton conductivity.[4] Many efforts to design new PEMs that can outperform Nafion have been made, and this area has been extensively reviewed over the last decade.[2,5] A brief overview of novel randomly sulfonated polymers was given in Chapter 1. Those materials have demonstrated appreciable thermal stabilities, reduced methanol diffusion, and similar proton conductivities to Nafion.

In most randomly sulfonated polymers, the ionic nanostructures were in general poorly controlled. Understanding the relationship between the morphology of PEM membrane candidates and their molecular structure is crucial for guiding future innovations. Over the last several years, nanostructured PEMs produced from block and graft copolymers containing sulfonated polystyrene (SPS) have been studied. Self-assembled block copolymers can lead to well-defined nanostructures where the morphology and domain size are tunable on the nanoscopic length scale.[6] More importantly, the physical attributes of the resultant materials can be independently tailored in many cases. For example, grafting SPS onto a fluorinated polymer using radiation-mediated polymerizations,[7] chemical grafting of SPS on PS, [8] poly(arylene ether), [9] poly(ethylene-tetrafluoroethylene), [10] poly(vinylidenedifluoride),[11] and poly(vinylidenedifluoride-chlorotrifluoroethylene)[12] have all been explored. Studies of these graft copolymer membranes presented compelling evidence that ionic conductivity was significantly enhanced by forming continuous

nanochannels of polyelectrolyte in the matrix material, and proton conductivity of all materials was an order of magnitude higher than that of randomly sulfonated PS (*r*-SPS), a material that exhibited no clear nanostructure at similar ionic contents.

Studies on other block polymers, such as sulfonated PS-*b*-poly(ethylene-*s*-butene)-*b*-PS,[13] PS-*b*-polyisobutene(PIB)-*b*-PS, [14] poly(ethylene-*s*-styrene) with short alternating PS segments, [15] and poly(vinylidenedifluoride-hexafluoropropylene)-*b*-SPS [16] have also indicated that the orientation of ionic domains in the PEM membrane could have a significant effect on the proton conductivity; the copolymer composition and the membrane preparation conditions are critically important in this regard. For example, Park *et al.*[17] studied a series of poly(methylbutylene) (PMB)-*b*-SPS diblock polymers and showed that the bicontinuous morphologies like gyroid or perforated lamellae benefited the proton conductivity. Moreover, they clearly demonstrated that the domain sizes formed by SPS block played a critical role in preventing membrane dehydration at high temperatures or lower humidity. For example, some PEMs with domain sizes < 5 nm in the dry state exhibited increases in conductivity with increasing temperature up to 90 °C. They proposed that the suppression of water evaporation from the PEMs was due to the capillary condensation of the water in confined nanochannels thus reducing its chemical potential. Based on these studies, the morphology in self-assembled PEMs and the size of the ionic phase are important to achieve a material with high proton conductivity at high temperatures and low humidity. The uncrosslinked PEMs with small ionic domains by Park *et al.* typically lacked of requisite thermal and mechanical stability and displayed high levels water uptake, which can be disadvantageous for DMFC applications due to increased methanol crossover under these conditions.

New crosslinked PEMs that (i) adopt a bicontinuous structure, (ii) contain a SPS phase, (iii) possess tunable domain sizes, and (iv) are mechanically and thermally robust are targeted. A series of poly(norbornenylethylstyrene-styrene)-poly(*n*-propyl-*p*-styrenesulfonate) (PNS-PSSP) block polymers are prepared by atom transfer radical polymerization (ATRP),

and these materials are utilized in a polymerization-induced phase separation scheme to yield robust precursor membranes (Figure 4.1).[18] These materials are readily converted into PEMs with a bicontinuous structure where the size of the ionic domains is easily tuned by changing the molecular weight of the PNS-PSSP copolymers. While the proton conductivities of some PEMs are similar to Nafion at high humidity, membrane swelling is managed by tuning the modulus of the structural phase. The PEMs that exhibit the least amount of swelling give the lowest methanol permeability while still retaining high saturated proton conductivities. Additionally, the use of these crosslinked PEMs in separating ammonia from gas mixtures is preliminarily examined.

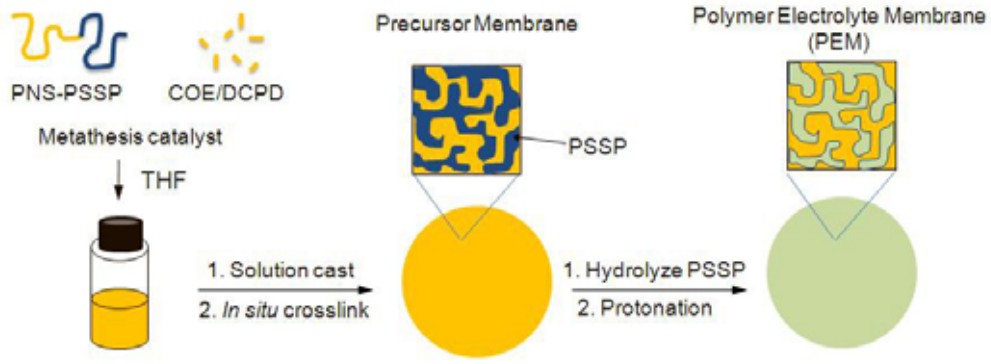

Figure 4.1. Preparation of a crosslinked PEM from PNS-PSSP and COE/DCPD by ring-opening metathesis polymerization induced phase separation.

4.2 Experimental section

4.2.1 Materials

All chemicals were purchased from Aldrich and used as received if not specified. Styrene and cyclooctene (COE) were purified by passage through short alumina columns to remove the radical inhibitors followed by distillation over CaH_2 under reduced pressure, and were refrigerated before use. Pyridine and dimethylformamide (DMF) were distilled over CaH_2 under reduced pressure. Norbornenylethylstyrene (N) was prepared according to the procedure described in Chapter 2. Purification of toluene was described elsewhere.[19] All

anhydrous alcohols were used without further purification in the synthesis of styrenesulfonate esters.

4.2.2 General methods

^{1}H NMR spectra of all samples were acquired on a Varian 300 VI spectrometer at RT and samples were dissolved in deuterated chloroform (Cambridge) at a concentration of about 1 wt %. Size exclusion chromatography (SEC) experiments were mostly performed in $CHCl_3$ with a flow rate of 1 mL/min at 35 °C using a Hewlett-Packard 1100 series liquid chromatograph equipped with three PLgel 5 μm mixed columns and a Hewlett-Packard 1047A refractive index detector. The SEC instrument was calibrated with polystyrene standards (Polymer Laboratories). Some SEC data were acquired on a SEC system consisting of a Wyatt Optilab RI detector, a Wyatt Dawn multiangle light scattering detector, and three Phenolgel columns of 10^5, 10^4, and 10^3 Å pore sizes, where THF was used as the mobile phase at 40 °C with a flow rate of 1 mL/min. In the THF SEC, molecular weight was calculated based on PS standards. Differential scanning calorimetry (DSC) experiments were conducted on a TA Instruments Q1000 with a heating rate of 10 or 20 °C min^{-1}. FT-IR spectra were acquired on a Nicolet Magna-Infrared Spectrometer 550, and free-standing membranes were pressed and measured directly. Tensile tests were performed on a Rheometric Scientific MINIMAT instrument at crosshead speed of 4 mm/min with a 200 N load cell installed under ambient conditions. Measured membranes were cut into rectangular bars (approximately 30×2×0.2 mm). Small angle X-ray scattering (SAXS) experiments were partially performed on a custom built beam line at the University of Minnesota described in Chapter 2. Some SAXS data for curve fitting were acquired at the Argonne National Lab using the synchrotron source. Scanning electron microscopy (SEM) experiments were performed on a Hitachi S-900 FE-SEM using 3.0 kV accelerating voltage. The SEM samples were mounted on brass shims and coated with 3 nm thick Pt. Transmission electron microscopy (TEM) micrographs were acquired on a JOEL 1210 transmission electron

microscope with accelerating voltage of 120 kV. Some crosslinked films were cryo-microtomed at −120 °C and then stained with a 4 wt % OsO_4 aqueous solution for 15 min; other samples were first soaked in a saturated aqueous solution of $Pb(acetate)_2$ overnight and then cryo-microtomed at −120 °C. Standard PEM measurements (methanol crossover, through-plane and in-plane proton conductivities, *et al.*) were performed at Drexel University and were described in details elsewhere.[14a,14b,20]

4.2.3 Material synthesis

4.2.3.1 Synthesis of norbornene-functionalized polystyrene (PNS)

A bromo-terminated PNS was prepared by atom transfer radical polymerizations following a reported procedure.[21] 1-bromoethyl styrene, CuBr, and bipyridine in a molar ratio of 1:1:2 were mixed with styrene and N (variable ratio) in an air free flask under argon atmosphere, followed by three freeze-pump-thaw cycles. The reaction vessels were sealed and placed in an oil bath at 110 °C. For bulk polymerizations (e.g., PNS(6) and PNS(10)), the molar ratio of monomers to the initiator was 162, and the polymerization time was 4 h and 6 h, respectively; for PNS(2), a 20 % solution in toluene was used (the molar ratio of monomers to the initiator was 28), and the reaction time was 4 h. After polymerization, the reaction mixture was diluted with THF and passed through a short alumina column to remove the residue Cu catalyst. The resultant polymer was recovered through precipitation in methanol followed by vacuum filtration, washed with extra methanol, and finally dried at 60 °C overnight under high vacuum. PNS was recovered in 30–60 % yield. ^{1}H NMR spectrum of PNS (multiplicity, identity) δ ppm: 6.2–7.3 (b, Ph-**H**), 5.9–6.2 (b, -C**H**=C**H**-), 4.3–4.6 (b,-C**H**-Br), 2.8 (b, -C**H**-CH=CH-C**H**-), 2.5 (b, Ph-C**H2**-), 0.6–2.0 (b, other C**H** or C**H2**). By ^{1}H NMR spectroscopy, the number average molecular weight (M_n) and the N composition in the polymer were determined. Specifically, based on the integration ratio of the norbornene double bonds to the end group (C**H**-Br) signal, the average number of N units per chain was calculated. The number of styrene units was calculated based on the Ph-**H** integration by

subtracting the contribution from the N units.

4.2.3.2 Synthesis of *n*-propyl-*p*-styrenesulfonate (SSP)

SSP was prepared following the reported steps (Scheme 4.1).[22] Sodium *p*-styrenesulfonate (9.0 g) was slowly added to thionyl chloride (23 mL) under argon atmosphere with stirring. After the mixture was cooled down to 0 °C, dry DMF (12 mL) was added dropwise to give a clear yellow solution. The reaction mixture was stirred for 6 h at RT and then poured into ice/water to quench unreacted thionyl chloride. The aqueous solution was extracted with diethyl ether three times. The ether solution was washed with cold DI water and cold brine sequentially, and then dried over $MgSO_4$ for 1 h. After removing $MgSO_4$, concentration of the ether phase afforded 4-vinylbenzenesulfonyl chloride (SSCl) as viscous yellow liquid in 83 % yield. To SSCl (4.0 g) in a round-bottom flask under argon atmosphere, anhydrous *n*-propanol (2.0 g) and dry pyridine (5 mL) were added slowly. A white solid formed immediately after mixing. The reaction was stirred in an ice bath for 2 h. After that, the solution was diluted with excess CH_2Cl_2 and poured into a mixture of ice and aqueous HCl. The organic layer was washed sequentially with water and brine, and dried over $MgSO_4$ for 1 h. After removing $MgSO_4$, concentration of the organic phase under vacuum yielded a viscous oil (SSP). This crude product was further purified by column chromatography using silica gel and methylene chloride in about 80 % yield. The resultant SSP was dried under high vacuum at 0 °C to remove residue volatiles and refrigerated before use.[b] ^{1}H and ^{13}C NMR analyses corroborated high purity of SSP. ^{1}H NMR spectrum of SSP (multiplicity, identity) δ ppm: 7.86 and 7.56 (d, d, Ph-**H**), 6.76 (t, -C**H**=CH2); 5.91 and 5.47 (d, d, CH=C**H2**), 4.01 (t, -C**H2**-CH2-CH3), 1.67 (m, -CH2-C**H2**-CH3), 0.90 (t, -CH2-CH2-C**H3**). ^{13}C NMR spectrum of SSP (75 MHz) δ ppm: 142.8, 135.2, 134.9, 128.2, 126.8, 118.0, 72.3, 22.2, 9.9.

4.2.3.3 Synthesis of other styrenesulfonate esters

[b] Due to the high reactivity of SSP, this monomer was stored at −10 °C and used within a few days.

Structures of other styrenesulfonate esters are shown below and synthesized in the same scheme.[22]

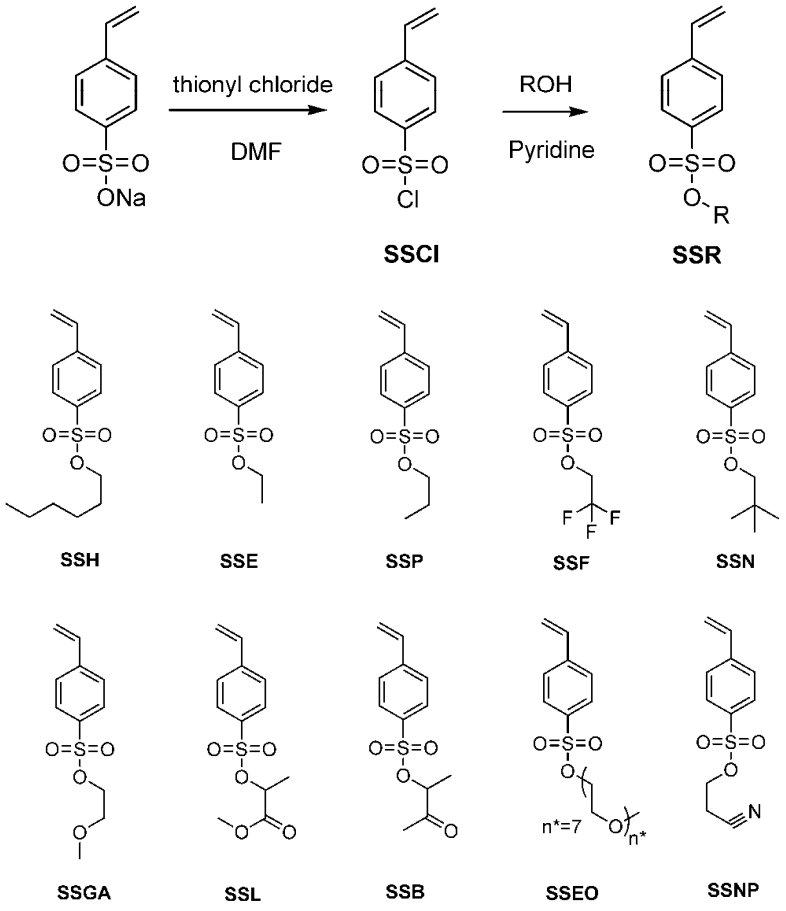

Scheme 4.1. General synthetic scheme and chemical structure of styrenesulfonate esters. R represents a protecting group.

n-Hexyl-*p*-styrenesulfonate (**SSH**): a viscous oil. ^{1}H NMR spectrum of SSH (multiplicity, identity) δ ppm: 7.86 and 7.55(d, d, Ph-**H**), 6.75 (q, -C**H**=CH2); 5.90 and 5.45 (d, d, -CH=C**H2**), 4.02 (t, -O-C**H2**-CH2-), 1.64 (m, -O-CH2-C**H2**-CH2-), 1.25 (m, other C**H2**), 0.83 (t, -CH2-C**H3**). ^{13}C NMR spectrum of SSH δ ppm: 142.7, 135.0, 134.7, 128.1, 126.6, 117.9, 70.7, 30.9, 28.6, 24.8, 22.2, 13.7.

Neopentyl-*p*-styrenesulfonate (**SSN**): a white solid. ^{1}H NMR spectrum of SSN (multiplicity, identity) δ ppm: 7.86 and 7.56 (d, d, Ph-**H**), 6.76 (q, -C**H**=CH2); 5.91 and 5.47

(d, d, -CH=C**H2**), 3.67 (s, -O-C**H2**-C(CH3)3), 0.90 (t, -C**H3**). ^{13}C NMR spectrum of SSN δ ppm: 142.6, 135.1, 134.6, 128.1, 126.6, 117.8, 79.5, 31.5, 25.8.

Trifluoroethyl-*p*-styrenesulfonate (**SSF**): a viscous oil. ^{1}H NMR spectrum of SSF (multiplicity, identity) δ ppm: 7.88 and 7.60 (d, d, Ph-**H**), 6.78 (q, -C**H**=CH2); 5.94 and 5.51 (d, d, -CH=C**H2**), 3.37 (q, -O-C**H2**-CF3), 0.90 (t, -C**H3**). ^{13}C NMR spectrum of SSF δ ppm: 143.7, 134.8, 133.2, 128.3, 126.9, CF3 (127.2 123.5, 119.9, 116.1), 118.6, CF3 (65.2, 64.7, 64.2, 63.7).

Methoxyethyl-*p*-styrenesulfonate (**SSGA**): a viscous oil. ^{1}H NMR spectrum of SSGA (multiplicity, identity) δ ppm: 7.87 and 7.56 (d, d, Ph-**H**), 6.76 (q, -C**H**=CH2); 5.91 and 5.47 (d, d, -CH=C**H2**), 4.18 (t, -O-C**H2**-CH2-O-CH3), 3.58 (t, -O-CH2-C**H2**-O-CH3), 3.30 (S, -O-C**H3**). ^{13}C NMR spectrum of SSGA δ ppm: 142.8, 135.0, 134.5, 128.2, 126.6, 117.9, 69.7, 69.1, 58.8.

Ethyl-*p*-styrenesulfonate (**SSE**): a white solid. ^{1}H NMR spectrum of SSE (multiplicity, identity) δ ppm: 7.86 and 7.55(d, d, Ph-**H**), 6.75 (q, -C**H**=CH2); 5.91 and 5.46 (d, d, -CH=C**H2**), 4.11 (q, -O-C**H2**-CH3), 1.29 (t, -C**H3**). ^{13}C NMR spectrum of SSE δ ppm: 142.7, 135.0, 134.8, 128.0, 126.7, 117.9, 66.8, 14.5.

Methyllactate-*p*-styrenesulfonate (**SSL**): a viscous oil. ^{1}H NMR spectrum of SSL (multiplicity, identity) δ ppm: 7.87 and 7.55 (d, d, Ph-**H**), 6.75 (q, -C**H**=CH2); 5.90 and 5.46 (d, d, -CH=C**H2**), 4.94 (q, -O-C**H**(CH3)), 3.65 (s, -O-C**H3**), 1.51 (d, -O-CH(C**H3**)). ^{13}C NMR spectrum of SSL δ ppm: 169.2, 142.9, 134.9, 134.7, 128.2, 126.5, 118.0, 74.0, 52.4, 18.2.

Acetoin-*p*-styrenesulfonate (**SSB**): a viscous oil. ^{1}H NMR spectrum of SSB (multiplicity, identity) δ ppm: 7.86 and 7.56 (d, d, Ph-**H**), 6.75 (q, -C**H**=CH2); 5.91 and 5.47 (d, d, -CH=C**H2**), 4.77 (q, -O-C**H**(CH3)), 2.21 (s, -C(=O)-C**H3**), 1.35 (d, -O-CH(C**H3**)). ^{13}C NMR spectrum of SSB δ ppm: 169.2, 143.1, 134.8, 134.5, 128.0, 126.8, 80.7, 25.4, 17.1.

Poly(ethyleneoxide)-*p*-styrenesulfonate (**SSEO**): a viscous oil. ^{1}H NMR spectrum of SSEO (multiplicity, identity) δ ppm: 7.85 and 7.54 (d, d, Ph-**H**), 6.74 (q, -C**H**=CH2); 5.89 and 5.45 (d, d, -CH=C**H2**), 4.16 (t, Ph-O-C**H2**-CH2-O-), 3.6 (m, other C**H2**-O-), 3.35 (S, -O-C**H3**). ^{13}C NMR spectrum of SSEO δ ppm: 142.8, 135.0, 134.5, 128.2, 126.6, 117.9, 71.7, 70.4(b), 69.3, 68.4, 58.8.

Propionitrile-*p*-styrenesulfonate (**SSNP**): a viscous oil. ^{1}H NMR spectrum of SSNP (multiplicity, identity) δ ppm: 7.87 and 7.58 (d, d, Ph-**H**), 6.76 (q, -C**H**=CH2); 5.92 and 5.48 (d, d, -CH=C**H2**), 4.22 (t, -O-C**H2**-), 2.75 (t, CH2-C**H2**-CN). ^{13}C NMR spectrum of SSNP δ ppm: 143.4, 134.8, 133.4, 128.2, 127.0, 118.4, 115.6, 63.7, 18.4.

4.2.3.4 Free radical polymerizations of the styrenesulfonate esters

SSP (2.0 g), toluene (2.0 mL), and AIBN (20 mg) were mixed in an air free flask followed by three freeze-pump-thaw cycles, and reacted at 65 °C for 2 h. The resultant polymer was precipitated in pentane as a white powder in about 50 % yield and then dried under reduced pressure.

4.2.3.5 Synthesis of PNS-PSSP

PNS-PSSP copolymer was synthesized via an ATRP scheme using the PNS macroinitiators. PNS (0.40 g), SSP (0.80–1.00 g), CuBr, and bipyridine were dissolved in dry toluene (1 mL), where the molar ratio of PNS:bipyridine:CuBr was 1:2:4. After three freeze-pump-thaw circles, the reaction solution was sealed under vacuum and reacted at 55 °C for 20 h. The resulting brown mixture was diluted with excess acetone, and the Cu catalyst was removed by passage through a short column filled with Dowex ion exchange resins (sodium form) several times until the solution was light blue or colorless. The resultant copolymer was recovered by precipitation in pentane followed by filtration and washed with cold pentane. After drying the product under high vacuum overnight, a nearly white powder was obtained in 60–80 % yield. The conversion of SSP was nearly complete based on NMR analysis of the

resulting block polymer, while the yield was lower due to mass loss during the step of removing the catalyst. By ^{1}H NMR spectroscopy, the M_n of PSSP was calculated based on the pre-determined PNS block. ^{1}H NMR spectrum of PNS-PSSP (multiplicity, identity) δ ppm: 6.2–7.3 (b, Ph-**H**), 5.9–6.2 (b, -C**H**=C**H**-), 4.0 (b, O-C**H2**-CH2), 2.8 (b, -C**H**-CH=CH-C**H**-), 2.5 (b, Ph-C**H2**-), 0.6–2.0 (m/b, other C**H** and C**H2**).

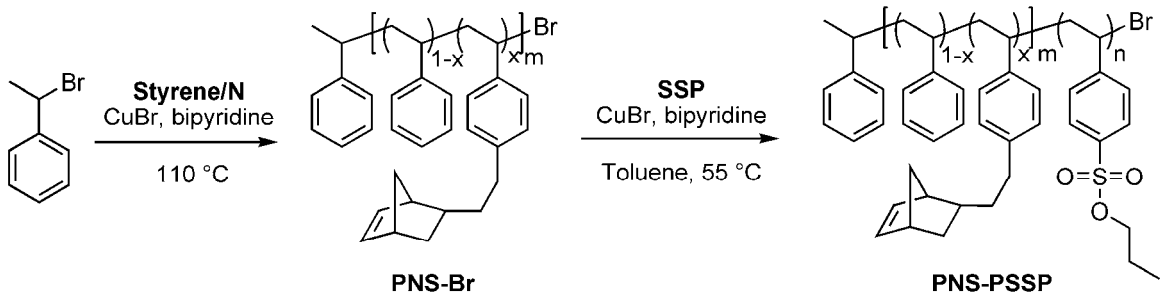

Scheme 4.2. Synthetic procedure for PNS-PSSP.

4.2.3.6 Synthesis of P(N-*s*-SSP)

SSP (1.77 g), N (0.32 g), toluene (2.0 mL), and AIBN (20 mg) were mixed in an air free flask followed by three freeze-pump-thaw cycles, and reacted at 65 °C for 4 h. The resultant polymer precipitated in pentane as a white powder in about 50 % yield. SEC analysis of the resultant polymer in $CHCl_3$ showed no signal, due to the strong interaction between the polymer and the column-packing material. ^{1}H NMR spectrum of P(N-*s*-SSP) (multiplicity, identity) δ ppm: 7.7 and 6.7 (b, b, Ph-**H** in SSP), 6.2–6.9 (b, Ph-**H** in N), 5.9 and 6.1 (b, b, CH-C**H**=C**H**-CH), 4.1 (b, O-C**H2**), 2.8 (b, C**H**-CH=CH-C**H**), other peaks were not assigned. By NMR spectroscopy, the M_n of the resultant polymer could not be determined, while based on the stoichiometry of the reaction and conversion, M_n was expected to be close to 8.5 kg mol^{-1}. Additionally, the mass ratio of N to SSP in the polymer of 0.11 was lower than a ratio of 0.18 in the feed, presumably due to the low reactivity of N compared with SSP.

4.2.3.7 Synthesis of PNS-PSSH

Using the same procedure described in 4.2.3.5, PNS-PSSH was synthesized from a PNS

macroinitiator (0.30 g, 12.5 kg mol^{-1}, 12 N units in PNS) and SSH (0.90 g) in dry toluene (0.9 mL). ^{1}H NMR spectrum of the PNS-PSSH (multiplicity, identity) δ ppm: 7.7 and 6.7 (b, b, Ph-**H** of SSH), 6.2–6.9 (b, Ph-**H** of N and styrene), 5.9 and 6.1 (b, b, CH-C**H**=C**H**-CH), 4.1 (b, O-C**H2**), 2.8 (b, C**H**-CH=CH-C**H**), other peaks were not specified. By NMR spectroscopy, M_n of the resultant copolymer was 12.5-29.0 kg mol^{-1}.

4.2.3.8 Synthesis of PNS-PSSL

PNS-PSSL was synthesized from a PNS macroinitiator (0.40 g, 4.5 kg mol, 4.5 N units in PNS) and SSL (0.80 g) in dry toluene (1.0 mL). ^{1}H NMR spectrum of PNS-SSL (multiplicity, identity) δ ppm: 7.7 and 6.7 (b, b, Ph-**H** in SSP), 6.2–6.9 (b, Ph-**H** in PNS), 5.9 and 6.1 (b, b, CH-C**H**=C**H**-CH), 5.05 (b, O-C**H**(CH3)-), 4.15 (b, O-C**H3**), 2.8 (b, C**H**-CH=CH-C**H**), other signals were not specified. By NMR spectroscopy, M_n of the resultant copolymer was 4.5-12 kg mol^{-1}.

4.2.4 Membrane fabrication

Crosslinked membranes were prepared using the same procedure in Chapter 3. In a vial, PNS-PSSP (0.4 g) was dissolved into THF (2.0 mL) until a homogeneous solution (clear or slightly opaque) was obtained, and then COE and/or DCPD was added in the solution and stirred for another 20 min. To the solution, a mixture of the 2nd generation Grubbs catalyst (**G2**) (2.5 mg, 0.4 wt % relative to overall mass of copolymer and monomers) and THF (0.4 mL) was quickly added and stirred for 10 s. Solution-cast film in an aluminum pan was covered with a petri dish and placed in a covered chamber. Gelation of the solution typically occurred within 5 min. The film was cured at RT overnight along with slow THF evaporation. After curing the film at 90 °C for 1 h, a transparent and slightly yellow film was peeled off the aluminum substrate and dried under high vacuum. Base hydrolysis of the PSSP component in the precursor film was conducted in a 30 wt % NaOH solution in H_2O/methanol (v/v=5:6) at 70 °C for 48 h, and then the film was rinsed with DI water and

soaked in a 20 wt % HCl aqueous solution at RT for 24 h. The resultant film was washed with DI water and dried at 60 °C under high vacuum. Finally, the film was cut into small pieces for further measurements: films of approximately 2.5×2.5 cm were for proton conductivity (through plane) and methanol permeability measurements; films of approximately 3×0.5 cm were for lateral swelling and four-electrode proton conductivity measurements at a range of temperatures and humidities.

4.3 Results and discussion

4.3.1 Polymer synthesis and characterization

Ionic block copolymers containing polystyrenesulfonic acid are typically produced by sulfonation of a PS-containing block[9–17] or by radical polymerization of sodium styrenesulfonate.[7,8] In these examples, the processabilities of the resultant copolymers can be compromised by their ionic character. The polymerization of styrenesulfonate esters, on the other hand, allows for the synthesis of copolymers with tailored levels of sulfonation using controlled free radical polymerization followed by base hydrolysis.[22b,23] The approach shown schematically in Figure 4.1 requires the synthesis of a reactive block copolymer containing a norbornene-functionalized PS block for ultimate metathesis crosslinking as in our previous work,[18] and a polystyrenesulfonate ester block as the precursor to a proton conducting phase. Thus, *n*-propyl-*p*-styrenesulfonate (SSP), was synthesized by the esterification of styrenesulfonate chloride and *n*-propyl alcohol (see Section 4.2.3.2), and norbornenylethyl styrene (N) was prepared by our previously reported method.[24]

Atom transfer radical polymerization (ATRP) has been utilized for the controlled polymerization of a variety of styrene derivatives including styrenesulfonate esters.[25] Poly(norbornenylethylstyrene-*s*-styrene) (PNS)-PSSP block polymers were prepared by sequential ATRP reactions (Scheme 4.2). The PNS block was prepared by ATR copolymerization of N and styrene, using 1-bromoethylstyrene as the initiator. By manipulating the relative amounts of the comonomers and the initiator, prepared

bromo-terminated PNS samples possessed tailored molecular weight and norbornene content as summarized in Table 1. SEC analyses of these polymers gave polydispersity indices (PDIs) around 1.5 consistent with styrene homopolymerizations under similar conditions.[26] The M_n and N content of PNS block were determined by NMR spectroscopy (Table 4.1). Between 4 and 12 norbornene groups were incorporated into the PNS blocks.

Table 4.1. Molecular characteristics of PNS macroinitiators and PNS-PSSP block polymers.

Entry[a]	NMR M_n (kg mol^{-1})	SEC M_n (kg mol^{-1})[b]	PDI	PSSP (wt%)	Avg. # of N per chain	Mol% N in PNS	D (nm)[d]
PNS (10)	10.1	9.2	1.55		12	0.14	
PNS-PSSP (10-23)	33.0	20.9[c]		70	12	0.14	24
PNS (6)	5.9	6.4	1.45		7	0.14	
PNS-PSSP (6-13)	18.9	14.4[c]		69	7	0.14	15
PNS (2)	2.0	2.5	1.23		4	0.32	
PNS-PSSP (2-5)	6.5	4.2	1.19	69	4	0.32	10

a. PNS (X) and PNS-PSSP (X-Y) denote a bromo-terminated PNS and a PNS-PSSP copolymer, where X and Y indicate the NMR M_n values for the PNS and PSSP blocks, respectively. *b*. SEC data acquired in $CHCl_3$ using a RI detector and PS standards. *c*. SEC data acquired in THF using a RI detector and PS standards. *d*. Domain spacing (D) in copolymers was obtained through SAXS analysis at 100 °C, and calculated based on $D=2\pi/q^*$, where the q^* is the primary peak position in 1D SAXS plot.

ATRP of SSP using the bromo-terminated PNS as a macro initiator resulted in near quantitative conversion of SSP and the formation of PNS-PSSP block copolymers in 60–80% isolated yield. The somewhat low yields were attributed to mass losses that occurred during removal of the Cu catalyst. The M_n of the PSSP was determined using ^1H NMR spectroscopy and the predetermined M_n of the PNS block. A representative NMR spectrum for PNS-PSSP (2-5) is shown in Figure 4.3; the retention of both norbornene and sulfonate ester functional groups is evident. The SEC data for PNS-PSSP(2-5) is shown in Figure 4.2; a clear shift to lower elution volume for this sample compared to PNS(2) confirms the conversion of the bromo-terminated PNS to the PNS-PSSP block copolymer. However, SEC analysis of the two higher molecular weight PNS-PSSP samples in $CHCl_3$ using a RI detector gave very

weak signals. This may be due to interactions between the sulfonate ester block and the column-packing material. The PNS-PSSP(6-13) and PNS-PSSP(10-23) copolymers were evaluated by SEC in THF containing 1 vol% N,N,N',N'-tetramethylethylenediamine and using a combination of refractive index and light scattering detectors. While a peak associated with the copolymer was observed, a high molecular weight tail was evident in both samples. This high molecular weight signal was attributed to aggregation of the PNS-PSSP block polymers in THF based on preliminary dynamic light scattering analysis of a dilute solution of PNS-PSSP(10-23). The peak molecular weights of these copolymers based on PS standards are given in Table 4.1.

DSC analysis of these copolymers (between −40 and 200 °C) only revealed one T_g associated with the PNS block (between 90 and 100 °C). Additionally, the morphologies of these copolymers were probed by small angle X-ray scattering (SAXS). Each of the copolymer samples exhibited a principal scattering peak indicative of microphase separation between the PNS and PSSP blocks. The domain spacing increased with increasing PNS-PSSP molecular weight as expected. However, due to lack of high-order reflections, even after annealing these copolymers at 150 °C for 10 min, no specific ordered morphology could be determined. Possibly, equilibrium morphology in these copolymers was hindered by the high glass transition temperature (T_g) of the PSSP block, which has been reported to be higher than 200 °C.[27] In further SAXS experiments, while heating these copolymers to 195 °C for 10 min, the irreversible change of domain spacing (Figure 4.4) indicated decomposition of the PSSP block before achieving an equilibrium morphology. It was further confirmed by IR spectra that the PSSP block was converted into polystyrene sulfonic acid (PSSA) after annealing in SAXS experiments (Figure 4.5). In fact, thermal decomposition of similar PS sulfonate esters has been previously reported.[22b] DSC analysis of PNS-PSSP(2-5) (Figure 4.6) indicated strong exothermic peak above 200 °C, likely associated with the thermal decomposition of the ester groups in PSSP. Overall, production of well-defined PNS-PSSP

copolymers with tunable molecular weights and compositions was successfully demonstrated.

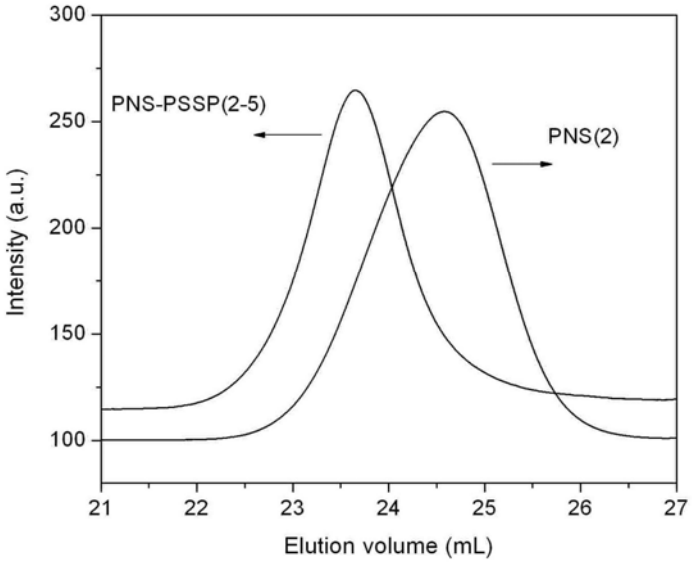

Figure 4.2. SEC traces of PNS(2) and PNS-PSSP (2-5).

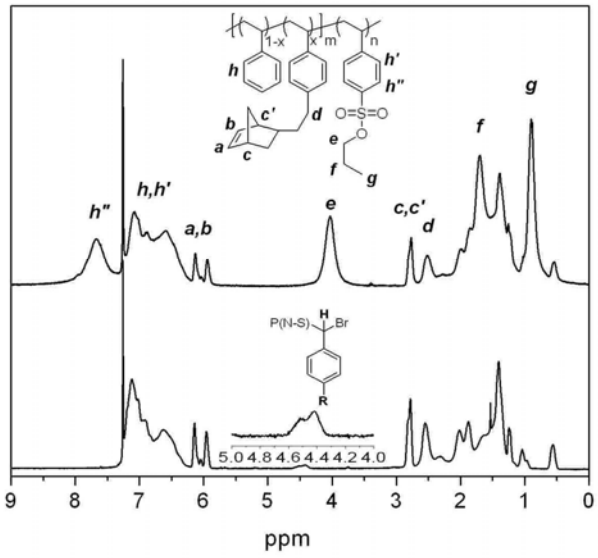

Figure 4.3. NMR spectra of PNS(2) and PNS-PSSP (2-5).

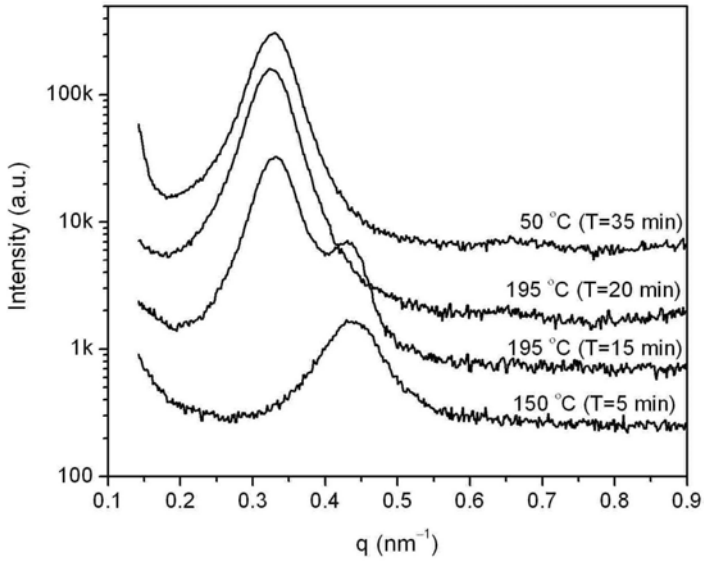

Figure 4.4. Temperature-dependent SAXS profiles of the PNS-PSSP (6-13) copolymer. The irreversible change of domain spacing indicates the decomposition of propyl sulfonate. The SAXS signals were vertically shifted.

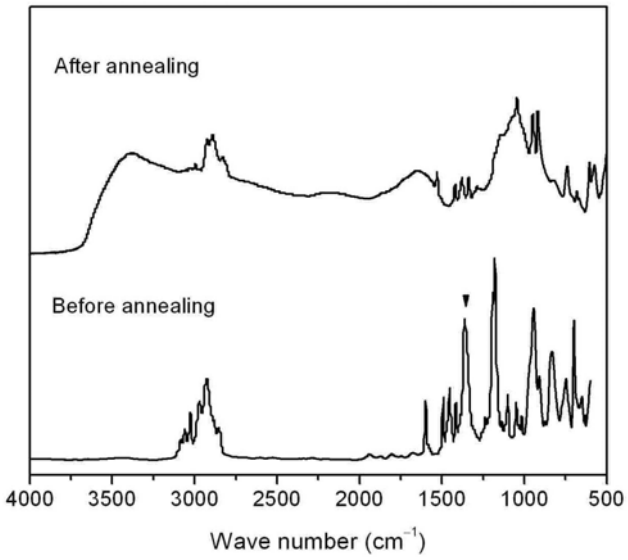

Figure 4.5. IR spectra of PNS-PSSP (6-13) before and after annealing at 195 °C for 10 min. The triangle indicates the absorbance associated with the sulfonate ester, which is significantly reduced after thermal annealing.

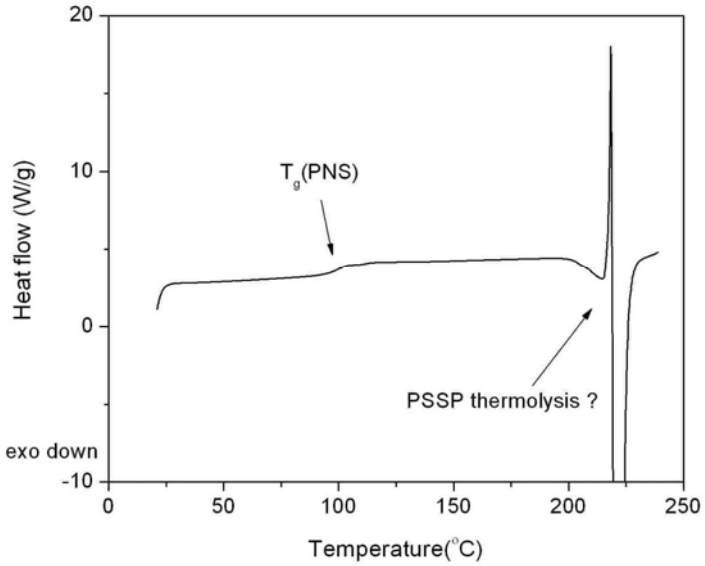

Figure 4.6. DSC traces of the PNS-PSSP(2-5) copolymer, using the 2nd heating run with a heating rate of 20 °C/min. The exothermic peak above 200 °C is likely associated with the thermolysis of PSSP.

4.3.2 Crosslinked precursor membranes

In our previously-reported nanoporous membrane synthesis, a PNS-polylactide (PLA) block polymer containing a metathesis-reactive segment (PNS) and a chemically etchable segment (PLA) was combined with DCPD and a ruthenium-based metathesis catalyst in a suitable solvent give robust nanostructured membrane upon casting, curing, and drying. Removal of the PLA component from these membranes yielded robust nanoporous membranes with a bicontinuous structure.[18]

Herein, a similar approach is taken using PNS-PSSP as the doubly reactive block polymer and DCPD and/or COE as the metathesis reactive comonomers (Figure 4.1). PNS-PSSP and reactive monomers were dissolved in THF to give an optically homogeneous solution. The 2nd generation Grubbs metathesis catalyst[28] dissolved in minimum amount of THF was added to the solution of PNS-PSSP and monomers. Cast films formed gels in about 2 min, and were allowed to cure at RT overnight and then at 90 °C for 1 h. For this study, five crosslinked precursor films containing roughly 42 wt % PSSP (Table 4.2) were prepared. The

resultant films were transparent and slightly yellow. The color is due to the low levels of metathesis catalyst that remains in the film.

Table 4.2. Summary of the crosslinked precursor films.

Entry[a]	PNS-PSSP sample	Monomer(s)	Wt % PNS-PSSP	PSSP[b] (wt%)	D[c] (nm)	f_a
PEM1e	PNS-PSSP (10-23)	COE	59.9	41.6	37.3	−0.48
PEM2e	PNS-PSSP (6-13)	COE	64.1	44.1	17.7	−0.87
PEM3e	PNS-PSSP (2-5)	COE	59.9	41.5	10.5	−0.86
PEM4e	PNS-PSSP (6-13)	COE:DCPD (1:1)	60.6	41.7	27.3	−0.72
PEM5e	PNS-PSSP (6-13)	DCPD	61.3	42.2	19.0	−0.71

a. "e" indicates these precursor membranes contain the sulfonated group in the ester form. *b*. PSSP content in the crosslinked precursor films, given all components were fully crosslinked. *c*. Domain spacing (D) and amphiphilicity factor (f_a) determined by SAXS.

TEM analysis of the PEMXe films (Table 4.2), where e indicates that the films contain sulfonate groups in the ester form, demonstrated that similar structures were adopted in all samples. As an example, a TEM micrograph of a cryo-microtomed slice of PEM2e is given in Figure 4.7. In this image, the bright domains correspond to the unstained PSSP phase, and the dark domains are the PCOE-containing phase as the backbone double bonds of PCOE were selectively stained by OsO_4. A disordered morphology with interconnected PSSP domains (ca. 18 nm) is evident from this image.

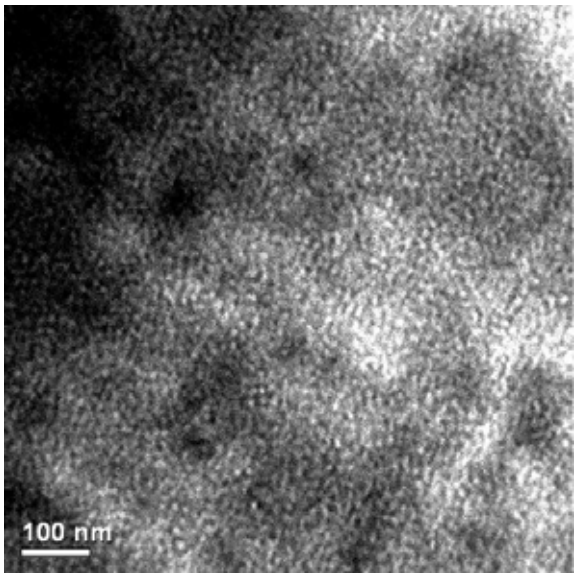

Figure 4.7. TEM micrograph of the PEM2e. The film was cryo-microtomed and stained with OsO_4, where the PNS/PCOE domains appear dark.

Synchrotron SAXS experiments were conducted to probe the microstructure in the resultant PEMXe samples. A single scattering peak was observed for each of the membranes and suggested a phase separated but disordered structure. The scattering data were analyzed using the Teubner-Strey model for a bicontinuous microemulsion.[29] The scattering profile and Teubner-Strey fit for PEM2e are shown in Figure 4.9 (SAXS profiles and fits for the other PEMXe membranes are given in Figure 4.13). A domain spacing (d) and amphiphilicity factor (f_a) could be extracted using this model. The amphiphilicity factor is a parameter that describes the character of bicontinuous microemulsions. For example, a value of f_a between −1 and 0 indicates a well-defined bicontinuous phase.[30] The values of f_a for the PEMXe membranes (Table 2) were between –0.86 and –0.48.

$$I(q) = \frac{1}{a_2 + c_1 q^2 + c_2 q^4} \qquad \textbf{4.1}$$

$$d = 2\pi \left[\frac{1}{2} \left(\frac{a_2}{c_2} \right)^{1/2} - \frac{1}{4} \frac{c_1}{c_2} \right]^{-1/2} \qquad \textbf{4.2}$$

$$f_a = \frac{c_1}{\left(4a_2c_2\right)^{1/2}} \qquad \textbf{4.3}$$

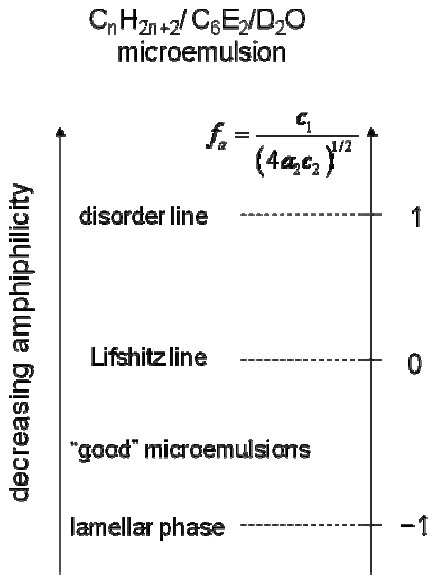

Figure 4.8. Structural definition of microemulsions.[30]

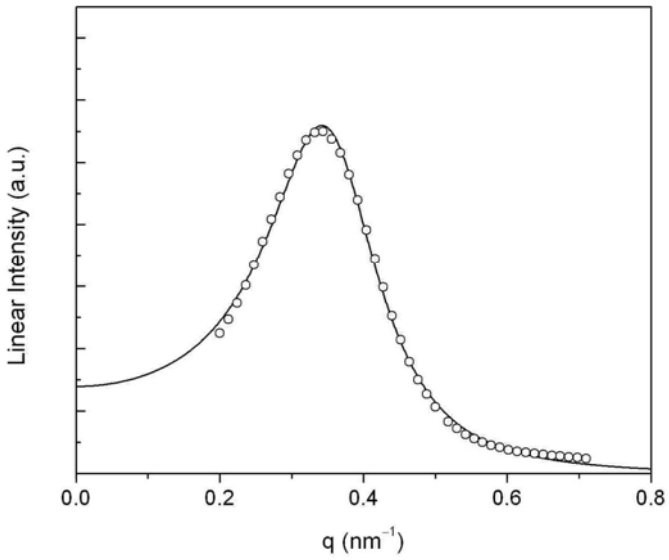

Figure 4.9. Synchrotron scattering profile of the PEM2e with curve fitting using the Teubner-Strey model.

The domain spacing of PEM2e was consistent with TEM data (Figure 4.7). Furthermore,

the domain spacings of PEMs 1e, 2e, and 3e decreased with the reduced molecular weight of PNS-PSSP. The domain spacing of PEMs 4e and 5e were both larger than that of PEM2e produced using the same copolymer. The difference could be partially accounted for by the higher monomer content in PEMs 4e and 5e, and the difference in the nature of the crosslinked matrix phase (see below).

The tensile properties of the PEMXe membranes were examined under ambient conditions (Figure 4.10), and are summarized in Table 4.3. The tensile strength and elongation at break for the PEM1e–4e are comparable to the parent PCOE homopolymer: elastic moduli between 280 and 500 MPa and elongations at break between 70 to 250 % were observed. PEM5e exhibited a higher modulus and tensile strength, but lower elongation at break due the higher level of DCPD in the monomer mix.

Table 4.3. Summary of tensile tests on the precursor films under ambient conditions.[a]

Entry	Elastic modulus G (GPa)	Tensile strength (MPa)	Elongation at break (%)
PEM1e	0.28	21.8	176
PEM2e	0.32	22.5	149
PEM3e	0.38	19.6	69
PEM4e	0.50	27.9	124
PEM5e	0.95	35.4	13
Nafion 117[b]	0.25	35.0	250

a. Values of elastic modulus, tensile strength, and elongation at break for each sample are the average of three measurements (two for PEM4e). b. Reported in Ref 31.

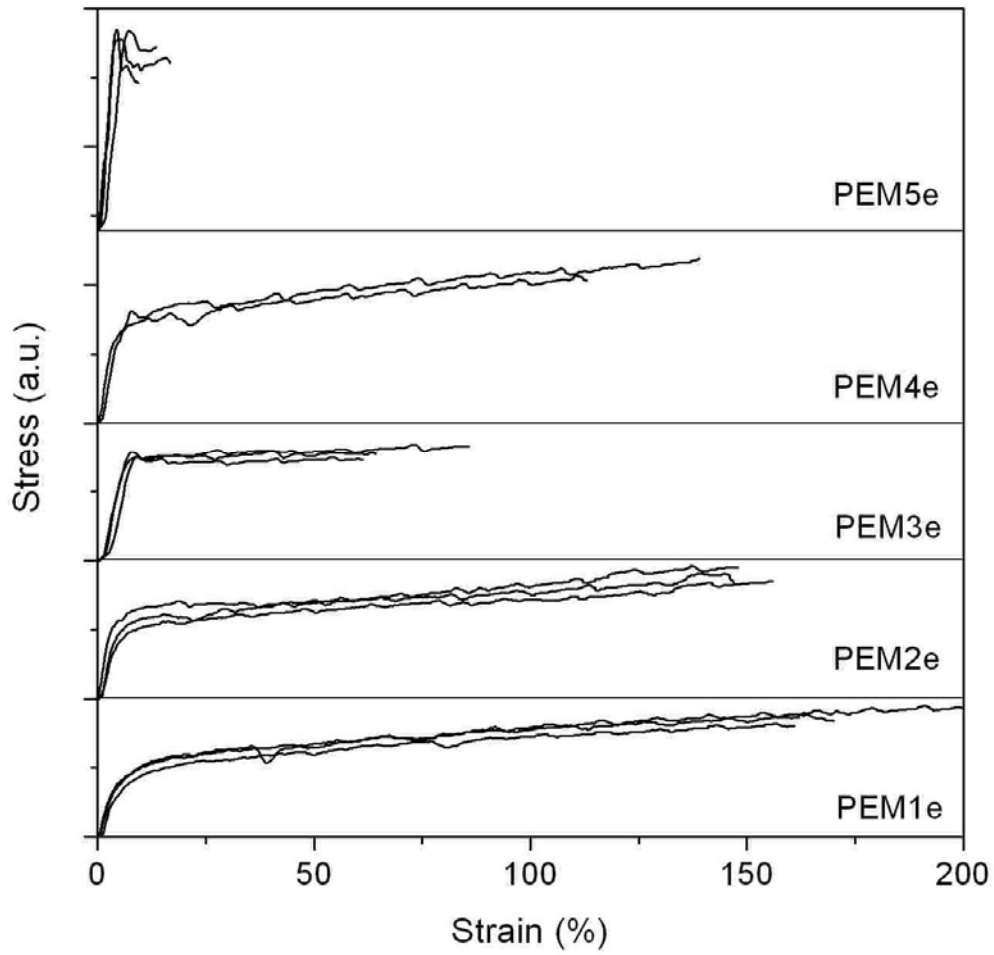

Figure 4.10. Tensile curves of the PEMXe membranes under ambient conditions.

4.3.3 PEMs synthesis

The PSSP block in these precursor films was hydrolyzed by treatment with a concentrated NaOH solution. Protonation of the sulfonate groups was accomplished using aqueous HCl (see Section 4.2.4). IR characterization confirmed that the PSSP component in all precursor films was fully converted to the acid form. The IR spectra of PEM2e and PEM2a (the "a" indicates the acid form of the membrane) are shown in Figure 4.11. The PEM2e membrane exhibited strong absorbance at 1370 and 1170 cm^{-1} for the SO_2 stretching of sulfonate ester; upon hydrolysis, this absorbance was absent and a characteristic stretching for the SO_2 stretching of sodium sulfonate group was observed at 1200 cm^{-1}; after protonation,

absorbance associated with the sulfonic acid group at 1155 cm^{-1} was observed.

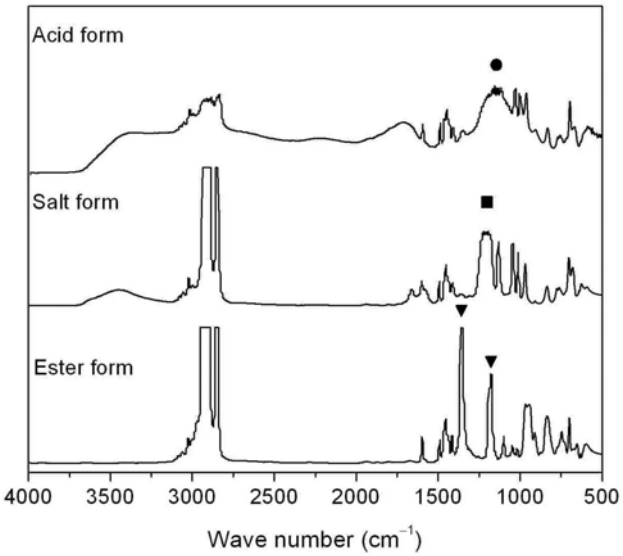

Figure 4.11. IR spectra of PEM2 films in different forms. The solid triangle indicates the absorbance for sulfonate ester, the solid square denotes the absorbance for sodium sulfonate, and the solid circle indicates the absorbance for sulfonic acid.

Synchrotron SAXS analysis of the resulting acid PEMXa dried samples at ambient conditions displayed a single scattering peak that was well fitted by the Teubner-Strey model as in the PEMXe samples.[30] Representative SAXS data for PEM2a is given in Figure 4.12 (see Figure 4.13 for SAXS data on the other PEMXa membranes).

A summary of the SAXS results (d and f_a) for the PEMXa membranes are given in Table 4.4. Interestingly, the domain spacings in the PEMXa membranes containing PCOE were consistently larger than their corresponding PEMXe precursors. This phenomenon is likely due to the increase in the Flory-Huggins parameter between PSSA and the matrix; the relatively soft and ductile PCOE domains could accommodate domain increases. Consistent with this, the polyDCPD containing membranes PEM4a and PEM5a exhibited domain spacings that were approximately the same size as the PEM4e and PEM5e samples. The sizes of the individual PSSA domains were estimated using simple cylindrical and lamellar models, and the averages are given in Table 4.4 (detailed calculation shown in Table 4.5). Ion

exchange capacity (IEC) in these PEMs was calculated based on the PSSA content, which were determined by mass and by elemental analysis (EA). Lower IEC values from EA were attributed to the absorbed moisture in these PEMXa films under ambient conditions.

Table 4.4. Summary of the resultant PEMXa membranes.

Entry	PSSA[a] (wt %)	D[b] (nm)	f_a	PSSA width (nm) SAXS[c]	PSSA width (nm) TEM[d]	IEC (mmol/g) Predicted[e]	IEC (mmol/g) Measured[f]
PEM1a	36.7	41.5	−0.50	18.7	19.0	2.00	1.98
PEM2a	39.1	22.6	−0.85	10.8	10.9	2.12	2.06
PEM3a	36.6	14.4	−0.86	6.6	6.5	1.99	1.93
PEM4a	36.8	28.3	−0.68	13.0	10.0	2.00	1.86
PEM5a	37.3	19.5	−0.71	9.0	7.5	2.03	1.96

a. Composition of the PSSA phase in each PEM was calculated based on the membrane composition based on the PSSP composition. *b*. Domain spacing was calculated from SAXS analysis. *c*. Estimated PSSA domain width from SAXS analysis described in Table 4.5. *d*. Estimated PSSA domain size from TEM micrographs, ±1 nm. *e*. Moles of sulfonic acid per gram of sample, calculated based on the PSSA content: IEC= 1× (PSSA wt %)/184×1000, in unit of mmol/g. *f*. Determined by elemental analysis.

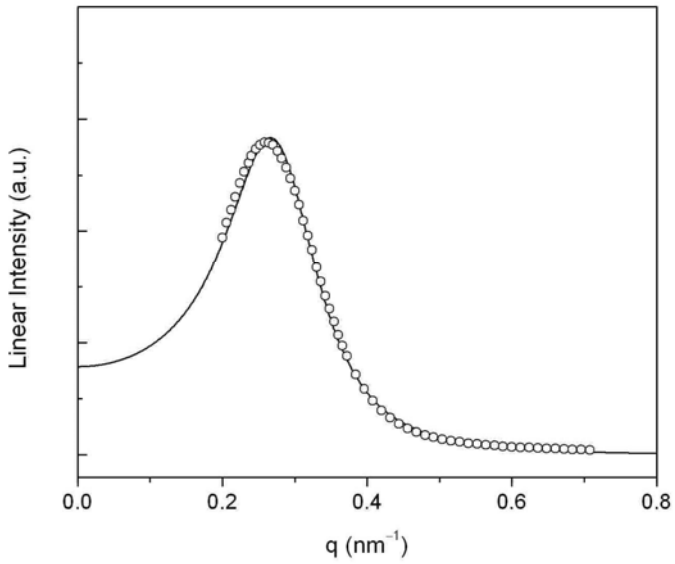

Figure 4.12. Synchrotron scattering profile of the PEM2a with curve fitting using the Teubner-Strey model.

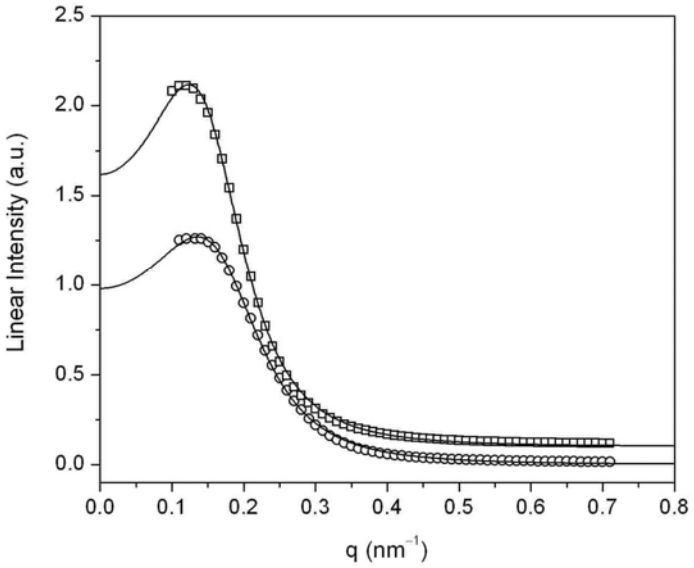
Linear Intensity (a.u.)
q (nm^{-1})
0.0
0.5
1.0
1.5
2.0
2.5
0.0
0.1
0.2
0.3
0.4
0.5
0.6
0.7
0.8

(a)

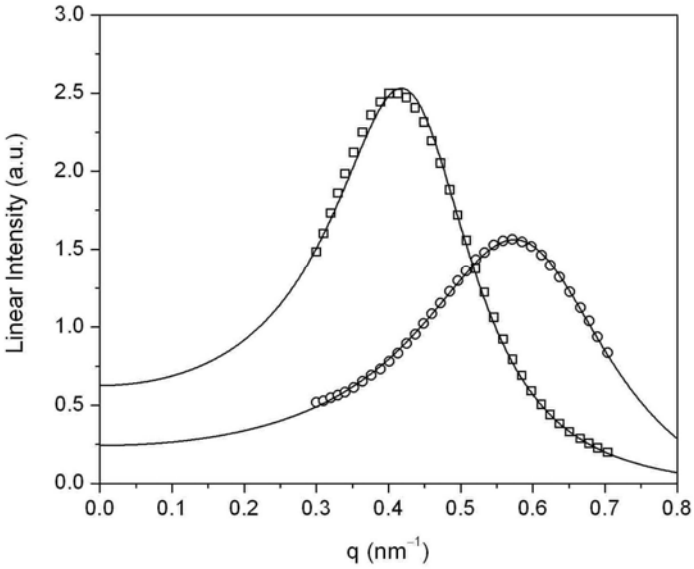
Linear Intensity (a.u.)
q (nm^{-1})
0.0
0.5
1.0
1.5
2.0
2.5
3.0
0.0
0.1
0.2
0.3
0.4
0.5
0.6
0.7
0.8

(b)

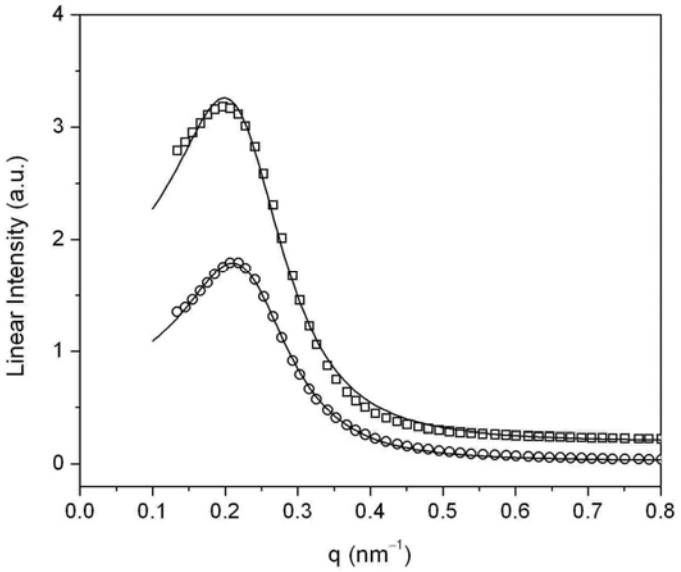

(c)

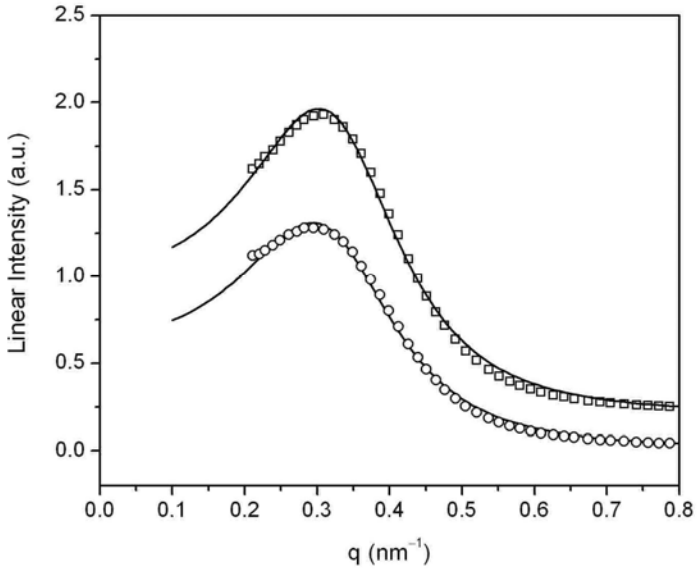

(d)

Figure 4.13. Synchrotron scattering profiles of the PEMXa films with curve fitting using the Teubner-Strey model. Figures a, b, c, and d correspond to PEMs 1a, 3a, 4a, and 5a, respectively. The open circles and squares represent the experimental data for PEMXe and PEMXa membranes, respectively.

Table 4.5. Calculation of PSSA domain size in the PEMXa films.

Entry	Weight fraction of PSSA (wt%)	Volume fraction Of PSSA (%)[a]	D (nm)	d (nm)		d (average)[b] (nm)
				lamellae	cylinders	
PEM1a	36.7	27.7	41.0	11.3	26.1	18.7
PEM2a	39.1	29.7	22.6	6.7	14.9	10.8
PEM3a	36.6	27.6	14.4	4.0	9.2	6.6
PEM4a	36.8	27.8	28.3	7.9	18.1	13.0
PEM5a	37.3	28.2	19.5	5.5	12.6	9.0

a. Based on the polymer densities ρ(PSSA)=1.44 g cm^{-3} at RT[32] and assuming ρ(PCOE/PNS) =0.95 g cm^{-3}. *b*. Correlation between the domain spacing (D) and the domain size (d) in a disordered bicontinuous morphology was unknown. However, based on the composition and domain spacing, the PSSA domain size assuming in a lamellar or a cylindrical morphology was calculated separately, and the PSSA domain sizes were estimated by taking the average of these two values.

Overall, the PSSA domain size (Figure 4.14) can be correlated with not only the molecular weight of the PSSP block but also the crosslinking density in the matrix.

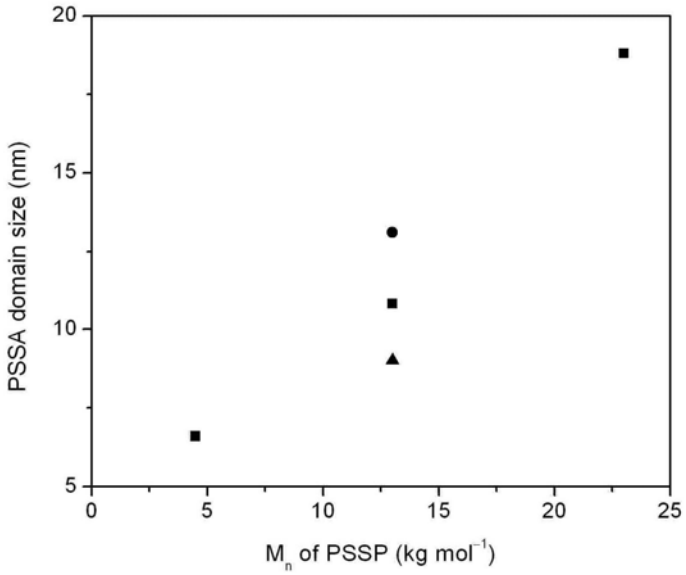

Figure 4.14. PSSA domain size of the PEMXa films plotted against the molecular weight of the PSSP block, determined from SAXS analysis. The solid square, circle, and triangle symbols indicate membranes containing PNS/PCOE, PNS/PCOE/polyDCPDE, and PNS/polyDCPD, respectively

From the Teubner-Strey analysis, amphiphilicity factors between −0.86 and −0.50 were extracted for the PEMXa membranes. Supporting evidence for the bicontinuous structure was

provided by TEM analysis. A TEM image of thin section of PEM2a is given in Figure 4.15; the bright domains correspond to the PSSA. Increased PSSA domain size upon hydrolysis is evident in this image, consistent with the SAXS data.

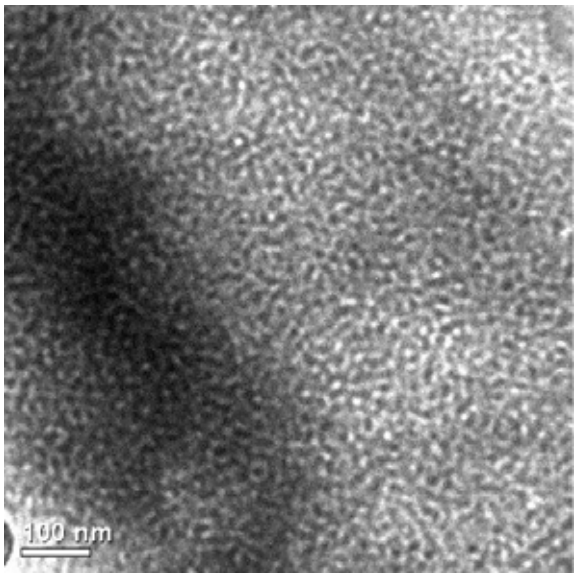

Figure 4.15. TEM image of PEM2a, the sample was cyro-microtomed and stained by OsO_4.

TEM analyses on PEMXa membranes were performed, where the PSSA domains stained by Pb^{2+} ions.[8] This reverses the contrast from the OsO_4 staining. For the TEM image for PEM2a shown in Figure 4.16, a similar structure and comparable domain spacing are visualized in comparison with Figure 4.15, implying the morphology and domain size in the resultant membrane is unaffected by the staining method. TEM images for other PEMXa films were shown in Figure 4.16. Moreover, the PSSA domain size in the resultant PEMXa membranes could be estimated from these TEM images. For PEMs 1a, 2a, and 3a, decrease of the PSSA domain size is consistent with the reduced PSSA block, and the PSSA domain sizes measured from TEM images were comparable with those values from previous SAXS analyses. For PEMs 2a, 4a and 5a, surprisingly, a consistent decrease in the PSSA size is observed with more polyDCPD content in the matrix phase. Such results are inconsistent with the previously SAXS data of PEMs 4a and 5a that roughly gave domain spacings roughly 30 % larger than the TEM results.

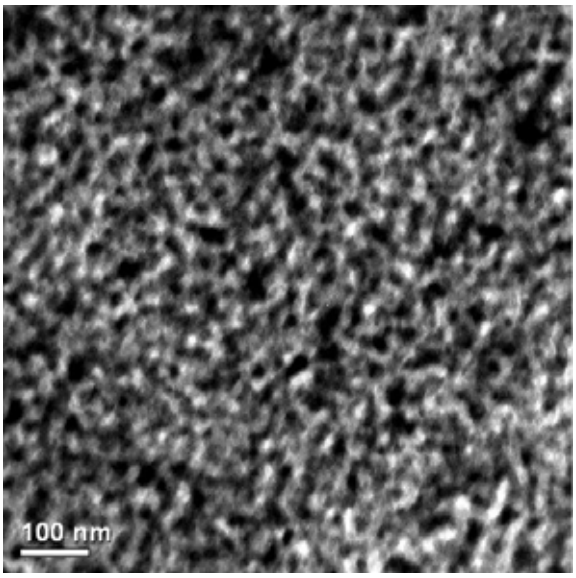

(a)

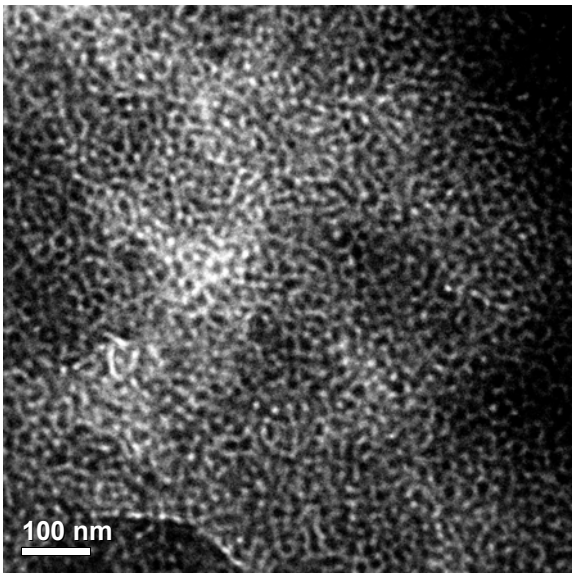

(b)

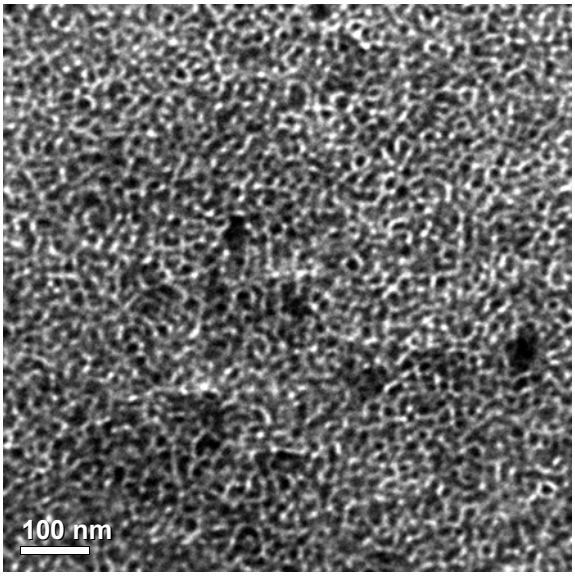

(c)

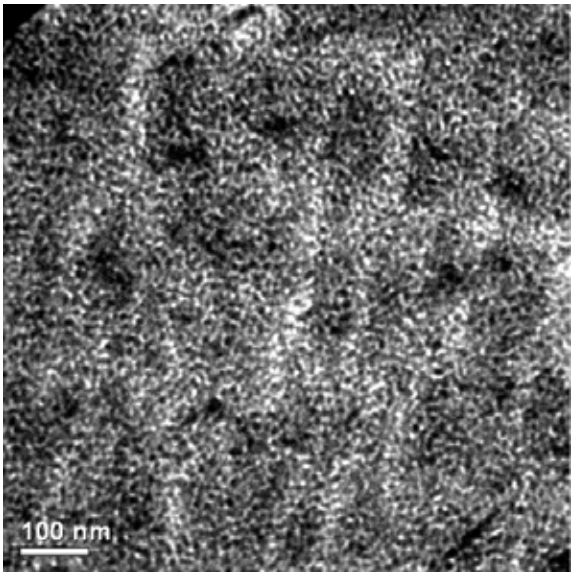

(d)

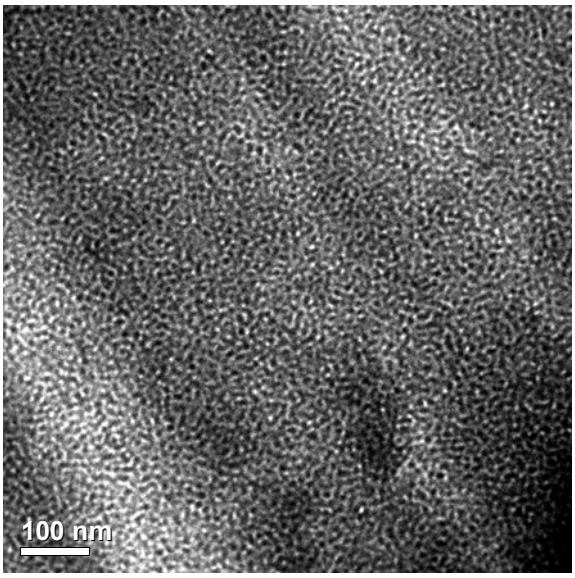

(e)

Figure 4.16. TEM images of five PEMa films. The membranes were cryo-microtomed and stained by $Pb(acetate)_2$, and dark domains correspond to the $PSSA/Pb^{2+}$ phase. Images (a), (b), (c), (d), and (e) correspond to PEMs 1a, 2a, 3a, 4a, and 5a, respectively.

Experiments were further conducted to understand the difference of domain spacings in PEMs 4a and 5a between SAXS and TEM experiments. Temperature-dependent SAXS experiments on PEM2a and PEM4a (Figure 4.17) were performed. The domain spacing in PEM2a maintained during heating, while the domain spacing of PEM4a shrank 30 % during annealing (q* increased 30 %). Thus, the decrease of domain spacing of PEMs 4a and 5a could be thermally induced. Similarly in TEM experiments, it was hypothesized that high-energy electron beams penetrating the polymer sample could generate heat and thereby caused the similar transition of domain spacing. Radical crosslinking of the double bonds in polyDCPD upon heating has been discussed.[33] Herein, for PEMs 4a and 5a, since polyDCPD segments were connected between PS chains, thermal reactions of polyDCPD could presumably cause the shrinkage of PNS/polyDCPD domains and the reduction of the PSSA domain sizes as well.

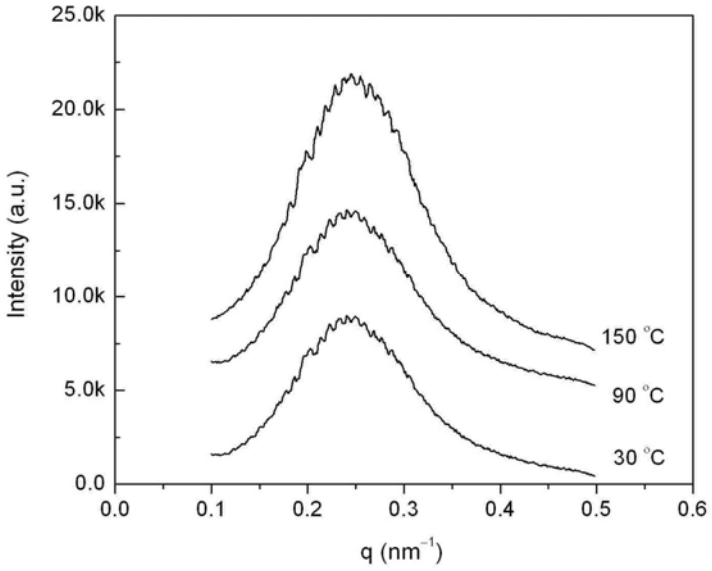

(a)

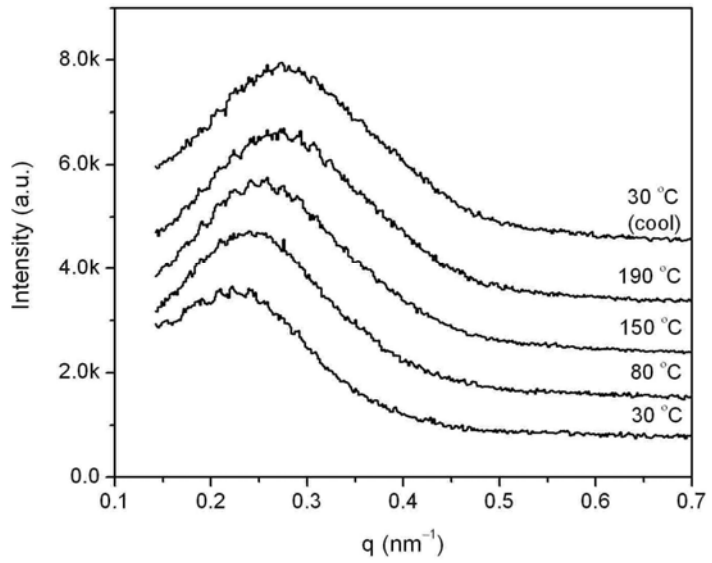

(b)

Figure 4.17. Temperature-dependent SAXS profiles of PEM2a (a) and PEM4a (b). Signals were offset vertically.

Lastly, thermal and mechanical stabilities of these PEMXa were evaluated. DSC analysis on PEM2 membranes (Figure 4.18a) between −40 and 140 °C does not show any T_g endotherms, since the matrix phase was crosslinked and the PS sulfonate phase had high thermal transition temperatures. Melting peaks of the PCOE component are observed, and the

intensity of the melting peaks of PCOE is attenuated from PEM1e to PEM1a. Additionally, DSC analyses of PEMs 1a, 2a, and 3a (Figure 4.18b) show melting endotherms between 0 and 50 °C upon heating consistent with the semi-crystalline nature of PCOE in the matrix phase. Decreases in melting temperature (T_m) and crystallinity of PCOE generally agree with the reduced PSSA domain size. No thermal transitions were observed for PEMs 4a and 5a up to 120 °C (Figure 4.18b), as the polyDCPD component was non-crystalline and disrupted the semi-crystalline PCOE phase. SAXS analysis of the PEMXa films indicated persistent scattering peaks at high temperatures, for example, the SAXS profiles for PEMs 2a and 4a shown in Figure 4.17, indicating the bicontinuous morphology is thermally stable to 200 °C. In contrast, morphologies of uncrosslinked PEMs from block copolymers could be sensitive to both humidity and temperature.[34] Moreover, the mechanical stability of the PEMXa films was largely maintained from the PEMXe films indicated from tensile measurements. As an example, tensile curves of PEM2a (Figure 4.19) under ambient conditions indicate an average elongation at break of 90 % and an average tensile strength of 21 MPa. Collectively, these PEMXa membranes were thermally and mechanically robust.

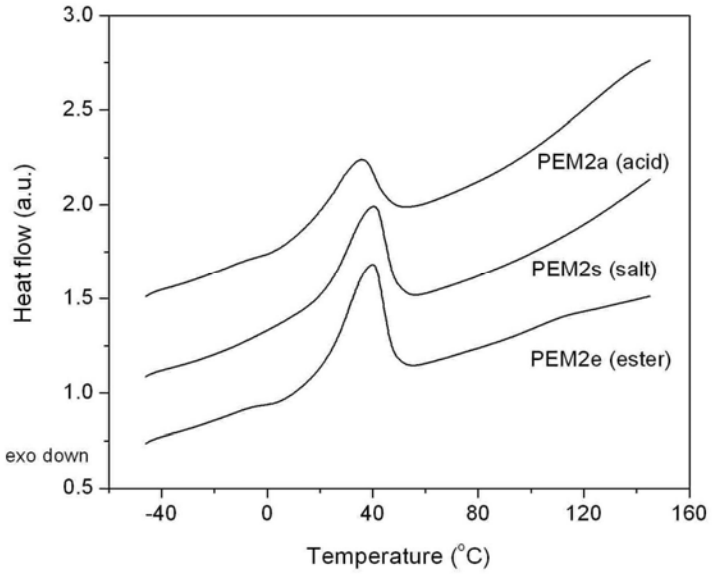

(a)

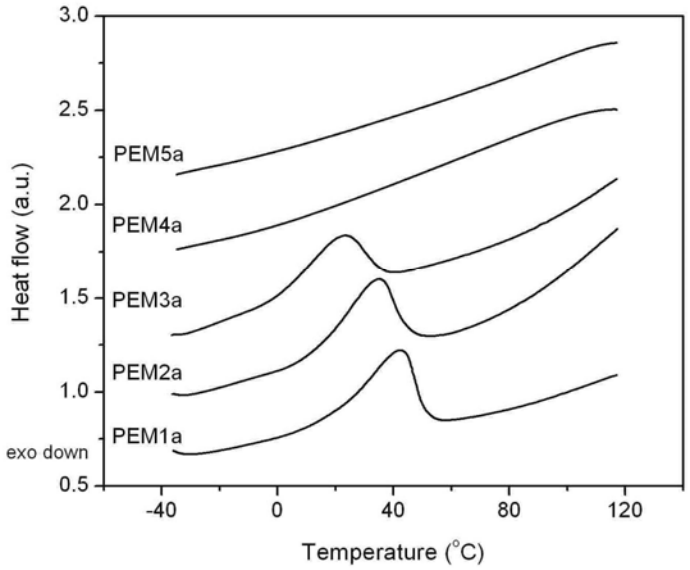

(b)

Figure 4.18. DSC traces of the PEM2 in three forms (a) and all membranes in acid form (b). The 2nd heating run was plotted for each PEM. The signals were vertically shifted.

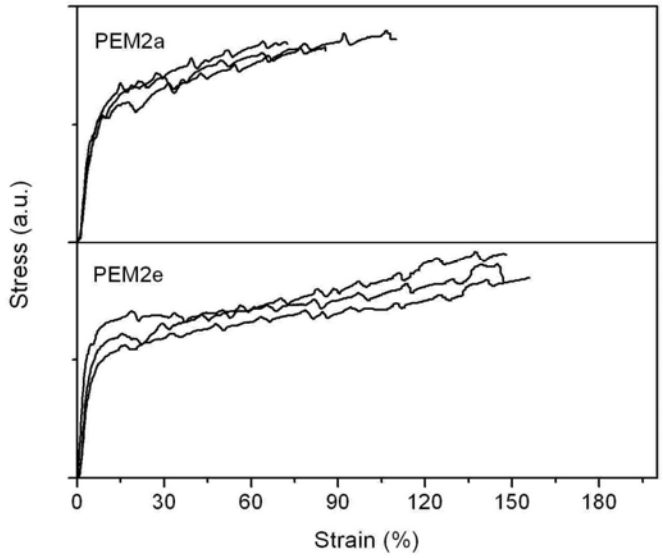

Figure 4.19. Tensile curves of the PEM2e and PEM2a membranes under ambient conditions.

4.3.4 Methanol permeability and proton conductivity measurements[c]

Before further characterization of the PEMXa films, the surface skin layer of these

[c] Experiments in this section were performed by Dan Hallinan at Drexal University.

membranes was completely removed using O_2 plasma etching.[18] XPS analysis (Figure 4.20) of the surface of PEM1a after etching indicates a sulfur composition (5.8 wt %) comparable to that in bulk (6.4 wt %).

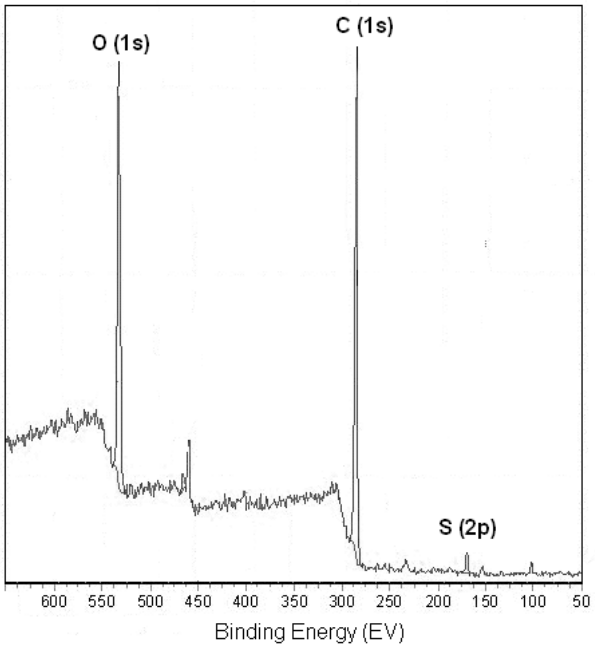

Figure 4.20. X-ray photoelectron spectroscopy (XPS) analysis of the surface of PEM2a, after 200 s O_2 plasma etching.

Methanol permeability through these PEMs in the fully hydrated state was examined using the FTIR-ATR technique,[14a] and summarized in Table 4.6. Experiments were conducted at 25 °C, and all membranes, unless noted, were soaking in water for four months before the permeability was measured. These hydrated PEMs were not in equilibrium state. For instance, the sorption and swelling induced by liquid water continually increased over four months. It is clear that during four months of non-equilibrium liquid water sorption the methanol permeability of PEM2a increased 20 %. Additionally, decrease in the mechanical strength of these hydrated PEMs was observed. For PEMs 1a, 2a, and 3a, slightly higher methanol permeability than Nafion 117 was observed; for PEMs 4a and 5a, due to increased crosslinking density in the matrix phase, reduced swelling of these PEMs in water was

observed thus causing lower methanol permeability. Therefore, methanol permeability was greatly suppressed by increasing the crosslinking density in the matrix phase of these PEMs.

Table 4.6. Methanol permeability through these crosslinked PEMs.

Membrane	Methanol Permeability × 10^6 (cm^2 s^{-1})
PEM1a	2.2
PEM2a[b]	2.2
PEM2a	2.7
PEM3a	3.0
PEM4a[b]	0.6
PEM5a[b]	0.5
Nafion 117	1.9

a. Measurements were performed by using 2 mol L^{-1} aqueous methanol at 25°C. *b*. Tested in the first week. Other PEMs were soaked in liquid water for 4 months prior to the measurements.

Table 4.7 shows proton conductivity (two electrodes, through plan conductivity), dimensional swelling, and weight uptake of these PEMs. Dry proton conductivity was measured on samples before contacting with water under ambient conditions (~25°C and ~20 % RH). Wet proton conductivity, dimensional swelling, and weight uptake were all measured after the fully hydrated PEMs that were soaked in water for 3 weeks. The dry proton conductivity was two orders of magnitude less than the wet proton conductivity for all samples. PEM1a took up much more water and swelled more than other PEMs. Wet proton conductivity of PEM1a appears to be higher than other PEMs and can be attributed to the lower modulus in the matrix phase of PEM1a (Table 4.3). In contrast, PEM5a having a rigid matrix took up the least amount of water.

Table 4.7. Two-electrode proton conductivity, dimensional swelling, and water uptake.

Membrane	Dry σ (mS/cm)	Wet σ (mS/cm)	Dimensional Swelling (%)	Water uptake (wt %)
PEM1a	0.43	34.0	28±2 %	118 ± 4
PEM2a	0.22	31.8	20±3 %	73 ± 12
PEM3a	0.53	28.7	20±5 %	78 ± 5
PEM4a		17.1	19±0.1 %	73 ± 2
PEM5a		20.0	11±1 %	42 ± 0.4
Nafion	4	35	19±1 %	34 ± 0.4

Four-electrode proton conductivities (in-plane conductivity) of these PEMs were depicted in Figure 4.21. First of all, for PEM3a having the smallest PSSA domain size exhibited comparable proton conductivity to Nafion at 90 % RH, while PEMs 1a and 2a showed significantly lower conductivities. These data are generally consistent with the previous observation that narrow ionic channels helped retain water and thus rendered high proton conductivity.[17] For the more crosslinked PEMs 4a and 5a, conductivities at low temperatures were comparable to PEM2a but substantially increased at 80 °C. These results are likely associated with the internal ion structure in the hydrated PSSA phase[4] and need to be further explored, for example, by characterizing the water structure in the hydrated PSSA phase. At RH=50 %, one order of magnitude lower conductivity than that of Nafion was observed, which is quite contradictory to previous observations that increased proton conductivity at high temperatures led to stronger water retention at low humidity.[17] Although a high acid content and a stable bicontinuous morphology were achieved in these PEMXa membranes, free energy of water in the PSSA domains was possibly high and somehow impeded the water uptake at low humidity. In sum, these crosslinked PEMs have demonstrated potential to improve the conductivity/permeability ratio at high humidity conditions.

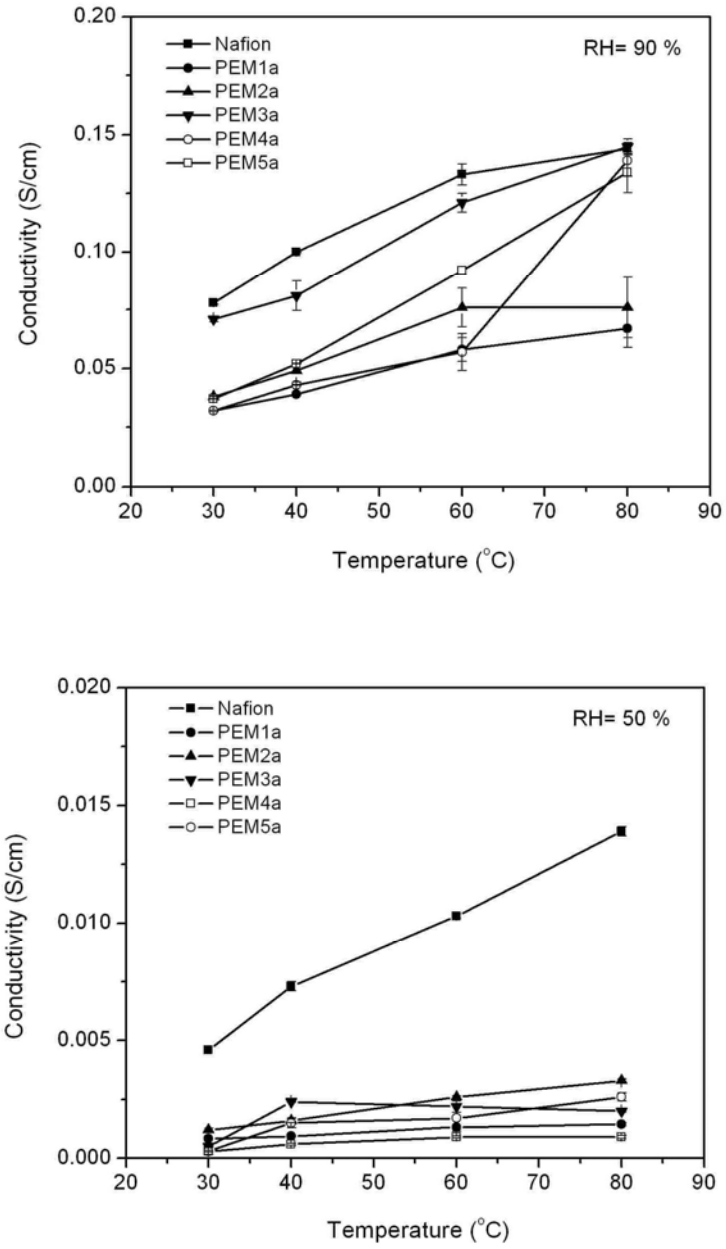

Figure 4.21. In-plan proton conductivity measurements on the PEMXa membranes at RH = 90 % and RH = 50 %.

4.3.5 Ammonia separation from gas mixtures[d]

Ammonia is produced from H_2 and N_2 in about 20 % conversion. The nitrogen and

[d] Ammonia separation experiments in this section were performed by Bill Phillip in CEMS at UMN.

hydrogen have to be separated from ammonia and recycled. Currently, dissolution and condensation of ammonia have been generally used to separation H_2 and N_2, and each method has some limitation. Polymer membranes containing a PSSA phase could be highly selective for ammonia over hydrogen and nitrogen due to the favorable interaction between the acid PSSA phase and the base NH_3. In practice, crosslinked PSSA membranes are preferred to sustain high operating pressures.[35]

In a recent paper, the crosslinked PEMs 1a, 2a, and 3a have been examined in the NH_3 separation process.[36] Another crosslinked PEM (PEM6a) studied in this paper was produced from PNS-PSSP (8.0-13 kg mol^{-1}) and COE/DCPD (1:1 ratio, 0.6 wt % to the copolymer) following the preparation steps in 4.3.2 and 4.3.3. Here are some characterization data for this membrane. Based on the SAXS data (Figure 4.22), a domain spacing of 26.6 nm is calculated. The PSSA domain size estimated from the TEM image (Figure 4.23) is 10 nm, and PSSA the composition in PEM6a is 33.9 wt %. PEM6a was less elastic compared with PEMs 1a–3a, due to the incorporation of polyDCPD in the matrix phase. During the measurements, PEM6a swelled less by NH_3 than the other three membranes.

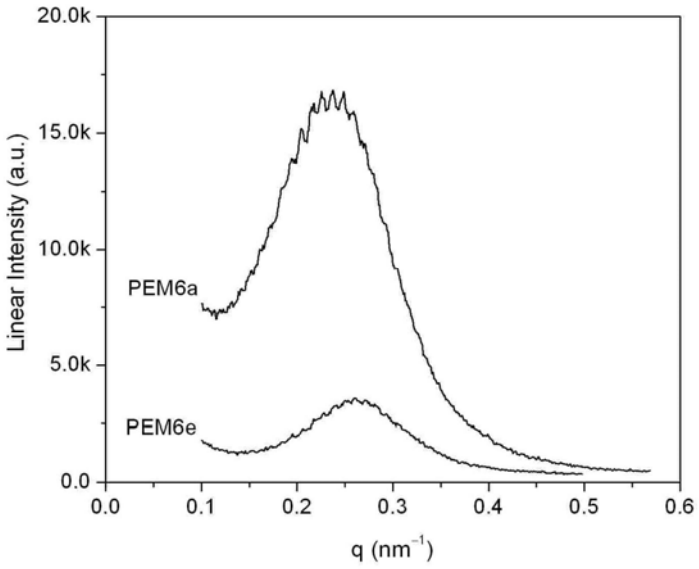

Figure 4.22. SAXS profiles of the PEM6e and PEM6a.

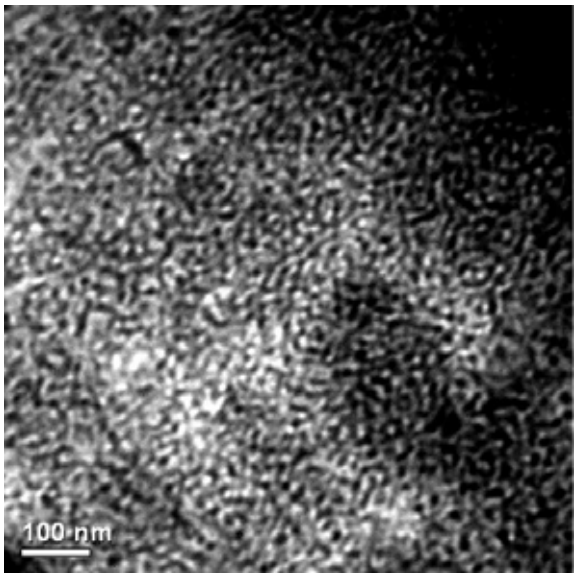

Figure 4.23. TEM image of PEM6a produced from PNS-PSSP (8-13) and COE/DCPD (1:1). The sample was stained in a saturated $Pb(acetate)_2$ aqueous solution and cryo-microtomed at −120 °C in 80 nm thick slices.

In this study, Nafion, a robust material possessing pendent sulfonic acid groups, was first examined in ammonia separation. Although high NH_3 flux and selectivity were achieved in single gas experiments, the NH_3 selectivity was completely lost in mixed gas experiments (Figure 4.24). This is because Nafion was plasticized by excess NH_3, so N_2 and H_2 fluxes were substantially increased.

In contrast, these crosslinked PEMXa films having a crosslinked matrix prevents the PSSA phase from swelling thereby allowing the membrane to remain NH_3 selectivity in the mixed gas experiments, for example, a representative graph shown in Figure 4.25. However, the ammonia permeabilities of these PEMs are much lower than that of Nafion, likely due to the crosslinked nature and high PSSA content.

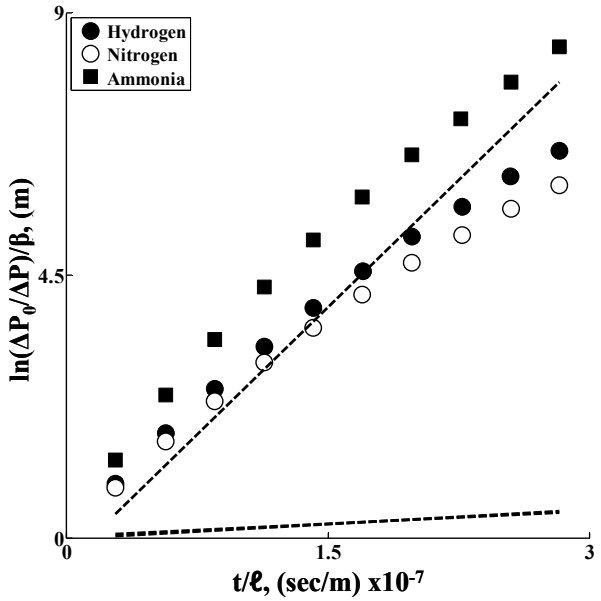

Figure 4.24. Gas diffusion experiments through Nafion. The data points show the results for the mixed gas experiments and the dashed lines show the permeabilities for experiments with single gases (N_2 and H_2 have lower permeabilities than NH_3). Reproduced with permission from Ref 36. Copyright 2009 Elsevier.

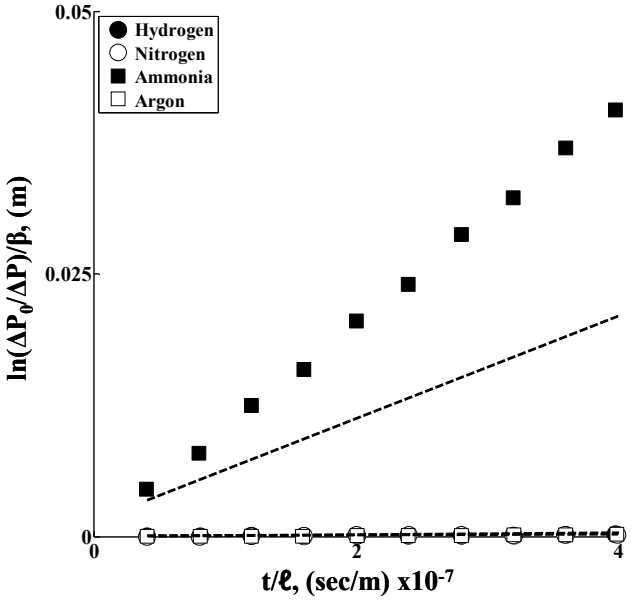

Figure 4.25. Gas diffusion experiments through the crosslinked PEMs. The data points show the results for the mixed gas experiments and the dashed lines show the permeabilities for experiments with single gases. Reproduced with permission from Ref 36. Copyright 2009 Elsevier.

Among these PEMs, PEM6a having a polyDCPD/PCOE matrix retained a high NH_3 selectivity (>100) from 50 kPa to 450 kPa. The ammonia permeability increased linearly, while the mixed gas nitrogen permeability remained constant, while other PEMs 1a–3a films containing an elastic PCOE component lost the NH_3 selectivity at high pressures. It was hypothesized that the more highly crosslinked PEM6a membranes have a lower dissolved ammonia concentration and are able to retain selectivity at high operating pressures.

4.3.6 Additional experimental aspects in PEM preparation

4.3.6.1 Deprotection of the PSSR phase

Successful deprotection of the PSSP phase in the precursor membrane is a key step in creating a proton-conducting phase. In the previous examples (Figure 4.11), reduction of the absorbance at 1370 cm^{-1} associated with the sulfonate ester has been utilized to indicate the PSSP deprotection. To confirm such a transition, a new copolymer PNS-PSSL (4.5-12 kg mol^{-1}) was synthesized (Section 4.2.3.8), as the PSSL block possesses a characteristic C=O group showing a strong absorbance by IR analysis. A crosslinked film was prepared from the PNS-PSSL (0.15 g) and COE (0.10 g) in THF (1.1 mL) with the catalyst **G2** (1.2 mg), and then PSSL phase was hydrolyzed following the standard procedure (Section 4.2.4). A similar bicontinuous morphology was observed in this film by SAXS. By IR spectroscopy (Figure 4.26), the C=O stretching peak at 1750 cm^{-1} completely disappears after hydrolysis, along with the decrease of a peak at 1360 cm^{-1}. This experiment unambiguously confirmed the complete deprotection of the sulfonated PS block in the crosslinked membranes.

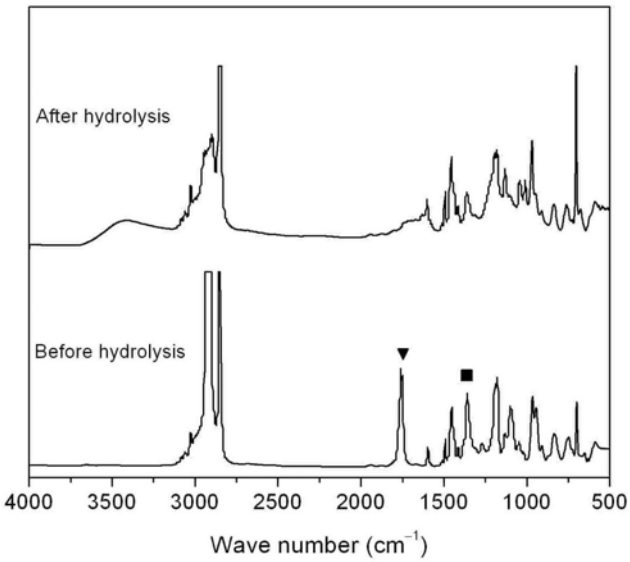

Figure 4.26. IR spectra of a crosslinked membrane prepared from PNS-PSSL (4.5-12) before and after PSSL hydrolysis. The triangle indicates the C=O stretching absorbance from the PSSL phase, and the square indicates the SO_2 absorbance.

4.3.6.2 An alternative approach to tune the PSSA domain size

Based on previous examples, a small PSSA domain size of less than 5 nm could facilitate the proton conductivity at high temperatures or low humidities.[17] Crosslinked PEMs with tunable PSSA domain sizes have been demonstrated in our preparation, but the PSSA domain sizes were all above 6 nm in the dry state. In this regard, crosslinked membranes produced from a lower molecular weight PNS-PSSP copolymer (e.g., 1 kg mol^{-1}) can be helpful. However, in order to maintain more reactive N groups (e.g., > 4 N units in the PNS block),[e] the PN block should contain exclusively N. Previous synthesis of PN by radical polymerization in Chapter 2 showed low conversion (10%), and thus production of low molecular weight PN in high efficiency could be challenging. Alternatively, low molecular weight hydroxyl terminated PN can be synthesized by anionic polymerization and thereby converted into a macroinitiator by end group modification, which can grow a PSSP block subsequently.

[e] This is critical to crosslink all copolymers and monomers together in high efficiency.

Herein, motivated by the work of producing crosslinked PSSA membranes by random copolymerization reactions,[37] a reactive copolymer was synthesized from N and SSP by conventional free radical copolymerization, where the ratio of PSSP to reactive sites could be simply adjusted, for example, a P(N-*s*-SSP) with N:SSP=1:9 (see Section 4.2.3.6). Following that, a crosslinked precursor membrane was produced from a solution of this polymer (0.30 g) and COE (0.27 g) in THF (2.4 mL) with **G2** (2.4 mg). Next, the PSSP component in the resultant film was successfully deprotected as indicated by IR analysis, suggesting that the PSSP phase was interconnected in the film. SAXS profiles of the resultant membranes (Figure 4.27) could not indicate a distinct morphology due to the lack of well-defined scattering peaks. Lastly, the resultant membrane was stained with $Pb(acetate)_2$, and the TEM image (Figure 4.28) indicates a disordered network structure and the PSSA domain size of < 5 nm.

In sum, by the same *in situ* crosslinking reactions of a P(N-*s*-SSP) copolymer and COE, a phase-separated PEM with a reduced PSSA domain size was facilely achieved, whereas the morphology of the PEM was ill-defined. The resulting membrane was relatively brittle comparing with the previous PEM3a, and it almost did not swell in water. To this end, no further characterization (e.g., proton conductivity, methanol permeability) has been performed on this membrane.

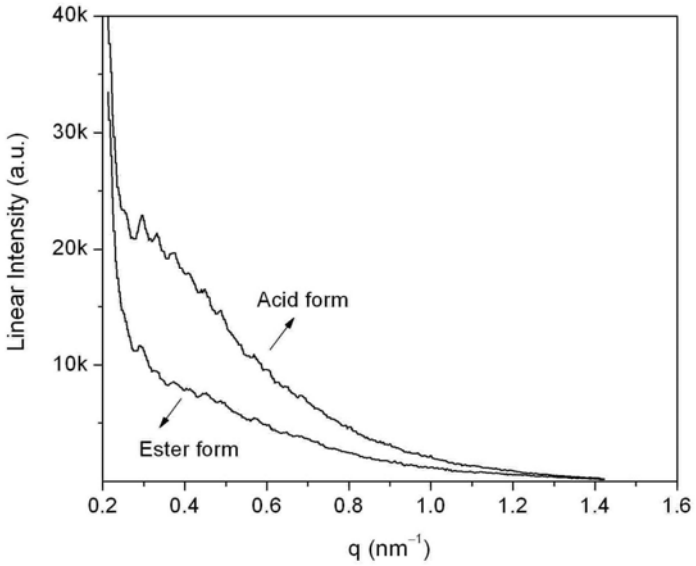

Figure 4.27. SAXS of crosslinked membranes produced from P(N-*s*-SSP) and COE.

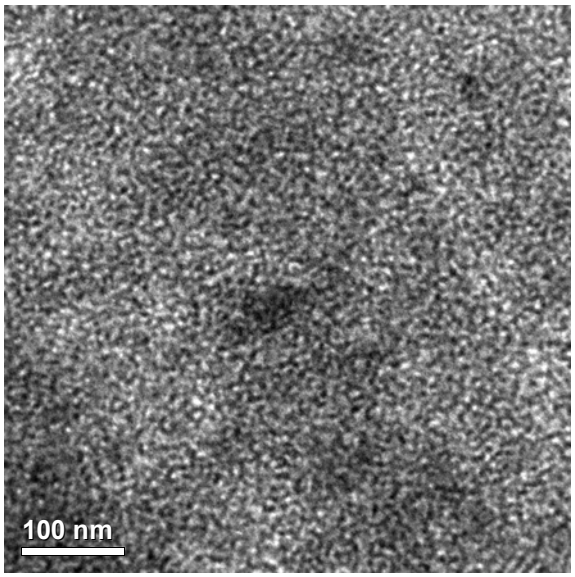

Figure 4.28. TEM image of the crosslinked PEM from P(N-*s*-SSP) and COE, the dark domains correspond to PSSA stained by Pb^{2+} ions.

4.3.6.3 Adjusting the acid content in the crosslinked PEMs

In most uncrosslinked PEMs, mechanical strength and thermal stability are often compromised by increase of the acid content.[11] In our membranes, the mechanical strength is governed by the crosslinked matrix phase, while the acid content can be independently

controlled. Experimentally, this aspect was demonstrated by using a PNS-PSSP copolymer containing a high PSSP content, while the bicontinuous morphology would be realized upon crosslinking with less COE. A PNS-PSSP (5-25 kg mol^{-1}, 6 N units per chain) copolymer was synthesized using the standard approach (Section 4.2.3.5). A precursor membrane was then synthesized from the PNS-PSSP (0.50 g) and 0.20 g COE in THF (2.8 mL) with **G2** (2.8 mg). After the deprotection step, the PSSP block was completely converted to PSSA (IR spectra not shown), and SAXS profiles of the resultant membrane (Figure 4.29) shows a scattering peak similar to previous PEMXa films, possibly indicative of a bicontinuous phase.

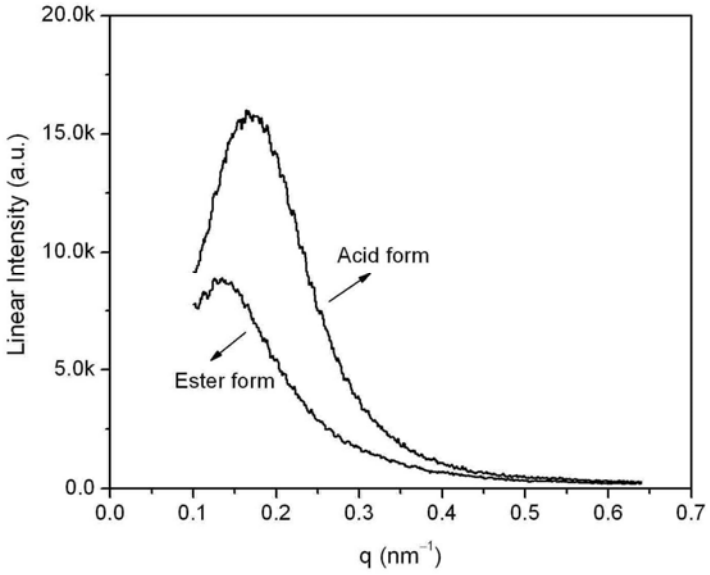

Figure 4.29. SAXS of the crosslinked membrane produced from PNS-PSSP(5-25) and COE.

4.3.6.4 Tuning mechanical strength of the PEMs

In previous experiments, the mechanical strength of the crosslinked films was adjusted by using different reactive monomers. Herein, a different method for tuning the mechanical strength was demonstrated by varying the mass ratio of PNS to the reactive monomers in the films. For simplicity, a PNS polymer was studied instead of using a PNS-PSSP copolymer. The model PNS polymer (30 kg mol^{-1}, 15 N units per chain) was synthesized by living

anionic polymerization following the description in Chapter 2. Next, several crosslinked films were prepared from the PNS and COE (or DCPD) (20 wt % in THF) by *in situ* metathesis crosslinking reactions, and summarized in Table 4.8. After drying the resultant films, tensile tests on these films were performed. The tensile curves (Figure 4.30) illustrates that the crosslinked films containing high PCOE contents (PNSPCOE37 and PNSPCOE55) exhibit elongations at break above 200 %. The elastic modulus (indicated by the initial slope of the tensile curves) increases along with incorporation of more PNS. In contrast, the crosslinked films containing low PCOE content or polyDCPD were relatively brittle.

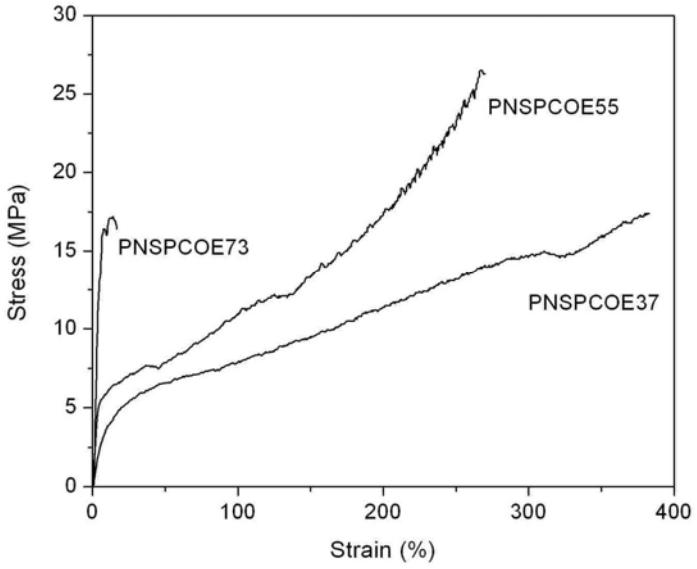

Figure 4.30. Tensile tests on the crosslinked films listed in Table 4.8.

Table 4.8. Crosslinked PNS films containing PCOE or polyDCPD.

Entry	Composition	Mass ratio	Swelling in THF
1	PCOE		dissolved
2	PolyDCPD		28%
2	Crosslinked PNS		20%
3	PCOE/PNS	3:7	40 %
4	PCOE/PNS	5:5	35%
5	PCOE/PNS	7:3	55%
6	PolyDCPD/PNS	7:3	25%

PNS was produced by anionic polymerization. By NMR: M_n = 30 kg mol^{-1} and on average 15 N groups in

the backbone. The cured films contained 0.25 wt % of the catalyst **G2**.

Swelling properties of these crosslinked films were examined by soaking these samples in toluene overnight and measuring the dimensional change. Generally, the crosslinked films containing polyDCPD or more PNS content had higher crosslinking densities and thus swelled less in toluene. Additionally, thermal properties of these films were examined by DSC experiments. Similar to the previous PEM1e, the melting endotherm of the PCOE component was observed in PNSPCOE37, while the films containing less PCOE became non-crystalline.

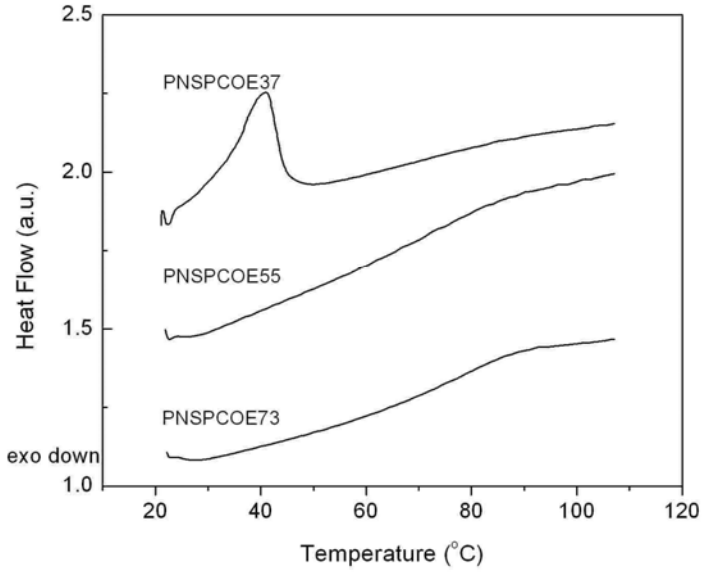

Figure 4.31. DSC traces (the 2nd heating run) of the crosslinked films from the PNS (30 kg mol^{-1}) and COE, at a heating rate of 10 °C/min. The signals were vertically shifted.

In sum, the above systematic examination of different experimental aspects indicated critical factors in control of PEM preparation from PNS-PSSP. Given a PNS-PSSP copolymer, the final morphology, PSSA content, and mechanical strength in the resultant PEM can be independently tailored through the PIPS process (Figure 4.1). In the next section, mechanistic examination of the structure formation in PEMs was conducted.

4.3.7 Mechanistic studies

4.3.7.1 Screening study of styrenesulfonate monomers

In Chapter 3, for the PIPS process during the ROMP of DCPD with a PLA homopolymer, macrophase separation occurred due to the incompatibility between the resultant polyDCPD and PLA. This phenomenon was simply indicated by the opaque appearance of the polyDCPD/PLA film, as the opaqueness is typically attributed to the difference of refractive indices between two macrophase-separated domains that are in the range of the wavelengths of visible light.[38] Furthermore, in a similar PIPS process with a PNS-PLA copolymer,[18] the reactive PNS block helped arrest phase separation and rendered nanoscopic PLA domains in a crosslinked PNS/polyDCPD matrix.

In this chapter, in order to realize the same bicontinuous structure through the crosslinking reaction of PNS-PSSR (R denotes a protecting group) and DCPD, strong phase segregation between the PSSR and polyDCPD blocks should be satisfied. Experimentally, the segregation strength between them could be adjusted by varying the protective group in the PSSR block. Several candidate styrenesulfonate esters were synthesized, and were subsequently polymerized by conventional radical polymerizations. After that, metathesis reactions of DCPD in the presence of these homopolymers were performed in THF.

For these PSSR copolymers (see Section 4.2.3.3), PSSF was produced in very low conversion (about 10 %), although the resultant polymers exhibited strong incompatibility with polyDCPD due to the trifluoromethyl groups in the polymer. PSSE and PSSNP showed limited solubility in organic solvents like THF, and thus were not suitable for further use. For other polymers like PSSH and PSSB, metathesis reactions of DCPD with them in THF yielded transparent films, presumably indicating no pronounced macrophase separation from polyDCPD; copolymers containing a PSSH or PSSB block might not be effective to form a bicontinuous structure. Lastly, PSSP turned out to be a promising candidate, as an opaque film was yielded through the crosslinking process of DCPD with PSSP in THF. As expected, the PEM5e film produced from the PNS-PSSP (6-13) copolymer and DCPD in a

bicontinuous structure was shown in Section 4.3.2.

4.3.7.2 Mechanism of structure formation in the PEMXe films

In 4.3.7.1, ROMP of DCPD in the presence of PSSH likely resulted in no macrophase separation. Regardless of this fact, in further experiments, a crosslinked film from a PNS-PSSH copolymer (12-29 kg mol^{-1}) and DCPD (0.6 wt % relative to PNS-PSSH) was prepared following the standard procedure (Section 4.2.4). The resultant film did not exhibit a distinct peak by SAXS in Figure 4.32. Next, base hydrolysis of the PSSH block in the crosslinked membrane was incomplete based on IR analysis. Both SAXS and IR results corroborated that a bicontinuous structure was likely absent in this crosslinked film as expected.

In previous experiments, COE was commonly utilized in the crosslinking process with PNS-PSSP, and yielded crosslinked films possessed high elasticity (e.g., PEMs 1e, 2e, and 3e). Herein, a crosslinked film was prepared from the same PNS-PSSH and COE (0.6 wt % relative to PNS-PSSH) following the standard procedure. SAXS analysis of the resultant film (Figure 4.32) exhibits a distinct scattering peak as evidence of a disordered but phase-separated structure, similar to the bicontinuous structure observed in PEM1e (Figure 4.9). Furthermore, the PSSH phase was successfully transformed to PSSA, implying that the PSSH phase was indeed continuous throughout the macroscopically crosslinked PNS-PSSH/PCOE membrane. Different microstructures resulted in these two examples may help elucidate the mechanism of structure formation in the PIPS process.

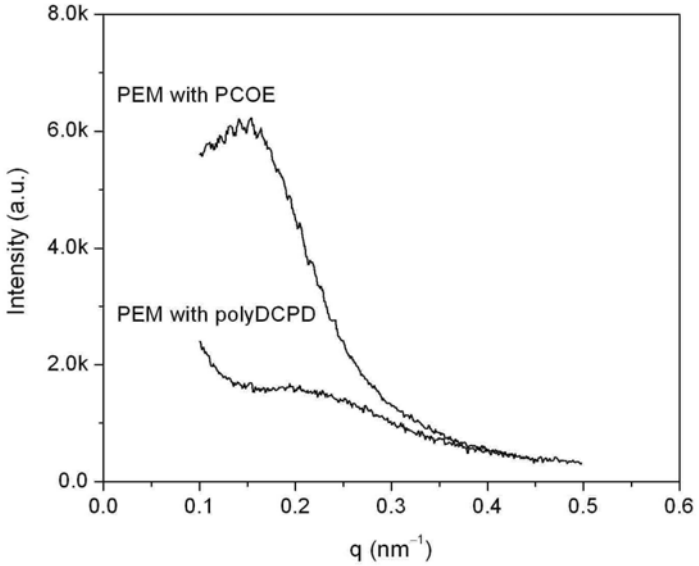

Figure 4.32. SAXS profiles of the crosslinked membranes produced with PNS-PSSH (12-29 kg mol^{-1}).

Apart from above experiments, crosslinked films from PNS-PSSP(6-13) and COE have been prepared in different solvents, such as CH_2Cl_2 and toluene, and the resultant films showed similar bicontinuous structures. Additionally, the solvent content in the crosslinking process could be flexible (5–10 times to copolymer/monomer by mass) without affecting the final morphology. These results are consistent with the observation in Chapter 3, and may infer that the formation a bicontinuous morphology in this chapter complies with the proposed mechanism in Chapter 3.

In Chapter 3, the formation of a bicontinuous morphology throughout the crosslinking process was not affected by the reactive monomers (e.g., DCPD and PCOE), and no supermolecular aggregates existed in the initial solution. Nevertheless, in the crosslinked films produced from PNS-PSSH, different nanostructures resulted in the cases of using DCPD or COE. Additionally, DLS analysis of solutions of these copolymers in THF or benzene indicated both free copolymer chains and micrometer-sized aggregates, as summarized in Table 4.9, contrasted with the PNS-PLA solution in THF. The aggregates in

the solutions were presumably caused by the PSSP block, as the PSSP homopolymer (>10 kg mol^{-1}) was not soluble in benzene and sub-micrometer aggregates were present in a PSSP/THF solution by DLS analysis. Next, structure of the aggregates in the PNS-PSSP solutions was further examined. Instead of resorting to complicated cryo-SEM experiments, regular SEM experiments were performed on the freeze-dried copolymers. SEM samples were prepared as follows: the copolymer/benzene in a glass vial was frozen in liquid nitrogen, immersed in an ice/water bath at 0 °C, and dried slowly under reduced pressure. Since the melting point of benzene is 4 °C, the copolymer structure in the solution could be largely preserved. As a result, SEM images for entries 2 and 7 in Table 4.9 (Figure 4.33) exhibit very different structures: the PNS-PSSP (2-5) sample shows a micrometer-scale porous cellular structure, while PNS-PLA (8-11 kg mol^{-1}) shows an isotropic sponge-like structure (< 100 nm). These results support that the PNS-PSSP solutions were not as homogeneous in the nanoscopic length scale as the PNS-PLA solution, qualitatively agreeable with the DLS results.

Table 4.9. DLS analysis of the copolymer solutions.[a]

Entry	Polymer	Solvent	DLS analysis
1	PNSPSSP(2-5)	THF	A+F[b]
2	PNSPSSP(2-5)	benzene	A+F
3	PNSPSSP(6-13)	THF	A+F
4	PNSPSSP(10-23)	THF	A+F
5	PNSPSSH(12-29)	THF	A+F
6	PNSPLA (8-11)	THF	F
7	PNSPLA (8-11)	benzene	F

a. Roughly 10 wt % copolymer in the solution. *b*. A and F denote micrometer scale aggregates and free copolymer chains, based on DLS analysis.

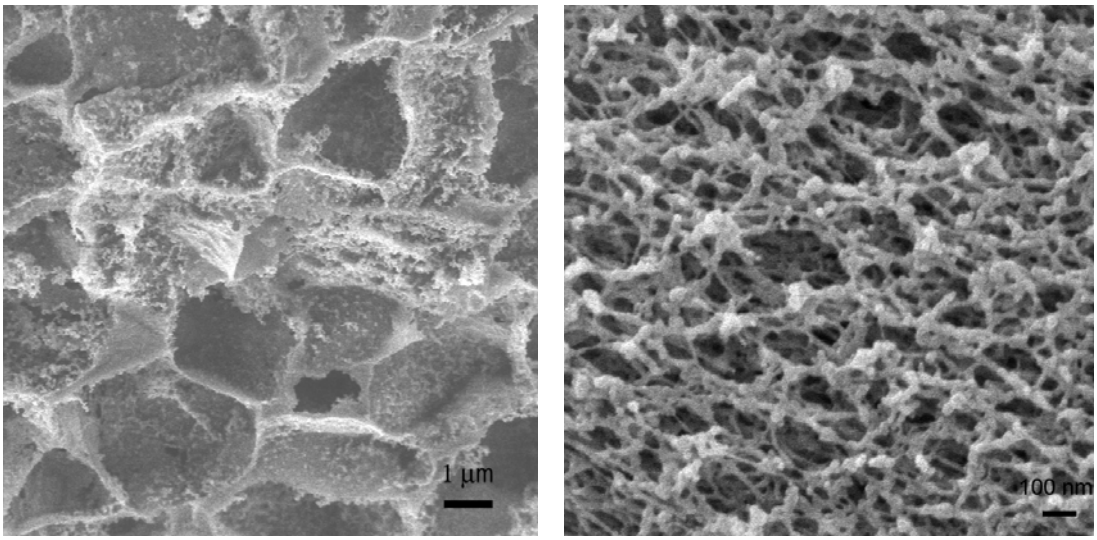

(a) (b)

Figure 4.33. SEM images of freeze-dried PNS-PSSP (2-5) (a) and PNS-PLA (8-11) (b) from 10 wt % benzene solutions, coated with 3 nm Pt.

Collectively, the PIPS process of PNS-PSSR and reactive cyclic alkenes (DCPD or COE) is generically depicted in Figure 4.34. Initially, in the THF solution of these components, the PNS and monomers are well mixed with THF, but the PSSR chains form some micrometer-sized aggregates in THF due to their limited solubility. In the PSSR/THF domains, some monomers and the catalyst are possibly mixed. Through the *in situ* metathesis reactions, the PNS component and monomers are efficiently polymerized to render a highly grafted structure, which would hypothetically favor a bicontinuous phase based on the example of reactive graft copolymers.[39] Specifically, for the crosslinking process of PNS-PSSR with COE, this grafting process can overcome any existing microstructure in the initial solution, and thus a bicontinuous structure is yielded. Importantly, during this process, any PCOE oligomers that are formed in the PSSR/THF domains could eventually segregate from PSSR after removing THF, since uncrosslinked PCOE oligomers may possess modest mobility in the crosslinked blend. In contrast, for the crosslinking process of PNS-PSSR with DCPD, the same scheme will still lead to a bicontinuous morphology, but the final structure can be compromised by the segregation strength between the resultant polyDCPD and PSSR. For example, if the segregation between PSSR and polyDCPD is weak (e.g., PSSH), some

polyDCPD oligomers can be crosslinked and trapped in PSSR domains after gelation, so the bicontinuous structure will be partially disrupted.

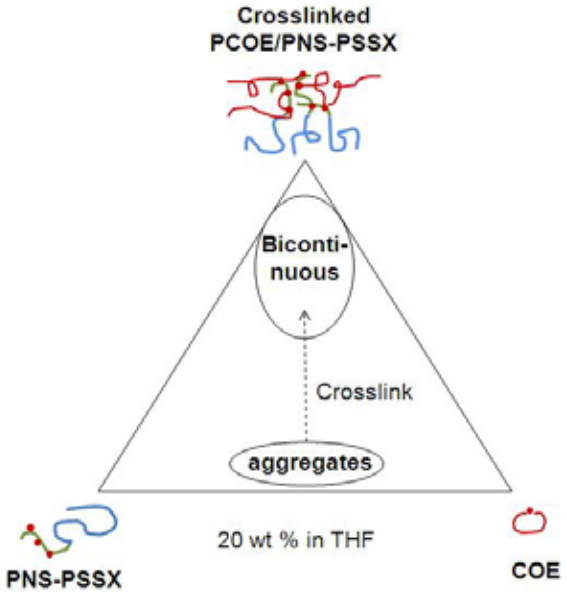

Figure 4.34. Schematic illustration of forming a crosslinked film in a bicontinuous morphology.

4.4 Conclusions and outlook

A facile approach has been demonstrated to prepare crosslinked PEMs from the PNS-PSSP block copolymers and reactive cyclic olefins. A morphology with continuous PSSA domains supported by a continuous and mechanically robust phase was evident in these films. Pronounced thermal and mechanical stabilities in the resultant PEMs were realized. The PSSA domain size was tuned by the copolymer molecular weight. Select PEMs showed much lower methanol crossover than Nafion while maintaining high saturated conductivities. Dehydration of these PEMs at low humidity was more severe than Nafion and deserved further investigation. For example, the internal ion structure of the hydrated PSSA phase at the hydrated state needs to be examined in the future. This reactive block polymer strategy for the preparation of PEMs is attractive due the ready formation of a bicontinuous structure, the facile control of the PSSA domain size and content, and the ability to independently

control mechanical and swelling properties of the PEMs.

4.5 References

[1] Hickner, M. A.; Ghassemi, H.; Kim, Y. S.; Einsla, B. R.; McGrath, J. E. *Chem. Rev.* **2004**, *104*, 4587–4612.

[2] Mauritz, K.; Moore, R. *Chem. Rev.* **2004**, *104*, 4535–4585.

[3] Ravikumar, M. K.; Shukla, A. K. *J. Electrochem. Soc.* **1996**, *143*, 2601–2606.

[4] Karlsson, L. E.; Wesslen, B.; Jannasch, P. *Electrochimica Acta* **2002**, *47*, 3269–3275.

[5] (a) Rikukawa, M.; Sanui, K. *Prog. Polym. Sci.* **2000**, *25*, 1463–1502. (b) Kreuer, K. D. *J. Membr. Sci.* **2001**, *185*, 29–39. (c) Li, Q.; He, R.; Jensen, J. O.; Bjerrum, N. J. *Chem. Mater.* **2003**, *15*, 4896–4915. (d) Hicker, M. A.; Pivovar, B. S. *Fuel Cells* **2005**, *5*, 213–229. (e) Souzv, R.; Ameduri, B. *Prog. Polym. Sci.* **2005**, *30*, 644–687. (f) Deluca, N. W.; Elabd, Y. A. *J. Polym. Sci. B: Polym. Phys.* **2006**, *44*, 2201–2225. (g) Neburchilov, V.; Martin, J.; Wang, H.; Zhang, J. *J. Power Sources* **2007**, *169*, 221–238.

[6] (a) Bates, F. S.; Fredrickson, G. H. *Physics Today* **1999**, 32–38. (b) Ruzette, A.-V.; Leibler, L. *Nature Mater.* **2005**, *4*, 10–31.

[7] (a) Wang, H.; Capuano, G. A. *J. Electrochem. Soc.* **1998**, *145*, 780–784. (b) Shen, M.; Roy, S.; Kuhlmann, J. W.; Scott, K.; Lovell, K. Horsfall, J. A. *J. Membr. Sci.* **2005**, *251*, 121–130.

[8] (a) Ding, J.; Chuy, C.; Holdcroft, S. *Chem. Mater.* **2001**, *13*, 2231–2233. (b) Ding, J.; Chuy, C.; Holdcroft, S. *Adv. Func. Mater.* **2002**, *12*, 389–394. (c) Yang, Y.; Holdcroft, S. *Fuel Cells* **2005**, *2*, 171–186.

[9] (a) Norsten, T. B.; Guiver, M. D.; Murphy, J.; Astill, T.; Navessin, T.; Holdcroft, S.; Frankamp, B. L.; Rotello, V. M.; Ding, J. *Adv. Funct. Mater.* **2006**, *16*, 1814–1822. (b) Nieh, M.-P.; Guiver, M. D.; Kim, D. S.; Ding, J.; Norsten, T. *Macromolecules* **2008**, *41*, 6176–6182.

[10] Zhai, M.; Chen, J.; Hasegawa, S.; Maekawa, Y. *Polymer* **2009**, *50*, 1159–1165.

[11] Zhang, Z.; Chalkova, E.; Fedkin, M.; Wang, C.; Lvov, S. N.; Komarneni, S.; Chung, T. C. M. *Macromolecules* **2008**, *41*, 9130–9139.

[12] Tsang, E. M. W.; Zhang, Z.; Shi, Z.; Soboleva, T.; Holdcroft, S. *J. Am. Chem. Soc.* **2007**, *129*, 15106–15107.

[13] Kim, J.; Kim, B.; Jung, B. *J. Membr. Sci.* **2002**, *207*, 129–137.

[14] (a) Elabd, Y. A.; Napadensky, E.; Sloan, J. M.; Crawford, D. M.; Walker, C.W. *J. Membr. Sci.* **2003**, *217*, 227–242. (b) Elabd, Y. A.; Beyer, F. L.; Walker, C.W. *J. Membr. Sci.* **2004**, *231*,181–188. (c) Elabd, Y. A.; Napadensky, E.; Walker, C. W.; Winey, K. I. *Macromolecules* **2006**, *39*, 399–407.

[15] Serpico, J. M.; Ehrenberg, S. G.; Fontanella, J. J.; Jiao, X.; Perahia, D.; McGrady, K. A.; Sanders, E. H.; Kellogg, G. E.; Wnek, G. E. *Macromolecules* **2002**, *35*, 5916–5921.

[16] Shi, Z.; Holdcroft, S. *Macromolecules* **2005**, *38*, 4193–4201.

[17] Park, M. J.; Downing, K. H.; Jackson, A.; Gomez, E. D.; Minor, A. M.; Cookson, D.; Weber, A. Z.;

Balsara, N. P. *Nano Lett.* **2007**, *7*, 3547–3552.

[18] Chen, L.; Phillip, W. A.; Cussler, E. L.; Hillmyer, M. A. *J. Am. Chem. Soc.* **2007**, *129*, 13786–13787.

[19] Schmidt, S. C.; Hillmyer, M. A. *Macromolecules* **1999**, *32*, 4794–4801.

[20] DeLuca, N. W.; Elabd, Y. A. *J. Membr. Sci.* **2006**, *282*, 217–224.

[21] Wang, J.-S.; Matyjaszewski, K. *J. Am. Chem. Soc.* **1995**, *117*, 5614–5615.

[22] (a) Ishizone, T.; Tsuchiya, J.; Hirao, A.; Nakahama, S. *Macromolecules* **1992**, *25*, 4840–4847. (b) Okamura, H.; Takatori, Y.; Tsunooka, M.; Shirai, M. *Polymer* **2002**, *43*, 3155–3162.

[23] Lienkamp, K.; Ruthard, C.; Lieser, G.; Berger, R.; Groehn, F.; Wegner, G. *Macromol. Chem. Phys.* **2006**, *207*, 2050–2065.

[24] Chen, L.; Hillmyer, M. A. *Macromolecules* in press.

[25] Lienkamp, K.; Schnell, I.; Groehn, F.; Wegner, G. *Macromol. Chem. Phys.* **2006**, *207*, 2066–2073.

[26] Wang, J.-S.; Matyjaszewski, K. *J. Am. Chem. Soc.* **1995**, *117*, 5614–5615.

[27] Aylward, N. N. *Polym. Lett.* **1970**, *8*, 377–380.

[28] Scholl, M.; Ding, S.; Lee, C. W.; Grubbs, R. H. *Org. Lett.* **1999**, *1*, 953– 956.

[29] Teubner, M.; Strey, R. *J. Chem. Phys.* **1987**, *87*, 3195–3200.

[30] Schubert, K.-V.; Strey, R.; Kline, S. R.; Kaler, E. W. *J. Chem. Phys.* **1994**, *101*, 5343–5355

[31] Liu, D.; Kyriakides, S.; Case, S. W.; Lesko, J. J.; Li, Y.; McGrath, J. E. *J. Polym. Sci. B: Polym. Phys.* **2006**, *44*, 1453–1465.

[32] DeLongchamp, D. M.; Vogt, B. D.; Brooks, C. M.; Kano, K.; Obrzut, J.; Richter, C. A.; Kirillov, O. A.; Lin, E. K. *Langmuir* **2005**, *21*, 11480–11483.

[33] Davidson, T. A.; Wagener, K. B.; Priddy, D. B. *Macromolecules* **1996**, *29*, 786–788.

[34] (a) Park, M. J.; Nedoma, A. J.; Geissler, P. L.; Balsara, N. P.; Jackson, A.; Cookson, D. *Macromolecules* **2008,** *41,* 2271–2277. (b) Park, M. J.; Balsara, N. P. *Macromolecules* **2008,** *41,* 3678–3687.

[35] Staudt-Bickel, C.; Koros, W. J. *J. Membr. Sci.* **1999***, 155*, 145–154.

[36] Phillip, W. A.; Martono, E.; Chen, L.; Hillmyer, M. A.; Cussler, E. L. *J. Membr. Sci.* **2009**, *337*, 39–46.

[37] Zhou, Z.; Dominey, R. N.; Rolland, J. P.; Maynor, B. W.; Pandva, A. A.; DeSimone, J. M. *J. Am. Chem. Soc.* **2006**, *128*, 12963–12972.

[38] Debye, P.; Bueche, A. M. *J. Appl. Phys.* **1949**, *20*, 518–525.

[39] Pernot, H.; Baumert, M.; Court, F.; Leibler, L. *Nature Mater.* **2002**, *1*, 54–58.

References

Chapter 1

1 Shannon, M. A.; Bohn, P. W.; Elimelech, M.; Georgiadis, J. G.; Marinas, B. J.; Mayes, A. M. *Nature* **2008**, *452*, 301–310.

2 Freeman, B. D.; Pinnau, I. *Polymer membranes for gas and vapor separation: chemistry and materials science*. Washington, DC: American Chemical Society, **1999**.

3 Chapman, P. D.; Oliveira, T.; Livingston, A. G.; Li, K. *J. Membr. Sci.* **2008**, *318*, 5–37.

4 Hickner, M. A.; Ghassemi, H.; Kim, Y. S.; Einsla, B. R.; McGrath, J. E. *Chem. Rev.* **2004**, *104*, 4587–4612.

5 (a) Sadoway, D. R. *J. Power Sources* **2004**, *129*, 1–3. (b) Armand, M.; Tarascon, J. M. *Nature* **2001**, *414*, 359–369.

6 (a) Koopal, C. G.; de Ruiter, B.; Nolte, R. J. M. *J. Chem. Soc. Chem. Commun.* **1991**, 1691–1692. (b) Wang, P.-C.; DeVoe, D. L.; Lee, C. S. *Electrophoresis* **2001**, *22*, 3857–3867. (c) Adhikari, B.; Majumdar, S. *Prog. Polym. Sci.* **2004**, *29*, 699–766. (d) Charcosset, C. *Biotech. Adv.* **2006**, *24*, 482–492.

7 Pastan, S.; Bailey, J. *New Engl. J. Med.* **1998**, *338*, 1428–1437.

8 Strathmann, H. *AIChE Journal* **2001**, *47*, 1077–1087.

9 Ulbricht, M. *Polymer* **2006**, *47*, 2217–2262.

10 (a) Koros, W. J.; Fleming, G. K. *J. Membr. Sci.* **1993**, *83*, 1–80. (b) Stern, S. A. *J. Membr. Sci.* **1994**, *84*, 1–65. (c) Koros, W. J.; Mahajan, R. *J. Membr. Sci.* **2000**, *175*, 181–196.

11 Nagai, K.; Masuda, T.; Nakagawa, T.; Freeman, B. D.; Pinnau, I. *Prog. Polym. Sci.* **2001**, *26*, 721–798.

12 Perry, J. D.; Nagai, K.; Koros, W. J. *MRS Bulletin* **2006**, *31*, 745–749.

13 Lin, H.; Freeman, B. D. *J. Mol. Struct.* **2005**, *739*, 57–74.

14 Ho, W. S.; Dalrymple, D. C. *J. Membr. Sci.* **1994**, *91*, 13–25.

15 (a) Tanaka, K.; Kita, H.; Okano, M.; Okamoto, K. *Polymer* **1992**, *33*, 585–592. (b) Ghosal, K.; Chern, R. T.; Freeman, B. D.; Daly, W. H.; Negulescu, I. I. *Macromolecules* **1996**, *29*, 4360–4369.

16 Ghanem, B. S.; McKeown, N. B.; Budd, P. M.; Selbie, J. D.; Fritsch, D. *Adv. Mater.* **2008**, *20*, 2766–2771

17 Park, H. B.; Jung, C. H.; Lee, Y. M.; Hill, A. J.; Pas, S. J.; Mudie, S. T.; Wagner, E. V.; Freeman, B. D.; Cookson, D. J. *Science* **2007**, *318*, 254–258.

18 Hillock, A. M. W.; Koros, W. J. *Macromolecules* **2007**, *40*, 583–587.

19 Lin, H.; Wagner, E. V.; Freeman, B. D.; Toy, L. G.; Gupta, R. P. *Science* **2006**, *311*, 639–642.

20 (a) Kim, T.-J.; Li, B.; Hagg, M.-B. *J. Polym. Sci. B: Polym. Phys.* **2004**, *42*, 4326–4336. (b) Zou, J.; Ho, W. *J. Membr. Sci.* **2006**, *286*, 310–321.

21 (a) Quinn, R.; Laciak, D. V.; Pez, G. P. *J. Membr. Sci.* **1997**, *131*, 49–60. (b) Quinn, R.; Laciak, D. V.; Pez, G. P. *J. Membr. Sci.* **1997**, *131*, 61–69.

22 Radosz, M.; Shen, Y. US Patent 0119302A1, **2007**.

23 Sridhar, S.; Smitha, B.; Aminabhavi, T. M. *Separation & Purification Reviews* **2007**, *36*, 113-174.

24 *Nature Mater.* **2008**, *7*, 341.

25 Fleischer, R. L.; Alter, H. W.; Furman, S. C.; Price, P. B.; Walker, R. M. *Science* **1972**, *178,* 255–263.

26 Michaels, A. S. High Flow Membrane, US Patent 3,615,024, **1971**.

[27] Bierenbaum, H. S.; Isaacson, R. B.; Bruin, M. L.; Plovan, S. G. *Ind. Eng. Chem. Prod. Res. Dev.* **1974**, *1*, 2–9.
[28] Gore, R. W. Porous Products and Process Therefore, US Patent 4,187,390, **1980**.
[29] Hester, J. F.; Mayes, A. M. *J. Membr. Sci.* **2002**, *202*, 119–135
[30] Ulbricht, M.; Oechel, A.; Lehmann, C.; Tomaschewski, G.; Hicke, H.-G. *J. Appl. Polym. Sci.* **1995**, *55*, 1707–1723.
[31] Pieracci, J.; Wood, D. W.; Crivello, J. V.; Belfort, G. *Chem. Mater.* **2000**, *12*, 2123–2133.
[32] Xu. D.; Hein, S.; Wang, K. *Mater. Sci. Tech.* **2008**, 1076–1087.
[33] Matsuyama, H.; Yuasa, M.; Kitamura, Y.; Teramoto, M.; Lloyd, D. R. *J. Membr. Sci.* **2000**, *179*, 91–100.
[34] (a) Reverchon, E.; Cardea, S. *Ind. Eng. Chem. Res.*, **2006**, *45*, 8939–8945. (b) Cardea, S.; Gugliuzza, A.; Sessa, M.; Aceto, M. C.; Drioli, E.; Reverchon, E. *ACS Appl. Mater. Interfaces*, **2009**, *1*, 171–180.
[35] (a) Ulbricht, M.; Belfort, G. *J. Membr. Sci.* **1996**, *111*, 193–215. (b) Nabe, A.; Staude, E.; Belfort, G. *J. Membr. Sci.* **1997**, *133*, 57–72.
[36] Nagendran, A.; Vijayalakshmi, A.; Arockiasamy, D. L.; Shobana, K. H.; Mohan, D. *J. Hazardous Mater.* **2008**, *155*, 477–485.
[37] Vainrot, N.; Eisen, M. S.; Semiat, R. *MRS Bulletin* **2008**, *33*, 16–20.
[38] Strathmann, H.; Kock, K.; Amar, P.; Baker, R. W. *Desalination* **1975**, *16*, 179–203.
[39] Freger, V. *Langmuir* **2003**, *19*, 4791–4797.
[40] Lonsdale,H. K.; Merten, U.; Riley, R. L. *J. Appl. Polym. Sci.* **1965***, 9*, 1341–1362.
[41] (a) Cadotte, J. E.; Petersen, R. J.; Larson, R. E.; Erickson, E. E. *Desalination* **1980**, *32*, 25–31. (b) Jeong, B.-H.; Hoek, E. M. V.; Yan, Y.; Subramani, A.; Huang, X.; Huiwitz, G.; Ghosh, A. K.; Jawor, A. *J. Membr. Sci.* **2007**, *294*, 1–7.
[42] http://www.osmolabstore.com.
[43] http://www.dow.com/liquidseps.
[44] Cadotte, J.; Forester, R.; Kim, M.; Petersen, R.; Stocker, T. *Desalination* **1988***, 70*, 77–88.
[45] Zhou, M.; Nemade, P. R.; Lu, X.; Zeng, X.; Hatakeyama, E.; Noble, R. D.; Gin, D. L. *J. Am. Chem. Soc.* **2007**, *129*, 9574–9575.
[46] (a) Datta, A.; Ebert, K.; Plenio, H. *Organometallics* **2003**, *22*, 4685–4691. (b) Akthakul, A.; Hochbaum, A. I.; Stellacci, F.; Mayes, A. M. *Adv. Mater.* **2005**, *17*, 532–535. (c) de Pater, J. J. M.; Deelman, B.-J.; Elsevier, C. J.; van Koten, G. *Adv. Synth. Catal.* **2006**, *348*, 1447–1458.
[47] (a) Carrette, L.; Friedrich, K. A.; Stimming, U. *ChemPhysChem* **2000**, *1*, 162–193. (b) Neburchilov, V.; Martin, J.; Wang, H.; Zhang, J. *J. Power Sources* **2007**, *169*, 221–238.
[48] Wieser, C. *Fuel Cells* **2004**, *4*, 245–250.
[49] Wasmus, S.; Küver, A. *J. Electroanal. Chem.* **1999**, *461*, 14–31.
[50] Olah, G. A.; Goeppert, A.; Prakash, G. K. S. *Beyond Oil and Gas: The Methanol Economy*; Wiley-VCH, **2006**.
[51] Service, R. F. *Science* **2002**, *296*, 1222–1224.
[52] Garland, N. L.; Kopasz, J. P. *J. Power Sources* **2007**, *172*, 94–99.
[53] McNicol, B. D.; Rand, D. A. J.; Williams, K. R. *J. Power Sources* **2007**, *83*, 15–31.
[54] Hicker, M. A.; Pivovar, B. S. *Fuel Cells* **2005**, *5*, 213–229.

[55] Pivovar, B. S.;Wang, Y.; Cussler, E. L. *J. Membr. Sci.* **1999**, *154*, 155–162.
[56] Souzy, R.; Ameduri, B. *Prog. Polym. Sci.* **2005**, *30*, 644–687.
[57] Mauritz, K.; Moore, R. *Chem. Rev.* **2004**, *104*, 4535–4585.
[58] Hsu, W. Y.; Gierke, T. D. *Macromolecules* **1982**, *15*, 101–105.
[59] Rajendran, R. G. *MRS Bulletin* **2005**, *30*, 587–590.
[60] Zhou, Z.; Dominey, R. N.; Rolland, J. P.; Maynor, B. W.; Pandva, A. A.; DeSimone, J. M. *J. Am. Chem. Soc.* **2006**, *128*, 12963–12972.
[61] Deluca, N. W.; Elabd, Y. A. *J. Polym. Sci. B: Polym. Phys.* **2006**, *44*, 2201–2225.
[62] (a) Rikukawa, M.; Sanui, K. *Prog. Polym. Sci.* **2000**, *25*, 1463–1502. (b) Smitha, B.; Sridhar, S.; Khan, A. A. *J. Membr. Sci.* **2005**, *259*, 10–26.
[63] Park, H. B.; Lee, C. H.; Sohn, J. Y.; Lee, Y. M.; Freeman, B. D.; Kim, H. J. *J. Membr. Sci.* **2006**, *285*, 432 –443.
[64] Alberti, G.; Casciola, M. *Annu. Rev. Mater. Res.* **2003**, *33*, 129–154.
[65] Karlsson, L. E.; Wesslen, B.; Jannasch, P. *Electrochimica Acta* **2002**, *47*, 3269–3275.
[66] Shao, P.; Huang, R. Y. M. *J. Membr. Sci.* **2007**, *287*, 162–179.
[67] Semenova, S. I.; Ohya, H.; Soontarapa, K. *Desalination* **1997**, *110*, 251–286.
[68] Xu, Y. X.; Chen, C. X.; Li, J. D. *Chem. Eng. Sci.* **2007**, *62*, 2466–2473.
[69] Chiang, W.-Y.; Lin, Y.-H. *J. Appl. Polym. Sci.* **2002**, *86*, 2854–2859.
[70] Nam, S. Y.; Lee, Y. M. *J. Membr. Sci.* **1999**, *153*, 155–162.
[71] Cabasso, I.; Liu, Z.-Z. *J. Membr. Sci.* **1985**, *24*,101–119.
[72] Bennett, M.; Brisdon, B. J.; England, R.; Feld, R. W. *J. Membr. Sci.* **1997***, 137*, 63–88.
[73] Uragami, T. *Polym. J.* **2008**, *40*, 484–494.
[74] Tanihara, N.; Tanaka, K.; Kita, H.; Okamoto, K. *J. Membr. Sci.* **1994**, *95*, 161–169.
[75] Neel, J.; Aptel, P.; Clement, R. *Desalination* **1985**, *53*, 297–326.
[76] Koval, C.A.; Spontarelli, T.; Nobel, R.D. *Ind. Eng. Chem. Res.* **1989**, *28*, 1020–1024.
[77] Teraguchi, M.; Suzuki, J.; Kaneko, T.; Aoki, T.; Masuda, T. *Macromolecules* **2003**, *36*, 9694–9697.
[78] Baker, R. W. *Ind. Eng. Chem. Res.* **2002**, *41*, 1393–1411.
[79] Tokarev, I.; Minko, S. *Adv. Mater.* **2008**, *20*, 1–7
[80] Baker, R. W. *Membrane technology and applications,* 2nd Ed. John Wiley & Sons Ltd, West Sussex, England, **2004**.
[81] Smit, E.; Mulder, M. H. V.; Smolders, C. A.; Karrenbeld, H.; van Eerden, J.; Feil, D. *J. Membr. Sci.* **1992**, *73*, 247–257.
[82] (a) Robeson, L. *J. Membr. Sci.* **1991**, *62*, 165–185. (b) Robeson, L. M.; Borgoyne, W. F.; Langsam, M.; Savoca, A. C.; Tien, C. F. *Polymer* **1994**, *35*, 4970-4978.
[83] Freeman, B. D. *Macromolecules* **1999**, *32*, 375–380.
[84] Pinnau, I.; Toy, L. G. *J. Membr. Sci.* **1996**, *116*, 199–209.
[85] Cussler, E. L. In *Diffusion, mass transfer in fluid systems;* Cambridge University Press: New York, **1997**; pp 580.
[86] Huizenga, D. G.; Smith, D. M. *AICHE J.* **1986***, 32*, 1–6.
[87] Bird, R. B.; Stewart, W. E.; Lightfoot, E. N. *Transport phenomena*; Wiley: New York, **2002**; pp 895.

[88] Khandpur, A. K.; Forster, S.; Bates, F. S.; Hamley, I. W.; Ryan, A. J.; Bras, W.; Almdal, K.; Mortensen, K. *Macromolecules* **1996**, *28*, 8796–8806.
[89] Matsen, M. W.; Bates, F. S. *Macromolecules* **1996**, *29*, 1091–1098.
[90] Cochran, E. W.; Garcia-Cervera, C. J.; Fredrickson, G. H. *Macromolecules* **2006**, *39*, 2449–2451.
[91] Bates, F. S.; Fredrickson, G. H. *Physics Today* **1999**, 32–38.
[92] (a) Bates, F. S.; Maurer, W. W.; Lipic, P. M.; Hillmyer, M. A.; Almdal, K.; Mortensen, K.; Fredrickson, G. H.; Lodge, T. P. *Phys. Rev. Lett.* **1997**, *79*, 849–852. (b) Jeon, H. S.; Lee, J. H.; Balsara, N. P. *Phys. Rev. Lett.* **1997**, *79*, 3274–3277. (c) Thompson, R. B.; Matsen, M. W. *Phys. Rev. Lett.* **2000**, *85*, 670–673.
[93] Bates, F. S.; Fredrickson, G. H. *J. Polym. Sci. B: Polym. Phys.* **1997**, *35*, 2775–2786.
[94] Lodge, T. P.; Pudil, B.; Hanley, K. J. *Macromolecules* **2002**, *35*, 4707–4717.
[95] Lai, C.; Russel, W. B.; Register, R. A. *Macromolecules* **2002**, *35*, 841–849.
[96] Hadjichristidis, N.; Pitsikalis, M.; Pispas, S.; Iatrou, H. *Chem. Rev.* **2001**, *101*, 3747–3792.
[97] Braunecker, W. A.; Matyjaszewski, K. *Prog. Polym. Sci.* **2007**, *32*, 93–146
[98] Moad, G.; Rizzardo, E.; Thang, S. H. *Polymer* **2008**, *49*, 1079–1131.
[99] Hawker, C. J.; Bosman, A .W.; Harth, E. *Chem. Rev.* **2001**, *101*, 3661–3688.
[100] Dechy-Cabaret, O.; Martin-Vaca, B.; Bourissou, D. *Chem. Rev.* **2004**, *104*, 6147–6176.
[101] Bielawski, C. W.; Grubbs, R. H. *Prog. Polym. Sci.* **2007**, *32*, 1–29.
[102] Discher, B.M.; Won, Y.-Y.; Ege, D.S.; Lee, J. C.-M.; Discher, D.E.; Hammer, D.A. *Science* **1999**, *284*, 1143–1146.
[103] Warren, S. C.; Messina, L. C.; Slaughter, L. S.; Kamperman, M.; Zhou, Q.; Gruner, S. M.; DiSalvo, F. J.; Wiesner, U. *Science* **2008**, *320*, 1748–1752.
[104] Ruzette, A.-V.; Leibler, L. *Nature Mater.* **2005**, *4*, 19–31.
[105] (a) Hamley, I. W. *The Physics of Block Copolymers*; Oxford University Press: Oxford, **1998**. (b) Hadjichristidis, N.; Pispas, S.; Floudas, G. A. *Block Copolymers: Synthetic Strategies, Physical Properties, and Applications*; Wiley-Interscience: New York, **2003**. (c) *Developments in block copolymer science and technology*, Hamley, I. W. Ed.; John Wiley & Sons Ltd, West Sussex, England; **2004**. (d) *Block copolymer in nanoscience*, Lazzari, M.; Liu, G.; Lecommandoux, S. Eds.; WILEY-VCH Verlag GmbH & Co. KGaA, Weinheim; **2006**.
[106] (a) Lodge, T. P. *Macromol. Chem. Phys.* **2003**, *204*, 265–273. (b) Hamley, I. W. *Angew. Chem. Int. Ed.* **2003**, *42*, 1692–1712. (b) Park, C.; Yoon, J.; Thomas, E. L. Polymer **2003**, *44*, 6725–6760. (d) Hillmyer, M. A. *Adv. Polym. Sci.* **2005**, *190*, 137–181. (e) Olson, D. A.; Chen, L.; Hillmyer, M. A. *Chem. Mater.* **2008**, *20*, 869–890.
[107] (a) Zalusky, A. S.; Olayo-Valles, R.; Taylor, C. J.; Hillmyer, M. A. *J. Am. Chem. Soc.* **2001**, *123*, 1519–1520. (b) Zalusky, A. S.; Olayo-Valles, R.; Wolf, J. H.; Hillmyer, M. A. *J. Am. Chem. Soc.* **2002**, *124*, 12761–12773.
[108] (a) Rzayev, J.; Hillmyer, M. A. *J. Am. Chem. Soc.* **2005**, *127*, 13373–13379. (b) Mao, H.; Arrechea, P. L.; Bailey, T. S.; Johnson, B. J. S.; Hillmyer, M. A. *Faraday Discuss.* **2005**, *128*, 149–162. (c) Bailey, T. S.; Rzayev, J.; Hillmyer, M. A. *Macromolecules* **2006**, *39*, 8772–8781.
[109] (a) Kim, S. H.; Misner, M. J.; Xu, T.; Kimura, M.; Russell, T. P. *Adv. Mater.* **2004**, *16*, 226–231. (b) Ryu, D. Y.; Shin, K.; Drockenmuller, E.; Hawker, C. J.; Russell, T. P. *Science* **2005**, *308*, 236–239. (c) Bang, J.;

Kim, S. H.; Drockenmuller, E.; Misner, M. J.; Russell, T. P.; Hawker, C. J. *J. Am. Chem. Soc.* **2006**, *128*, 7622–7629. (d) Tang, C.; Lennon, E. M.; Fredrickson, G. H.; Kramer, E. J.; Hawker, C. J. *Science* **2008**, *322*, 429–432.

110 Hawker, C. J.; Russell, T. P. *MRS Bull.* **2005**, *30*, 952–966.

111 Thurn-Albrecht, T.; Schotter, J.; Kastle, G. A.; Emley, N.; Shibauchi, T.; Krusin-Elbaum, L.; Guarini, K.; Black, C. T.; Tuominen, M. T.; Russell, T. P. *Science* **2000**, *290*, 2126–2129.

112 (a) Yang, S. Y.; Ryu, I.; Kim, H. Y.; Kim, J. K.; Jang, S. K.; Russell, T. P. *Adv. Mater.* **2006**, *18*, 709–712. (b) Phillip, W. A.; Rzayev, J.; Hillmyer, M. A.; Cussler, E. L. *J. Membr. Sci.* **2006**, *286*, 144–152.

113 (a) Walheim, S.; Schaffer, E.; Mlynek, J.; Steiner, U. *Science* **1999**, *283*, 520–522. (b) Joo, W.; Park, M. S.; Kim, J. K. *Langmuir* **2006**, *22*, 7960–7963.

114 Uehara, H.; Yoshida, T.; Kakiage, M.; Yamanobe, T.; Komoto, T.; Nomura,K.; Nakajima, K.; Matsuda, M. *Macromolecules* **2006**, *39*, 3971–3974.

115 Uehara, H.; Kakiage, M.; Sekiya, M.; Sakuma, D.; Yamonobe, T.; Takano, N.; Barraud, A.; Meurville, E.; Ryser, P. *ACS Nano* **2009**, *3*, 924–932.

116 Yang, S. Y.; Park, J.; Yoon, J.; Ree, M.; Jang, S. K.; Kim, J. K. *Adv. Funct. Mater.* **2008**, *18*, 1371–1377.

117 Cooney, D. T.; Hillmyer, M. A.; Cussler, E. L.; Moggridge, G. D. *Crystallogr. Rev.* **2006**, *12*, 13–24.

118 Peinemann, K.-V.; Abetz, V.; Simon, P. F. W. *Nature Mater.* **2007**, *6*, 992–996.

119 Yang, Y.; Holdcroft, S. *Fuel Cells* **2005**, *2*, 171–186.

120 Ding, J.; Chuy, C.; Holdcroft, S. *Chem. Mater.* **2001**, *13*, 2231–2233.

121 Ding, J.; Chuy, C.; Holdcroft, S. *Macromolecules* **2002**, *35*, 1348–1355.

122 Ding, J.; Chuy, C.; Holdcroft, S. *Adv. Func. Mater.* **2002**, *12*, 389–394.

123 Shi, Z.; Holdcroft, S. *Macromolecules* **2005**, *38*, 4193–4201.

124 Tsang, E. M. W.; Zhang, Z.; Shi, Z.; Soboleva, T.; Holdcroft, S. *J. Am. Chem. Soc.* **2007**, *129*, 15106–15107.

125 Zhang, Z.; Chalkova, E.; Fedkin, M.; Wang, C.; Lvov, S. N.; Komarneni, S.; Chung, T. C. M. *Macromolecules* **2008**, *41*, 9130-9139.

126 Norsten, T. B.; Guiver, M. D.; Murphy, J.; Astill, T.; Navessin, T.; Holdcroft, S.; Frankamp, B. L.; Rotello, V. M.; Ding, J. *Adv. Funct. Mater.* **2006**, *16*, 1814–1822.

127 Nieh, M.-P.; Guiver, M. D.; Kim, D. S.; Ding, J.; Norsten, T. *Macromolecules* **2008**, *41*, 6176–6182.

128 Kim, J.; Kim, B.; Jung, B. *J. Membr. Sci.* **2002**, *207*, 129–137.

129 Elabd, Y. A.; Napadensky, E.; Walker, C. W.; Winey, K. I. *Macromolecules* **2006**, *39*, 399–407.

130 Serpico, J. M.; Ehrenberg, S. G.; Fontanella, J. J.; Jiao, X.; Perahia, D.; McGrady, K. A.; Sanders, E. H.; Kellogg, G. E.; Wnek, G. E. *Macromolecules* **2002**, *35*, 5916–5921.

131 Park, M. J.; Balsara, N. P. *Macromolecules* **2008**, *41*, 3678–3687.

132 Park, M. J.; Nedoma, A. J.; Geissler, P. L.; Balsara, N. P.; Jackson, A.; Cookson, D. *Macromolecules* **2008**, *41*, 2271–2277.

133 Park, M. J.; Downing, K. H.; Jackson, A.; Gomez, E. D.; Minor, A. M.; Cookson, D.; Weber, A. Z.; Balsara, N. P. *Nano Lett.* **2007**, *7*, 3547–3552.

134 (a) Bullock, S. E.; Kofinas, P. K. *J. Power Sources* **2004**, *132*, 256–260. (b) Bullock, S. E.; Kofinas, P. *Macromolecules* **2004**, *37*, 1783–1786. (c) Xue, C.; Meador, M. A. B.; Zhu, L.; Ge, J. J.; Cheng, S. Z. D.;

Putthanarat, S.; Eby, R. K.; Khalfan, A.; Bennett, G. D.; Greenbaum, S. G. *Polymer* **2006**, *47*, 6149–6155. (d) Olivetti, E. A.; Kim, J. H.; Sadoway, D. R.; Asatekin, A.; Mayes, A. M. *Chem. Mater.*, **2006**, *18*, 2828–2833

135 (a) Miyata, T.; Obata, S.; Uragami, T. *Macromolecules* **1999**, *32*, 8465–8475. (b) Dutta, B. K.; Sikdar, S. K. *Environ. Sci. Technol.*, **1999**, *33*, 1709–1716. (c) Arnold, M. E.; Nagai, K.; Spontak, R. J.; Freeman, B. D.; DeSimone, J. M. *et al. Macromolecules* **2002**, *35*, 3697–3707. (d) Ray, S.; Ray, S. K. *J. Membr. Sci.* **2006**, *270*, 73–87. (e) Zhao, Q.; Qian, J.; An, Q.; Zhu, Z.; Zhang, P.; Bai, Y. *J. Membr. Sci.* **2008**, *311*, 284–293. (f) Koh, J. H.; Kim, Y. W.; Park, J. T.; Min, B. R.; Kim, J. H. *Polym. Adv. Technol.* **2008**, *19*, 1643–1648.

136 (a) Kim, J. H.; Ha, S. Y.; Lee, Y. M. *J. Membr. Sci.* **2001**, *190*, 179–193. (b) Zhao, H.-Y.; Cao, Y-M.; Ding, X.-L.; Zhou, M.-Q.; Yuan, Q. *J. Membr. Sci.* **2008**, *310*, 365–373. (c) Car, A.; Stropnik, C.; Yave, W.; Peinemann, K.-V. *Adv. Funct. Mater.* **2008**, *18*, 2815–2823

137 (a) Ying, L.; Wang, P.; Kang, E. T.; Neoh, K. G. *Macromolecules* **2002**, *35*, 673–679. (b) Nyknen, A.; Nuopponen, M.; Ruokolainen, J. *et al. Macromolecules* **2007**, *40*, 5827–5834. (c) Wang, W.; Chen, L. *J. Appl. Polym. Sci.* **2007**, *104*, 1482–1486. (d) Xue, J.; Chen, L.; Wang, H. L.; Zhang, Z. B., Zhu, X. L. Kang, E. T.; Neoh, K. G. *Langmuir* **2008**, *24*, 14151–14158.

138 Nobelprize.org. http://nobelprize.org/chemistry/laureates/2005/index.html.

139 (a) Murdzek, J. S.; Schrock, R. R. *Organometallics* **1987**, *6*, 1373–1374. (b) Schrock, R. R.; Murdzek, J. S.; Bazan, G. C.; Robbins, J.; DiMare, M.; O'Regan, M. *J. Am. Chem. Soc.* **1990**, *112*, 3875–3886.

140 (a) Schwab, P.; France, M. B.; Ziller, J. W.; Grubbs, R. H. *Angew. Chem., Int. Ed. Engl.* **1995**, *34*, 2039–2041. (b) Scholl, M.; Ding, S.; Lee, C. W. Grubbs, R. H. *Org. Lett.* **1999**, *1*, 953–956.

141 *Handbook of Metathesis*; Grubbs, R. H., Ed.: Wiley-VCH: Weinheim, **2003**; Vol. 1.

142 *Handbook of Metathesis*; Grubbs, R. H., Ed.: Wiley-VCH: Weinheim, **2003**; Vol. 3.

143 (a) Davidson, T. A.; Wagener, K. B.; Priddy, D. B. *Macromolecules* **1996,** *29,* 786–788. (b) Rule, J. D.; Moore, J. S. *Macromolecules* **2002**, *35*, 7878–7882.

144 White, S. R.; Sottos, N. R.; Geubelle, P. H.; Moore, J. S.; Kessler, M. R.; Sriram, S. R.; Brown, E. N.; Viswanathan, S. *Nature* **2001**, *409*, 794–797

145 Kelsey, D. R.; Chuan, H. H.; Ellison, R. H. *J. Polym. Sci. A: Polym. Chem.* **1997**, *35*, 3049–3063.

146 Jeong, W.; Kessler, M. R. *Chem. Mater.* **2008**, *20*, 7060–7068.

147 (a) Sinner, F.; Buchmeiser, M. R. *Macromolecules* **2000,** *33,* 5777–5786. (b) Martina, A. D.; Hilborn, J. G. *J. Mater. Res.* **2001**, *16*, 2045–2052.

148 Bandari, R.; Prager-Duschke, A.; Kuhnel, C.; Decker, U.; Schlemmer, B.; Buchmeiser, M. R. *Macromolecules* **2006**, *39*, 5222–5229.

149 Liu, C.; Chun, S. B.; Mather, P. T. *Macromolecules* **2002**, *35*, 9868–9874.

150 (a) Bielawski, C. W.; Morita, T.; Grubbs, R. H. *Macromolecules* **2000**, *33*, 678–680. (b) Mahanthappa, M. K.; Bates, F. S.; Hillmyer, M. A. *Macromolecules* **2005**, *38*, 7890–7894.

Chapter 2

1 Lee, J. S.; Hirao, A.; Nakahama, S. *Macromolecules* **1988**, *21*, 274–276.

[2] (a) Zalusky, A. S.; Olayo-Valles, R.; Taylor, C. J.; Hillmyer, M. A. *J. Am. Chem. Soc.* **2001**, *123*, 1519–1520. (b) Mao, H.; Hillmyer, M. A. *Macromolecules* **2005**, *38*, 4038–4039.

[3] Jeong, U.; Kim, H.-C.; Rodriguez, R. L.; Tsai, I. Y.; Stafford, C. M.; Kim, J. K.; Hawker, C. J.; Russell, T. P. *Adv. Mater*. **2002**, *14*, 274–276.

[4] (a) Thurn-Albrecht, T.; Schotter, J.; Kastle, G. A.; Emley, N.; Shibauchi, T.; Krusin-Elbaum, L.; Guarini, K.; Black, C. T.; Tuominen, M. T.; Russell, T. P. *Science* **2000**, *290*, 2126–2129. (b) Johnson, B. J. S.; Wolf, J. H.; Zalusky, A. S.; Hillmyer, M. A. *Chem. Mater*. **2004**, *16*, 2909–2917. (c) Tseng, W.-H.; Chen, C.-K.; Chiang, Y.-W.; Ho, R.-M.; Akasaka, S.; Hasegawa, H. *J. Am. Chem. Soc.* **2009**, *131*, 1356–1357. (d) Zschech, D.; Kim, D. H.; Milenin, A. P.; Scholz, R.; Hillebrand, R.; Hawker, C. J.; Russell, T. P.; Steinhart, M.; Gosele, U. *Nano Lett.* **2007**, *7*, 1516−1520. (e) Crossland, E. J. W.; Ludwigs, S.; Hillmyer, M. A.;Steiner, U. *Soft Matter* **2007**, *3*, 94–98.

[5] (a) Yang, S. Y.; Ryu, I.; Kim, H. Y.; Kim, J. K.; Jang, S. K.; Russell, T. P. *Adv. Mater.* **2006**, *18*, 709–712. (b) Phillip, W. A.; Rzayev, J.; Hillmyer, M. A.; Cussler, E. L. *J. Membrane Sci.* **2006**, *286*, 144–152. (c) Yang, S. Y.; Park, J.; Yoon, J.; Ree, M.; Jang, S. K.; Kim, J. K. *Adv. Funct. Mater.* **2008**, *18*, 1371–1377.

[6] (a) Walheim, S.; Schaffer, E.; Mlynek, J.; Steiner, U. *Science* **1999**, *283*, 520–522. (b) Joo, W.; Park, M. S.; Kim, J. K. *Langmuir* **2006**, *22*, 7960–7963.

[7] Wolf, J. H.; Hillmyer, M. A. *Langmuir* **2003**, *19*, 6553–6560.

[8] Zalusky, A. S.; Olayo-Valles, R.; Wolf, J. H.; Hillmyer, M. A. *J. Am. Chem. Soc.* **2002**, *124*, 12761–12773.

[9] (a) Drockenmuller, E.; Li, L. Y. T.; Ryu, D. Y.; Harth, E.; Russell, T. P.; Kim, H-C.; Hawker, C. J. *J. Polym. Sci. A: Polym. Chem.* **2005**, *43*, 1028–1037. (b) Leiston-Belanger, J. M.; Russell, T. P. Drockenmuller, E.; Hawker, C. J. *Macromolecules* **2005**, *38*, 7676–7683.

[10] Cavicchi, K. A.; Zalusky, A. S.; Hillmyer, M. A.; Lodge, T. P. *Macromol. Rapid Commun.* **2004**, *25*, 704–709.

[11] Guo, F.; Andreasen, J. W.; Vigild, M. E.; Ndoni, S. *Macromolecules* **2007**, *40*, 3669–3675.

[12] Zhou, N.; Bates, F. S.; Lodge, T. P. *Nano. Lett.* **2006**, *6*, 2354–2357.

[13] Uehara, H.; Yoshida, T.; Kakiage, M.; Yamanobe, T.; Komoto, T.; Nomura, K.; Nakajima, K.; Matsuda, M. *Macromolecules* **2006**, *39*, 3971–3974.

[14] Jones, B. H.; Lodge, T. P. *J. Am. Chem. Soc.* **2009**, *131*, 1676–1677.

[15] Bluemle, M. J.; Fleury, G.; Lodge, T. P.; Hillmyer, M. A.; Bates, F. S. *Soft Matter* **2009**, *5*, 1587–1590.

[16] Bluemle, M. J. *et al.* unpublished results.

[17] (a) Hillmyer, M. A.; Lipic, P. M.; Hajduk, D. A.; Almdal, K.; Bates, F. S. *J. Am. Chem. Soc*. **1997**, *119*, 2749–2750. (b) Grubbs, R. B.; Dean, J. M.; Broz, M. E.; Bates, F. S. *Macromolecules* **2000**, *33*, 9522–9534.

[18] Carter, K. R.; DiPietro, R. A.; Sanchez, M. I.; Russell, T. P.; Lakshmanan, P. McGrath, J. E. *Chem. Mater.* **1997**, *9*, 105−118.

[19] Trimmer, M. S. In *Handbook of Metathesis*; Grubbs, R. H., Ed.: Wiley-VCH: Weinheim, **2003**; Vol. 3, 407− 418.

[20] Pangborn, A. B.; Giardello, A.; Grubbs, R. H.; Rosen, R. K.; Timmers, F. J. *Organometallics* **1996**, *15*, 1518–1520.

[21] Roe, R. J. *Methods of X-ray and Neutron Scattering in Polymer Science, Topics in Polymer Science*; Oxford University Press: New York, **2000**.

[22] deGennes, P. G.; Prost, J. *The Physics of Liquid Crystals*; Oxford University Press: New York, **1993**.

[23] Mao, H. Ph.D. thesis "Nanoporous Polymers with Functionalized 1D and 3D Channels from Ordered Block Copolymer Templates", University of Minnesota, **2006**, Chapter 2.
[24] Gregg, S. J.; Sing, K. S. W. *Adsorption, Surface Area and Porosity*; Academic Press: London, **1982**.
[25] Brunauer, S.; Emmett, P. H.; Teller, E. *J. Am. Chem. Soc.* **1938**, *60*, 309–319.
[26] Barrett, E. P.; Joyner, L. G.; Halenda, P. P. *J. Am. Chem. Soc.* **1951**, *73*, 373–380.
[27] Wang, Y.; Hillmyer, M. A. *Macromolecules* **2000**, *33*, 7395–7403.
[28] Bennett, M. A.; Smith, A. K. *J. Chem. Soc., Dalton Trans.***1974**, 233–241.
[29] Lai, J. T.; Filla, D.; Shea, R. *Macromolecules* **2002**, *35*, 6754–6756.
[30] Rzayev, J.; Hillmyer, M. A. *Macromolecules* **2005**, *38*, 3–5.
[31] Willy, W. E.; McKean, D. R.; Garcia, B. A. *Bull. Chem. Soc. Jpn.* **1976**, *49*, 1989–1995.
[32] Dolman, S. J.; Hultzsch, K. C.; Pezet, F.; Teng, X.; Hoveyda, A. H.; Schrock, R. R. J. *Am. Chem. Soc.* **2004**, *126*, 10945–10953.
[33] Kelsey, D. R.; Chuan, H. H.; Ellison, R. H. *J. Polym. Science A: Polym. Chem.* **1997**, *35*, 3049–3063.
[34] Stille, J. K.; Frey, D. A. *J. Am. Chem. Soc.* **1959**, *81*, 4273-4275.
[35] Stubbs, L. P.; Weck, M. *Chem. Eur. J.* **2003**, *9*, 992–999.
[36] (a) Lai, C.; Russel, W. B.; Register, R. A. *Macromolecules* **2002**, *35*, 841–849. (b) Ding, J.; Carver, T. J.; Windle, A. H. *Comp. Theo. Polym. Sci.* **2001**, *11*, 483–490.
[37] Lodge, T. P.; Pudil, B.; Hanley, K. J. *Macromolecules* **2002**, *35*, 4707–4717.
[38] Fetters, L. J.; Lohse, D. J.; Richter, D.; Witten, T. A.; Zirkel, A. *Macromolecules* **1994**, *27*, 4639–4647.
[39] Witzke, D. R.; Narayan, R.; Kolstad, J. J. *Macromolecules* **1997**, *30*, 7075–7085.
[40] Du, Y.; Xue, Y.; Frisch, H. L. in *Physical Properties of Polymers Handbook*; Mark, J. E. *Ed*; AIP Press, **1996**, Chapter 16, Page 232.
[41] Lodge, T. P.; Hanley, K. J.; Pudil, B.; Alahapperuma, V. *Macromolecules* **2003**, *36,* 816–822.
[42] Davidson, T. A.; Wagener, K. B.; Priddy, D. B. *Macromolecules* **1996**, *29*, 786–788.
[43] Hafner, A.; Mühlebach, A.; van der Schaaf, P. A. *Angew. Chem. Int. Ed. Engl.* **1997**, *36*, 2121–2124.
[44] Runge M. B.; Dutta, S.; Bowden, N. B. *Macromolecules* **2006**, *39*, 498–508.
[45] Patton, D. L.; Advincula, R. C. *Macromolecules* **2006**, *39*, 8674–8683.
[46] Cheng, C.; Yang, N.-L. *Macromol. Rapid Commun.* **2005**, *26*, 1395–1399.
[47] Detrembleur, C.; Jérôme, C.; Claes. M.; Louette, P.; Jérôme, R. *Angew. Chem. Int. Ed.* **2001**, *113*, 1308–1311.
[48] (a) Hirao, A.; Loykulnant, S.; Ishizone, T. *Prog. Polym. Sci.* **2002**, *27*, 1399–1471. (b) Hawker, C. J.; Bosman, A. W.; Harth, E. *Chem. Rev.* **2001**, *101*, 3661–3688. Matyjaszewski, K. *Current Org. Chem.* **2002**, *6*, 67–82. (c) Le, T. P.; Moad, G.; Rizzardo, E.; Thang, S. H. PCT Int. Appl. WO 9801478 A1 980115.
[49] (a) Robello, D. R.; Levy, D. H.; Reynolds, J. H.; Southby, D. T.; Twist, S. L. *Macromolecules* **2006**, *39*, 5686–5695. (b) Yamada, S.; Mrozek, T.; Rager, T.; Owens, J.; Rangel, J.; Willson, C. G. M*acromolecules* **2004**, *37*, 377–384. (c) Wang, S.; Li, X.; Xun, S.; Wan, X.; Wang, Z. Y. *Macromolecules* **2006**, *39*, 7502–7507. (d) Mitsukami, Y.; Donovan, M. S.; Lowe, A. B.; McCormick, C. L. *Macromolecules* **2001**, *34*, 2248–2256. (e) Gortz, V.; Ritter, H. *Macromolecules* **2002**, *35*, 4258–4265. (f) Hashimoto, K.; Ohsawa, R.; Imai, N.; Okada, M. *J. Polym. Sci. A: Polym. Chem.* **1999**, *37*, 303–312.
[50] (a) Zhang, H.; Ruckenstein, E. *Macromolecules* **1999**, *32*, 5495–5500. (b) O'Reilly, R. K.; Joralemon,

M. J.; Hawker, C. J.; Wooley, K. L. *Chem. Eur. J.* **2006**, *12*, 6776–6786. (c) Trakhtenberg, S.; Warner, J. C.; Nagarajan, R.; Bruno, F. F.; Samuelson, L. A.; Kumar, J. *Chem. Mater.* **2006**, *18*, 2873–2878.

51 Mirviss, S. B. *J. Org. Chem.* **1989**, *54*, 1948–1951.

52 Hillmyer, M. A.; Bates, F. S. *Macromolecules* **1996**, *29*, 6994–7002.

53 Buckley, D. A.; Augostini, P. P. *J. Appl. Polym. Sci.* **1979**, *23*, 311–314.

54 (a) Leibler, L. *Macromolecules* **1980**, *13*, 1602–1617. (b) Matsen, M. W., Bates, F. S. *J. Chem. Phys.* **1997**, *106*, 2436–2448.

55 Ren, Y.; Lodge, T. P.; Hillmyer, M .A. *Macromolecules* **2002**, *35*, 3889–3894.

56 Couchman, P. R. *Macromolecules* **1978**, *11*, 1156–1161.

57 Sanford, M. S.; Love, J. A.; Grubbs, R. H. *J. Am. Chem. Soc.* **2001**, *123*, 6543–6554.

58 Muralidharan, V.; Hui, C.-Y. *Macromol. Rapid Commun*. **2004**, *25*, 1487–1490.

59 Keitz, B. K.; Grubbs, R. H. *J. Am. Chem. Soc.* **2009***, 131*, 2038–2039.

Chapter 3

1 Strathmann, H.; Kock, K. *Desalination* **1977**, *21*, 241–255.

2 (a) Peinemann, K.-V.; Abetz, V.; Simon, P. F. W. *Nature Mater.* **2007**, *6*, 992–996. (b) Xue, J.; Chen, L.; Wang, H. L.; Zhang, Z. B., Zhu, X. L. Kang, E. T.; Neoh, K. G. *Langmuir*, **2008**, *24*, 14151–14158.

3 Olson, D. A.; Chen, L.; Hillmyer, M. A. *Chem. Mater.***2008**, *20*, 869–890.

4 Bates, F. S.; Fredrickson, G. H. *Physics Today* **1999**, 32–38. Ruzette, A.-V.; Leibler, L. *Nature Materials* **2005**, *4*, 10-31. Bates, F. S. *MRS Bulletin* **2005**, *30*, 525–532**.**

5 Mao, H.; Hillmyer, M. A. *Soft Matter* **2006**, *2*, 57–59.

6 Crossland, E. J. W.; Kamperman, M.; Nedelcu, M.; Ducati, C.; Wiesner, U.; Smilgies, D.-M.; Toombes, G. E. S.; Hillmyer, M. A.; Ludwigs, S.; Steiner, U.; Snaith, H. J. *Nano Lett.* **2009**, in press.

7 Chan, V. Z.-H.; Hoffman, J.; Lee, V. Y.; Iatrou, H.; Avgeropoulos, A.; Hadjichristidis, N.; Miller, R. D.; Thomas, E. L. *Science* **1999**, *286*, 1716–1719.

8 Matsen, M. W. *Macromolecules* **1995**, *28*, 5765–5773.

9 (a) Sun, P.; Yin, Y.; Li, B.; Chen, T.; Jin, Q.; Ding, D.; Shi, A.-C. *Phys. Rev. E* **2005**, *72*, 061408. (b) Lammertink, R. G. H.; Hempenius, M. A.; Thomas, E.; Vancso, G. J. *J. Polym. Sci. B: Polym. Phys.* **1999**, *37*, 1009–1021.

10 (a) Okumura, A.; Nishikawa, Y.; Hashimoto, T. *Polymer* **2006**, *47*, 7805–7812. (b) Hashimoto, T.; Nishikawa, Y.; Tsutsumi, K. *Macromolecules* **2007**, *40*, 1066–1072.

11 (a) Scriven, L. E. *Nature* **1976**, *263*, 123–125. (b) Kaler, E. W.; Davis, H. T.; Scriven, L. E. *J. Chem. Phys.* **1983**, *79*, 5685-5692. (c) Langevin, D. *Acc. Chem. Res.* **1988**, *21*, 255–260.

12 Zhou, N.; Lodge, T. P.; Bates, F. S. *J. Phys. Chem. B* **2006**, *110*, 3979–3989.

13 Ruegg, M. L.; Reynolds, B. J.; Lin, M. Y.; Lohse, D. J.; Balsara, N. P. *Macromolecules* **2006,** *39,*1125–1134.

14 Hillmyer, M. A.; Maurer, W. W.; Lodge, T. P.; Bates, F. S.; Almdal, K. *J. Phys. Chem. B* **1999**, *103*, 4814–4824.

15 Zhou, N.; Bates, F. S.; Lodge, T. P. *Nano. Lett.* **2006**, *6*, 2354–2357.

16 Jones, B. H.; Lodge, T. P. *J. Am. Chem. Soc.* **2009**, *131*, 1676–1677.
17 Almdal, K.; Koppi, K. A.; Bates, F. S.; Mortensen. K. *Macromolecules* **1992**, *25*, 1743–1751.
18 Takenaka, M.; Wakada, T.; Akasaka, S.; Nishitsuji, S.; Saijo, K.; Shimizu, H.; Kim, M. I.; Hasegawa, H. *Macromolecules* **2007**, *40*, 4399–4402.
19 Uehara, H.; Yoshida, T.; Kakiage, M.; Yamanobe, T.; Komoto, T.; Nomura, K.; Nakajima, K.; Matsuda, M. *Macromolecules* **2006**, *39*, 3971–3974.
20 Qi, S., Chakraborty, A. K.; Balsara, N. P. *J. Chem. Phys.* **2001**, *115*, 3387–3400.
21 Pernot, H.; Baumert, M.; Court, F.; Leibler, L. *Nature Mater.* **2002***, 1*, 54–58.
22 Ryan, A. J. *Nature Mater.* **2002**, *1*, 8–10.
23 (a) Martina, A. D.; Hilborn, J. G.; Mühlebach, A. *Macromolecules* **2000**, *33*, 2916–2921. (b) Lee, J. K.; Gould, G. L. *J. Sol-Gel Sci. Technol.* **2007**, *44*, 29–40.
24 Inoue, T. *Prog. Polym. Sci.* **1995**, *20*, 119–153.
25 Kiefer, J.; Hedrick, J. L.; Hilborn, J. G. *Adv. Polym. Sci.* **1999**, *147*, 161–247.
26 Pan, C.; Maurer, W.; Liu, Z.; Lodge, T. P.; Stepanek, P.; von Meerwall, E. D.; Watanabe, H. *Macromolecules* **1995**, *28*, 1643–1653.
27 Rzayev, J.; Hillmyer, M. A. *Macromolecules* **2005**, *38*, 3–5.
28 Hillmyer, M. A.; Laredo, W. R.; Grubbs, R. H. *Macromolecules* **1995**, *28*, 6311–6316.
29 Kelsey, D. R.; Chuan, H. H.; Ellison, R. H. *J. Polym. Sci. A: Polym. Chem.* **1997**, *35*, 3049–3063.
30 Bielawski, C. W.; Scherman, O. S.; Grubbs, R. H. *Polymer* **2001**, *11*, 4939 – 4945.
31 Zalusky, A. S.; Olayo-Valles, R.; Wolf, J. H.; Hillmyer, M. A. *J. Am. Chem. Soc.* **2002**, *124*, 12761–12773.
32 Meuler, A. J.; Mahanthappa, M. K.; Hillmyer, M. A.; Bates, F. S. *Macromolecules* **2007**, *40*, 760–762.
33 Fetters, L. J.; Lohse, D. J.; Richter, D.; Witten, T. A.; Zirkel, A. *Macromolecules* **1994**, *27*, 4639–4647.
34 Witzke, D. R.; Narayan, R.; Kolstad, J. J. *Macromolecules* **1997**, *30*, 7075–7085.
35 Dinger, M. B.; Mol, J. C. *Organometallics* **2003**, *22,* 1089–1095.
36 Gregg, S. J.; Sing, K. S. W. *Adsorption, Surface Area and Porosity*; Academic Press: London, **1982**.
37 He, Y.; Lodge, T. P. *Chem. Comm.* **2007**, 2732–2734.
38 He, Y.; Boswell, P. G.; Bühlmann, P.; Lodge, T. P. *J. Phys. Chem. B* **2007**, *111*, 4645–4652.
39 Barrett, E. P.; Joyner, L. G.; Halenda, P. P. *J. Am. Chem. Soc.* **1951**, *73*, 373–380.
40 Guo, S.; Rzayev, J.; Bailey, T. S.; Zalusky, A. S.; Olayo-Valles, R.; Hillmyer, M. A. *Chem. Mater.* **2006**, *18*, 1719–1721.
41 Chen, L.; Phillip, W. A.; Cussler, E. L.; Hillmyer, M. A. *J. Am. Chem. Soc.* **2007**, *129*, 13786–13787.
42 Cussler, E. L. In *Diffusion, mass transfer in fluid systems;* Cambridge University Press: New York, **1997**; page 580.
43 Phillip, W. A.; Amendt, M. A.; O'Neil, B.; Chen, L.; Hillmyer, M. A.; Cussler, E. L. *ACS Appl. Materials & Interfaces* **2009**, *1*, 472–480.
44 ASTM International Standard Test Method for Molecular Weight Cutoff Evaluation of Flat Sheet Ultrafiltration Membranes; **2001**; ASTME 1343–1390.
45 Bailey, T. S.; Rzayev, J.; Hillmyer, M. A. *Macromolecules* **2006**, *39*, 8772–8781.
46 Ishii, Y.; Ryan, A. J. *Macromolecules* **2000**, *33,* 158–166.

47 (a) Ide, N.; Fukuda, T. *Macromolecules* **1999**, *32,* 95–99. (b) Kanamori, K.; Hasegawa, J.; Nakanishi, K.; Hanada, T. *Macromolecules* **2008**, *41*, 7186–7193.
48 Tseng, W.-H.; Chen, C.-K.; Chiang, Y.-W.; Ho, R.-M.; Akasaka, S.; Hasegawa, H. *J. Am. Chem. Soc.* **2009**, *131*, 1356–1357.
49 Roerdink, M. *et al.* unpublished results.

Chapter 4

1 Hickner, M. A.; Ghassemi, H.; Kim, Y. S.; Einsla, B. R.; McGrath, J. E. *Chem. Rev.* **2004**, *104*, 4587–4612.
2 Mauritz, K.; Moore, R. *Chem. Rev.* **2004**, *104*, 4535–4585.
3 Ravikumar, M. K.; Shukla, A. K. *J. Electrochem. Soc.* **1996**, *143*, 2601–2606.
4 Karlsson, L. E.; Wesslen, B.; Jannasch, P. *Electrochimica Acta* **2002**, *47*, 3269–3275.
5 (a) Rikukawa, M.; Sanui, K. *Prog. Polym. Sci.* **2000**, *25*, 1463–1502. (b) Kreuer, K. D. *J. Membr. Sci.* **2001**, *185*, 29–39. (c) Li, Q.; He, R.; Jensen, J. O.; Bjerrum, N. J. *Chem. Mater.* **2003**, *15*, 4896–4915. (d) Hicker, M. A.; Pivovar, B. S. *Fuel Cells* **2005**, *5*, 213–229. (e) Souzv, R.; Ameduri, B. *Prog. Polym. Sci.* **2005**, *30*, 644–687. (f) Deluca, N. W.; Elabd, Y. A. *J. Polym. Sci. B: Polym. Phys.* **2006**, *44*, 2201–2225. (g) Neburchilov, V.; Martin, J.; Wang, H.; Zhang, J. *J. Power Sources* **2007**, *169*, 221–238.
6 (a) Bates, F. S.; Fredrickson, G. H. *Physics Today* **1999**, 32–38. (b) Ruzette, A.-V.; Leibler, L. *Nature Mater.* **2005**, *4*, 10–31.
7 (a) Wang, H.; Capuano, G. A. *J. Electrochem. Soc.* **1998**, *145*, 780–784. (b) Shen, M.; Roy, S.; Kuhlmann, J. W.; Scott, K.; Lovell, K. Horsfall, J. A. *J. Membr. Sci.* **2005**, *251*, 121–130.
8 (a) Ding, J.; Chuy, C.; Holdcroft, S. *Chem. Mater.* **2001**, *13*, 2231–2233. (b) Ding, J.; Chuy, C.; Holdcroft, S. *Adv. Func. Mater.* **2002**, *12*, 389–394. (c) Yang, Y.; Holdcroft, S. *Fuel Cells* **2005**, *2*, 171–186.
9 (a) Norsten, T. B.; Guiver, M. D.; Murphy, J.; Astill, T.; Navessin, T.; Holdcroft, S.; Frankamp, B. L.; Rotello, V. M.; Ding, J. *Adv. Funct. Mater.* **2006**, *16*, 1814–1822. (b) Nieh, M.-P.; Guiver, M. D.; Kim, D. S.; Ding, J.; Norsten, T. *Macromolecules* **2008**, *41*, 6176–6182.
10 Zhai, M.; Chen, J.; Hasegawa, S.; Maekawa, Y. *Polymer* **2009**, *50*, 1159–1165.
11 Zhang, Z.; Chalkova, E.; Fedkin, M.; Wang, C.; Lvov, S. N.; Komarneni, S.; Chung, T. C. M. *Macromolecules* **2008**, *41*, 9130–9139.
12 Tsang, E. M. W.; Zhang, Z.; Shi, Z.; Soboleva, T.; Holdcroft, S. *J. Am. Chem. Soc.* **2007**, *129*, 15106–15107.
13 Kim, J.; Kim, B.; Jung, B. *J. Membr. Sci.* **2002**, *207*, 129–137.
14 (a) Elabd, Y. A.; Napadensky, E.; Sloan, J. M.; Crawford, D. M.; Walker, C.W. *J. Membr. Sci.* **2003**, *217*, 227–242. (b) Elabd, Y. A.; Beyer, F. L.; Walker, C.W. *J. Membr. Sci.* **2004**, *231*,181–188. (c) Elabd, Y. A.; Napadensky, E.; Walker, C. W.; Winey, K. I. *Macromolecules* **2006**, *39*, 399–407.
15 Serpico, J. M.; Ehrenberg, S. G.; Fontanella, J. J.; Jiao, X.; Perahia, D.; McGrady, K. A.; Sanders, E. H.; Kellogg, G. E.; Wnek, G. E. *Macromolecules* **2002**, *35*, 5916–5921.
16 Shi, Z.; Holdcroft, S. *Macromolecules* **2005**, *38*, 4193–4201.
17 Park, M. J.; Downing, K. H.; Jackson, A.; Gomez, E. D.; Minor, A. M.; Cookson, D.; Weber, A. Z.; Balsara, N. P. *Nano Lett.* **2007**, *7*, 3547–3552.

[18] Chen, L.; Phillip, W. A.; Cussler, E. L.; Hillmyer, M. A. *J. Am. Chem. Soc.* **2007**, *129*, 13786–13787.
[19] Schmidt, S. C.; Hillmyer, M. A. *Macromolecules* **1999**, *32*, 4794–4801.
[20] DeLuca, N. W.; Elabd, Y. A. *J. Membr. Sci.* **2006**, *282*, 217–224.
[21] Wang, J.-S.; Matyjaszewski, K. *J. Am. Chem. Soc.* **1995**, *117*, 5614–5615.
[22] (a) Ishizone, T.; Tsuchiya, J.; Hirao, A.; Nakahama, S. *Macromolecules* **1992**, *25*, 4840–4847. (b) Okamura, H.; Takatori, Y.; Tsunooka, M.; Shirai, M. *Polymer* **2002**, *43*, 3155–3162.
[23] Lienkamp, K.; Ruthard, C.; Lieser, G.; Berger, R.; Groehn, F.; Wegner, G. *Macromol. Chem. Phys.* **2006**, *207*, 2050–2065.
[24] Chen, L.; Hillmyer, M. A. *Macromolecules* **2009**, *42*, 4237–4243.
[25] Lienkamp, K.; Schnell, I.; Groehn, F.; Wegner, G. *Macromol. Chem. Phys.* **2006**, *207*, 2066–2073.
[26] Wang, J.-S.; Matyjaszewski, K. *J. Am. Chem. Soc.* **1995**, *117*, 5614–5615.
[27] Aylward, N. N. *Polym. Lett.* **1970**, *8*, 377–380.
[28] Scholl, M.; Ding, S.; Lee, C. W.; Grubbs, R. H. *Org. Lett.* **1999**, *1*, 953– 956.
[29] Teubner, M.; Strey, R. *J. Chem. Phys.* **1987**, *87*, 3195–3200.
[30] Schubert, K.-V.; Strey, R.; Kline, S. R.; Kaler, E. W. *J. Chem. Phys.* **1994**, *101*, 5343–5355
[31] Liu, D.; Kyriakides, S.; Case, S. W.; Lesko, J. J.; Li, Y.; McGrath, J. E. *J. Polym. Sci. B: Polym. Phys.* **2006**, *44*, 1453–1465.
[32] DeLongchamp, D. M.; Vogt, B. D.; Brooks, C. M.; Kano, K.; Obrzut, J.; Richter, C. A.; Kirillov, O. A.; Lin, E. K. *Langmuir* **2005**, *21*, 11480–11483.
[33] Davidson, T. A.; Wagener, K. B.; Priddy, D. B. *Macromolecules* **1996**, *29*, 786–788.
[34] (a) Park, M. J.; Nedoma, A. J.; Geissler, P. L.; Balsara, N. P.; Jackson, A.; Cookson, D. *Macromolecules* **2008,** *41,* 2271–2277. (b) Park, M. J.; Balsara, N. P. *Macromolecules* **2008,** *41,* 3678–3687.
[35] Staudt-Bickel, C.; Koros, W. J. *J. Membr. Sci.* **1999***, 155*, 145–154.
[36] Phillip, W. A.; Martono, E.; Chen, L.; Hillmyer, M. A.; Cussler, E. L. *J. Membr. Sci.* **2009**, *337*, 39–46.
[37] Zhou, Z.; Dominey, R. N.; Rolland, J. P.; Maynor, B. W.; Pandva, A. A.; DeSimone, J. M. *J. Am. Chem. Soc.* **2006**, *128*, 12963–12972.
[38] Debye, P.; Bueche, A. M. *J. Appl. Phys.* **1949**, *20*, 518–525.
[39] Pernot, H.; Baumert, M.; Court, F.; Leibler, L. *Nature Mater.* **2002**, *1*, 54–58.

Appendix

Crosslinked Amine-Functionalized Membranes from a PNS-Containing Copolymer

This chapter represents our efforts to synthesize amine-functionalized block polymers and subsequently prepare crosslinked amine-functionalized polymer membranes by metathesis reactions. The resulting membranes exhibit attractive mechanical and thermal stabilities and are amenable to chemical modification. These membranes are potentially useful in separating CO_2 from gas mixtures.

A1 Introduction

Effective separation of CO_2 from gas mixtures will play a critical role in solving the greenhouse effect; removing the CO_2 impurity in natural gas is of particular interest to promote efficiency harvesting of methane.[1] To date, all commercial CO_2 capture plants use processes based on chemical absorption, for example, using a monoethanolamine solvent (MEA).[2] MEA reversibly absorbs CO_2 and releases it upon heating. In the future, in order to improve the separation efficiencies of CO_2, several disadvantages of the MEA system, such as high energy cost in separation and degradation of MEA, must be overcome.

In addition to chemical adsorption, inorganic zeolite membranes[3] and nanocomposite membranes[4] have been studied as a means of CO_2 separation. These materials have exhibited good chemical durability and CO_2 separation efficiencies. Particularly, functional polymer membranes have drawn much attention to realize continuous CO_2 isolation from gas mixtures in a facile and inexpensive way.[5] For dense polymer membranes, one challenging aspect is to promote the flux and selectivity of CO_2 over other gases. The gas flux can be promoted by using composite membranes, which are typically comprised of an active skin polymer layer over a macroporous substrate.[6] Gas diffusion through polymer membranes typically follows a solubility-diffusion mechanism. As a result, selective CO_2 transport can be facilitated by increasing the interaction between polymer and CO_2. Among various polymers, complex polyimides,[7] crosslinked amorphous poly(ethylene oxide)[8] and amine-functionalized polystyrene[9] have exhibited appealing CO_2 selectivities over other gases. Additionally, poly(*N*,*N*-dimethylaminoethyl methacrylate) (PDMAEMA) is another suitable polymer for CO_2 separation, where the pendant amine groups favor the interaction with CO_2 and thus increase selective CO_2 transport. In practice, PDAMEA membranes have been employed by either grafting PDMAEMA on a polyethylene backbone[10] or by chemically crosslinking the thin PDMAEMA layer.[11]

Herein, a new method of fabricating crosslinked PDMAEMA membranes with a

bicontinuous morphology is demonstrated. The synthesis of a new block copolymer PNS-*b*-PDMAEMA is first described. The production of crosslinked membranes via metathesis reactions of PNS-PDMAEMA and cyclooctene (COE) or dicyclopentadiene (DCPD) is discussed, following the same procedure described in Chapter 4. Additionally, post modification reactions are conducted on the PDMAEMA block to convert it into a zwitterionic polymer. These functional membranes are thermally and mechanically robust and can potentially help elucidate the relationship between the chemical functionality and CO_2 permeability.

A2 Experimental section

A2.1 Materials and characterization

All chemicals were purchased from Aldrich and used as received if not specified. All solvents were purified following the description in Chapter 2. N,N-dimethylaminoethyl methacrylate (DMAEMA), 3-(dimethylamino)propyl methacrylamide (DMAPAM), methyl methacrylate (MMA), styrene, and anisole were passed through short alumina columns to remove the inhibitors and then distilled over CaH_2 under reduced pressure. Syntheses of 2-hydroxymethyl-5-norbornene and 4-norbornenylethyl styrene (N) were described in previous chapters. Synthesis of a polylactide-attached chain transfer reagent for RAFT polymerization (PLATC) was described in Chapter 2.

All characterization methods (NMR, SEC, IR, DSC, SAXS, and TEM) were illustrated in the previous chapters.

A2.2 Material synthesis

A2.2.1 Synthesis and polymerization of norbornenylmethyl methacrylate (NMMA)

NMMA was synthesized using a reported procedure.[12] 2-Hydroxymethyl-5-norbornene (5.0 g, mainly the *endo* isomer), triethylamine (4.23 g), and BHT (0.01 g) were mixed in dry THF (60 mL) under argon. After cooling to 0 °C, a solution of methacrylic acid chloride (5.0

g) in dry CH_2Cl_2 (16 mL) was added dropwise, and a white solid formed. The solution was warmed up to RT and reacted for 1 h. After removing the solid by filtration, the organic phase was washed sequentially with aqueous HCl, DI water, aqueous Na_2CO_3, and brine (50 mL each). The organic phase was dried over Na_2SO_4 for 1 h. After removing Na_2SO_4, the solution was concentrated under vacuum to yield crude product, which was purified by vacuum distillation to yield approximately 8.0 g of product as a colorless oil (NMMA). ^{1}H NMR spectrum of NMMA (300 MHz, $CDCl_3$) δ ppm: 5.91–6.16 (m, CH-C**H**=C**H**-CH), 6.09 and 5.56 (m, -C(CH3)=C**H2**); 3.73 and 3.96 (m, m, -C(O)-O-C**H2**), 2.81 and 2.89 (s, s, C**H**-CH=CH-C**H**), 2.43 (m, -C**H**-CH2-O-C(=O)), 1.93(s, C**H3**), 1.84 (m, -CH-C**H2**(*exo*)-CH-), 1.45 and 1.26 (m, -CH-C**H2**-CH-), 0.57 (m, 1H, -CH-C**H2**(*endo*)-CH-). ^{13}C NMR spectrum of NMMA (75 MHz) δ ppm: 167.3, 137.4, 136.4, 132.0, 125.0, 67.9, 49.1, 43.7, 42.0, 37.6, 28.7, 18.1.

NMMA (1.0 g) and AIBN (17 mg) were mixed in dry Tu (2.0 mL) followed by three freeze-pump-thaw cycles. The mixture was reacted at 65 °C for 0.5 h until gelation occurred. The gel was insoluble in any organic solvent and likely attributed to extensive crosslinking of the norbornene groups in the resultant polymer.

NMMA (0.30 g), MMA (1.27 g), toluene (3.0 mL), and AIBN (15 mL) were mixed in an air free flask followed by three freeze-pump-thaw cycles, and reacted at 60 °C for 2 h. The resultant polymer was precipitated in pentane as a white powder in about 50 % yield. ^{1}H NMR spectrum of P(NM-M)MA δ ppm: 5.7–6.5 (b, CH-C**H**=C**H**-CH), 3.6 (b, O-C**H3** and O-C**H2-**), 2.8–2.95 (d/b, C**H**-CH=CH-C**H**), other peaks were not specified. The mass ratio of NMMA to MMA in the polymer was 0.22, consistent with a ratio of 0.24 in the feed.

A2.2.2 Synthesis and polymerization of 4-nitrobenzyl methacrylate

4-Nitrobenzyl methacrylate (NBMA) was synthesized from 4-nitrobenzyl alcohol (6.17 g) and methacrylic acid chloride (5.0 g) using the same procedure in 2.2.1. The crude product was purified by recrystallization from a mixture of ethyl acetate and pentane and dried at RT

overnight. ^{1}H NMR spectrum of NBMA δ ppm: 8.23 and 7.53(m, t, Ph-**H**), 6.21 and 5.66 (s, t, C(CH3)=C**H2**), 5.29 (s, O-C**H2**), 1.99 (s, -C**H3**). ^{13}C NMR spectrum δ ppm: 166.6, 143.2, 135.5, 128.0, 126.4, 123.6, 64.7, 18.1.

MMA (2.0 g), NBMA (0.40 g), and AIBN (25 mg) were mixed in dry toluene (4 mL) followed by three freeze-pump-thaw cycles, and reacted at 65 °C for 3 h until gelation occurred. The white powder-like polymer was recovered through precipitation in methanol followed by vacuum filtration. ^{1}H NMR spectrum of P(NB-M)MA δ ppm: 8.27 and 7.55 (b, b, Ph-**H**), 5.09 (O-C**H2**), 3.6 (b, O-C**H3**), other peaks were not determined. By NMR analysis, the mass ratio of NBMA to MMA in the polymer was 0.187, agreeable with a ratio of 0.20 in the feed.

A2.2.3 Reduction reaction of P(NB-M)MA

Selective reduction of nitro groups was following a reported step.[13] In an autoclave, P(NB-M)MA (1.50 g) was dissolved in ethyl acetate (50 mL) and hydrogenated under 5 atm of H_2 atmosphere in the presence of Pearlman's catalyst ($Pd(OH)_2$ on activated carbon (100 mg) at 40 °C for 48 h. The catalyst was removed by vacuum filtration, and the solvent was removed under reduced pressure. The resultant polymer was dissolved in toluene (100 mL) and subjected to azeotropic distillation to remove the residue water. Finally, a light yellow polymer was obtained (1.1 g). ^{1}H NMR spectrum δ ppm: 6.95, 6.60 (d, d, NH2-Ph-**H**), other peaks were not specified. The conversion from nitro group to amine group was approximately 60 % based on NMR analysis, and other groups in the polymer were intact after hydrogenation.

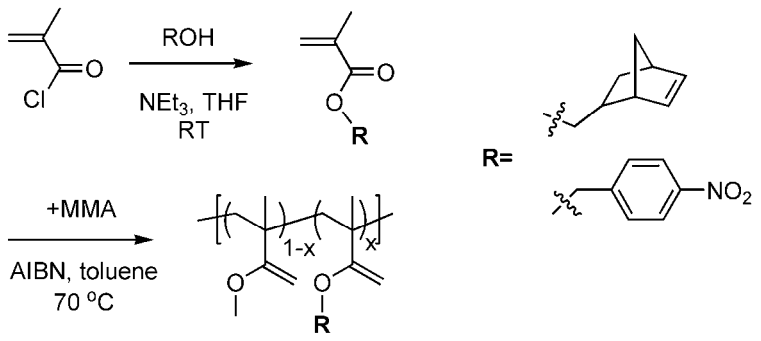

Scheme A1. Syntheses and polymerizations of two methacrylate derivatives.

A2.2.4 Synthesis and polymerization of Boc-protected 4-amino-styrene

4-Nitro-1-bromoethyl benzene (NBEBr): in a three-necked flask, acetic anhydride (55 g) and acetic acid (33 g) were mixed at 0 °C. After cooling the mixture in an ethylene glycol/dry ice bath, fuming nitric acid (38 g) was added slowly. After that, 2-bromoethyl benzene (55 g) was added dropwise into the solution over 1.5 h. During this process, the solution temperature was maintained below 0 °C. The mixture was stirred for 3 h in an ice bath and subsequently quenched with a mixture of aqueous Na_2CO_3 and ice. About 36 g of crude product as a yellow solid was collected by filtration. The resulting product was washed with water and recrystallized from a mixture of 20 % toluene in petroleum ether to yield 29 g of clean product (a yellow needle-like crystal). ^{1}H NMR spectrum of NBEBr δ ppm: 8.20 and 7.40 (d, d, Ph-**H**), 3.62 (t, -C**H2**-Ph), 3.29 (t, -C**H2**-Br).

4-Nitro-styrene:[14] NBEBr (29 g), triethanolamine (100 mL), and DI water (80 mL) were refluxed in a round-bottom flask equipped with Stark and Dean trap and a reflux condenser. About 14 g of heavy yellow oil[a] was isolated within 2 h. This product was recrystallized from methanol at −40 °C and dried at 0 °C, to yield 11g of product as a light yellow needle-like crystal. ^{1}H NMR spectrum of 4-nitro-styrene δ ppm: 8.20 and 7.54 (d, d, Ph-**H**), 6.79 (q, C**H**=CH2), 5.94 and 5.51 (d, d, CH=C**H2**).

4-Amino-styrene:[15] to a solution of 4-nitrostyrene (10.0 g) in acetone (100 mL) added a

[a] Low yield was obtained by the slow reflux, and some product decomposed during heating.

solution of ammonium chloride (7.5 g) in water (30 mL). The mixture was heated to boiling. The bath was removed and zinc dust (15.0 g) was slowly added in small portions. After the zinc was added, another batch of zinc dust (5.0 g) was added and the reaction was refluxed for 30 min. The solution was hot-filtered and the solid was washed with acetone. Concentration of the organic mixture afforded 6.6 g of crude product as orange liquid that froze at 0 °C. ^{1}H NMR spectrum of 4-amino-styrene δ ppm: 7.24 and 6.64 (d, d, Ph-**H**), 6.62 (q, C**H**=CH2), 5.55 and 5.05 (d, d, CH=C**H2**), 3.71 (s, N**H2**).

Boc-protected 4-amino-styrene (BocNSt):[16] 4-aminostyrene (6.6 g) was dissolved in dioxane (100 mL) into a three-necked round-bottom flask. To the solution, a di-*t*-butylcarbonate [$(Boc)_2O$] (18.0 g) solution in dioxane (20 mL) was slowly added under N_2 atmosphere. The solution was stirred overnight and then concentrated under reduced pressure. The solid product was dissolved in ethyl acetate, while maintaining the temperature at 0 °C, and then a $KHSO_4$ aqueous solution was added until pH=5 was reached. The organic phase was separated and dried over Na_2SO_4. After removing Na_2SO_4 by filtration, the solvent was removed under reduced pressure. Recrystallization of the crude BocNSt as an orange solid from *n*-hexane afforded a white solid in 50 % yield.[b] ^{1}H NMR spectrum of BocNSt δ ppm: 7.34 (t, Ph-**H**), 6.66 (q, C**H**=CH2), 6.52 (s, -N**H-**), 5.66 and 5.16 (d, d, CH=C**H2**), 1.52 (s, C**H3**). ^{13}C NMR spectrum δ ppm: 137.7, 135.9, 126.6, 118.2, 115.1, 112.2, 28.1.

PLATC (11.0 kg mol^{-1}, 0.2 g), BocNSt (0.05 g), styrene (0.36 g), and AIBN (0.2 mg) were mixed in an air free flask followed by three freeze-pump-thaw cycles, and reacted at 60 °C for 18 h. The resulting polymer was recovered by precipitation in methanol. By NMR spectroscopy, on average only 1.3 BocNSt units were incorporated in each copolymer (1 mol % in the P(S-BocNSt) block), significantly lower than 6 mol % of BocNSt in the monomer feed.

[b] By heating the compound in *n*-hexane an insoluble solid formed. To circumvent this problem, more *n*-hexane was used to dissolve the crude product at RT, and the solution was placed in a dry ice/isopropanol bath until a white solid precipitated. By this step, the product was recovered in low yield.

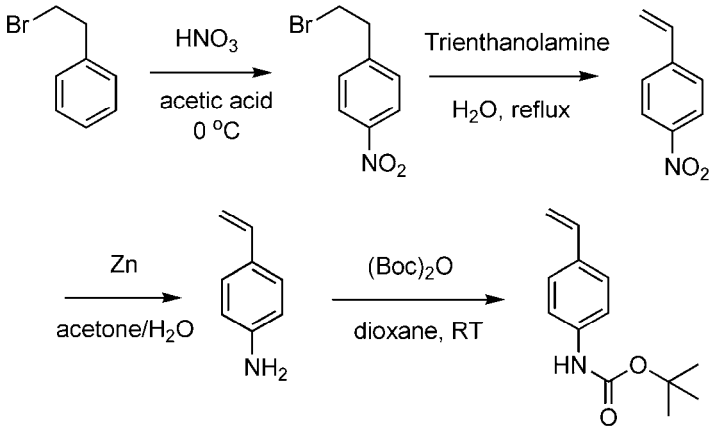

Scheme A2. Synthesis of Boc-protected 4-amino-styrene.

A2.2.5 Synthesis of 2-phenylprop-2-yl dithiobenzoate (CTA2)[17]

Bromobenzene (5.6 g, 0.036mol) and magnesium (0.82g, 0.036mol) in anhydrous diethyl ether (100ml) formed the Grignard reagent and then reacted with carbon disulide (2.7 g, 0.036mol) in dry THF (30 ml) at −5 °C for 1 h. The mixture was decomposed with aqueous HCl and ice (100 ml). The organic layer was separated and washed with cold aqueous NaOH (10 wt %, 50 ml) three times. The combined aqueous solution was washed with diethyl ether three times and acidified with cold aqueous HCl (10 wt %). Finally, the aqueous layer was extracted with diethyl ether (50 mL) three times. The ether fractions were concentrated to afford 5 g of dithiobenzoic acid. A mixture of dithiobenzoic acid (5.0 g), α-methylstyrene (4.4 mL) and CCl_4 (40 mL) was heated at 70 °C for 5 h under N_2. The resultant mixture was concentrated to a crude oil, which was further purified by column chromatography (silica gel, hexanes) twice to afford about 2.0 g of product as a purple oil. ^{1}HNMR of **CTA2** δ ppm: 7.2–7.4 (m, C(CH3)2-Ph-**H**), 7.4–7.9 (m, C(=S)-Ph-**H**), 2.04 (s, C**H3**).

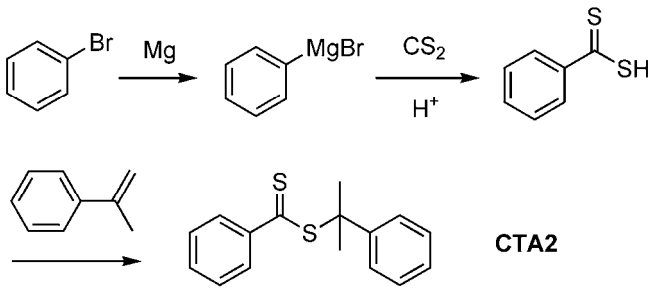

Scheme A3. Synthesis of a RAFT chain transfer reagent.

A2.2.6 Synthesis of PNS-*b*-PDMAEMA

The norbornene-functionalized polystyrene (PNS-Br) was prepared by atom transfer radical polymerization (ATRP).[18] 1-Bromoethyl styrene (70 mg), CuBr (54 mg) and bipyridine (117 mg) at a molar ratio of 1:1:2 were mixed in styrene (3 mL) and monomer N (1 mL) in an air free flask under argon atmosphere followed by three free-pump-thaw cycles. The reaction vessel was sealed under vacuum and placed in an oil bath at 110 °C for 4.5 h. After polymerization, the reaction mixture was diluted with THF and passed through a short alumina column to remove the Cu catalyst. The polymer was precipitated in methanol followed by filtration and washed with extra methanol. The resultant polymer was dried at 60 °C overnight under reduced pressure. The number average molecular weight (M_n) was derived from NMR end group analysis. ^{1}H NMR spectrum of PNS-Br δ ppm: 6.2–7.3 (b, Ph-**H**), 5.9–6.2 (b, -C**H**=C**H**-), 4.3–4.6 (b,-C**H**-Br), 2.8 (b, -C**H**-CH=CH-C**H**-), 2.5 (b, Ph-C**H2**-), 0.6–2.0 (b, other C**H** and C**H2**).

PNSBr (0.40 g), DMAEMA (1.2 g), CuBr (8.2 mg), and bipyridine (17.8 mg) were mixed in dry anisole (1.0 mL) followed by three free-pump-thaw cycles, and reacted at 90 °C for 1 h. The resultant solution was diluted with acetone, passed through a short alumina column to remove the catalyst, and precipitated in cold pentane. The polymer was dried at RT under reduced pressure overnight. ^{1}H NMR spectrum of PNS-PDMAEMA δ ppm: 6.2–7.3 (b, Ph-**H**), 5.9–6.2 (b, -C**H**=C**H**-), 4.05 (b, O-C**H2-**), 2.55 (b, O-CH2-**CH2**), 2.27 (b, -N(C**H3**)2), other signals were not specified. By NMR spectroscopy, the M_n of PDMAEMA was

determined based on the PNS block.

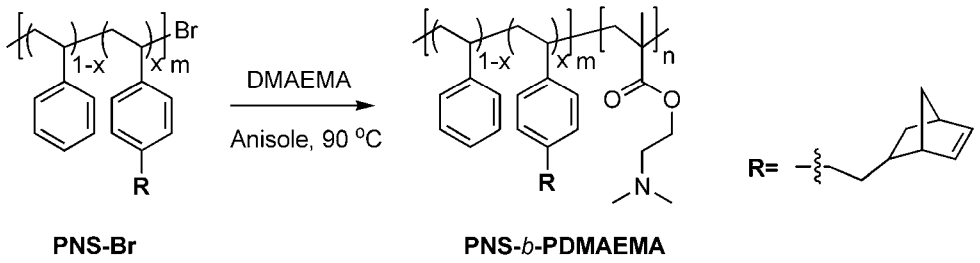

Scheme A4. Synthesis of a PNS-*b*-PDMAEMA copolymer.

A2.2.7 Synthesis of PDMAPAM

Conventional free radical polymerization: DMAPAM (2.0 g) and AIBN (40 mg) were mixed in dry toluene (2 mL) followed by three freeze-pump-thaw cycles, and reacted at 70 °C for 2 h until gelation occurred. The gel was dissolved in acetone and precipitated in hexanes. A white powder-like polymer (1.20 g) was obtained. This polymer was extremely soluble in water. ^{1}H NMR spectrum of PDMAPAM δ ppm: 7.5 (b, N**H**), 3.18 (b, -NH-C**H2**), 2.35 (b, -C**H2**-N(CH3)2), 2.22 (b, -N(C**H3**)2, other peaks were not determined.

RAFT polymerization: **CTA2** (20 mg), AIBN (3.3 mg), DMAPAM (2.0 mL) were mixed in dry toluene (2.0 mL) followed by three free-pump-thaw cycles, and reacted at 65 °C for 24 h. After polymerization, toluene was removed under vacuum and NMR analysis of the resulting mixture indicated 10 % conversion of DMAEMA, significantly lower than the conversion of the previous polymerization with AIBN.

ATRP: PNSBr (0.40 g, 5 kg mol^{-1}), DMAPAM (1.2 g), CuBr (8.2 mg), and bipyridine (17.8 mg) were mixed in dry anisole (1.0 mL) followed by three free-pump-thaw cycles, and reacted at 90 °C for 2 h. NMR analysis of the recovered polymer indicated negligible conversion of DMAPAM.

A2.3 Membrane preparation

PNS-PDMAEMA (e.g., 0.3 g) was dissolved into THF (1.6 mL) until a homogeneous

solution was obtained. COE or DCPD (variable, e.g., 0.23 g) was then added to the polymer solution and stirred for another 20 min. To the mixture a solution of the 2nd generation Grubbs catalyst (2.5 mg) in THF (0.4 mL) was quickly mixed and stirred for 20 s, and then casted onto an aluminum pan. Gelation of the solution occurred within 5 min. After curing the mixture at RT overnight along with slow THF evaporation and at 90 °C for 1 h, a transparent membrane was peeled off the substrate and dried under high vacuum. The amine groups were modified following a reported step.[19] PDMAEMA-containing membranes or PNS-PDMAEMA were stirred in a solution of 1,3-propanesultone (10 times in excess relative to the amine groups) in ethyl acetate at 40 °C overnight. After reaction, the copolymer was collected by filtration; the resultant membrane was rinsed with DI water and dried under high vacuum.

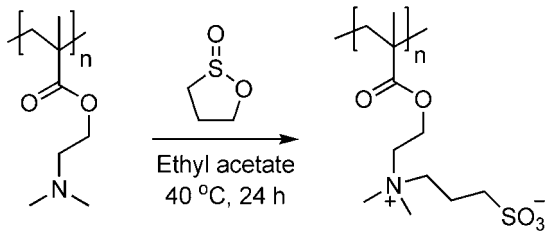

Scheme A5. Chemical modification of the amine group in PDMAEMA.

A3 Results and discussion

In order to produce crosslinked amine-functionalized membranes using the reaction induced phase separation scheme in Chapter 4, a desirable block copolymer should contain a PNS block reactive to metathesis catalysts and another block containing amine groups. Initial efforts were made to identify a proper candidate amine-functionalized polymer. Amine-functionalized polymers are normally produced in aqueous solution due to their high solubility in water, but synthesis of PNS-containing block copolymers having an amine-functionalized block in water is less facile, due to the hydrophobicity of the PNS block. Additionally, amine groups are easily charged in water, which could reduce the polymer solubility in organic solvents. Several strategies have been examined to synthesize

amine-functionalized polymers in organic solvents. First, a Boc-protected amine-functionalized styrene (BocNSt) was synthesized and polymerized. The protected amine group would be stable during the polymer synthesis and later could be selectively deprotected. Nevertheless, the low reactivity of BocNSt in the copolymerization with styrene could hinder the facile synthesis of copolymers with high amine contents. Second, an amine-functionalized PMMA was produced by selectively reducing a nitro-functionalized precursor polymer. Although the reduction step was selective, this synthetic scheme was relatively complicated and might not be suitable for bulk polymer membranes. Alternatively, DMAPAM is an attractive commercial monomer that is not susceptible to hydrolysis, and it is amenable to subsequent chemical modification.[20] Nevertheless, controlled radical polymerization of DMAPAM was not successful. For example, RAFT polymerization and ATRP of this monomer were retarded, as the initiators were likely decomposed by this base monomer.

Finally, synthesis of a PNS-PDMAEMA copolymer was accomplished using sequential ATRPs (Scheme A4). The resulting PNSBr macro-initiator and the PNS-PDMAEMA copolymer are summarized in Table A1. The NMR spectra in Figure A1 indicate well-defined molecular structures; SEC data show decent molecular polydispersity indices (PDI) around 1.5. From DSC analysis, the PNSBr homopolymer displays a glass transition temperature (T_g) at 88 °C, but the PNS-PDMAEMA copolymer only exhibits a single T_g at 29 °C, implying no phase segregation between the PNS and PDMAEMA blocks. According to the literature, PDMAEMA (M_n > 100 kg mol^{-1}) has a glass transition temperature (T_g) of 18 °C.[21] In the PNS-PDMAEMA copolymer, assuming the PNS and PDMAEMA blocks are completely miscible, a single T_g at 32 °C will be expected based on the Fox equation[22] and the T_gs of two blocks. This value is consistent with the experimental value at 29 °C, given that the T_g of 22 kg mol^{-1} PDMAEMA could be lower than 18 °C.

SAXS analysis of this copolymer gave no scattering peak at temperatures between RT and

150 °C (for example, the scattering profile at RT shown in Figure A3), suggesting no phase separation between the PNS and PDMAEMA blocks. Additionally, a reported χ between PS and PDMAEMA is 0.055 at about 160 °C,[23] so χN in PNS-PDMAEMA at RT would be less than 11 assuming a volume fraction of PS around 30 %. According to the theoretical phase diagram,[24] no phase segregation in this PNS-PDMAEMA copolymer would be expected.

Table A1. Summary of the resultant polymers.

	SEC[a]		NMR M_n	T_g	N groups
	M_n (kg mol^{-1})	PDI	(kg mol^{-1})	(°C)	per chain
PNS-Br	6.5	1.45	7.0	88	7.6
PNS-PDMAEMA	32.9	1.56	29.4	29	7.6

a. PNSBr was measured using a $CHCl_3$ SEC with a Refractive Index detector; PNS-PDMAEMA was characterized in a THF SEC containing 1 vol % N,N,N',N'-tetramethylethylenediamine with a Light Scattering detector, and *dn/dc* for this copolymer in THF of 0.130 mL/g was estimated from the *dn/dc* values of poly (dimethylaminoethyl acrylate) and PS.

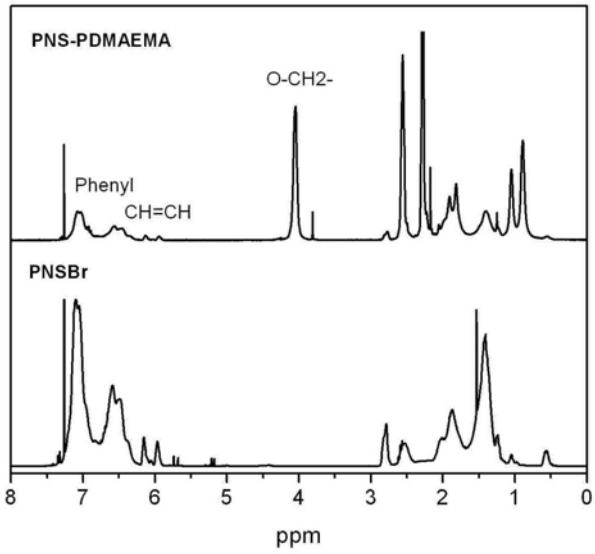

Figure A1. NMR spectra for the PNSBr and PNS-PDMAEMA.

Three crosslinked membranes were fabricated from the above copolymer, and summarized in Table A2. Chemical modification of the amine groups in CM1 and 2 was conducted as described in Section 2.2.8 and monitored by IR spectroscopy using the PNS-PDMAEMA

copolymer as reference. The PNS-PDMAEMA copolymer was initially soluble in ethyl acetate; after reaction with 1,3-propanesultone, an insoluble solid resulted, indicative of the formation of a zwitterionic copolymer. For the crosslinked membranes, following the same modification procedure, transparent membranes were obtained. IR analysis of the resulting samples indicated similar changes, for example, IR spectra for CM1 shown in Figure A2. Disappearance of the peak at 2770 cm^{-1} with the appearance of the strong absorbance at 1210 cm^{-1} suggest the full conversion of the -$N(CH_3)_2$ group to the zwitterionic group.

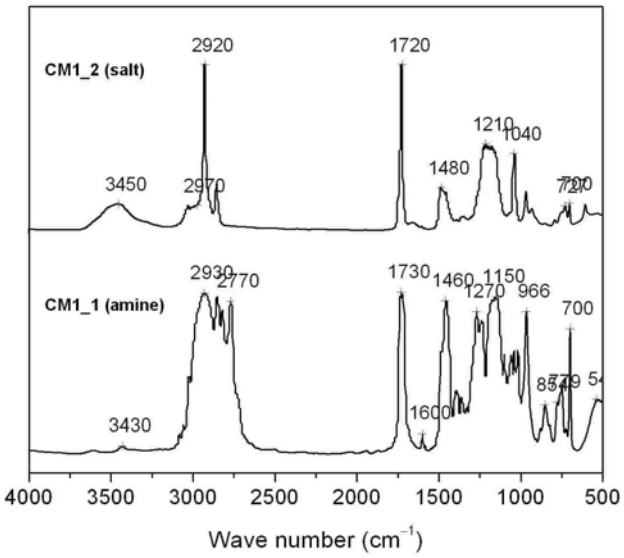

Figure A2. IR spectra of CM1_1 (amine) and CM1_2 (salt).

SAXS experiments were conducted to determine the morphology in these membranes. For membranes CM1_1 and CM2_1 produced from the PNS-PDMAEMA copolymer and COE, a single scattering peak was observed (Figure A3), indicating microphase separation between the crosslinked PNS/PCOE and PDMAEMA phases, similar to those crosslinked membranes in Chapter 4. For CM3 produced from the copolymer and DCPD, no scattering peak appeared in SAXS analysis, suggesting no phase separation in CM3. After modification of amine groups, the scattering peaks were retained in CM1_2 and CM2_2, but the domain spacings inferred by the peak position ($D=2\pi/q^*$) slightly increased.

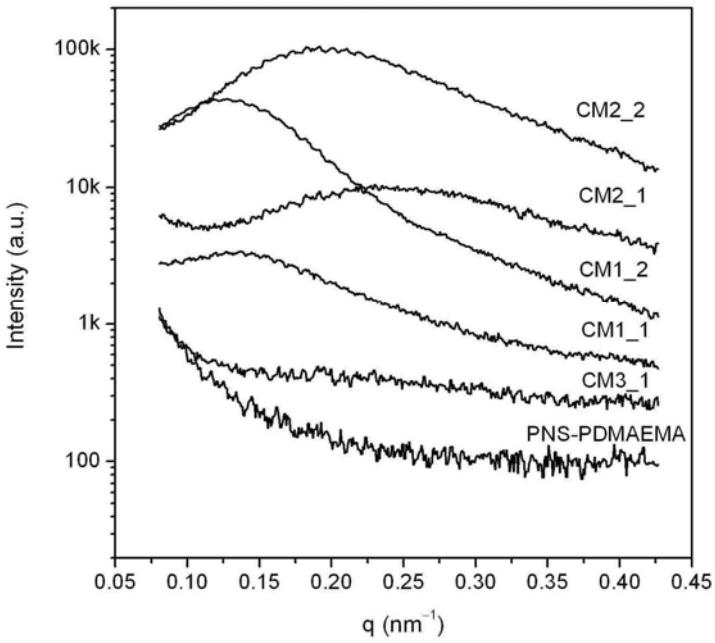

Figure A3. SAXS profiles of CMs 1, 2, and 3 at RT. The signals were intentially shifted vertically.

Table A2. Summary of the crosslinked PDMAEMA membranes.[a]

	PNS-PDMAEMA (mg)	Monomer (mg)	$f_{PDMAEMA}$ (wt %)	Domain spacing[c] (nm)
CM1_1[b]	300	223	42.8	45
CM2_1	400	150	54.4	25
CM3	300	223	42.8	

a. Membranes 1, 2, and 3 were casted from a 20 wt % THF solution of PNS-PDMAEMA, reactive monomers (1 and 2 using COE and 3 using DCPD), the 2nd generation Grubbs catalyst (0.5 wt % to the total mass of reactive components) onto aluminum pans, and cured at RT overnight. *b*. Membranes CM1_2 and CM2_2 in the zwitterionic form were produced from CM1_1 and CM1_2, respectively (see Scheme A5). *c*. SAXS domain spacing was estimated from the peak position q^* by the equation $D=2\pi/q^*$.

In further experiments, DSC analysis on the resultant membranes was conducted. Chemical modification of the PDMAEMA phase in CM1_1 could not be inferred from the DSC traces (Figure A4), as the T_g of PDMAEMA was embedded in the melting peak of PCOE in CM1_1, although after membrane modification the melting endotherm of CM1_2 was substantially decreased. For the DSC analysis of CM2_1 with less PCOE incorporated,

the matrix PNS/PCOE phase was nearly amorphous. A T_g endotherm was observed around 5 °C, possibly associated with the T_g of PDMAEMA. The lower T_g for PDMAEMA (a reported value was 18 °C) can be attributed to low molecular weight of PDMAEMA and some impurities (possibly some PCOE oligomers) in the PDMAEMA phase. After modification of the amine groups, the original T_g at 5 °C completely disappeared in CM2_2 (Figure A4), agreeable with the formation of the zwitterionic polymer, which would have a high T_g. Additionally, no thermal transition for CM3 by DSC indicated that PDMAEMA was possibly mixed in the PNS/polyDCPD phase, consistent with the previous SAXS result.

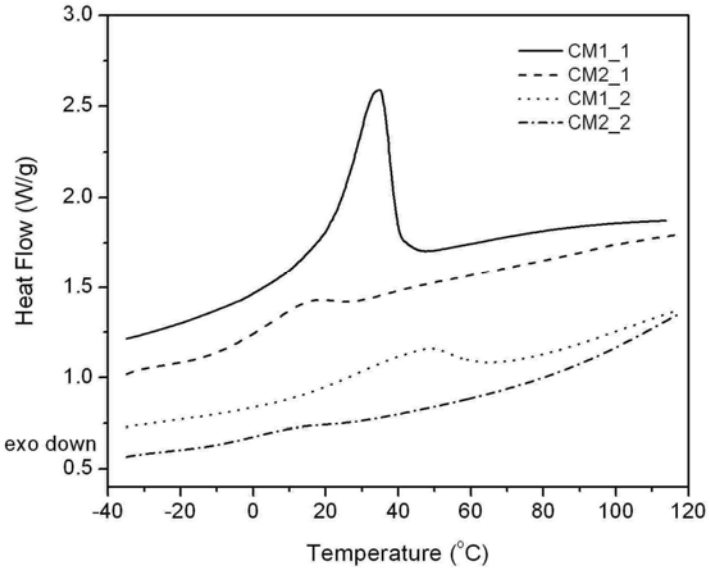

Figure A4. DSC traces of crosslinked amine-functionalized membranes (the 2nd heating run).

Next, TEM experiments were conducted on CM1_1 and CM1_2 to probe the microstructure. The TEM micrograph of CM1_1 in Figure A5 clearly shows microphase separation: dark PCOE/PNS nanodomains stained by OsO_4 percolate through bright PDMAEMA domains. For CM1_2, a similar structure is observed, indicating that the chemical modification did not affect the morphology. For the TEM image for CM3, no distinct microphase separation was observed.

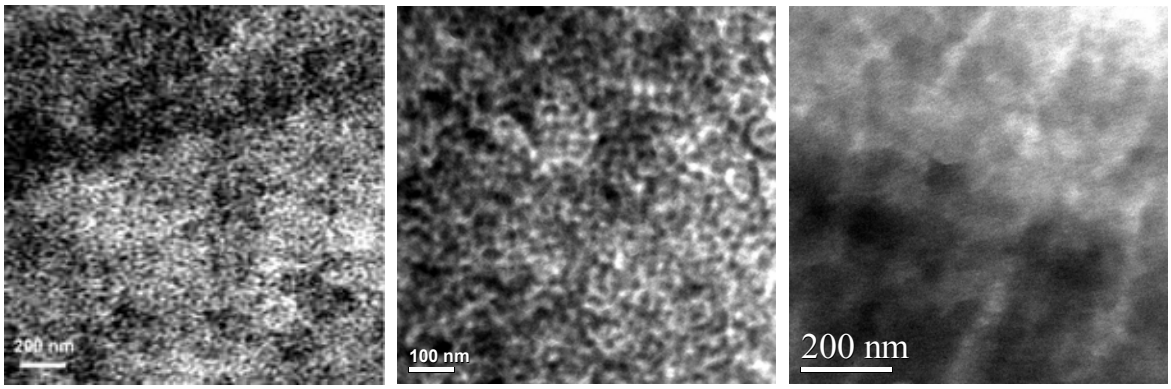

CM1_1 CM1_2 CM3

Figure A5. TEM images of CMs 1_1, 1_2, and 3. The membranes were cryo-microtomed into 80 nm thick slices and selectively stained by a 4 wt % OsO_4 aqueous solution at RT for 15 min. The dark regions in CM1_1 and CM1_2 correspond to the stained PCOE/PNS phase.

Additionally, these crosslinked membranes can swell in water (dimensional change of 10–20 %) and are stable in many organic solvents. Thermally, membranes CM1 and CM2 were stable to up 200 °C. Mechanically, dry membranes were very elastic similar to those membranes in Chapter 4. Collectively, the robustness of these crosslinked membranes has not been achieved in previous PDMAEMA membranes.[10,11] These structural attributes could be beneficial to address the relationship between the polymer functionality and CO_2 separation performance, since the membrane morphology is well resolved and stable under a variety of conditions.

Lastly, based on the crosslinked samples with PNS-PDMAEMA, the mechanism of structure formation proposed in Chapters 3 and 4 is further corroborated. While using COE in the crosslinking reaction of PNS-PDMAEMA, the grafting mechanism determines the final morphology. Despite low χs between PNS (PCOE) and PDMAEMA, when a highly grafted polymer (χN large enough) is formed, phase separation between PDMAMEA and PNS/PCOE finally results, and thereby a bicontinuous morphology is adopted.[25] During this process, any PCOE oligomers formed in the PDMAEMA/THF domains can eventually segregate from PDMAEMA after drying. In contrast, for the crosslinking process with DCPD, χ(PDMAEMA/polyDCPD) is presumably low, and thus the segregation between polyDCPD

and PDMAEMA may not occur before solution gelation. Consequently, some crosslinked polyDCPD oligomers would remain in the PDMAEMA phase due to their low mobility and thus lead to no distinct microphase separation.

A4 Conclusions and outlook

The fabrication of crosslinked PDMAEMA membranes with a well-defined morphology and enhanced robustness has been demonstrated. Currently, CO_2 separation from a CO_2/CH_4 gas mixture by using these PDMAEMA membranes is under exploration. In the future, other chemical modification methods of the amine component could be explored, such as forming a $-N(CH_3)_3^+ F^-$ structure.[9] Eventually, the influence of the membrane functionality on CO_2 separation from gas mixtures can be addressed.

A5 References

[1] Sridhar, S.; Smitha, B.; Aminabhavi, T. M. *Sep. Purif. Rev.* **2007**, *36*, 113–174.

[2] http://www.netl.doe.gov/newsroom/backgrounder/mb-0002.html

[3] Sebastian, V.; Kumakiri, I.; Bredesen, R.; Menendez, M. *J. Membr. Sci.* **2007**, *292*, 92–97.

[4] Cornelius, C. J.; Marand, E. *J. Membr. Sci.* **2002**, *202*, 97–118

[5] Lin, H.; Freeman, B. D. *J. Mol. Struct.* **2005**, *739*, 57–74.

[6] Baker, R. W. *Membrane technology and applications,* 2nd Ed. John Wiley & Sons Ltd, West Sussex, England, **2004**.

[7] Ghanem, B. S.; McKeown, N. B.; Budd, P. M.; Selbie, J. D.; Fritsch, D. *Adv. Mater.* **2008**, *20*, 2766–2771.

[8] Lin, H.; Wagner, E. V.; Freeman, B. D.; Toy, L. G.; Gupta, R. P. *Science* **2006**, *311*, 639–642.

[9] Quinn, R.; Laciak, D. V.; Pez, G. P. *J. Membr. Sci.* **1997**, *131*, 61–69.

[10] Matsuyama, H.; Teramoto, M.; Sakakura, H. *J. Membr. Sci.* **1996**, *114*, 193–200.

[11] Du, R.; Feng, X.; Chakma, A. *J. Membr. Sci.* **2006**, *279*, 76–85.

[12] Schitter, R. M. E.; Jocham, D.; Stelzer, F.; Moszner, N.; Volkel, T. *J. Appl. Polym. Sci.* **2000**, *78*, 47–60.

[13] Carter, K. R.; DiPietro, R. A.; Sanchez, M. I.; Russell, R. P. *Chem. Mater.* **1997**, *9,* 105–118.

[14] Strassburg, R. W.; Gregg, R. A.; Walling, C. *J. Am. Chem. Soc.* **1947**, *69*, 2141–2143.

[15] Boyer, J. H.; Alul, H. *J. Am. Chem. Soc.* **1959**, *81*, 2136–2137

[16] Covolan, V. L.; Ruggeri, G.; Chiellini, E. *J. Polym. Sci. A: Polym. Chem.* **2000**, *38*, 2910–2918.

[17] Le, T.P.; Moad, G.; Rizzardo, E.; Thang, S. H. WO 9801478, **1998**.

[18] Wang, J.-S.; Matyjaszewski, K. *J. Am. Chem. Soc.* **1995**, *117*, 5614–5615.

[19] Ward, R. S.; Davies, J.; Hodges, G.; Roberts, D. W. *Synthesis* **2000**, 2431–2439.

[20] (a) Schmitz, S.; Ritter, H. *Macromol. Rapid Commun.* **2007**, *28*, 2080–2083. (b) Hara, N.; Ohashi, H.; Ito, T.; Yamaguchi, T. *Macromolecules* **2009**, *42*, 980–986.

[21] Arce, A.; Fornasiero, F.; Rodriguez, O.; Radke, C. J.; Prausnitz, J. M. *Phys. Chem. Chem. Phys.* **2004**, *6*, 103–108.

[22] Couchman, P. R. *Macromolecules* **1978**, *11*, 1156–1161.

[23] Costa, A. K.; Geoghegan, M.; Vlcek, P.; Composto, R. J. *Macromolecules* **2003**, *36,* 9897–9904.

[24] Matsen, M. W.; Bates, F. S. *Macromolecules* **1996**, *29*, 1091–1098.

[25] Pernot, H.; Baumert, M.; Court, F.; Leibler, L. *Nature Mater.* **2002***, 1*, 54–58.